

HEAT FLOW IN SOLIDIFICATION OF ALLOYS

by

ALAN J. CAMPAGNA

S.B. Massachusetts Institute of Technology 1966

Submitted in Partial Fulfillment

of the Requirement for the

Degree of


DOCTOR OF PHILOSOPHY

at the

MASSACHUSETTS INSTITUTE OF TECHNOLOGY

(1970)

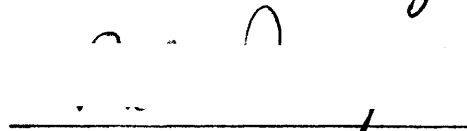
Signature of Author



Signature of Professor  
in Charge of Research



Signature of Chairman  
of Departmental Committee  
on Graduate Students



## HEAT FLOW IN SOLIDIFICATION OF ALLOYS

by

ALAN J. CAMPAGNA

Submitted to the Department of Metallurgy on May 14, 1970  
in partial fulfillment of the requirements for the degree  
of DOCTOR OF PHILOSOPHY.

-----

## ABSTRACT

A mathematical model for heat flow during solidification of alloys has been postulated. This model treats the heat of fusion released upon solidification separately for three distinct regions of a casting; a portion is released isothermally at the liquidus temperature, a second portion is released over the range of temperature between the liquidus and solidus in a specified manner, and the remainder is released at the solidus.

The mathematical model is solved numerically, by means of a finite difference technique, on a computer. Results of the solutions are presented for unidirectional heat flow, radial heat flow, and two dimensional heat flow in thin plates. For each of these cases, effects are considered of heat transfer coefficient at the chill surface, superheat, heat input, and liquid convection.

Results are presented in terms of positions of liquidus and solidus isotherms as a function of time, width of the liquid-solid zone as a function of time, and "local solidification time". Detailed numerical solutions are presented, as example, for an end chilled plate cast in various molding media. The local solidification time of an alloy is shown to decrease at a given distance from the chill, as (a) the heat transfer coefficient increases, (b) the superheat increases, (c) the gradient of temperature at the solidification front increases, (d) the characteristic distance over which heat flow occurs decreases, and (e) the multi-dimensionality of the heat flow path increases.

Thesis Supervisor: Merton C. Flemings  
Title: Professor of Metallurgy

## TABLE OF CONTENTS

| <u>Chapter<br/>Number</u> |   | <u>Page<br/>Number</u> |
|---------------------------|---|------------------------|
|                           | ABSTRACT  |                        |
|                           | LIST OF FIGURES   |                        |
|                           | LIST OF TABLES  |                        |
|                           | ACKNOWLEDGEMENTS  |                        |
| I                         | INTRODUCTION  | 1                      |
| II                        | RESULTS   | 28                     |
| III                       | DISCUSSION  | 96                     |
| IV                        | CONCLUSIONS   | 111                    |
| V                         | SUGGESTIONS FOR FUTURE WORK   | 115                    |
| VI                        | BIBLIOGRAPHY  | 118                    |
| VII                       | APPENDICES  | 137                    |
|                           | A: Numerical Procedure Used in<br>Calculation of Heat Flow in<br>Unidirectional Solidification<br>of Alloys | 137                    |
|                           | B: Modifications of the<br>Unidirectional Procedure to<br>Solve Radial and Sidewise<br>Heat Flow            | 148                    |
|                           | C: Dimensional Analysis Results   | 150                    |
|                           | D: The Program  | 153                    |
|                           | E: Error Estimates  | 191                    |
|                           | F: Thin Plate Castings  | 213                    |
|                           | BIOGRAPHICAL NOTE   | 221                    |

## LIST OF FIGURES

| <u>Figure<br/>Number</u> |   | <u>Page<br/>Number</u> |
|--------------------------|---|------------------------|
| 1                        | Approximation of distribution of liquid in the mushy zone. (a) Steady state solute redistribution, Scheil equation. (b) Linear $f_L$ versus $x$ , finite eutectic. (c) Linear $f_L$ versus $x$ , no eutectic. | 22                     |
| 2                        | Aluminum rich portion of aluminum-copper phase diagram  | 23                     |
| 3                        | Linear distribution of $f_L$ versus $x$ , with finite eutectic and undercooling   | 24                     |
| 4                        | Parallel plates of solid and liquid representing a simplified view of parallel or series heat flow. (a) Parallel. (b) Series  | 25                     |
| 5                        | Equi-axed growth, schematic representation of mushy region cut along length   | 26                     |
| 6                        | Description of parameters in finite difference procedure  | 27                     |
| 7                        | Position of the liquid-solid interface versus $\sqrt{t}/L$ , unidirectional heat flow, pure aluminum, $h_{BL}/\bar{K} = \infty$ , $\Delta T_s = 0$ , for three values of heat of fusion.                      | 61                     |
| 8                        | Position of the liquid-solid interface versus $\sqrt{t}/L$ , unidirectional, pure aluminum, $h_{BL}/\bar{K} = \infty$ for four values of superheat  | 62                     |
| 9                        | Position of the liquid-solid interface versus $\sqrt{t}/L$ , unidirectional, pure aluminum, $\Delta T_s = 0$ , for four values of $h_{BL}/\bar{K}$  | 63                     |
| 10                       | Position of the liquid-solid interface versus $\sqrt{t}/L$ , unidirectional, pure aluminum, comparing computer solutions to analytic results  | 64                     |
| 11                       | Local solidification time at $\lambda = 0.75$ versus fraction solid at the tip, Al-4.5% Cu alloy, unidirectional, no convection, no superheat, for two growth morphologies.                                   |                        |

| <u>Figure<br/>Number</u> |  | <u>Page<br/>Number</u> |
|--------------------------|--|------------------------|
| 12                       | Position of the tip and root versus $\sqrt{t}/L$ , Al-4.5% Cu alloy, unidirectional, $h_B L/\bar{K} = \infty$ , for four values of superheat                                       | 66                     |
| 13                       | Local solidification time versus distance for conditions of Figure 12  | 67                     |
| 14                       | Position of the tip and root versus $\sqrt{t}/L$ , Al-4.5% Cu alloy, unidirectional, no superheat, for four values of $h_B L/\bar{K}$  | 68                     |
| 15                       | Local solidification time versus distance for conditions of Figure 14  | 69                     |
| 16                       | Position of the tip and root versus $\sqrt{t}/L$ , Al-4.5% Cu alloy, radial heat flow, $h_B L/\bar{K} = \infty$ , for four values of superheat.                                    | 70                     |
| 17                       | Local solidification time versus distance for conditions of Figure 16  | 71                     |
| 18                       | Position of the tip and root versus $\sqrt{t}/L$ , Al-4.5% Cu alloy, radial heat flow, no superheat, for four values of $k_B L/\bar{K}$  | 72                     |
| 19                       | Local solidification time versus distance for conditions of Figure 18  | 73                     |
| 20                       | Position of the tip and root versus $\sqrt{t}/L$ , Al-4.5% Cu alloy, unidirectional, no superheat, $h_B L/\bar{K} = \infty$ , for four values of heat input with higher convection | 74                     |
| 21                       | Local solidification time versus distance for conditions of Figure 20  | 75                     |
| 22                       | Position of the tip and root versus $\sqrt{t}/L$ , Al-4.5% Cu alloy, no convection, no superheat, $h_B L/\bar{K} = \infty$ , for four values of side heat loss ( $h_s L^2/W$ )     | 76                     |
| 23                       | Local solidification time versus distance, for conditions of Figure 22   | 79                     |

| <u>Figure<br/>Number</u> |  | <u>Page<br/>Number</u> |
|--------------------------|--|------------------------|
| 24                       | Local solidification time at $\lambda = 0.75$ versus $h_s$ , for conditions of Figure 23   | 80                     |
| 25                       | Positions of the tip and root versus $\sqrt{t}/L$ , Al-4.5% Cu alloy, no convection, $h_B L/\bar{K} = \infty$ , $h_s L^2/W = 0.232$ , for four values of superheat                     | 81                     |
| 26                       | Local solidification time versus distance for conditions of Figure 25  | 82                     |
| 27                       | Local solidification time at $\lambda = 0.75$ versus $\Delta T_s$ , for four values of $h_s L^2/W$   | 83                     |
| 28                       | Position of the tip and root versus $\sqrt{t}/L$ , Al-4.5% Cu alloy, no superheat, $h_B L/\bar{K} = \infty$ , $h_s L^2/W = 0.232$ , for four values of heat input with high convection | 84                     |
| 29                       | Local solidification time versus distance for conditions of Figure 28  | 85                     |
| 30                       | Position of the tip and root versus $\sqrt{t}/L$ , Al-4.5% Cu alloy, no superheat, $h_B L/\bar{K} = \infty$ , heat input with high convection  | 86                     |
| 31                       | Local solidification time versus distance, for conditions of Figure 30   | 87                     |
| 32                       | Local solidification time at $\lambda = 0.75$ versus dimensionless heat input, no superheat, $h_B L/\bar{K} = \infty$ , for four values of $h_s L^2/W$                                 | 88                     |
| 33                       | Position of the tip and root versus $\sqrt{t}/L$ , Al-4.5% Cu alloy, $h_B L/\bar{K} = \infty$ , $\Delta T_s = 150^\circ\text{C}$ , for four values of parabolic side heat loss, $aL/W$ | 89                     |
| 34                       | Local solidification time versus distance for conditions of Figure 33  | 90                     |
| 35                       | Position of the tip and root versus $\sqrt{t}/L$ , Al-4.5% Cu alloy, $h_B L/\bar{K} = 0$ , no convection, $aL/W = 136$ , for four values of superheat                                  | 91                     |

| <u>Figure<br/>Number</u> |  | <u>Page<br/>Number</u> |
|--------------------------|--|------------------------|
| 36                       | Local solidification time versus distance, for conditions of Figure 35   | 92                     |
| 37                       | Local solidification time at $\lambda = 0.25$ versus $\Delta T_s$ , $h_B L / \bar{K} = \infty$ , for four values of $aL/W$   | 93                     |
| 38                       | Position of the tip and root versus $\sqrt{t}/L$ , Al-4.5% Cu alloy, high convection, equi-axed growth morphology, $h_B L / \bar{K} = \infty$ , no superheat for three values of critical fraction solid | 94                     |
| 39                       | Local solidification time versus distance for conditions of Figure 38  | 95                     |
| 40a                      | Fraction liquid versus reduced time at $\lambda = 0.5$ , comparing radial and unidirectional heat flow   | 120                    |
| 40b                      | Dimensionless temperature versus reduced time for conditions of Figure 40a   | 121                    |
| 41a                      | Fraction liquid versus reduced time at $\lambda = 0.5$ , comparing unidirectional growth with no convection to equi-axed growth with high convection   | 122                    |
| 41b                      | Dimensionless temperature versus reduced time for conditions of Figure 41a   | 123                    |
| 42a                      | Fraction liquid versus reduced time at $\lambda = 0.5$ , comparing unidirectional heat flow with sidewise heat loss  | 124                    |
| 42b                      | Dimensionless temperature versus reduced time for conditions of Figure 42a   | 125                    |
| 43                       | Fraction liquid versus reduced time for conditions of Figure 40, with Scheil distribution of fraction liquid versus temperature used for the mushy region  | 126                    |

| <u>Figure<br/>Number</u> |  | <u>Page<br/>Number</u> |
|--------------------------|--|------------------------|
| 44                       | Fraction liquid versus reduced time for conditions of Figure 41, with Scheil distribution of fraction liquid versus temperature used for the mushy region  | 127                    |
| 45                       | Fraction liquid versus reduced time, for conditions of Figure 42, with Scheil distribution of fraction liquid versus temperature used for the mushy region | 128                    |
| 46                       | Local solidification time versus distance from the chill, 12" end chilled plate casting, 6" wide, 1.57" thick, insulated mold ( $a = 0$ )                  | 129                    |
| 47                       | Local solidification time versus distance for casting of Figure 46 in a sand mold ( $a = 8.9$ )  | 130                    |
| 48                       | Local solidification time versus distance for casting of Figure 46 in a plaster mold ( $a = 4.95$ )  | 131                    |
| 49                       | Local solidification time versus distance for casting of Figure 46 in a foamed plaster mold ( $a = 1.57$ )   | 132                    |
| 50                       | Width of the mushy zone versus position of the root for conditions of Figure 46  | 133                    |
| 51                       | Width of the mushy zone versus position of the root for conditions of Figure 47  | 134                    |
| 52                       | Width of the mushy zone versus position of the root for conditions of Figure 48  | 135                    |
| 53                       | Width of the mushy zone versus position of the root for conditions of Figure 49  | 136                    |
| 54                       | Schematic representation of solidification of a plate casting  | 220                    |



## LIST OF TABLES

| <u>Table<br/>Number</u> |  | <u>Page<br/>Number</u> |
|-------------------------|--|------------------------|
| I                       | Definition of Symbols  | 20                     |
| II                      | Simulated Results for Laboratory end<br>Chilled Casting  | 110                    |
| III                     | Computer Output, Unidirectional Heat<br>Flow, for Several Simulation Parameters                  | 197                    |
| IV                      | Sensitivity of the Results to Changes<br>in Time Step and Mesh Size, Unidirectional<br>Heat Flow | 204                    |
| V                       | Computer Output, Side Heat Loss, for<br>Several Simulation Parameters                            | 205                    |
| VI                      | Sensitivity of the Results to Changes<br>in Time Step and Mesh Size, Side Heat<br>Loss           | 212                    |

## ACKNOWLEDGEMENTS

The author would like to thank Professor Merton C. Flemings for his guidance and encouragement throughout the course of this research, which was invaluable. I also wish to thank Professor Flemings for his understanding and concern which he has shown during both my undergraduate and graduate school careers.

I wish to thank also the following people for their help during the course of my work; Mr. Anthony J. Zona, Mr. James Stack, and Mr. John McCarthy.

Lastly, I thank my wife Sharon, for patience and encouragement, and my children Carol and Matthew for understanding as much as they are able.

## Chapter I

### INTRODUCTION

The important influence of dendrite arm spacing on mechanical properties of cast aluminum alloys, and of wrought material produced from cast ingots, is now well documented. (1,2) Also well documented is the experimental observation that the major factor influencing dendrite arm spacing of a given alloy is "local cooling rate" (or "local solidification time") which is inversely proportional to local cooling rate. (3-5)

Thus, it has been evident that a method, and perhaps the only method, of significantly reducing dendrite arm spacing in cast ingots is to alter heat flow conditions within the solidifying ingot. Much attention has therefore been given recently in applied studies to do this; all of these studies have been aimed at seeking ways to accelerate rate of heat extraction, thereby increasing local cooling rate and reducing dendrite arm spacing.

In this work, the aim is to study analytically heat flow in a solidifying "mushy" alloy. The major aim, following successful computer modelling of the heat flow problem, is to determine if there are ways, other than by increasing rate of heat extraction, of increasing local cooling rate, and therefore reducing dendrite arm spacing. This and other questions to be studied in this work are listed below:

- (1) What is the effect of convection on local solidification time?
- (2) What is the effect on local solidification time of addition of heat to the liquid or liquid-plus-solid zone of a solidifying ingot?
- (3) Will the grain structure of an ingot appreciably affect heat flow, including local solidification time?
- (4) In addition to increasing overall rate of heat extraction, are there practical ways to control heat flow in ingot solidification to reduce local solidification time?
- (5) What is the effect of geometry? Specifically, how does the local solidification time at specific points in an ingot change as heat is removed in more than one dimension, as in cylindrical ingots or those in which heat is lost through the side of the ingot as well as the bottom or chill.
- (6) How important is the heat transfer rate at the surface of an ingot to the local solidification time at points within the ingot.

The problem of solving heat flow equations when melting or solidification takes place is not a new one. Classically, the one dimensional problem of solidification of a pure material is known as the Stefan problem; and analytic solutions have been given for several important

cases. (6-9) Several approximate analytic solutions have been presented for the case of binary alloys, (10-12) and these will be discussed in a later section. Two extensive reviews of past work on the general problem of heat flow in solidification have appeared, (13-14) and an excellent review of Ruddle describes much experimental and analytical work prior to 1950. (29)

Finite difference methods have been used in solution of a wide variety of solidification problems, including solidification of alloys and of complex shapes. Examples are work of Mizikar, (15) Pehlke, (16) Kroeger (27), Campagna and Eisen, (17) and Adenis. (18) In all cases, these works have not employed "moving boundaries" as will be used in this work. Instead, heat of solidification has been approximately accounted for by treating it as an effective addition to specific heat. Heat released abruptly (as by a pure metal at its melting point or at the eutectic isotherm in an alloy solidifying with a eutectic) cannot be treated directly. The studies referred to above have assumed this heat was released over a small but finite temperature region.

In this work, the finite difference method was employed, but with moving boundaries, so finite heat release at discrete temperatures (e.g., at eutectic isotherms) can be treated. The following sections discuss:

- (1) the general mathematical statement of the problem of unidirectional solidification of binary alloys, in which the last liquid to freeze is of eutectic composition,
- (2) the solidification model employed for calculations,
- (3) methods employed previously in solution of similar problems, and
- (4) the numerical procedure employed for solution of the problem.

### Mathematical Statement of the Problem

#### A. Unidirectional Heat Flow

We consider here heat flow in unidirectional solidification of an alloy cast against a flat chill wall. The equation for heat flow through the metal ingot during solidification is then:

$$(\rho C_p) \frac{\partial T}{\partial t} = \frac{\partial}{\partial x} (\bar{K} \cdot \frac{\partial T}{\partial x}) + (\rho H) \frac{\partial f_s}{\partial t} \quad (1)$$

where:

- T = temperature, °C
- ρ = density (gms/cc)
- C<sub>p</sub> = local average heat capacity (cal/gms/cc)
- $\bar{K}$  = local average thermal conductivity (cal/cm<sup>2</sup>sec)
- t = time, sec
- x = distance, cm

$H$  = heat of fusion (cal/gm)

$f_s$  = fraction solid (weight or volume)

The underlying assumptions in use of Equation (1) are:

- (1) Isotherms are parallel to the chill wall and gradients perpendicular to the heat flow direction are small.
- (2) There are no discontinuities in temperature in the region to which Equation (1) applies. Therefore, the three regions of the casting (solid, mushy, and liquid) will require separate solutions, coupled by the boundary conditions at the interfaces (dendrite tip and root).

Taking  $x = 0$  at the chill face, the following boundary conditions apply:

$$q|_{x=0} = F_1(t) \quad t > 0 \quad (2)$$

$$q|_{x=L} = F_2(t) \quad t > 0 \quad (3)$$

where:

$L$  = length of casting (cm)

$F_1(t), F_2(t)$  = specified functions.

For liquid poured rapidly in the mold at uniform temperature,  $T$ , initial temperature of the melt is uniform:

$$T = T_0(\text{constant}) \quad t = 0 \quad (4)$$

$$0 \leq x \leq L$$

After some time,  $t$ :

$$T = T_E \quad t > 0 \quad (4a)$$

$$x = x_E$$

$$T = T_L \quad t > 0 \quad (4b)$$

$$x = x_t$$

On cooling below the liquidus temperature, solidification begins, and thermal properties in the liquid-solid "mushy zone" are specified functions of fraction solid and, therefore, of temperature:

$$\bar{K} = F_3(T); \quad C_p = F_4(T); \quad \rho = F_5(T); \quad \text{for } T < T < T_L \quad (5)$$

Assuming no significant undercooling at the dendrite tips (of an alloy such as Al-4.5% Cu alloy that freezes over a range of temperature) the solidification "front" is at the eutectic isotherm and there is no discontinuity in fraction solid at the liquidus temperature. Fraction solid is infinitesimally small at the liquidus temperature and increases smoothly with decreasing temperature. The boundary condition across the isotherm marks the boundary between the liquid-solid region, and the liquid region is then:

$$\bar{K}_m \left( \frac{dT}{dx} \right)_{x_t - \epsilon} = K_L \left( \frac{dT}{dx} \right)_{x_t + \epsilon} \quad (6a)$$

where:

$\bar{K}_m$  and  $K_L$  are the thermal conductivities of the



mushy and liquid zone, respectively, and  $\epsilon$  is a differential distance on the  $x$  axis.  $x_t$  is the location of the dendrite tips, in this case equal to the location of the liquidus isotherm,  $x_L$ .

If, however, there is significant undercooling at the solidification front, and if this undercooling is dissipated very close behind the front, then a finite amount of solid forms very near  $x_t$ ; and the boundary condition becomes:

$$\bar{K}_m \left( \frac{dT}{dx} \right)_{x_t - \epsilon} = K_L \left( \frac{dT}{dx} \right)_{x_t + \epsilon} + H \cdot \rho_\ell f_t \frac{dx_t}{dt} \quad (6b)$$

where:

$f_t$  = fraction solid forming discretely at the dendrite tips (weight or volume)

Again for an alloy such as Al-4.5% Cu, a finite amount of solid forms at the location of the eutectic isotherm,  $x_E$  and the boundary condition at this end of the liquid-solid region is

$$\bar{K}_s \left( \frac{dT}{dx} \right)_{x_E - \epsilon} = \bar{K}_m \left( \frac{dT}{dx} \right)_{x_E + \epsilon} + H \cdot f_E \rho_E \frac{dx_E}{dt} \quad (7)$$

where:

$f_E$  is fraction eutectic (weight or volume) which forms at  $x_E$ .

### B. Radial Heat Flow

Consider the case of a solidifying ingot whose shape is cylindrical, with radius  $R$  and of arbitrarily long length.

The heat flow equation equivalent to Equation (1) becomes:

$$(\rho C_p) \frac{\partial T}{\partial t} = \frac{1}{r} \frac{\partial}{\partial r} (\bar{K} \cdot r \cdot \frac{\partial T}{\partial r}) + H \rho_\ell \frac{\partial f_s}{\partial t} \quad (1R)$$

All initial and boundary conditions (Equations 2-7) apply, where the position  $x$  now refers to position  $R-r$ .

### C. Sidewise Heat Loss

Consider an ingot of length  $L$ , with heat flowing through a chill in the  $x$  direction, and of width  $2W$ , in the  $y$  direction. If heat flows across the boundaries in the  $x$ - $y$  planes at  $y = W$  and at  $y = -W$  and we assume this heat loss takes place slowly enough that there are no temperature gradients in the  $y$  direction (refer to Appendix F), then Equation (1) becomes:

$$(\rho C_p) \frac{\partial T}{\partial t} = \frac{\partial}{\partial x} (\bar{K} \frac{\partial T}{\partial x}) + H \rho_\ell \frac{\partial f_s}{\partial x} + q_x \quad (1S)$$

All initial and boundary conditions (Equations 2-7) still apply, with the additional conditions;

$$q_x = h(T_A - T) \quad 0 \leq x \leq L$$

$$\text{at } y = W, y = -W, \quad t > 0 \quad (1S,a)$$

If heat loss at the side boundary takes place by radiation and/or convection, the above condition may be suitable. For the case of a chill and plate casting, made in sand, a more appropriate "boundary condition" for heat loss to the sand would be:

$$q_x = a/(t)^{1/2} \quad 0 \leq x \leq L \quad (1S,b)$$

at  $y = W, y = -W, t > 0$

where  $a = -(T_m - T_o) \cdot (\bar{K}_{sand} \rho_{sand} C_p(sand) / \pi)^{1/2}$

The two conditions (1Sa) and (1Sb) are not only boundary conditions, they are also additive terms in the heat flow Equation (1S).

The functions  $F_1$  and  $F_2$  above are external boundary conditions, to be specified as part of the problem. The functions  $F_3$  to  $F_4$ ,  $f_{st}$  and  $f_E$  are based on a specific model of the solidification process, given in the following section and based on solidification studies at Massachusetts Institute of Technology over the last several years. (3,19,20)

#### Solidification Model

Alloy solidification is characterized by the presence of a region of finite thickness within the casting in which solidification takes place. This mushy region is delineated by two isothermal boundaries, the solidification "front" (at or near the liquidus temperature) and non-equilibrium solidus (at the eutectic temperature in binary alloys which contain some eutectic in the final solidified structure). It is this liquid-solid\* region which separates the problem of

---

\* In this thesis, these boundaries are hereafter referred to as the dendrite "tips" and "roots" respectively. It is important to recognize, however, that in most cases, a single dendrite does not extend across the entire "mushy zone". In equiaxed growth in particular, many randomly oriented dendrites fill this space. Figure 5 is an example. The terms dendrite "tips" employed herein, or "solidification front" is equivalent to the term "start of freezing isotherm" used by other investigators. (29) The term dendrite "roots" or "non-equilibrium solidus" is equivalent to the term "end of freeze isotherm" used by other investigators. (29)

alloy solidification from that of pure materials. For alloys, the characteristics of the mushy region which must be taken into account in the heat flow analysis are:

- (1) The boundary conditions at the tip and root, Equations (6a) or (6b) and (7) above.
- (2) The distribution of solid and liquid through the length of the zone, ( $f_s$  versus  $x$ ) and the amount of liquid which solidifies isothermally (eutectic),  $f_E$ , at the roots. The distribution  $f_s$  versus  $x$  or  $f_s$  versus  $T$  (since  $T$  versus  $x$  will be available) is referred to as  $F_6(T)$ .
- (3) Taking the distribution  $f_s$  versus  $x$  into account, the distribution of  $\bar{K}$ ,  $\rho$ , and  $C_p$  must be specified as functions of  $f_s$  (or  $f_L$ ). These distributions are referred to as  $F_3(x)$ ,  $F_4(x)$ ,  $F_5(x)$  above.

The solidification model presented below is based on physical arguments concerning the nature of the mushy region, and much of this has been presented elsewhere. (19,20)

For the case of no diffusion of solute in the solid (and other assumptions as previously stated), the Scheil Equation applies. (20) The solution of this equation, for constant partition ratio is:

$$C_L = C_O (1 - f_s)^{k-1} \quad (8)$$

or,

$$f_s = 1 - \left(\frac{C_L}{C_0}\right)^{1/k-1} \quad (9)$$

where:

$C_0$  = starting alloy composition

$f_s$  = fraction solid

$k$  = equilibrium partition ratio,  $C_s/C_L$

$C_L$  = interdendritic liquid composition in the region of  $f_s$  fraction solid

Fraction eutectic,  $f_e$ , is readily determined by letting  $C_s = kC_E$  where  $C_E$  is eutectic composition. It is, for example, .09 for Al-4.5% Cu alloy, assuming constant  $k$ . This value of  $f_e$  will be used in Equation (7).

A distribution of  $f_s$  (or  $f_L$ ) versus  $T$  is readily obtained by combining Equation (9) with the equation describing the liquidus line of the binary alloy. For constant liquidus slope,  $m$ :

$$m = \frac{C_L - C_0}{T - T_L} \quad (10)$$

The resulting distribution is termed the Scheil distribution and is shown in Figure 1a for Al-4.5% Cu alloy. Al-rich end of the Al-Cu binary diagram is shown in Figure 2. Alternate distributions which have been explored for simplicity in previous work on macrosegregation are a linear distribution of solid with finite eutectic (Figure 1b), and linear distribution of solid, neglecting eutectic (Figure 1c).

In this work, we will assume finite undercooling at the dendrite tips so that boundary condition Equation (6b) applies. Then, assuming further linear distribution of fraction solid in the mushy zone, the model for  $f_s$  vs  $T$  is schematically as in Figure 3, and is described by:

$$f_L = f_E + (1-f_t - f_E) \frac{T - T_E}{T_t - T_E} \quad (11)$$

The densities of the solid and liquid phase are assumed herein independent of temperature and composition, and so, average density in the mushy zone is a linear function of fraction solid:

$$\rho_m = \rho_s f_s + \rho_L f_L \quad (12)$$

Similarly, heat capacity is assumed to be a linear function of fraction solid in the mushy zone:

$$C_{pm} = C_{ps} f_s + C_{pL} f_L \quad (13)$$

where:

$C_{pm}$  is local average heat capacity in the mushy zone;  $C_{ps}$  and  $C_{pL}$  are heat capacities of the solid and liquid phase respectively, and  $f_s, f_L$  = volume or weight fraction of each phase. It should be noted that for an Al-4.5% Cu alloy, the error introduced in Equation (12) by assuming weight fraction equals volume fraction is less than 0.03%.

The final distribution to be developed, that of thermal conductivity versus  $T$  or  $x$ , cannot be expressed without taking dendrite morphology into account. For this investigation, two extreme cases of heat flow through multiphase media will be considered. The model for the mushy region is assumed to be parallel plates of alternating phase (Figure 4). If heat flow takes place parallel to these plates (columnar dendritic growth), the conductivity of the composite is: (21)

$$\bar{K}_m = (f_s K_s + f_L K_L) \quad (14)$$

If heat flow takes place perpendicularly to the plates (which would correspond to an exaggerated model of equi-axed growth), then the expression for the total conductivity is: (21)

$$\bar{K}_m = \frac{K_L K_S}{f_s K_L + f_L K_S} \quad (15)$$

Since equi-axed morphology in reality can be pictured as in Figure 5, the total conductivity should lie between Equations (14) and (15).

#### Solution of the Problem

It is appropriate to the following discussion of solutions to the problem stated above to point out that it is the terms on the right hand of (6b) and (7) that separates this problem of solidification from other heat flow problems. It is the way in which these terms are taken into account

that separates the various methods of solution to the problem.

The presence of the free internal boundaries, represented by Equations (6) and (7), has given rise to the name "Free boundary problem" in connection with a class of problems which contain boundary conditions whose position is a function of the conditions around them.

Many analytic solutions (referenced below) have been presented for various cases, but there is one common fact which is used to take the motion of the solid front into account. This is the use of the Boltzman similarity variable,  $x/(\alpha t)^{1/2}$ . Danckwerts(8) presents some interesting extensions to these exact solutions, but the basic method depends on the existence of the similarity variable. Adams(10) has presented a derivation based on this method for the case of a binary alloy freezing, which involves two free boundaries.

The methods of Boley,(9) Koump et al.,(11) and Hills(12) do not depend on the existence of the similarity variable; however, each involves approximations concerning the shape of the temperature curve in either the liquid or the solid, and thus constrains the velocity of the interface to be a function of surface conditions. This allows an integral to be developed, in Boley's method, which is then solved numerically; in Koump's method, an equation is derived which is solved for the position of the root and tips



of the dendrites, but temperature profiles cannot be found. In both these methods, approximations are made which make the solutions less meaningful to use as a tool for investigating large ranges of external conditions.

Hills uses an integral profile technique to obtain an approximate analytic solution, as do Boley and Koump. The equations are derived for the case of a pure material (12) and compared to experimental results (22) with very good agreement. In addition, the derivation of this equation is performed such that the extension of the method to mushy freezing alloys is straightforward, with the major assumptions being:

- (1) the temperature profiles in the solid, mushy and liquid regions are chosen by parabolic fitting to the boundary conditions;
- (2) the cooling rate across each of the three regions is assumed to vary linearly with distance; that no sharp thermal perturbations occur in these regions;
- (3) the assumed solidification model in the mushy region is generally similar (although not identical) to the one presented above.

In work yet to be published, Hills has indicated that the agreement between predicted results with this integral profile method compare well with experimental results of solidification studies done with lead-tin and lead-antimony alloys which were solidified with moderately

slow surface cooling.

The integral profile technique as presented by Hills is an accurate and efficient method of solution for the boundary conditions he employs. However, the numerical method will be used here because of its flexibility in dealing with, for example, different variations in fraction solid with temperature, variations of thermal properties with temperature, or very high value of interface heat transfer coefficient,  $h$ .

In order to avoid the need to use the similarity variable, and also to facilitate if not improve the accuracy of the solution, a numerical approach was considered. The only solutions presented which have been obtained through numerical means have been for the case of a pure materials. (23,24) It should be possible, however, to extend the methods presented from one free boundary to two. The method of Murray and Landis (23) is presented here.

Instead of assuming a velocity of the interface which is proportional to  $x/(\alpha t)^{1/2}$ , as was done for the analytic solution, Equations (6a) and (7) can be solved numerically at each time step of a numerical integration of the heat flow equation, Equation (1). This is the basis of the method which was used in this research, and the details will be presented later with the rest of the numerical integration description.

It should be noted that the need to consider the dendrite tips as a free internal boundary comes from the physical consideration of the fact that the liquid in front of the tips may have an apparent thermal conductivity which is higher than the interdendritic liquid, due to convection in the liquid melt, and from the consideration of the small but finite undercooling at the tips necessary for growth. It is for these reasons that the liquidus temperature position must be considered a boundary, Equation (6b). In other words, there is a discontinuity in  $C_p$  versus  $x$  at the tips. The apparent discontinuity in  $\bar{K}$  results from thermal convection. Vigorous convection is present in large ingots, (25) and this convection results in a high apparent thermal conductivity; however, this convection is very low at the dendrite tips and within the mushy zone.

### Numerical Procedure

A detailed account of the method used to solve Equation (1) with initial conditions and boundary conditions (2), (3), and (4) is given in the Appendix. It is described briefly below.

A finite difference equation is substituted for Equation (1), and the temperature at a given increment in time is calculated for the temperature distribution at the preceding time interval. The boundary conditions are satisfied by including them in the finite difference equation set, and the internal free boundary conditions are satisfied

by resetting the temperatures in their neighborhood at each time step. The functions F1 and F2 are read in and used directly as driving functions for the surface and center of the simulated casting. Various other parameters, such as mode of growth (Equations 13 or 14) and amount of convection (liquid thermal conductivity), are also read in, thus giving the program the capability to simulate a wide range of solidification problems.

Beside the two free boundaries which this numerical method takes into account, there is another feature of it which is worth pointing out. Most finite difference schemes which are derived from a parabolic differential equation, such as the heat flow equation, result in a set of equations (linear) which must be solved at each time step. The usual method of solution is a straight-forward substitution of the old temperatures (at time,  $t$ ) to obtain the new temperatures (at time,  $t + \Delta t$ ). This is known as an explicit technique, and it is known to place severe restrictions on the size of the time step which may be used in the calculations. If the critical time step is exceeded, the solution becomes unstable, that is, the temperatures start to oscillate in an uncontrolled fashion. Thus, many numerical solutions become unfeasible in terms of computer time because of the time step restrictions. In order to prevent this, an implicit solution technique was used, which was presented by, and is given the name, Crank-Nicholson (technique). The details of this method are presented in Appendix A, but the

theory behind the method is that the temperature at time  $t + \Delta t$  is used (as well as the temperature at time,  $t$ ) to calculate the temperature at time  $t + \Delta t$ . This means the solution to each difference equation is implicit in its formulation, thus, the name "implicit technique." As indicated above, this method was adopted in order to reduce the computer time necessary to obtain a solution, at a corresponding loss in accuracy. Estimates of the error involved (presented in the Appendix) showed that the accuracy of the Crank-Nicholson method is quite sufficient (temperature to four places), which implies that the accuracy of explicit techniques is far too great to justify their use in this type of heat flow calculation.

Table I. Definition of Symbols

|                                |  |
|--------------------------------|--|
| $a$                            | constant for parabolic side heat loss,<br>cal/cm <sup>2</sup> /sec <sup>1/2</sup>  |
| $A_{\text{heat}}$              | constant for parabolic heat input, cal/cm <sup>2</sup> /sec  |
| $C_{\text{pm}}$                | local average heat capacity in liquid-solid<br>region, cal/gm°C  |
| $C_{\text{pL}}, C_{\text{ps}}$ | $C_p$ for liquid solid respectively  |
| $C_o, C_L$                     | liquid metal compositions, wt percent, original<br>and local, respectively   |
| $f_L, f_s$                     | weight or volume fractions liquid and solid,<br>respectively   |
| $f_{\text{sc}}$                | weight or volume fractions solid at the critical<br>position at which convection stops                                     |
| $f_t, f_E$                     | weight or volume fractions solid at the tip or<br>root, respectively   |
| $H$                            | heat of fusion, cal/gm   |
| $h_B$                          | heat transfer coefficient at mold-metal interface<br>in the x-direction, cal/cm <sup>2</sup> sec°C                         |
| $h_s$                          | heat transfer coefficient at mold-metal interface<br>in the y-direction (sidewise heat flow),<br>cal/cm <sup>2</sup> sec°C |
| $\bar{K}$                      | local average thermal conductivity, cal/cm.sec°C   |
| $K_L, \bar{K}_m, K_S$          | $\bar{K}$ for liquid, mushy, or solid region   |
| $k$                            | equilibrium partition ratio  |
| $L$                            | length in the x direction, cm  |
| $q$                            | heat input, as boundary condition, cal/cm <sup>2</sup> /sec  |
| $q'$                           | dimensionless heat   |
| $R$                            | radius, cm   |
| $r$                            | radial distance from center of a cylinder, cm  |
| $r_t, r_E$                     | radial position of the tip or root, respectively   |

Table I , continued

|                              |   |
|------------------------------|---|
| $t$                          | time, (sec)   |
| $t_f$                        | time at finish of solidification (sec)                                    |
| $t_o$                        | time at start of solidification (sec)                                     |
| $t_{Lst}$ or $t_{lst}$       | local solidification time (sec)   |
| $T$                          | temperature, $^{\circ}\text{C}$   |
| $T_m$                        | melting temperature (liquidus), $^{\circ}\text{C}$                        |
| $T_E$                        | solidus or eutectic temperature, $^{\circ}\text{C}$                       |
| $T_p$                        | pouring temperature of a melt, $^{\circ}\text{C}$                         |
| $T_o$                        | starting temperature, $^{\circ}\text{C}$                                  |
| $T_a$                        | ambient temperature (x-direction), $^{\circ}\text{C}$                     |
| $T_{a,s}$                    | ambient temperature, side (y-direction), $^{\circ}\text{C}$               |
| $W$ or $w$                   | width, in y-direction, cm   |
| $x$                          | distance from the chill, cm   |
| $x_s$ or $x_E$               | position of the solidus or eutectic, cm                                   |
| $x_t$                        | position of the tip, cm   |
| $\alpha$                     | thermal diffusivity, $(\bar{K}/\rho C_p)$ , $\text{cm}^2/\text{sec}$      |
| $\alpha_s, \alpha_L$         | solid or liquid thermal diffusivity, respectively                         |
| $\beta$                      | dimensionless constant, appearing in the analytic solution, Equation (R1) |
| $\epsilon$                   | differential distance, cm   |
| $\lambda$                    | dimensionless distance from the chill                                     |
| $\tau_{Lst}$ or $\tau_{lst}$ | local solidification time/ $L^2$ , $\text{sec}/\text{cm}^2$               |
| $\rho$                       | density, $\text{gms}/\text{cm}^3$   |
| $\rho_L, \rho_m, \rho_s$     | liquid, mushy, and solid densities, respectively                          |
| $\Delta T_s$                 | superheat, $T_p - T_m$ , $^{\circ}\text{C}$                               |

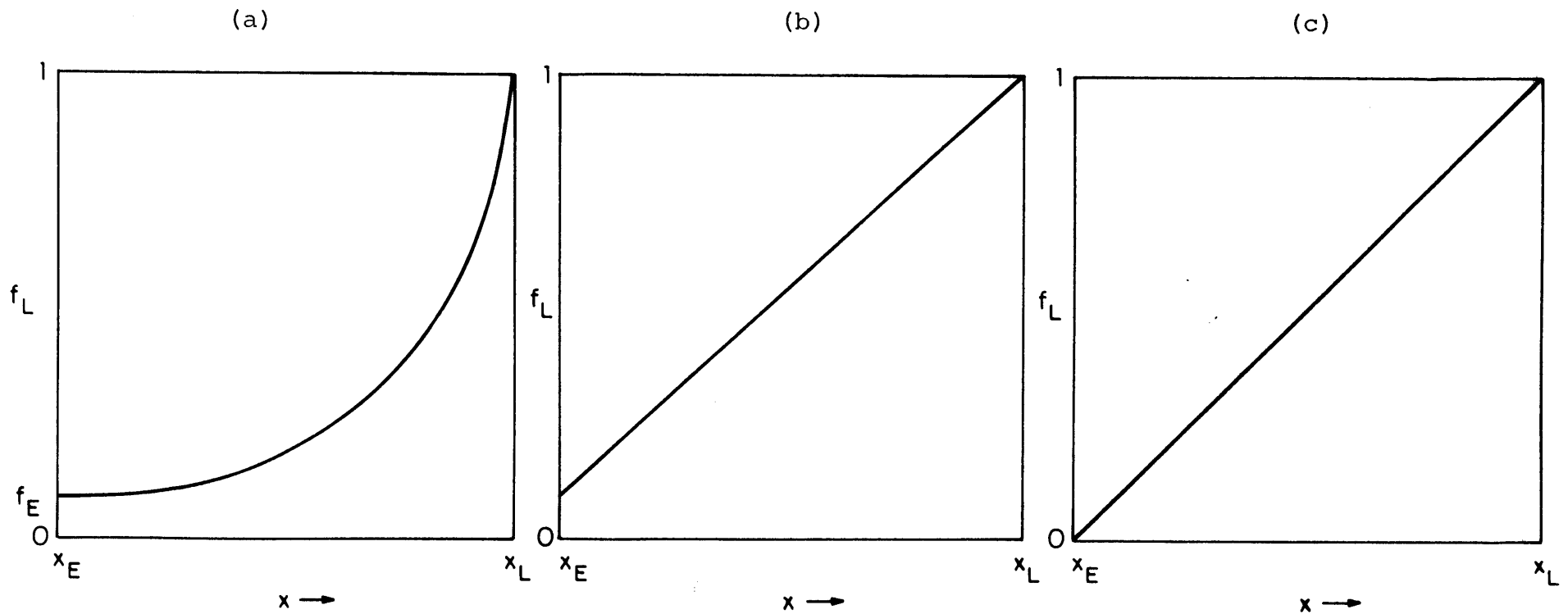


Figure 1. Approximations of distribution of liquid in the mushy zone. (a) Steady state solute redistribution, Scheil equation. (b) Linear  $f_L$  vs.  $X$ , finite eutectic. (c) Linear  $f_L$  vs.  $X$ , no eutectic.



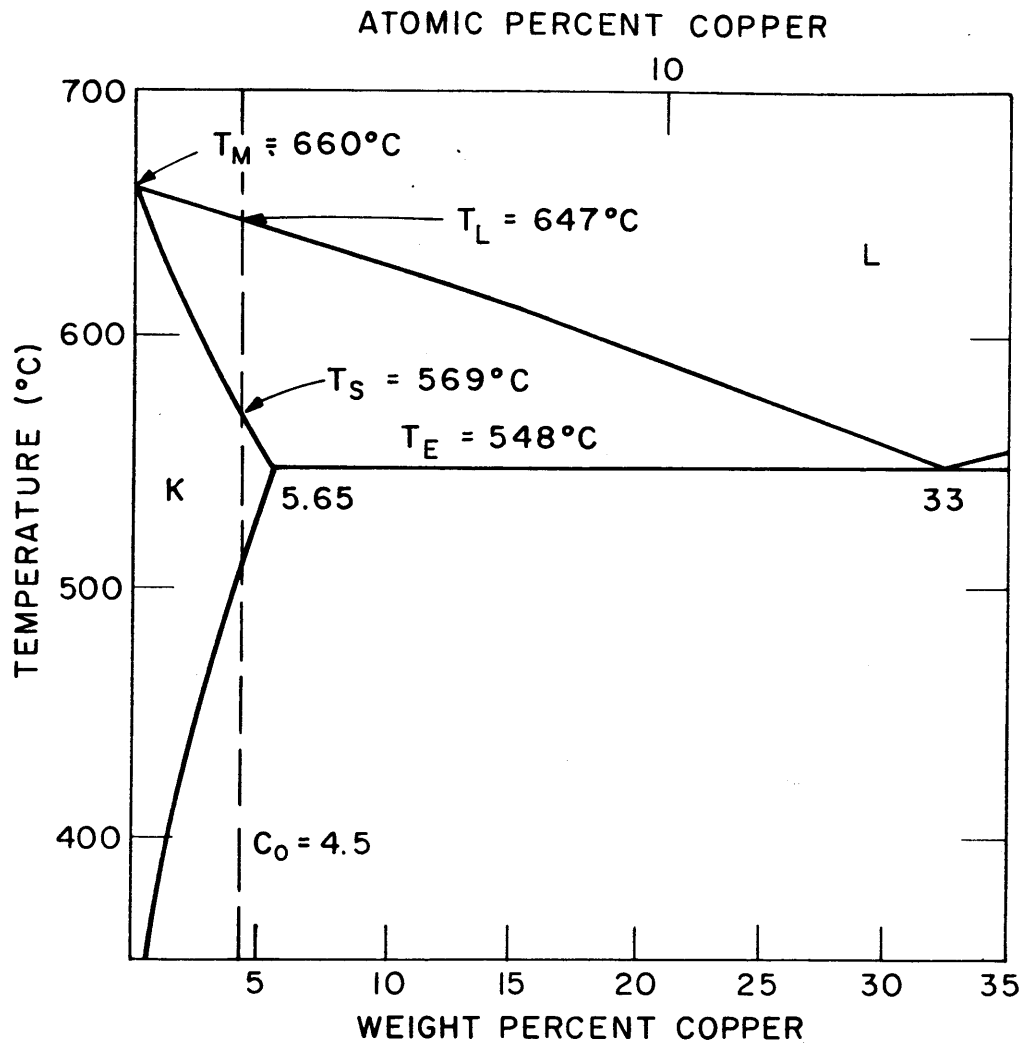


Figure 2. Aluminum rich portion of aluminum-copper phase diagram.

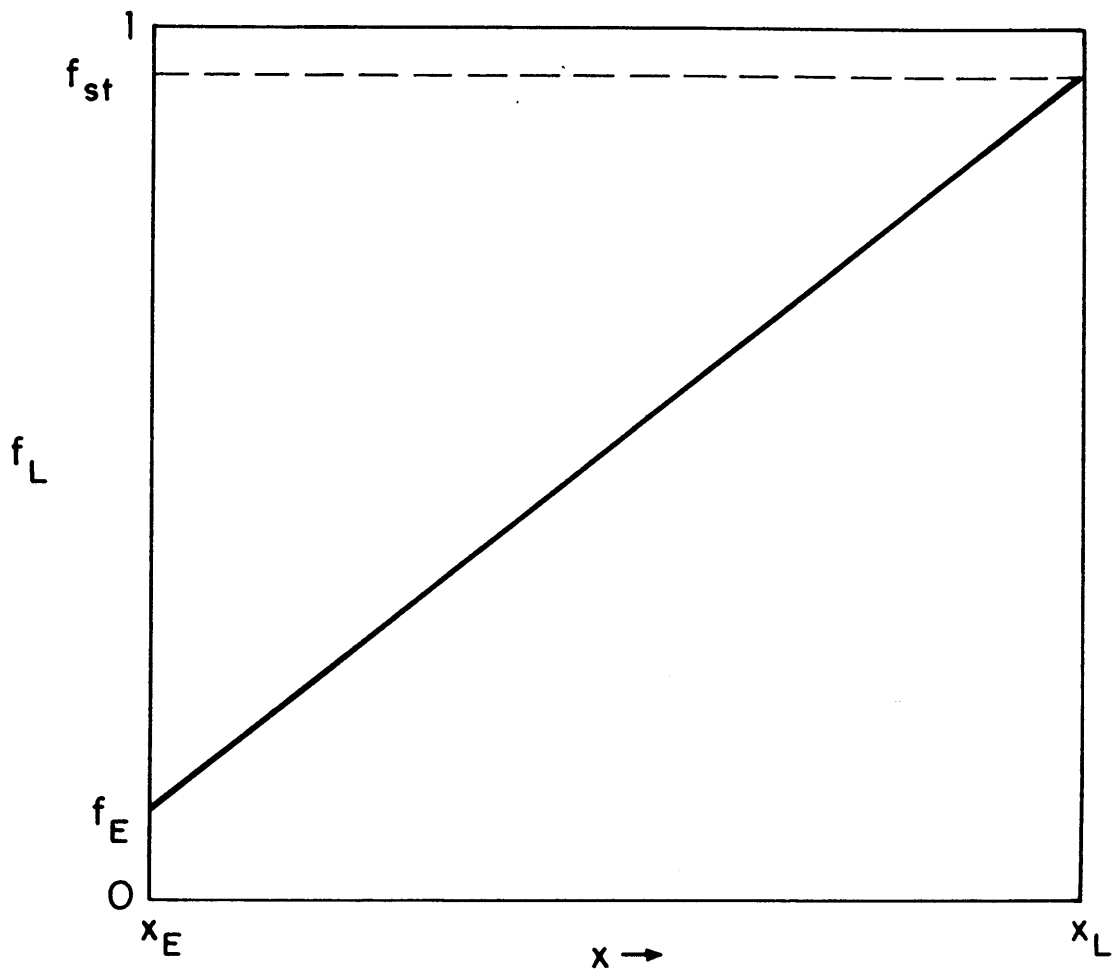


Figure 3. Linear distribution of  $f_L$  vs.  $X$ , with finite eutectic and undercooling.

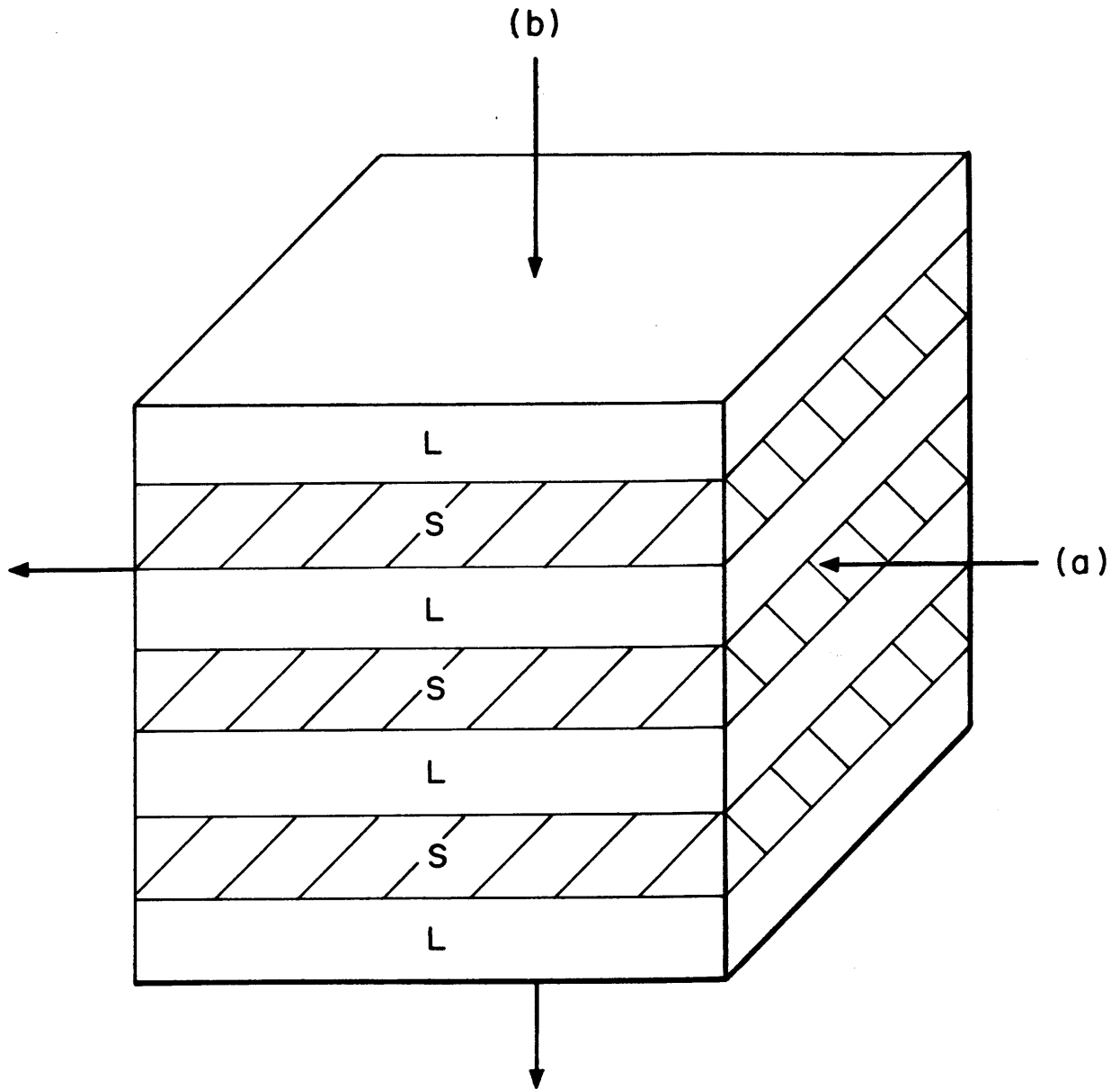


Figure 4. Parallel plates of solid and liquid, representing simplified view of parallel or series heat flow. (a) Parallel. (b) Series.

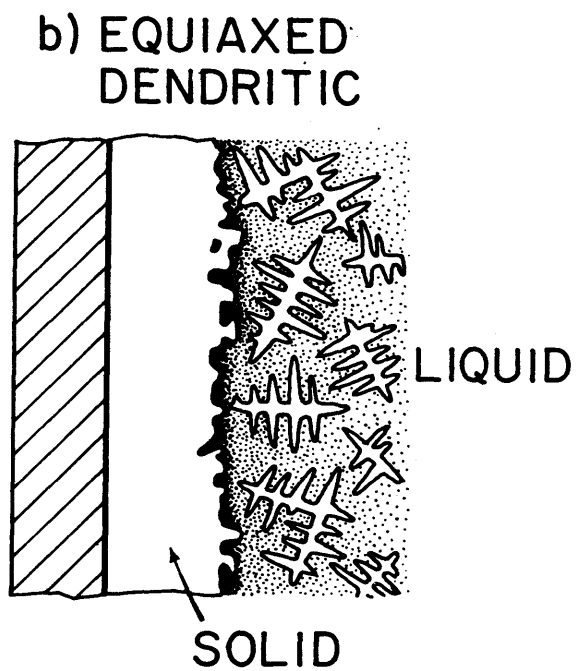


Figure 5. Equiaxed growth, schematic representation of mushy region cut along length.

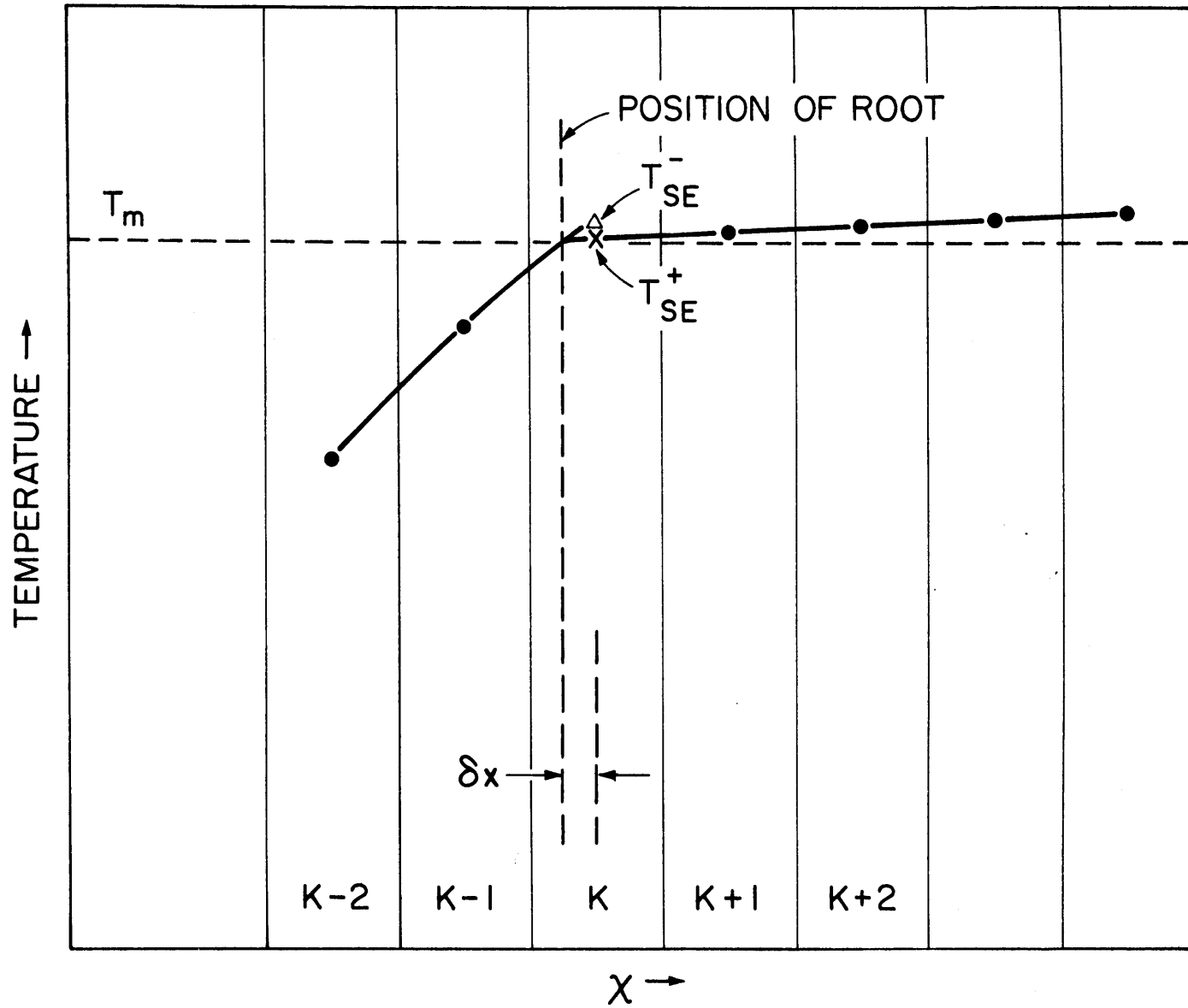


Figure 6. Description of parameters in finite difference procedure.

## Chapter II

### RESULTS

This section is organized in the following manner;

(A) Dimensional analysis; pertinent dimensionless numbers to be used to simplify the presentation of the results.

(B) Analytical correlation; a comparison of the results of the program for conditions of solidification of a pure material for which there is an analytic solution.

(C) Pure material, aluminum; the effect of  $h$  coefficient and superheat on the solidification behavior of pure aluminum.

(D) Unidirectional solidification of an alloy; results for various fraction solid at the tip, for columnar and equiaxed cases.

(E) Unidirectional solidification of an alloy; results for various surface cooling rates and superheats.

(F) Radial solidification of an alloy; results for various surface cooling rates and superheats.

(G) Heat input with convection; results for various parabolic heat inputs to a highly convecting melt.

(H) Side heat loss, without heat; results for various side cooling rates and superheats.

(I) Side heat loss, with heat input and convection; results for various parabolic heat inputs at two values of side heat loss.

(J) Side heat loss to a sand mold; results for parabolic heat loss, similar that in a sand mold.

(K) Equi-axed growth with high convection; results for a convecting melt in which equi-axed grains are carried into the melt ahead of the mushy region.

A. Dimensional Analysis

The problem of organizing the study of many engineering problems is often simplified through the use of dimensional analysis. In a case such as this one, a large number of independent and dependent variables appear in the equations, and the task of measuring and presenting the results (independent variables) as a function of all the dependent variables would be tedious if not impossible. Dimensional analysis provides a method of revealing the relationships between the variables, with dimensionless groups, which reduces the number of parameters which must be studied and also provides insight into the nature of the process. Such an analysis was made on this problem of heat flow during solidification and the results are presented in Appendix C.

The variables of major interest in this study are (1) the position of the tip and root as a function of time (or position in the ingot), and (2) the local solidification time as a function of position in the ingot. The dimensionless form of these variables is:

$\lambda$  dimensionless position;

$\alpha t_f / L^2$  dimensionless local solidification time.

The independent variables of major interest are:

$\alpha t / L^2$  dimensionless time;

$hL/K$  Biot number (dimensionless thermal conductance ratio);

$\frac{Q\sqrt{t}\sqrt{\alpha}}{LK(T_m - T_s)}$  dimensionless heat input, parabolic.

Since the dimensional analysis included the thermal properties of the material, these properties appear in many of the dimensionless groups. For many studies this form would be desirable, since a change of materials would then be easily accounted for. For this study, however, it is more desirable that the reader have a more direct measure of the values of the variables used, and since the study was undertaken only for one alloy composition, that of Al-4.5% Cu, much of the results will be presented in a modified form, that is, the dimensionless group has been stripped of the material property, with the understanding that this simply affects the numerical value of the dimensionless group, without affecting the functional relationships between the groups, and that these numbers now only apply to Al-4.5% Cu.

In particular, the group  $h_B L / \bar{K}$  will be reduced to  $h_B L$ , the group  $\alpha t / L^2$  will be reduced to  $t / L^2$  ( $\tau_{Lst}$ ), and the group  $(T - T_a) / (T_m - T_a)$  will be reduced to  $T - T_a$  ( $\Delta T_s$ ).



## B. Analytic Correlation

The program was set up to simulate the solidification of a pure material cast at its melting point. The analytic solution for the movement of the solidification front of an alloy that solidifies at a single temperature is:

$$x_E = 2 \beta (\alpha t)^{1/2} \quad (R1)$$

where:

- $x_E$  = position of the liquid-solid interface
- $\alpha$  = thermal diffusivity,  $K/\rho C_p$
- $t$  = time
- $\beta$  = dimensionless parameter, constant for a particular material and surface temperature

The constant  $\beta$  is found from the transcendental equation:

$$\beta e^{\beta^2} \operatorname{erf} \beta = (T_m - T_s) \frac{C_{ps}}{H\sqrt{\pi}} \quad (R2)$$

where:

- $C_{ps}$  = heat capacity of solid
- $T_m, T_s$  = melting temperature and surface temperature, respectively
- $H$  = heat of fusion

Figure 7 shows the results of the program,  $\lambda$  versus  $\sqrt{t}/L$  (the points plotted) for three values of  $H'$ , dimensionless heat of fusion. The straight lines are the analytic solutions for these cases (Equations R1 and R2), and as can be seen, the computer model correctly predicts the position

of the interface. The initial conditions for this case are:  $T = T_m$ ,  $t < 0$ ,  $0 \leq x \leq L$ , and the boundary conditions are  $T = T_a$  at  $t > 0$  at  $x = 0$ ,  $q = 0$  at  $x = L$ . The material properties used for this run were;  $T_m = 650^\circ\text{C}$ ,  $C_{ps} = .22$ ,  $\bar{K} = .24$ ,  $\rho = 2.645$ .

It is worth noting that in order to achieve the condition that the surface temperature drops to the ambient temperature at time  $t = 0$  sec., a special start-up procedure was used. Since this start-up procedure is used in the rest of the results to be presented whenever infinite surface cooling is desired, it will be described here.

At time  $t = 0$ , the positions of the liquid and solid interfaces (just the solid interface for pure materials) are set by means of a parabolic curve through the temperatures at the surface and at the first interior node. The temperature of the first node is interpolated also, and as long as an interface resides in it, it is set by interpolation. Thereafter, it is set to the ambient temperature.

Thus, the procedure for start-up causes a slight error to be introduced, since the calculations proceed from positions which are small but finite at time  $t = 0$ , whereas in the analytic solution, the position is  $x = 0$ , at time  $t = 0$ . This error can be corrected for, with the result that the positions of the interfaces are adjusted slightly at early times, but remain practically unchanged at later times.

The ability of the computer model to correctly predict the analytic solution for the case of a pure material

solidifying shows that the major source of error in the following results will be; (1) values of the data used for material properties, (2) assumptions made concerning the mode of solidification of the alloy in the mushy region, (3) the interaction of the tip and root when they are close to each other, and (4) the exact method of handling the boundary conditions at the surface and center of the ingot, where these conditions are not the same as they were above, namely, that the surface cools infinitely fast, and there is no heat lost or gained at the center.

Since there is an analytic solution for the case of a pure metal solidified with an infinite surface cooling rate, which predicts that the position of the interface will be proportional to the square root of time, the rest of the results presented will be plotted using the square root of the dimensionless time,  $\sqrt{t}/L$ . There are theoretical reasons that alloys should behave in the same fashion as the pure metals, as seen in the approximate analytic solutions of Adams (10).

#### C. Pure Metal, Aluminum

The effect of superheat and surface heat transfer coefficient on the solidification of pure aluminum is shown in Figures 8 and 9. The position of the interface is given as the dimensionless number  $\lambda$ , versus the dimensionless  $\sqrt{t}/L$ , as before for Figure 7.

Superheat has the effect of shifting the curves to the right, or, of retarding the motion of the interface. The early time portion of the curves are straight, indicating that the superheat can be treated as an additive heat term to the heat of fusion. It can also be seen that there is an end effect present in the curves at higher superheat, and this effect will later be shown to be a very characteristic effect in the solidification of alloys. The speed up of the interface in pure metals at high superheat near the centerline of the ingot is due to the dissipation of the superheat which has taken place over most of the length of the ingot, so that while the interface was growing into the superheated region at early times, which retarded the velocity of the interface, at later stages, the superheat has been dissipated (through the interface), and the velocity increases near the end.

The effect of lowering the heat transfer coefficient at the surface, with no superheat, is presented in Figure 9. The major change in the  $\lambda$  versus  $\sqrt{t}/L$  curves is that they are shifted to the right (higher times) and that they are no longer straight. This is to be expected, since the rate of heat removal from the ingot is changing from that of being controlled by the thermal diffusivity (or conductance) of the metal, to control by the heat transfer rate at the surface. As Figure 10 shows, when the heat transfer coefficient is sufficiently low, the position of the interface is governed only by the rate at which heat can be removed from the surface.

For this case of 'h controlled' heat flow, the position of the interface is given by:

$$x_t = h_B (T_m - T_o / \rho H) t \quad (R3)$$

which is what Figure 10 shows in the dotted lines. The error which the computer model introduces at the early time is due to the fact that at positions near the surface, only a two-point interpolation can be made in calculating the velocity of the interface (see Appendix A for details of the method), but this error can be corrected for, since the model predicts the correct slope of the line after the initial transient.

In general, the effects of superheat and surface heat removal rate are distinct; the superheat changes the amount of heat which must be removed for a given amount of solidification to take place, but does not alter the basic character of the relationship between position and time, however, the surface heat removal rate does alter the character of the curves, as the rate controlling factor shifts from conductance through the metal to conductance across the surface.

As to what value of  $h_B L / \bar{K}$  is sufficiently low such that Equation (R3) applies, Figure 10 shows that any choice of a number is somewhat arbitrary, but one criteria for determining whether heat flow is 'k controlled' or 'h controlled' could well be whether the curve obeys Equation (R3) or not. For  $h_B L / \bar{K} = .1$ , the straight lines are parallel, therefore heat

flow can be said to be 'h controlled'. For the  $h_B L / \bar{K} = .635$ , the dashed line diverges from the curve after a short period of time, indicating that heat flow was controlled initially by the surface removal rate, but that it was controlled by the heat flow rate through the metal at later times. The value of  $h_B x_t / \bar{K}$  at the time at which the curve diverged from the linear relationship is .1, indicating that this number may be useful in determining how long an ingot will be in the 'h control' region. That is, if  $h_B L / \bar{K}$  is less than .1, the solidification will be h controlled over its entire length, but if  $h_B L / \bar{K}$  is larger than .1, the heat flow will be h controlled until the interface moves out to a distance  $x_t = .1 \bar{K} / h_B$  from the chill, then it will start to be controlled by thermal diffusivity through the metal as well.

D. Unidirectional Alloy; Fraction Solid at the Tip, Columnar and Equi-Axed

Figure 11 shows the local solidification time, at a specific dimensionless distance away from the chill ( $\lambda = 0.75$ ), versus fraction solid at the tip, for two cases: (a) columnar growth; and (b) equi-axed growth. All other thermal properties remain as before, with the conditions being no superheat, and infinite surface cooling rate.

The investigation of the change in behavior as a function of the fraction solid at the tip was undertaken in order to have a quantitative measure of what effect the assumption of Equation (6b) would have. As the two curves of

Figure 11 show, the actual numerical value of the fraction solid at the tip, which must come from physical arguments concerning the undercooling necessary at the tip (due to radius of curvature and kinetic restrictions) does not have a large effect on the local solidification times, although the extrapolation of these curves back to zero fraction solid would cause difficulty; this might be a consequence of the nature of Equation (6b), which clearly is undefined at  $f_t = 0$ .

The most interesting feature of Figure 11 is the lack of difference between the assumption of columnar and equi-axed structures, at a given value of  $f_t$ . The model which separates the columnar heat flow from the equi-axed is given in the introduction, and the main result of that model is that the thermal conductivity in the mushy region, which is a function of fraction solid at a point, is slightly different for each of these cases, with the conductivity for equi-axed morphology being slightly lower, at a given fraction solid, than for the columnar. The closeness of the curves indicates that differences between equi-axed and columnar structures, which are observed in practice to be much larger than the effect seen here, must come from some other effect than just the difference in thermal conductivities. This difference will be shown in Section K of the Results, to be more probably a result of the convection in the melt which carried equi-axed grains, or dendrites, out into the melt

ahead of the unidirectional interface. Therefore the curves in Figure 11 are significant in the sense that they show that an effect is not the result of simple thermal conductivity differences between the growth morphologies.

#### E. Unidirectional Alloy Solidification

The variable of major concern to the solidification behavior of alloys is the time which the material spends between the liquidus temperature and the solidus temperature, at a given point within the ingot. But in order to see how this local solidification time is influenced by a particular casting variable (superheat, for instance), the positions of the tip and root as functions of time are valuable pieces of information. Therefore, the dimensionless positions of the tip and root versus  $\sqrt{t}/L$  will be presented in each of the following cases, as an aid to understanding the way in which the local solidification time is affected.

The conditions and properties used for this case of a binary alloy, Al-4.5% Cu, are:

Thermal properties; (cgs units) (26)

$$K_l = .24$$

$$K_s = .43$$

$$C_{pl} = .22$$

$$C_{ps} = .21$$

$$\rho_l = 2.645$$

$$\rho_s = 2.75$$



$$\begin{aligned}
 H &= 75 \\
 T_L &= 650 \\
 T_e &= 548 \\
 f_t &= .05 \\
 f_e &= .09
 \end{aligned}$$

Initial conditions;

$$T = T_m + \Delta T_s \text{ degrees superheat for } 0 \leq x \leq L; t = 0$$

Boundary conditions;

$$T = T_a \text{ at } x = 0 \text{ for } t > 0 \text{ or } T = h(T - T_a) \text{ at } x = 0 \text{ for } t > 0$$

$$q = 0 \text{ at } x = L \text{ for } t > 0$$

The thermal properties and initial conditions will be the same for all following cases, except where noted.

Figure 12 shows the  $\lambda$  versus  $\sqrt{t}/L$  curves for four values of superheat at a constant heat transfer coefficient =  $\infty$ . The most obvious effect observed is that both the tip and root velocities are retarded by the presence of superheat, and that for early times, the curves are straight lines. The root curves always have the speed up effect at the end of solidification, since there is always a superheat of  $102^\circ\text{C}$  ( $T_L - T_E$ ) in front of the root interface. This speed up effect of the root, and of the tip in cases of high superheat, is important to note; it is the cause of one of the characteristics of the local solidification time versus distance curves, which will be pointed out below.

Perhaps a less obvious feature of these curves is that while both the tip and root velocities are retarded by the presence of superheat, the tip is pushed closer to the root as the amount of superheat increases, that is, the root is less strongly affected by the superheat than the tip, but this is a small effect.

Figure 13 shows the dimensionless local solidification time as a function of dimensionless position from the chill. The effect of the superheat on the positions of the tip and root can now be seen more clearly, as the characteristics of the curves in Figure 13 are examined: (1) the early time portion (distances close to the chill) of the curves are parabolic upwards, governed by the straight line  $\lambda$  versus  $\sqrt{t}$  behavior of the tip and root; (2) the peak in the curves at  $\lambda \approx .9$ , due to the speed up effect of the root, mentioned earlier; (3) the peak local solidification time is lower as the superheat becomes larger, due to the fact that the superheat had more of an effect on the velocity of the tip than that of the root; (4) the peak occurs at a position closer to the centerline as the superheat becomes greater, due to the fact that at higher superheats the tip also has a speed up effect, which reduces the effect of the root speed up; (5) the effect of the superheat is diminishingly small, that is, for a given increase in the degrees of superheat, the peak in the  $\tau_{1st}$  curves drops by smaller and smaller amounts, due to the fact that although the velocity of the tip is

retarded by superheat, the width of the mushy region is also becoming smaller, since the superheat that the root 'sees' is always  $102^{\circ}\text{C}$  higher than that which the tip sees, and thus has a smaller effect.

In general, the effect of superheat is to lower the local solidification time at a given position in the ingot, but this effect is a maximum at  $\lambda \approx 0.9$  or so, and the effect is diminishing as superheat becomes large.

Figure 14 shows the  $\lambda$  versus  $\sqrt{t}/L$  curves for four values of  $h_{\text{P}}L/\bar{K}$  at a superheat of  $0^{\circ}\text{C}$ . The major characteristics of these curves are: (1) the tip behaves generally in the same way as the solid-liquid interface did for the case of pure aluminum, i.e., as the heat transfer coefficient at the surface decreases, the tip curves take on a curved portion at early times, corresponding to the h control which is evident in the early stages of solidification; (2) the root curves also take on the curved nature of controlled heat flow at early times, with the added effect that they start out at larger times as h decreases, due to the increasing amount of time which it takes to remove the 102 degrees superheat which the root has in front of it; (3) the tip curves are straight lines, after the initial transient; whereas the root curves are non-linear over almost all their length, especially the ones at the lower h values, indicating that the initial transient of h control is overlapping with the end effect; (4) the slope of the tip and root curves are

similar for a given  $h$ , indicating that, as  $h$  becomes lower, each interface sees approximately the same thermal conditions ahead of it.

The local solidification time curves are presented in Figure 15. The chief characteristics of these curves are: (1) they are less sharply peaked than the curves at various superheats, meaning that the maximum local solidification time in these cases is closer to the average than for the high superheat, high  $h$  curves; (2) the effect on the average  $\tau_{1st}$  as  $h$  decreases is increasing rapidly, i.e., as  $h_B$  goes from infinity to .1, the average  $\tau_{1st}$  is doubled, whereas as  $h$  goes from .1 to .01, the average is increased about 10 times; (3) the peak in the curves appears near the center-line, but moves inward toward the chill as  $h$  decreases, due to the fact that at low values of  $h$ , the root is much more affected by the rate of heat removal at the surface than the tip, since the root always has a superheat in front of it.

The question of determining whether and for how long a casting will be  $h$  controlled, for a given  $h$ , is more difficult in the case of an alloy, since both the tip and root behavior must be considered. For the tip, the same criterion could be applied as was used for pure aluminum, namely, that the process is  $h$  controlled as long as the position versus time curve for the tip is linear; this again is true for values of  $h_B x_t / \bar{K}$  on the order of .1. For the

root, the process is controlled by  $h$  for the early portion (curved portions at early times), then is controlled by diffusion through the metal for intermediate times, and finally controlled by the end effect. In the low  $h$  cases, the  $h$  control overlaps the end effect, so the process is not clearly defined, although if  $h$  were low enough ( $h_B L / \bar{K} = .1$ ) such that the temperature gradients in the metal were very small when the surface reached the solidus temperature, the process should then be completely  $h$  controlled, since there would be no superheat effect to consider. This implies that at these very small values of  $h_B L / \bar{K}$  both the tip and root positions would be linear functions of time (Equation R3), and therefore that the local solidification time would be a constant across the length of the ingot.

#### F. Radial Alloy Solidification

Figures 16, 17, 18, and 19 summarize the behavior of an alloy cast in a cylindrical mold, chilled from the outside, with thermal properties, initial conditions, and boundary conditions as listed previously for the case of unidirectional solidification, where the characteristic length is now the radius of the cylinder,  $R$ , and the positions of the tip and root from the chill are now  $R - r_t$  or  $R - r_e$ , respectively. The general nature of the curves is completely analogous to that of the unidirectional case, except for the following effects of geometry: (1) the tip

and root positions, for a given superheat and  $h$  coefficient, progress at a faster rate than for the unidirectional case, due to the fact that the volume from which heat must be removed is decreasing as solidification progresses; (2) the end effect is much more pronounced and takes place at earlier times, so that the resultant local solidification time curves have peaks (again, for a given superheat and  $h$ ) at distances closer to the chill than in the unidirectional case; (3) the local solidification time, for a specific  $h$  and superheat, is on the order of  $1/3$  that of the unidirectional case, at a given position in the ingot.

#### G. Heat Input with High Convection

The effect on local solidification time of superheat, presented above, suggests a practical method of controlling the solidification process, in order to reduce the local solidification time and therefore the dendrite arm spacing. If the presence of heat at the dendrite tip causes the velocity of the tip to be retarded, while the effect on the root is somewhat less, then if the exact amount of heat at the tip could be controlled, the velocity of the tip could be directly controlled. Just such a control of the tip could be attained if two conditions can be obtained:

- (1) sufficiently vigorous convection can be maintained in the liquid melt ahead of the dendrite tips, such that any heat introduced at the centerline of the ingot will be

carried to the tip almost immediately, and (2) heat may be introduced in a controlled fashion at the centerline of the ingot, perhaps by means of a resistance heating element immersed in the melt, with little or no surface contact resistance at this boundary.

Specifically, the results of this section are for the case of a unidirectionally cast ingot, with all thermal properties and boundary conditions as before, except that:

- (1) thermal conductivity of the bulk liquid ahead of the dendrite tips is treated as if it were 200 times that of still liquid, and
- (2) the centerline boundary condition now becomes:  
 $q = f(t)$  at  $x = L$ , for  $t > 0$ .

The exact method used to handle this high convection by the computer model is presented in Appendix A.

The center heat input boundary condition, function  $f(t)$ , was chosen, for simplicity and similarity to the rate of motion of the tip, to be a parabolic function of time, i.e.

$$f(t) = A_{\text{heat}}/\sqrt{t}$$

where  $A_{\text{heat}}$  is a specified constant for  $t > 0$ .

The results for the case of various values of  $A_{\text{heat}}$  are shown in Figure 20. The general characteristics of the curves are: (1) both the tip and root velocities are slowed by the presence of the heat at the tip, as they were in the case of superheat, (2) unlike the effect of superheat,

however, the curves start to take on a sigmoidal nature as the amount of heat is increased; (3) the tip and root seem to be closely coupled, that is, the rate of growth of the thickness of the mushy region is remarkably constant over the time from start to finish of solidification.

Figure 21 shows the local solidification time curves for the values of  $q'$  used in Figure 20. The characteristic nature of the curves is as it was for the no heat input cases, above (Figure 13). The effect of the heat input can be seen more clearly in curve A, Figure 32, in which the local solidification time at a given position ( $\lambda = .75$ ) is plotted against the value of  $A_{\text{heat}}$ . There is a minimum in this curve, at  $q' \approx 1.27 \times 10^{-2}$  ( $A_{\text{heat}} = 50$ ). This minimum in the curve indicates that the heat at the tip has a large effect on the tip motion (the curves in Figure 20 show this) but the retardation of the tip is closely coupled to the motion of the root, with the overall result that the width of the mushy region is approximately constant, but the velocities of the tip and root are less, so that at higher values of heat input, the local solidification time at a given point is becoming larger. The retarding of the tip motion is beneficial (lowers  $\tau_{1st}$ ) at low values of  $q'$ , because the mushy region is shortened, but as  $q'$  becomes larger, this shortening becomes smaller, and is overridden by the slowing of the velocities.



The general effect of heat input with high convection is that a small amount of heat at the tip shortens the mushy region and lowers the local solidification time at a given position, but increasing amounts of heat only slow the tip and root velocities, without shortening the mushy region appreciably. The result is that the local solidification time at given positions becomes larger.

This result indicates that there is potentially a method for reducing the local solidification time, and therefore the dendrite arm spacing, over the interior portions of an ingot (where the maximum times occur) which could be easily implemented in commercial foundry practice, in which there is typically a large amount of natural convection present during solidification.

#### H. Heat Loss from the Side

If heat can flow in the y-direction as well as the x-direction, the problem of solving the heat flow equation becomes much more complex. In order to simplify this problem, yet retain the nature of the effect of two-dimensional heat flow, one assumption was made about the rate of heat removal in the y-direction (as was stated in the Introduction). We consider heat to be removed from the side (y-direction) slowly enough that the process in this direction is completely 'h controlled', which implies, from Section E, that we chose values of  $h_s$  and  $W$  (half width), such that  $h_s W / \bar{K}$  is less than .1. (Refer to Appendix F for details.)

With this restriction, Figure 22 shows the effect of side heat loss, with no convection or superheat, for four values of side heat transfer coefficient. From Appendix C, the pertinent dimensionless number for this situation is  $h_s L^2/W$ . It should be noted that two dimensionless numbers are required to describe this situation, but the second number  $h_s/h_b$ , can be eliminated if we chose  $h_b = \text{infinity}$  at the chill (x-direction). This was done to simplify the results, and all cases of side heat loss presented here and in the following sections were obtained using  $h_b = \text{infinity}$ . The thermal properties and boundary conditions are as before.

Figure 22e shows the effect of side heat loss for a special case; that is, if heat is removed from the side such that the temperature is lowered very slightly, the tip position moves infinitely fast (along the vertical axis), since nucleation of the solid takes place ahead of the x-direction tip interface. In this special case, it is assumed that the root position is not affected, so that this case represents the maximum effect of side heat loss on the local solidification time. The other curves in Figure 22 show that the effect of side heat loss on the tip and position is:\*

(1) at zero superheat, the tip position becomes the vertical axis, as nucleation of the solid takes place along the entire length; (2) the root position is speeded up as the heat transfer coefficient at the side becomes larger, with the end effect becoming more pronounced at the high values of  $h_s$ .

---

\* It is important to emphasize here that "tip" and "root" positions are simply short hand designations of locations of "start of freeze" isotherms and "end of freeze" isotherms.

The effect on the local solidification time curves is shown in Figure 23. The largest change in the characteristics of the curves is that the drop off, due to the end effect, is somewhat eliminated. The effect on the local solidification time at a given position in the ingot of the side heat loss is seen more clearly in Figure 24, where  $\tau_{1st}$  at  $\lambda = 0.75$  is plotted versus  $h_s$ . This curve reveals two things: (1) as heat loss out the side becomes larger, the local solidification time at a point in the ingot is reduced, due to the speed up of the root position; (2) a small amount of heat loss is worse than no side heat loss. For values of  $h_s L^2/W$  less than 0.3, the local solidification time is increased at a given position, and for values greater than 0.3, it is decreased. Figure 24 also shows that the effect is diminishing, due to the fact that the root position at the high values of  $h_s$  is still controlled by the rate of heat removal in the x-direction. At very large values of  $h_s W/K$ , where the condition that  $h_s W/K$  be less than .1 becomes violated, it is expected that heat flow would be controlled by thermal diffusion through the metal in both the x and y directions.

The general effect of side heat loss, in the presence of no convection or superheat, is that the tip position is accelerated rapidly, and the root position to a smaller extent, such that the overall effect is that the local solidification time at a given x may be increased or decreased, depending on the value of  $h_s L^2/W$ .

Figure 25 shows the effect of superheat on the tip and root positions in the case for which the side heat transfer coefficient,  $h_s = 0.001$ . The primary characteristics of these curves are: (1) the tip can no longer shoot out from the chill, as nucleation from the side of the ingot is prevented by the superheat; (2) both the tip and root show a pronounced end effect, due to the fact that the superheat ahead of either of the interfaces is being dissipated in two directions, and thus enhances the speed up effect; (3) as superheat becomes larger, the width of the mushy region is becoming shorter (the tip is closer to the root at any given time), and the velocities of both are slowed. The effect on the local solidification time is shown in Figure 26, where it can be seen that the shortening of the mushy region out-weighs the slowing of the velocities, so that as the superheat becomes larger, the local solidification time at a given position drops. Figure 27 shows that this effect is diminishing, that is, for a given increase in the superheat, the  $\tau_{1st}$  decreases by smaller amounts, but that the effect is still present at superheats of  $250^{\circ}\text{C}$ .

The implication of this result is that in situations of heat loss out the side of an ingot, the more superheat which can be maintained at the start of solidification, the better the dendrite arm spacings will be in the final solidified structure. It should be noted, however, that the conditions for these results were that heat loss through the bottom (chill) was infinitely fast, and that there was

no convection present. Neither of these conditions is truly representative of what is obtained in a foundry casting situation, especially the no convection condition. In fact, it is more probable that there is a high amount of convection present in large cast ingots, so that any superheat present at the time of pouring will be lost by the time solidification starts at the chill or bottom of the ingot. Therefore, a large cast ingot situation may be more truly represented by the no superheat curves, Figures 22, 23 and 24; but Figures 25, 26 and 27 indicate that it might be well worth while, in terms of dendrite arm spacing in the final cast structure of commercially produced ingots, to prevent convection in these ingots in order to preserve superheat during the solidification process.

#### I. Side Heat Loss, with Heat Input and Convection

With the results of Sections G and H in mind, we consider here an alternative method of reducing dendrite arm spacing in large cast ingots in the presence of high convection; namely, that of inputting heat to the convecting melt, ahead of the tip interface in order to shorten the mushy region without slowing the motion of the tip very much.

Figures 28 and 30 show the effect of four values of heat input, in the presence of convection, for two values of  $h_s L^2/W$ . The general characteristics of these curves are:

(1) with the presence of heat at the tip interface, the tip can no longer shoot forward; (2) the tip and root are closely coupled, so that the slowing effect on the tip, as heat input becomes larger, is experienced almost to the same extent by the root; (3) this means that the width of the mushy region, at a given time, is approximately constant for each of the different heat input levels.

The effect on local solidification time is shown in Figure 29 for  $h_s L^2/W = .232$  and in Figure 31 for  $h_s L^2/W = .696$ . The characteristics of these curves are: (1) the local solidification time at positions near the center of the ingot has been reduced; (2) an end effect has re-appeared, indicating that in the final stages of solidification, when the root is approaching the centerline, there is very little heat in front of the root interface, and a speed up effect takes place. The most interesting result, showing how much of a drop in local solidification time results from a given amount of heat input, is shown in Figure 32. These curves reveal that (1) there is a minimum in the local solidification time at a given position versus  $q'$  curve for all values of  $h_s L^2/W$ , due to the fact that a small amount of heat input reduces the width of the mushy region as much as a large amount of heat, and therefore as more heat is input, the effect is to retard the velocities of both the tip and root, so that a given point in the ingot spends more time between the passage of the tip and root; (2) this minimum occurs at a higher value of  $q'$  for

higher values of  $h_s L^2/W$ . This shift in the minimum is due to the fact that as  $h_s L^2/W$  becomes larger, more heat is required to overcome the control which the side heat loss has on the motion of the tip and root interfaces. This can be seen by comparing Figures 28b and 30b, in which the same amount of heat was input at a given time, for the two different values of side heat loss. Figure 28b shows that at this lower value of side heat loss, the heat flow at the tip and root was controlled by the heat input over the entire length of the ingot, evidenced by the smooth, almost straight line character of the curves. Figure 30b shows that at the higher value of side heat loss, the heat flow was controlled by the heat input in the early stages, but that after some time ( $\sqrt{t}/L$  about 0.3) the curves showed the speed up effect characteristic of the side heat control seen in Figure 22. Figures 30c and 30d show that at these higher levels of heat input, the heat flow was controlled by the heat input, which was greater than the rate at which heat could be removed through the side. It is to be expected, therefore, that for even higher values of  $h_s L^2/W$ , the minimum will be shifted to higher values of  $q'$ , until the  $h_s W/\bar{K}$  criteria becomes important, and heat flow will be diffusion controlled in both the x and y directions, in which heat input will have similar effects as in the case of Section G.

As a practical method of reducing dendrite arm spacing, the introduction of a controlled amount of heat into a convecting melt could be quite feasible, judging from the results of this section. One major area which has not been touched upon here is an investigation of other heat input functions, i.e., the parabolic function used here was chosen for convenience and from the physical reasoning that the motion of the tip is governed by an inverse relation to the square root of time, in the case in which there is no heat in front of the tip (no temperature gradient in the melt ahead of the interface), therefore if heat is introduced in front of the tip in an inverse square root of time fashion, the overall effect should be that the tip motion is held to a constant, controlled velocity. This argument is justified in the results in Figures 28 and 30, as the curves are smooth and almost linear, but it is quite possible that there are many other  $q$  versus  $t$  functions which would give more beneficial results. This is an area which would benefit greatly from a mathematical analysis of the effect of heat input on the tip and root positions as a function of time; there is also available in the literature of numerical analysis a technique for optimization of unsteady state processes which could be utilized to determine optimal heat input functions for particular sets of conditions. This will be discussed later.



J. Side Loss to a Sand Mold; Parabolic Side Boundary Conditions

In castings made in sand molds, the assumption that the heat loss into the sand can be described by a constant heat transfer coefficient is not valid. Instead, the process is better described by assuming that the heat flux at the metal/sand interface is inversely proportional to the square root of time, as stated in an earlier section in the introduction. The results of the dimensional analysis on this special boundary condition reveal the dimensionless group  $aL/W$  to be the pertinent one.

Figure 33 shows the tip and root positions\* for four values of  $aL/W$ , where the numbers were chosen to be similar to thin plates ( $L/W$  about 15) cast in sand. As before a value of  $h_b = \text{infinity}$  was chosen in order to eliminate the need to consider two separate dimensionless variables. The characteristics of these curves are:

- (1) the characteristic speed up effect on the tip and root of sidewise heat loss is observed as  $aL/W$  increases;
- (2) this effect is more pronounced and takes place at earlier times as  $aL/W$  increases. Since the curves presented in Figure 33 are for the case of metal poured at 150 degrees superheat with no convection, there is no shooting out effect of the tip position. Figure 34 shows the effect on local solidification times of this side heat loss, which shows two things: (1) the curves are flat, with no drop in  $\tau_{1st}$  near the center, due to the fact that both the tip and

---

\*Note as described on page 9 that "tip" and "root" positions are simply short band designations of "start of freeze" and "end of freeze" isotherms, respectively.

root experience a speed up as they approach the centerline, and (2) at any given point within the ingot, the local solidification time is decreased as  $aL/W$  increases, due to the fact that the heat loss out the side is controlling the process over the entire length of the casting.

The implications of these results concerning the relationship of side heat loss to tip and root motion are the same as they were in Section H.

Figure 35 shows the tip and root curves for four values of superheat at a constant value of  $aL/W = 136$ . These curves reveal that; (1) at low superheats, the process is controlled by the side heat removal rate, as seen in the accelerated motion of the tip for the 0 and 50 degree superheat cases; (2) this effect is diminished as the superheat becomes higher, but is never completely eliminated. The local solidification time curves, shown in Figure 36, show that there are two effects to be considered; (1) at the low superheats, 0 and 50°C, the speed up effect of the root takes place over a large portion of the ingot, so that the  $\tau_{1st}$  curves are flat near the centerline, whereas at the higher superheats, 150 and 250°C, the speed up has been confined to very late stages of solidification so that the  $\tau_{1st}$  curves are inclined much more near the centerline; (2) the width of the mushy region is becoming much smaller as superheat increases, along with the slowing down of the tip and root velocities. The combination of these effects can be seen more clearly in curve D, Figure 37d in which the  $\tau_{1st}$  at

$\lambda = 0.75$  is plotted versus superheat. This curves shows a maximum occurring at a superheat of about  $150^{\circ}\text{C}$ , which is due to the fact that at superheats below 150 degrees the mushy region is still large, and the slowing effect of the superheat on the velocities of the tip and root is the major effect; at higher values of superheat, the size of the mushy region is much smaller, and this causes the drop in local solidification time. The position  $\lambda = .75$  was chosen to be consistant with other sections in which this sort of analysis was made, however, as can be seen from Figure 36, the choice of a different position would have resulted in a shift in the position of the maximum, although a maximum would still have been present.

A consideration of Figures 35a and 12a shows that if convection had been present in the melt in these simulated castings, and any superheat present at the time of pouring was lost through the chill or the sand mold due to this convection, the presence of this side heat loss is deleterious to the local solidification time at a given point within an ingot. The same argument can be made as was in Section H that for large commercial foundary castings, there are two avenues open to reducing the dendrite arm spacing within an ingot: (1) eliminate convection during solidification in order to preserve the superheat at pouring, although the amount of superheat which will lower the local solidification time depends on the exact

conditions present, as seen in Figure 37; or (2) input heat into this convecting melt, as in Section J, to shorten the mushy region and lower the local solidification times.

K. Equi-Axed Growth with High Convection

In large commercial foundry castings, in which it is probable that there is a high amount of convection in the melt during solidification, and when the growth morphology of the mushy region is highly equi-axed, there is good reason to believe that dendrites (equi-axed grains) are carried out into the melt ahead of the mushy region by the convection. (5) This would give rise to the following situation; the temperature of the convecting liquid would drop to a temperature at which the liquid would be in equilibrium with the solid dendrites carried out by convection, this temperature would be somewhat lower than the liquidus temperature, and can be determined from the non-equilibrium freezing relationship of fraction solid versus temperature (Scheil equation), Equation (9) and Figure 1a; solidification would take place in the mushy region (somewhere behind the dendrites at the edge of the region at which convection stops) normally, as if there were no convection. This situation can be modeled easily, and is worth investigating with the computer model since it represents a situation common to many large castings.

The conditions used to simulate this situation were:

- (1) high convection in the melt;
- (2) a new liquidus temperature exists,  $10^{\circ}\text{C}$  lower than the equilibrium liquidus;
- (3) the fraction solid at which convection stops (or up to which dendrites are carried into the melt) is assumed ( $f_{sc}$ );
- (4) the initial condition of the ingot is that there is no superheat, due to the presence of the high convection, therefore,

$$T = T_{le}; \quad 0 \leq x \leq L; \quad \text{at } t > 0.$$

- (5) heat loss through the chill is infinitely fast (no contact resistance), and heat flow, for this case, will be considered unidirectional.

The results for solidification taking place with the above conditions, for four values of the critical fraction solid,  $f_{sc}$ , are presented in Figure 38. The characteristics of these curves are: (1) the nucleation or presence of dendrites in the melt at time  $t = 0$ , causes the effective position of the tip to lie along the vertical axis; (2) the root curves are very similar, since the fraction solid at the tip only has a slight effect on the heat capacity of the mushy region ahead of the root interface (the more solid which solidifies at the tip interface; the less solidifies over the temperature range in the mushy region, which lowers

the apparent heat capacity of the region). These curves are summarized by the local solidification time curves shown in Figure 39. As is to be expected, the difference between the three curves representing the high convection case is very small, but the difference between these curves and that for no convection is large. This is due entirely to the fact that the start of local solidification takes place at time  $t = 0$ , in the high convection cases, which leads to the high local solidification times shown.

As in the previous sections, in which conditions were presented in which the start of freeze isotherm shoots out across the length of the casting at an early time, this undesirable effect could be eliminated by the addition of heat to this convecting melt; superheat would be lost during the early stages of pouring and cooling. If convection could be eliminated instead, it is to be expected that the same results as before would obtain, namely, that the start of freeze isotherms would no longer be able to shoot out, especially if some superheat were present, so that the local solidification time would be reduced at a given point in the ingot.

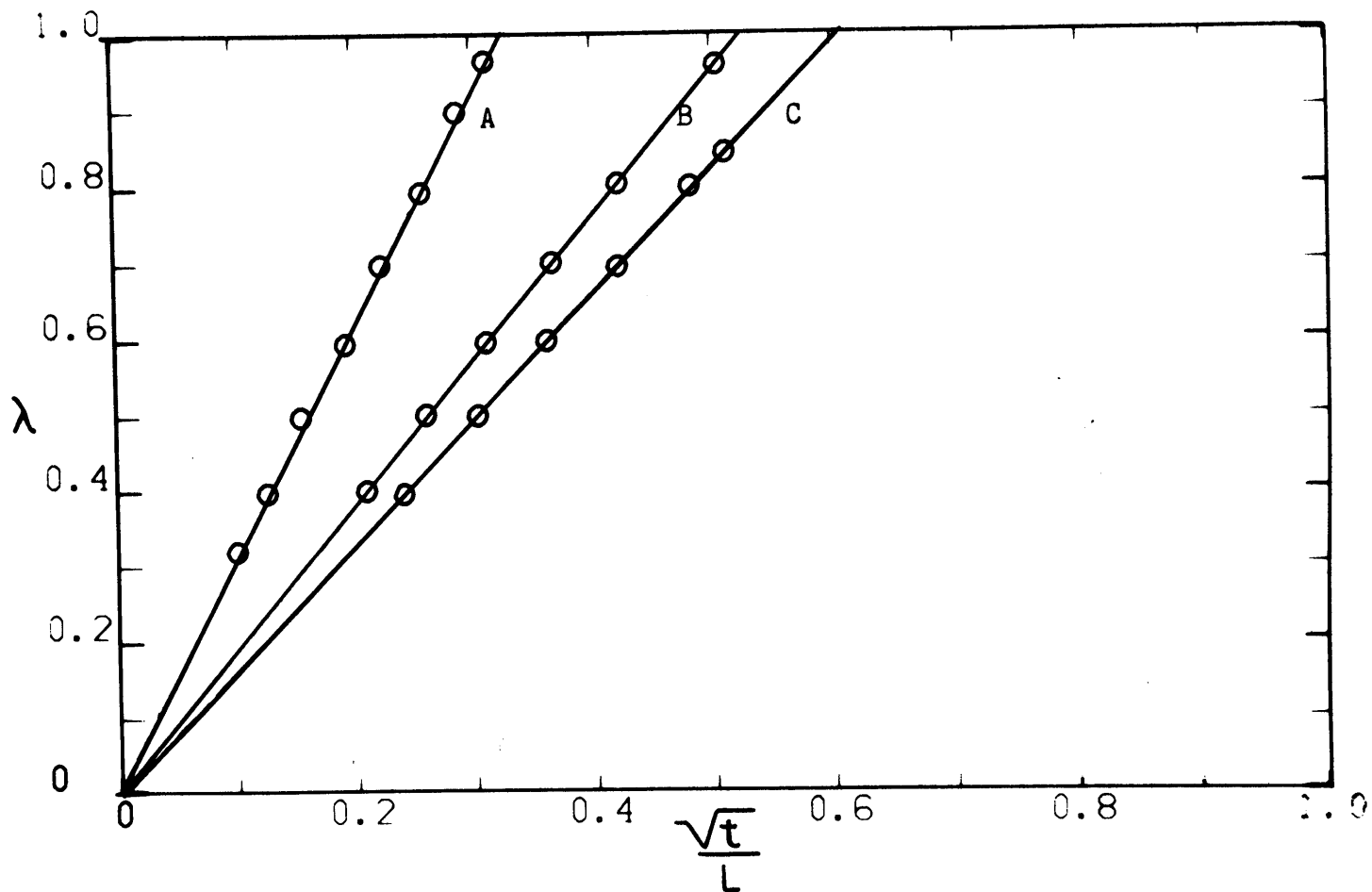


Figure 7. Position of the liquid-solid interface versus  $\sqrt{t}/L$ ,  $h\beta L/\bar{K} = \infty$ , no superheat, for (A) Heat of Fusion = 5 cal/gm, (B) Heat of Fusion = 50 cal/gm, (C) Heat of Fusion = 75 cal/gm., curves are solution to equation (R1), points are computer output.

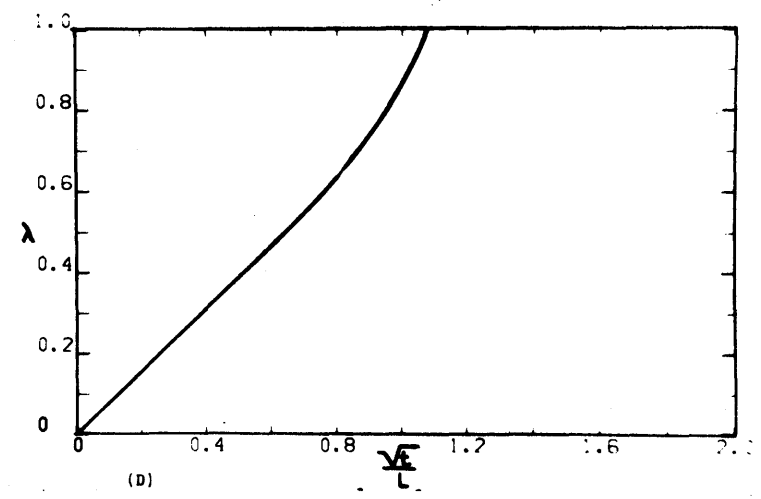
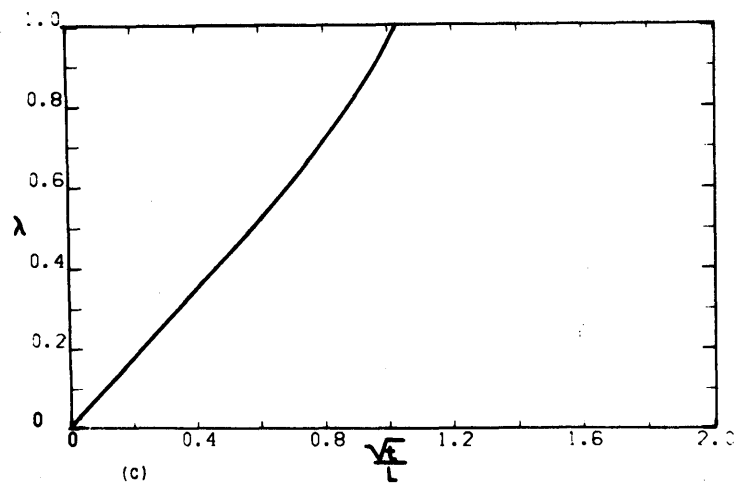
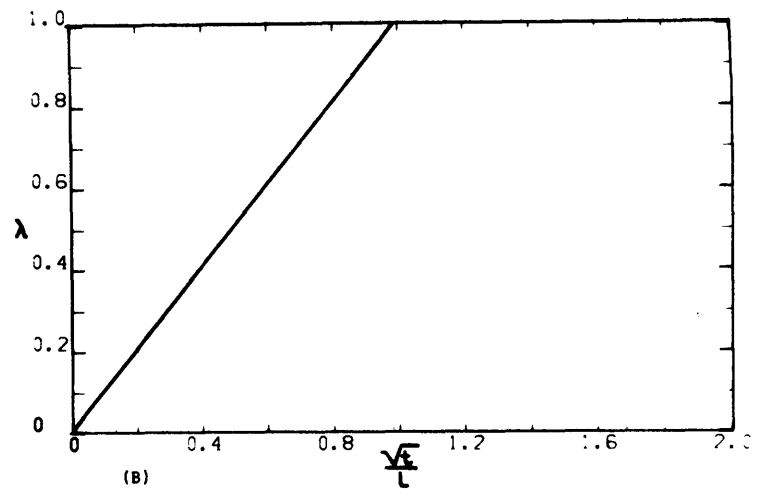
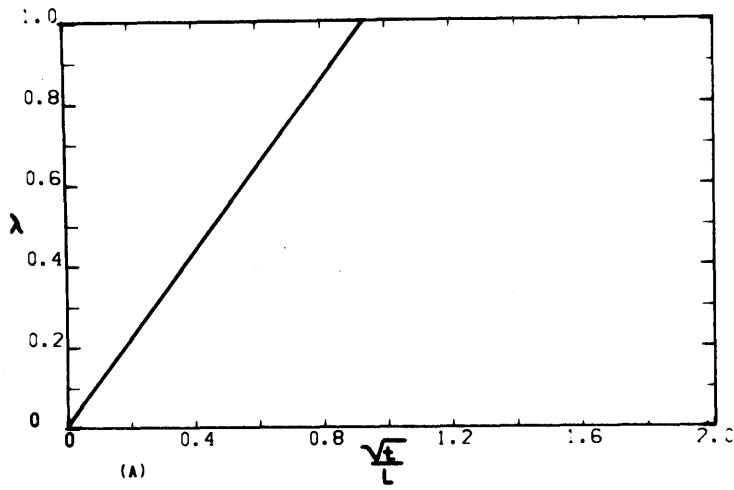


Figure 8. Position of the liquid-solid interface versus  $\sqrt{t}/L$ ,  $h_B L / \bar{K} = \infty$ , for pure metal, Heat of Fusion = 75 cal/gm, for (A)  $\Delta T_S = 0^\circ\text{C}$ , (B)  $\Delta T_S = 50^\circ\text{C}$ , (C)  $\Delta T_S = 150^\circ\text{C}$ , (D)  $\Delta T_S = 250^\circ\text{C}$ .



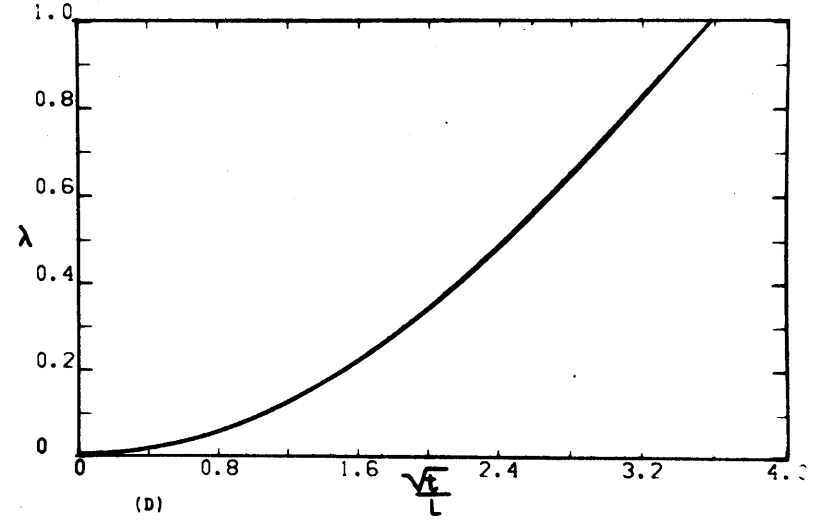
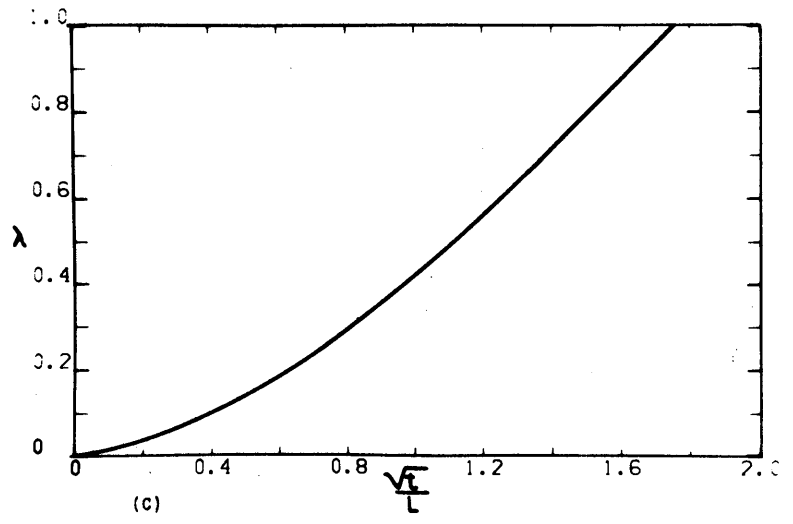
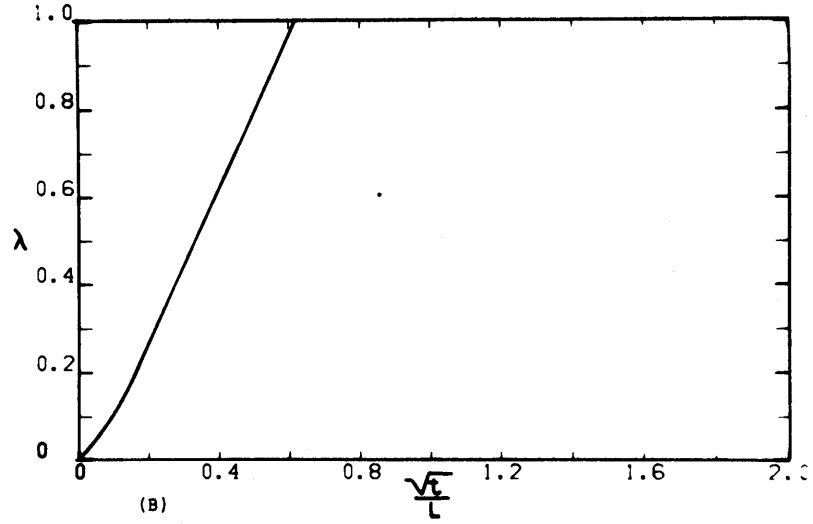
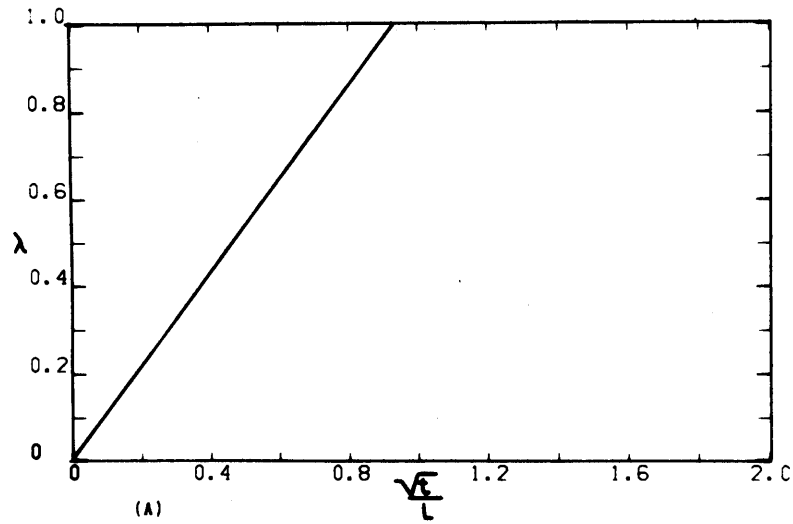


Figure 9. Position of the liquid-solid interface versus  $\sqrt{t}/L$ , for pure metal, Heat of Fusion = 75 cal/gm, no superheat, for (A)  $h_B L / \bar{K} = \infty$ , (B)  $h_B L / \bar{K} = 6.35$ , (C)  $h_B L / \bar{K} = 0.635$ , (D)  $h_B L / \bar{K} = 0.1$ .

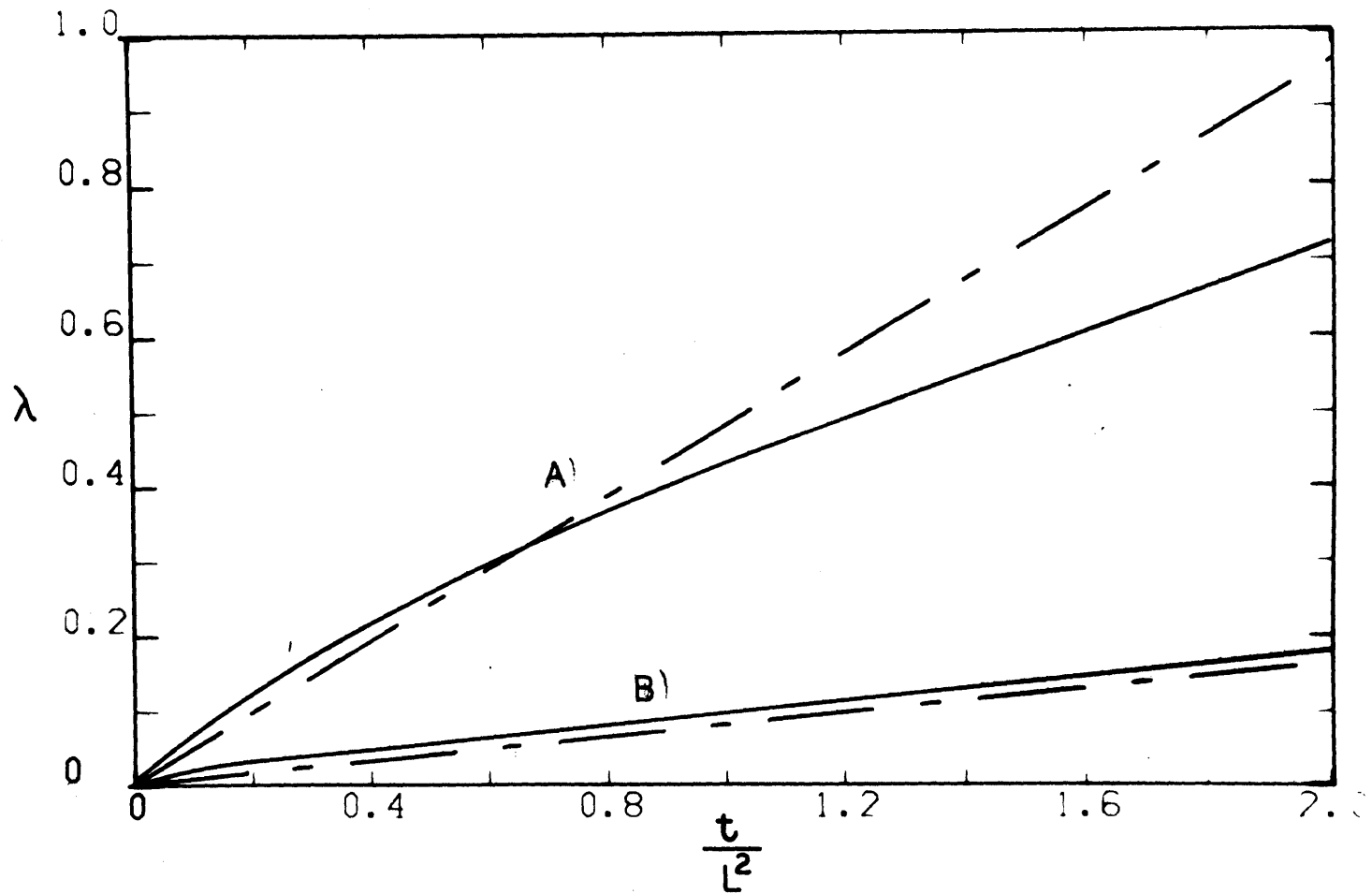


Figure 10. Position of the liquid-solid interface versus  $t/L^2$ , for (A) Figure 9 C, and (B) Figure 9 D, dashed line is solution to equation (R3), solid lines are computer solutions.

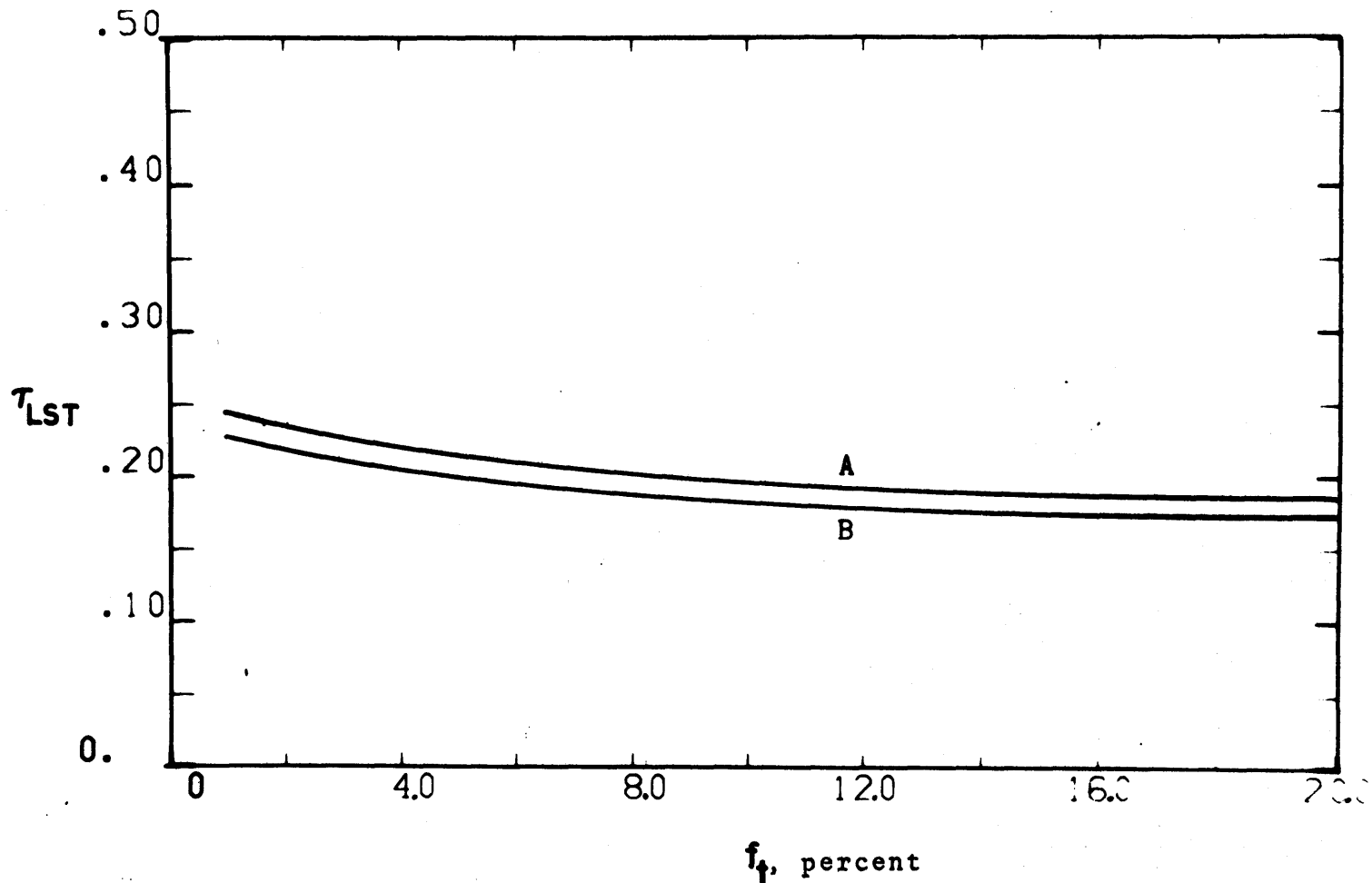


Figure 11. Local solidification time at  $\lambda = 0.75$  versus fraction solid at the tip, Al-4.5% Cu alloy,  $h_B L / \bar{K} = \infty$ , no superheat, no convection, for (A) columnar growth (parallel heat flow), (B) equi-axed growth (series heat flow).

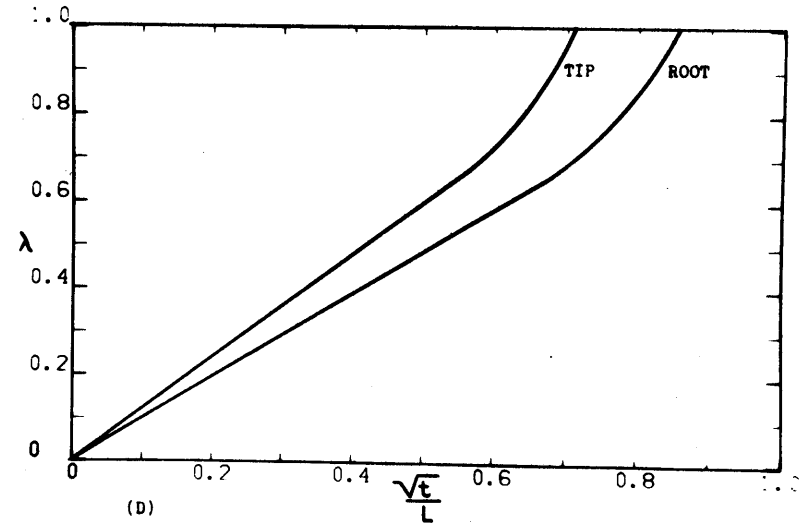
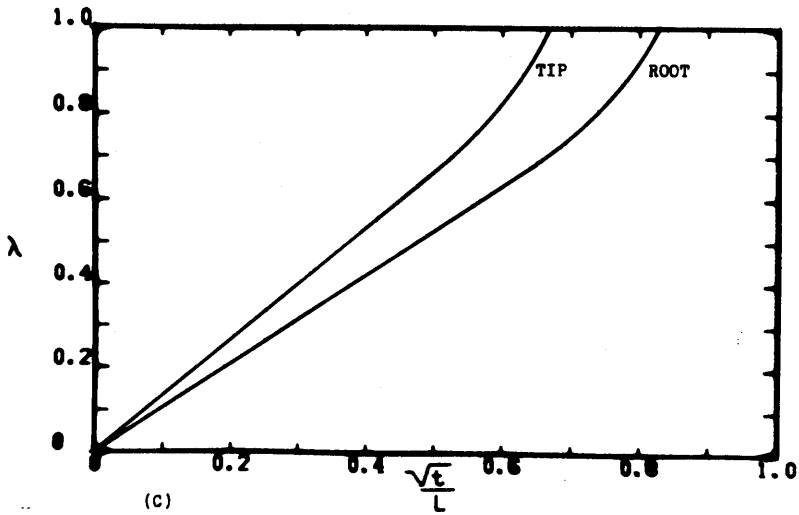
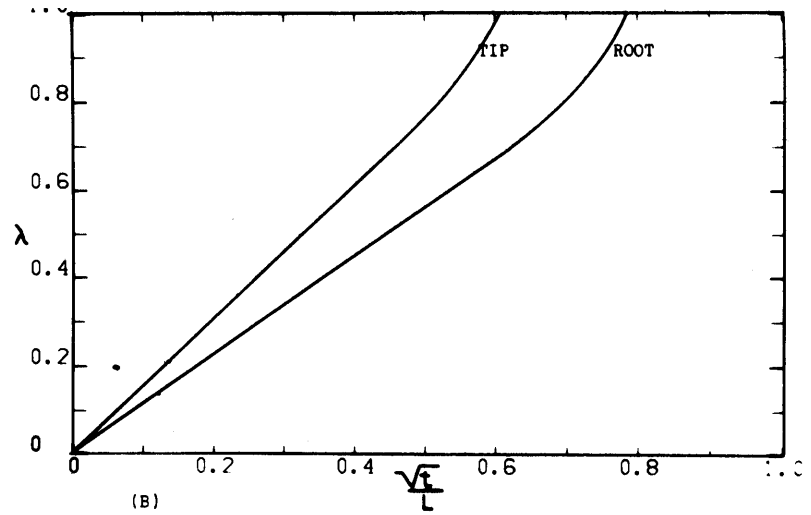
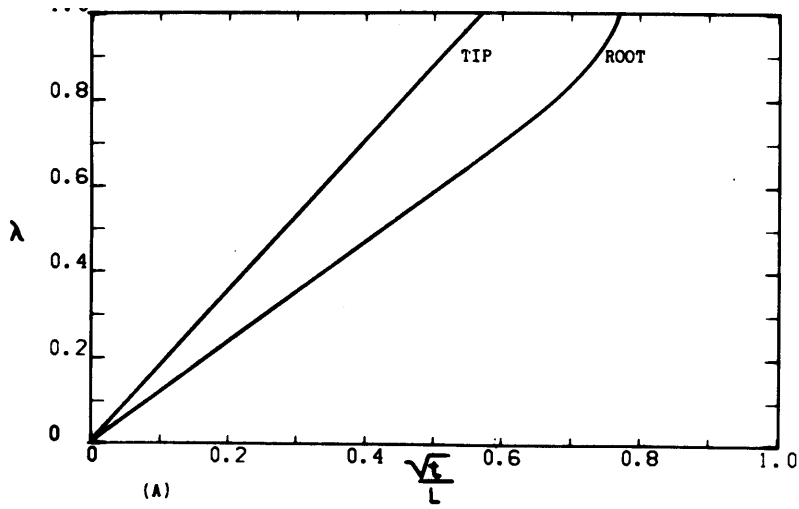


Figure 12. Position of the tip and root versus  $\sqrt{t}/L$ , Al-4.5% Cu alloy, unidirectional heat flow,  $h_B L / \bar{K} = \infty$ , for (A)  $\Delta T_S = 0^\circ\text{C}$ , (B)  $\Delta T_S = 50^\circ\text{C}$ , (C)  $\Delta T_S = 150^\circ\text{C}$ , (D)  $\Delta T_S = 250^\circ\text{C}$ .

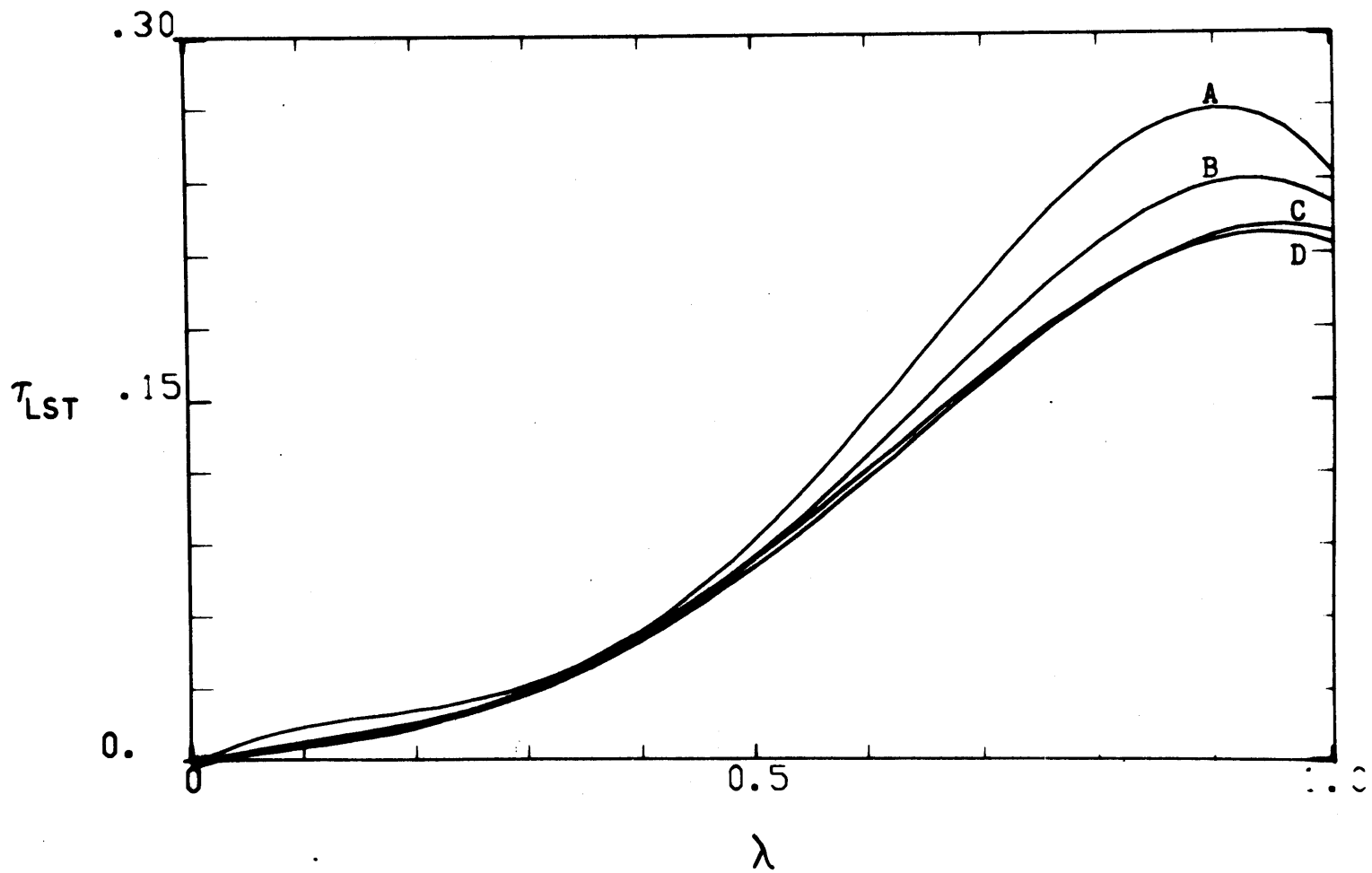


Figure 13. Local solidification time versus position, Al-4.5% Cu alloy, unidirectional,  $h_B L / \bar{K} = \infty$ , (A)  $\Delta T_S = 0^\circ\text{C}$ , (B)  $\Delta T_S = 50^\circ\text{C}$ , (C)  $\Delta T_S = 150^\circ\text{C}$ , (D)  $\Delta T_S = 250^\circ\text{C}$ .

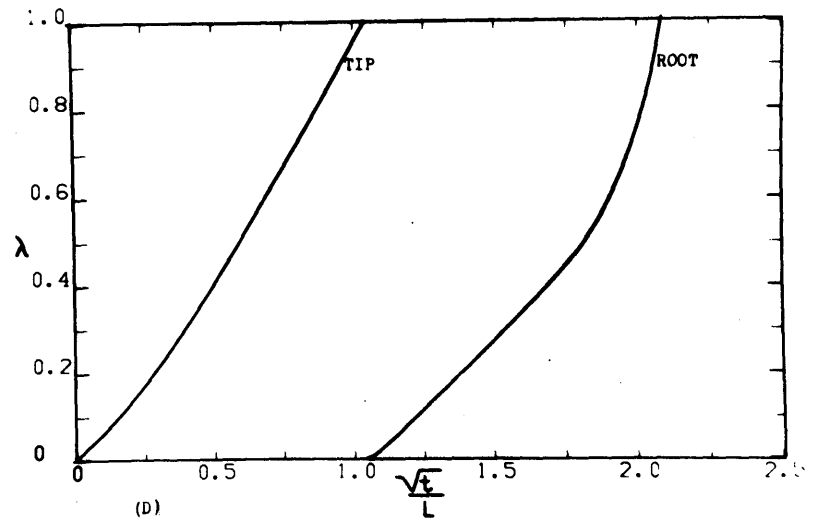
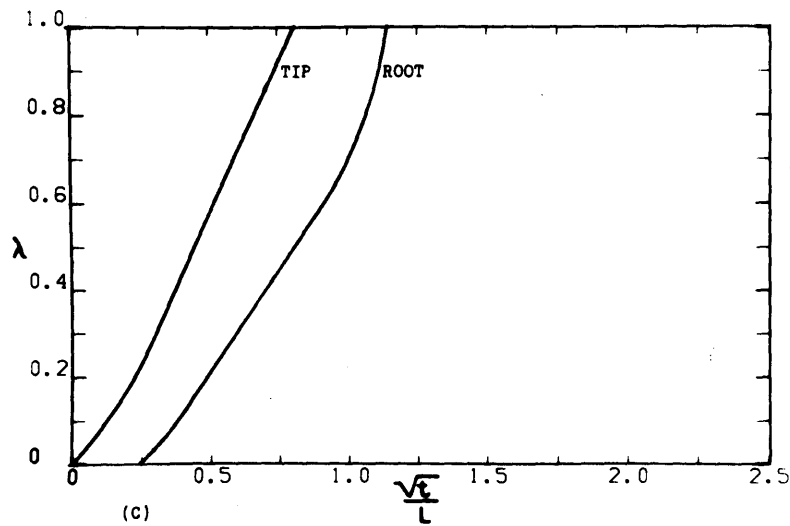
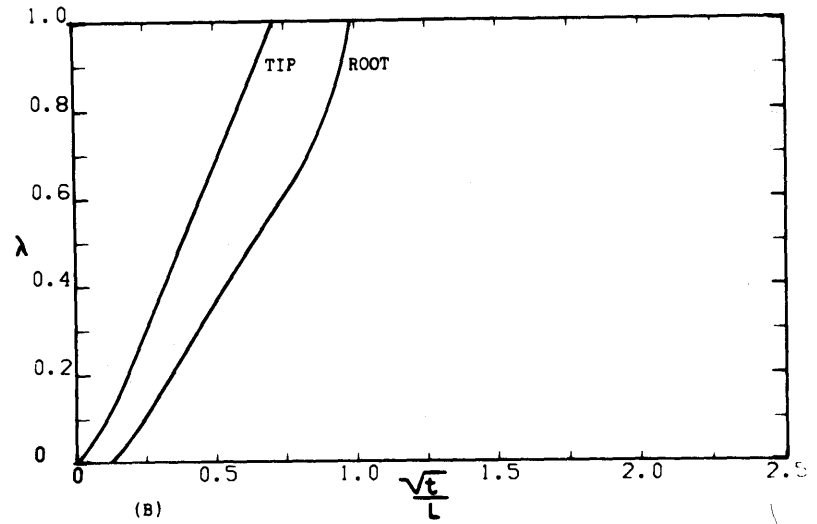
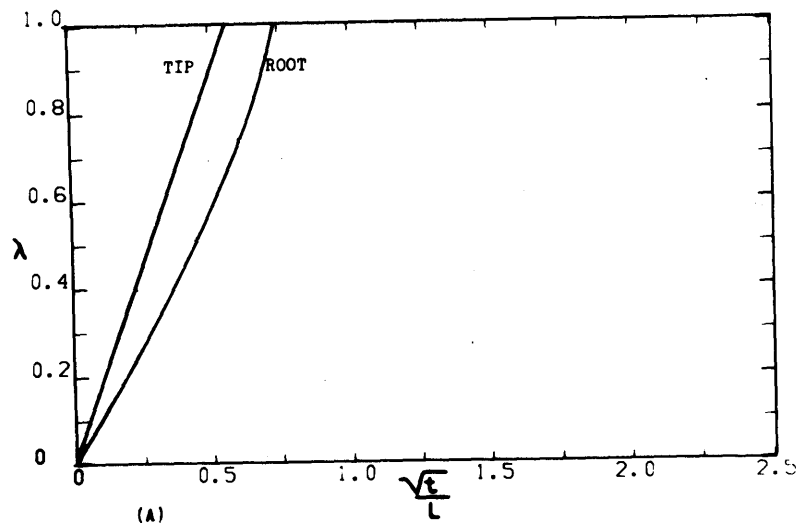


Figure 14. Position of the tip and root versus  $\sqrt{t}/L$ , Al-4.5% Cu alloy, unidirectional no superheat, for (A)  $h_B L / \bar{K} = \infty$ , (B)  $h_B L / \bar{K} = 6.35$ , (C)  $h_B L / \bar{K} = 3.17$ , (D)  $h_B L / \bar{K} = 0.635$ .

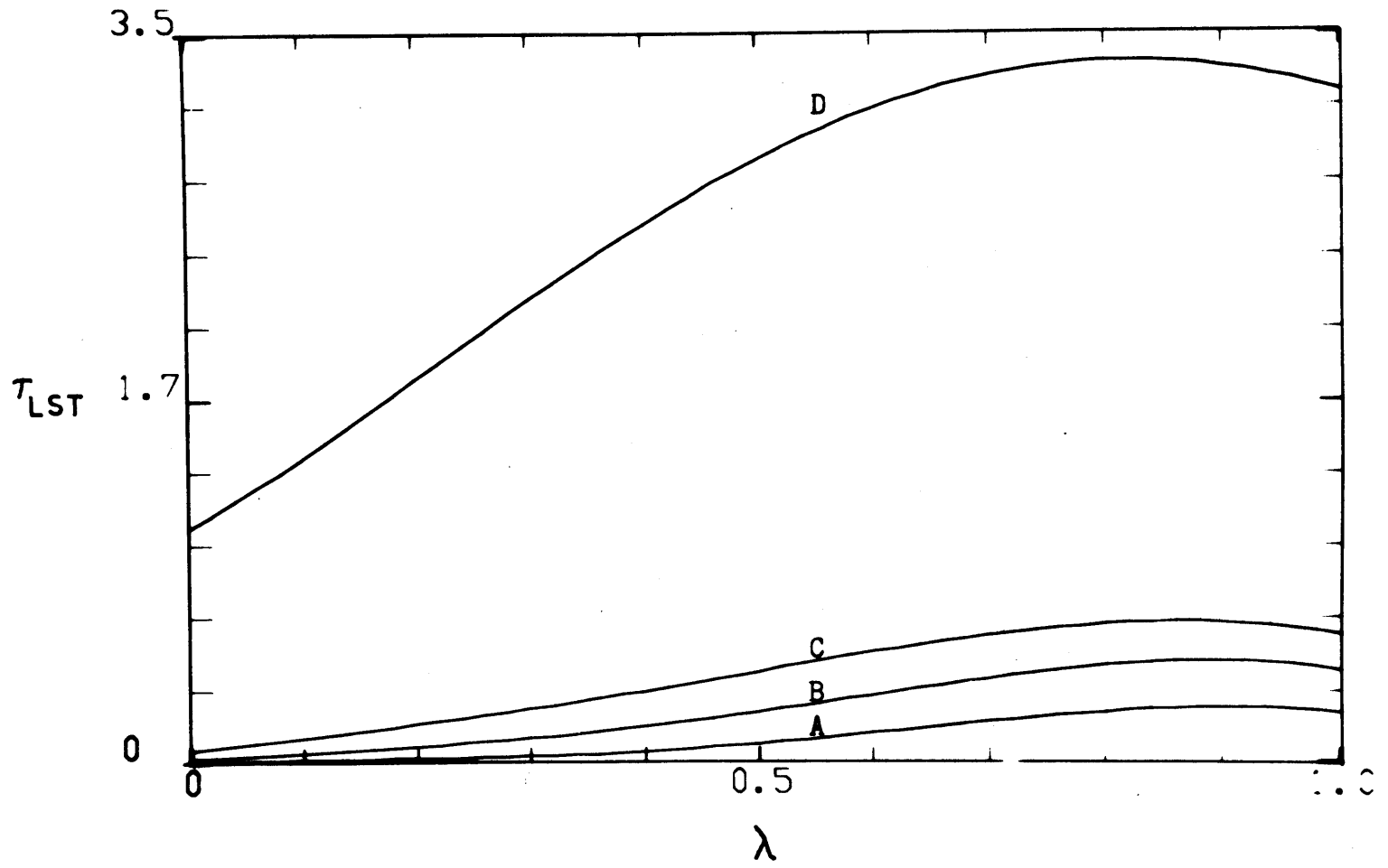


Figure 15. Local solidification time versus position for conditions of Figure (14).

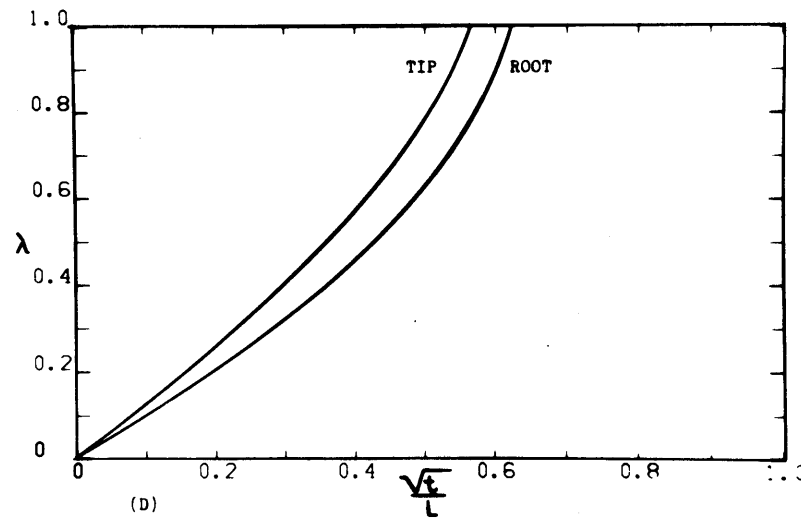
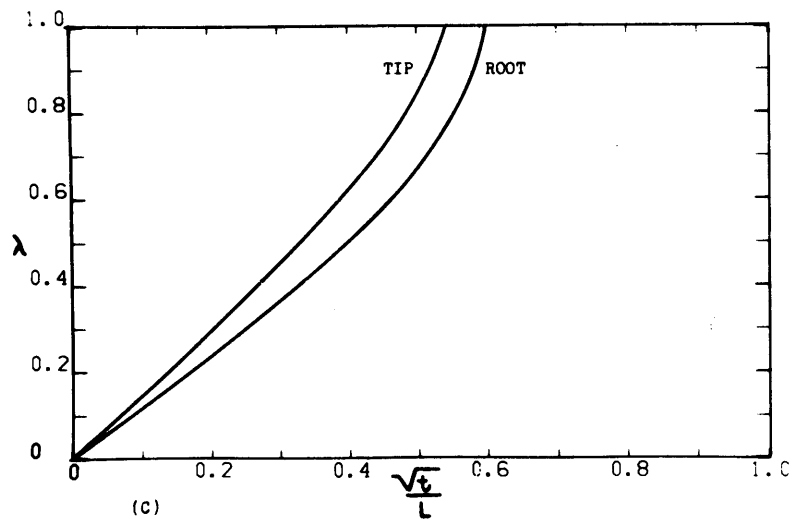
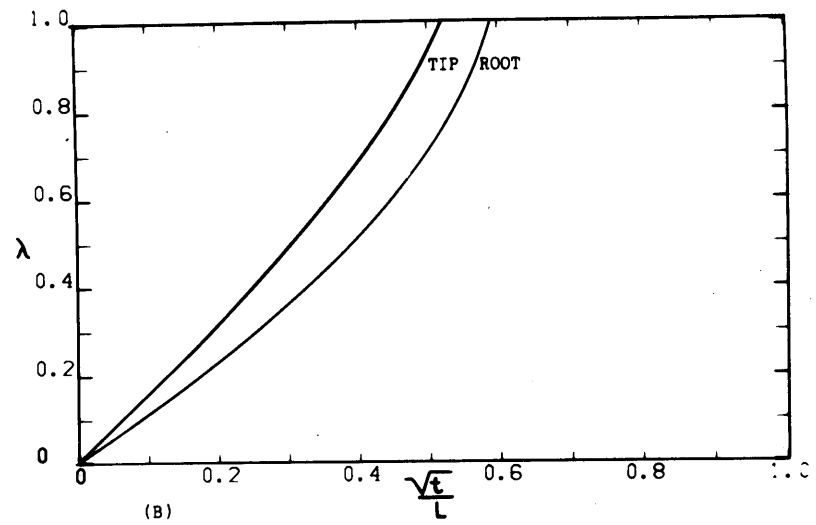
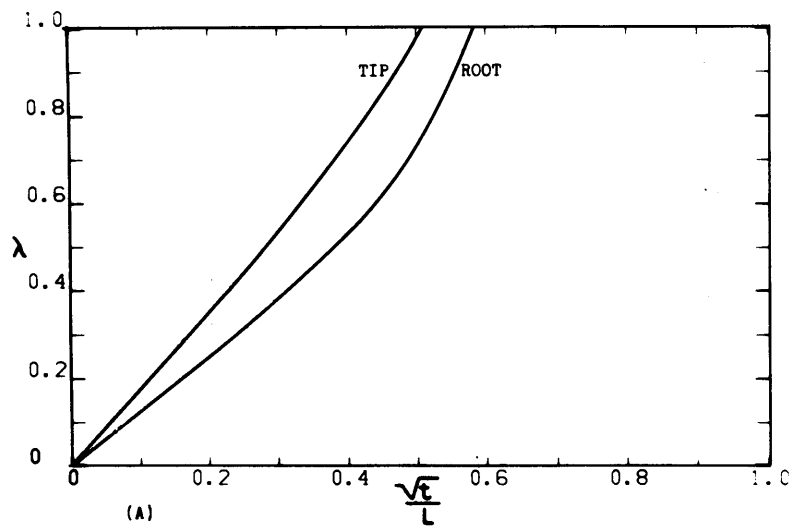


Figure 16. Position of the tip and root versus  $\sqrt{t}/L$ , Al-4,5% Cu alloy, radial heat flow,  $h_p R/\bar{K} = \infty$ , for (A)  $\Delta T_S = 0^\circ\text{C}$ , (B)  $\Delta T_S = 50^\circ\text{C}$ , (C)  $\Delta T_S = 150^\circ\text{C}$ , (D)  $\Delta T_S = 250^\circ\text{C}$ .



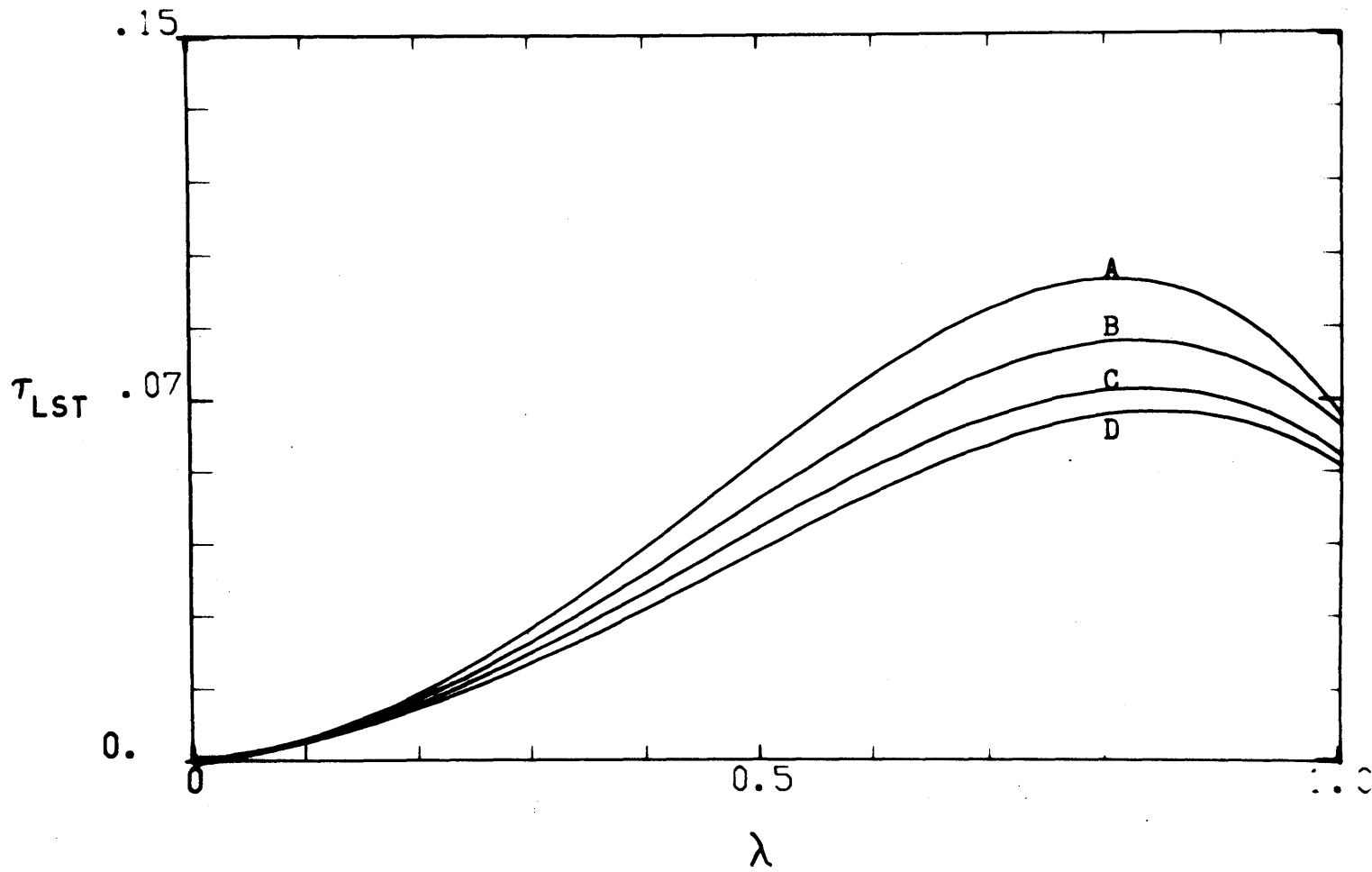


Figure 17. Local solidification time versus position, for conditions of Figure (16).

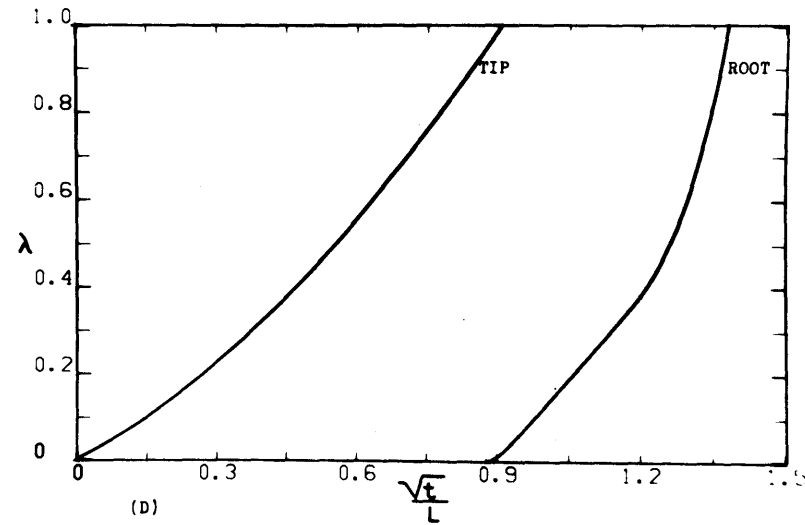
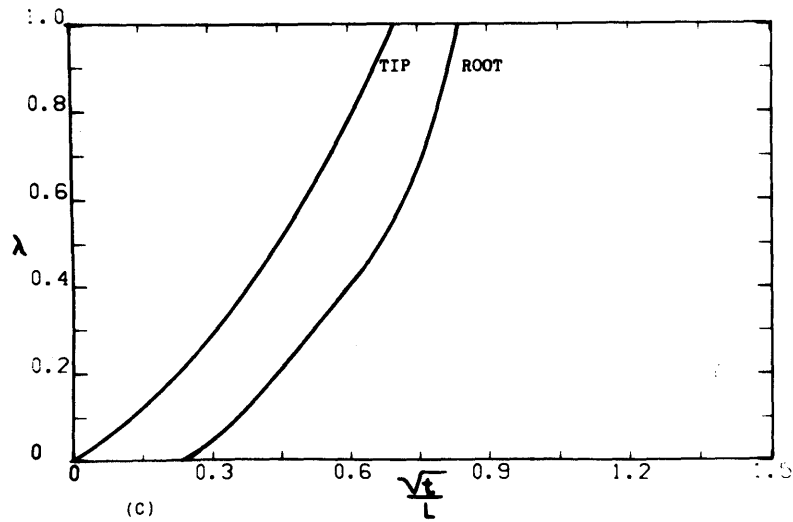
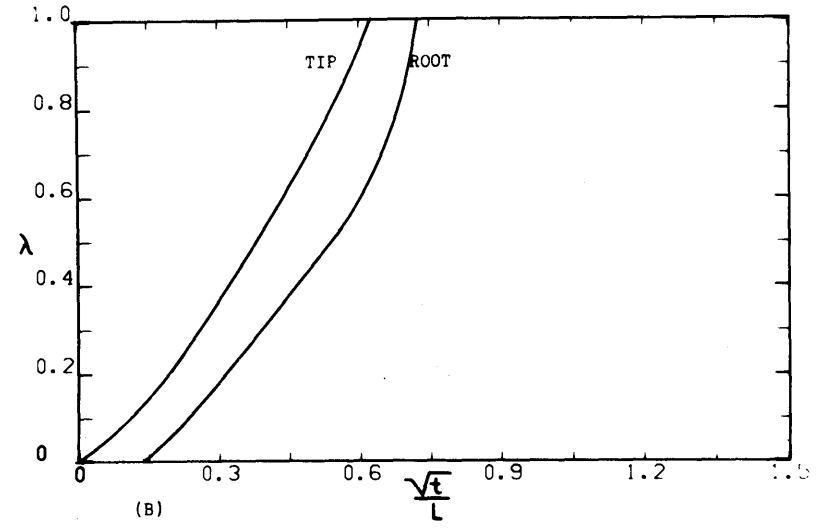
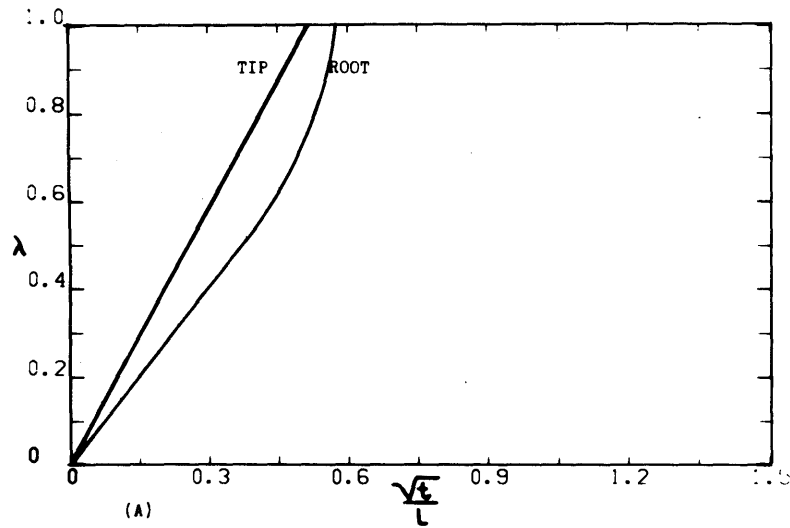


Figure 18. Position of the tip and root versus  $\sqrt{t}/L$ , Al-4.5% Cu alloy, radial heat flow, no superheat, for (A)  $h_B L / \bar{K} = \infty$ , (B)  $h_B L / \bar{K} = 6.35$ , (C)  $h_B L / \bar{K} = 3.17$ , (D)  $h_B L / \bar{K} = 0.635$ .

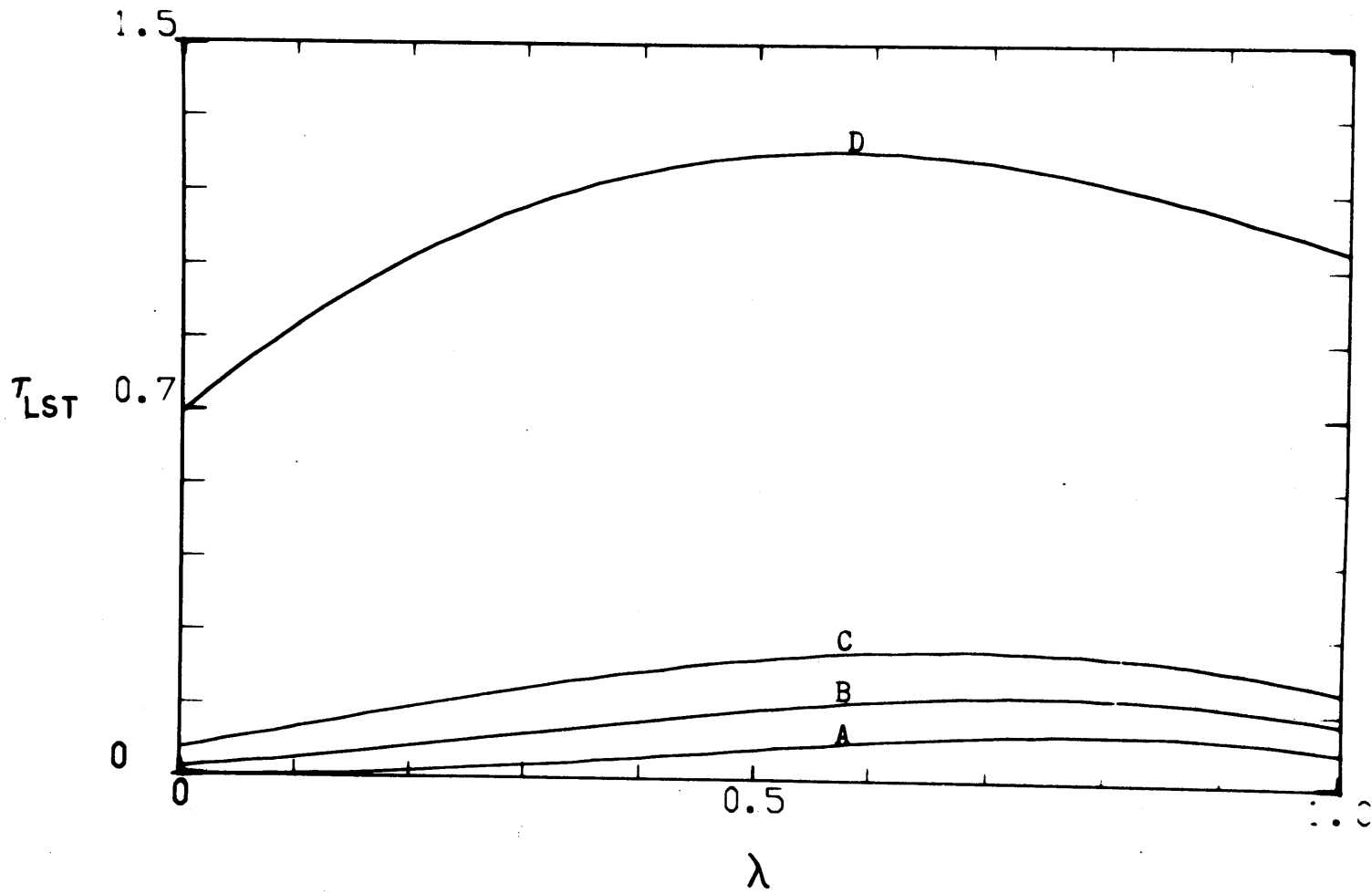


Figure 19. Local solidification time versus position, for conditions of Figure (18).

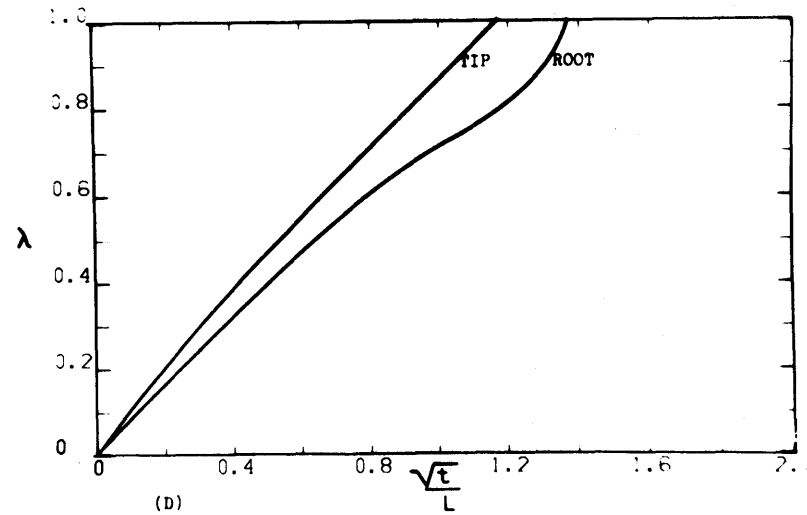
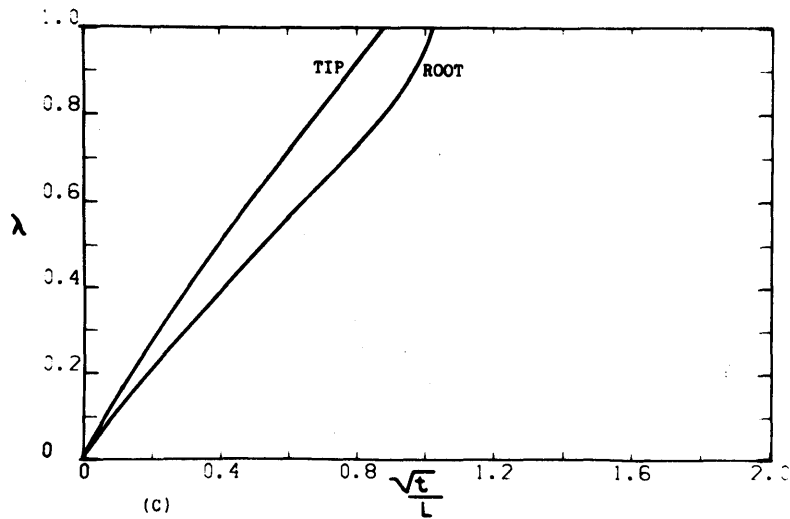
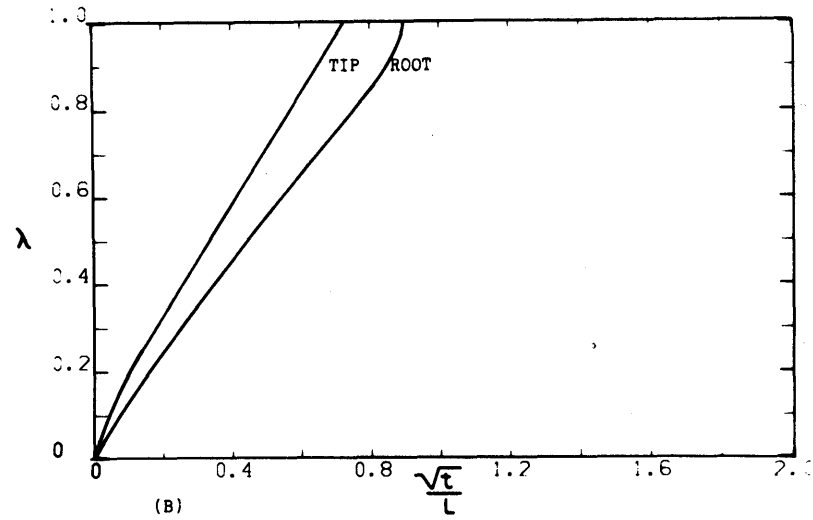
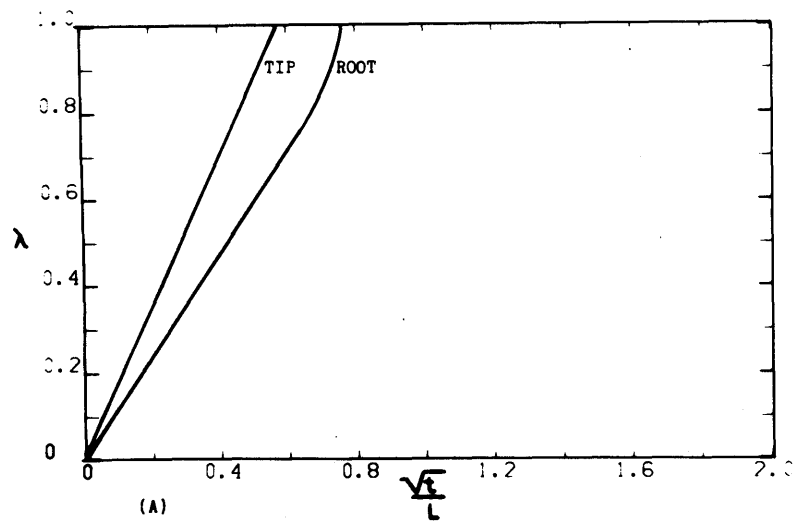


Figure 20. Position of the tip and root versus  $\sqrt{x}/L$ , Al-4.5% Cu alloy, unidirectional heat flow, no superheat,  $h_B L/\bar{K} = \infty$ , high convection, for (A) no heat input, (B)  $q'' = 1.27 \times 10^{-2}$ , (C)  $q'' = 2.54 \times 10^{-2}$ , (D)  $q'' = 5.08 \times 10^{-2}$ .

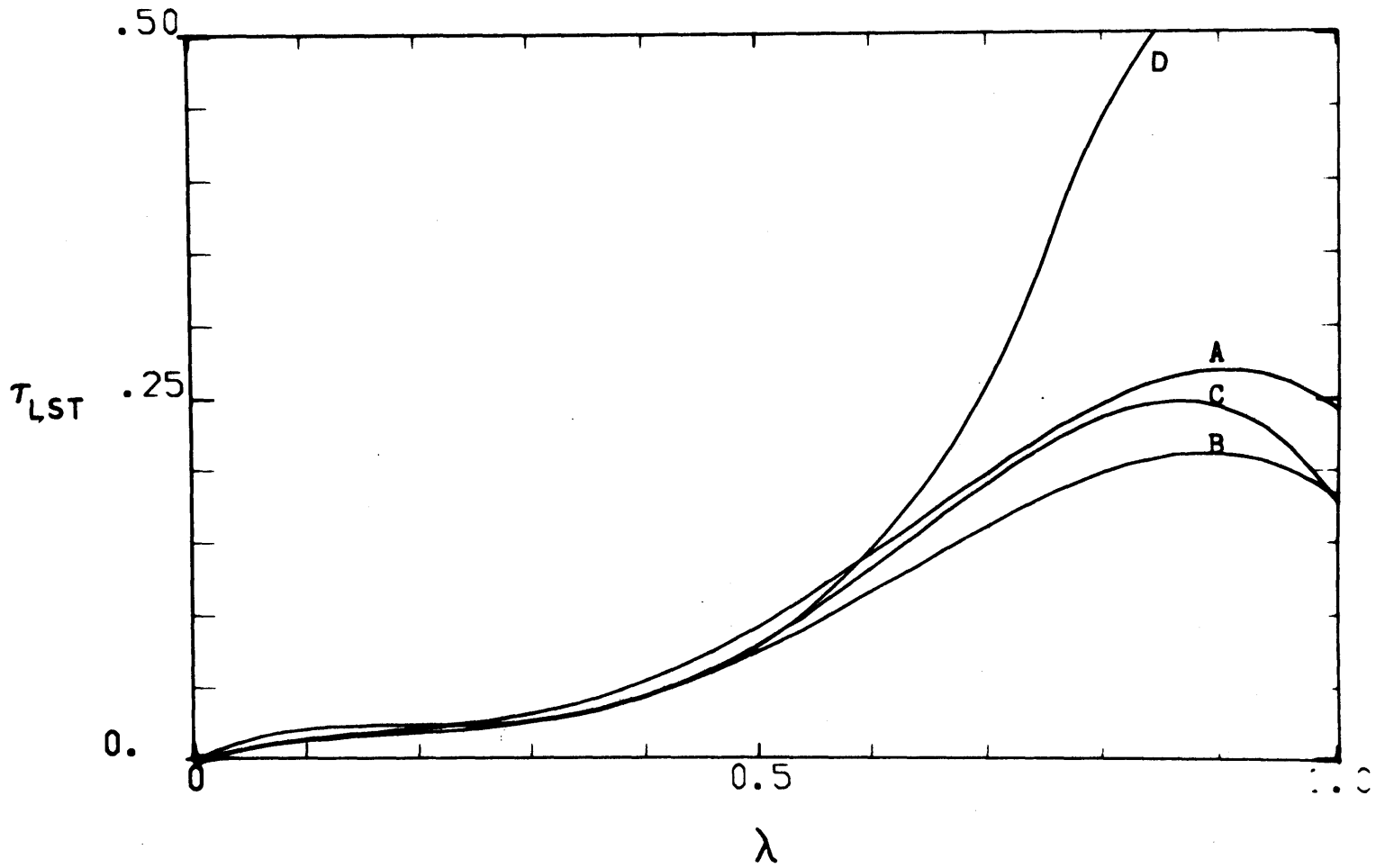
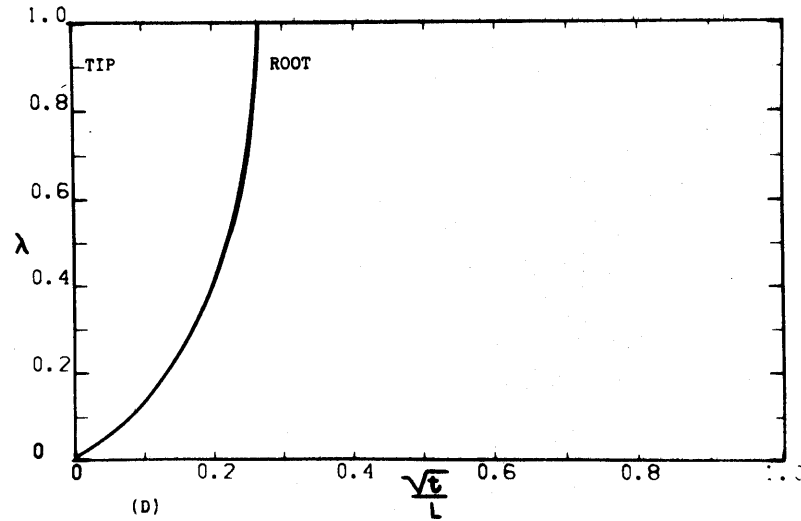
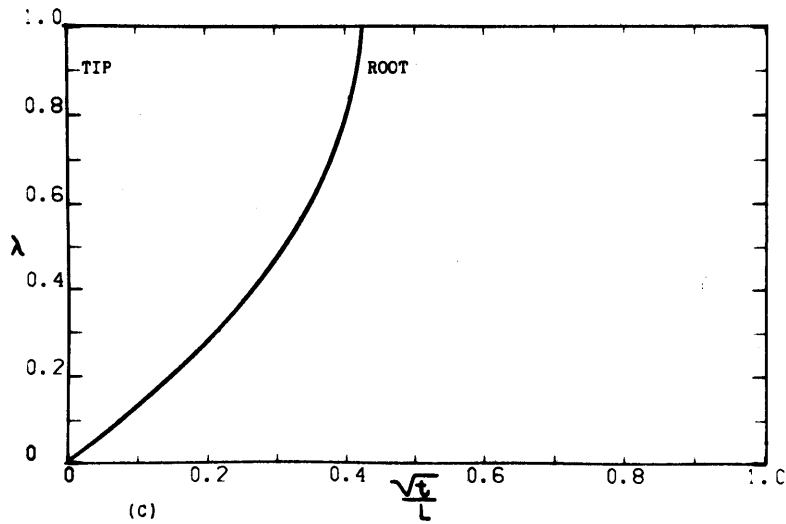
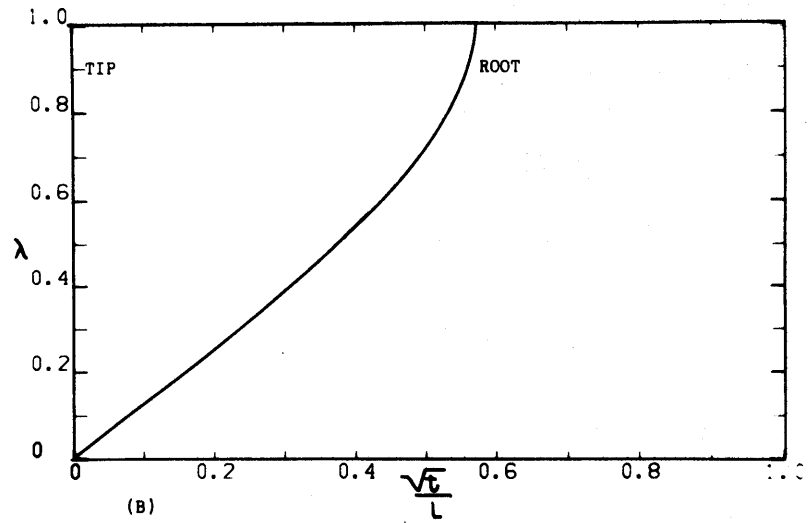
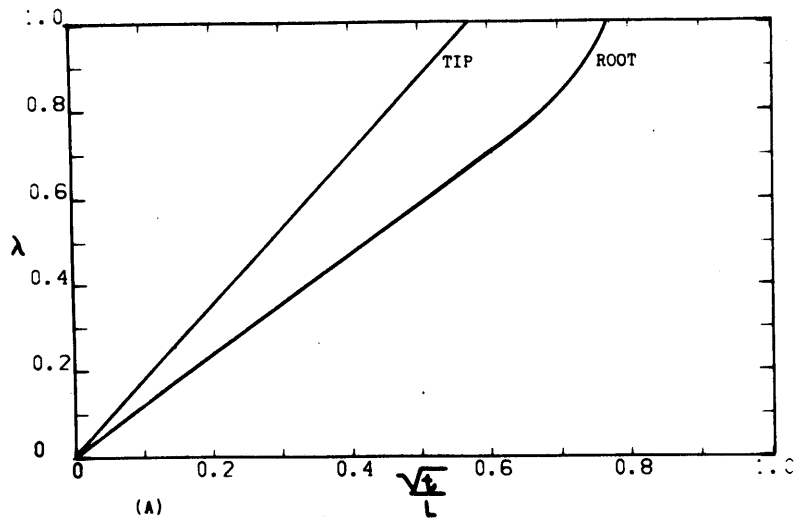
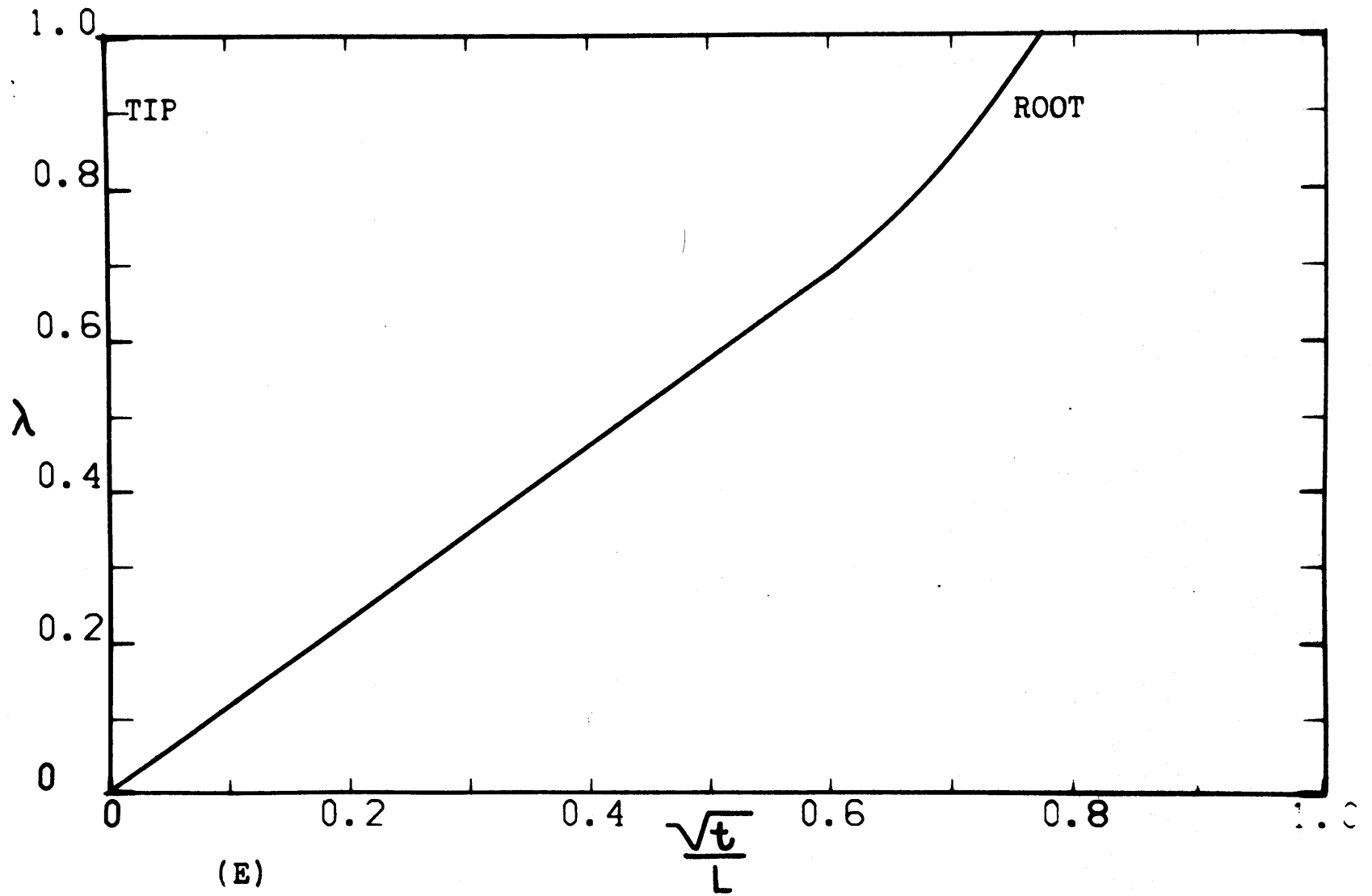


Figure 21. Local solidification time versus position, for conditions of Figure (20).

Figure 22. Position of the tip and root versus  $\sqrt{t}/L$ , Al-4.5% Cu alloy, side heat flow, no superheat,  $h_B L / \bar{K} = \infty$ , for (A) no side heat flow, (B)  $h_S L^2 / W = 0.232$ , (C)  $h_S L^2 / W = 0.696$ , (D)  $h_S L^2 / W = 2.32$ , (E)  $h_S L^2 / W > 0$  (minimum).







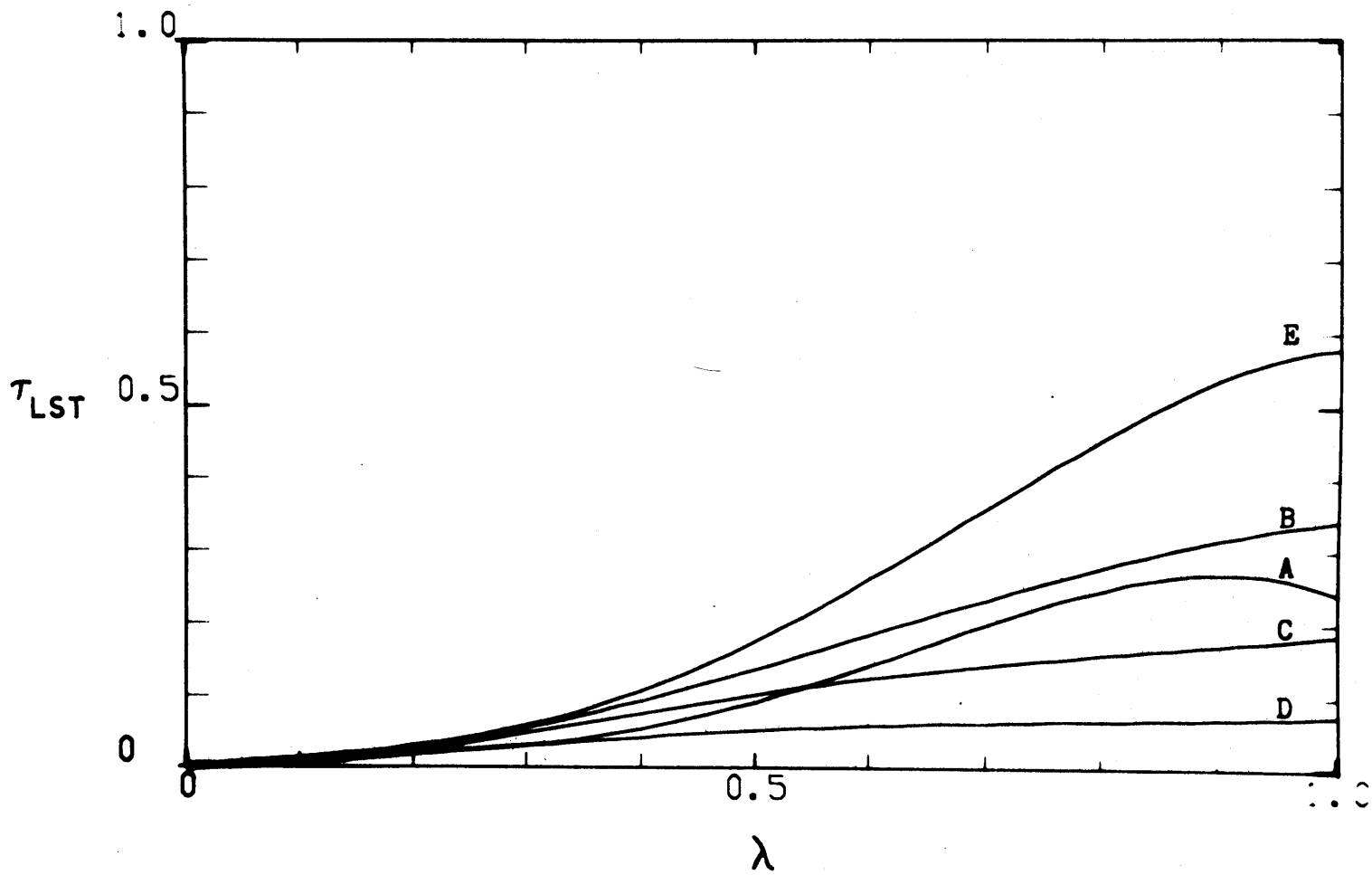


Figure 23. Local solidification time versus position, for conditions of Figure (22).

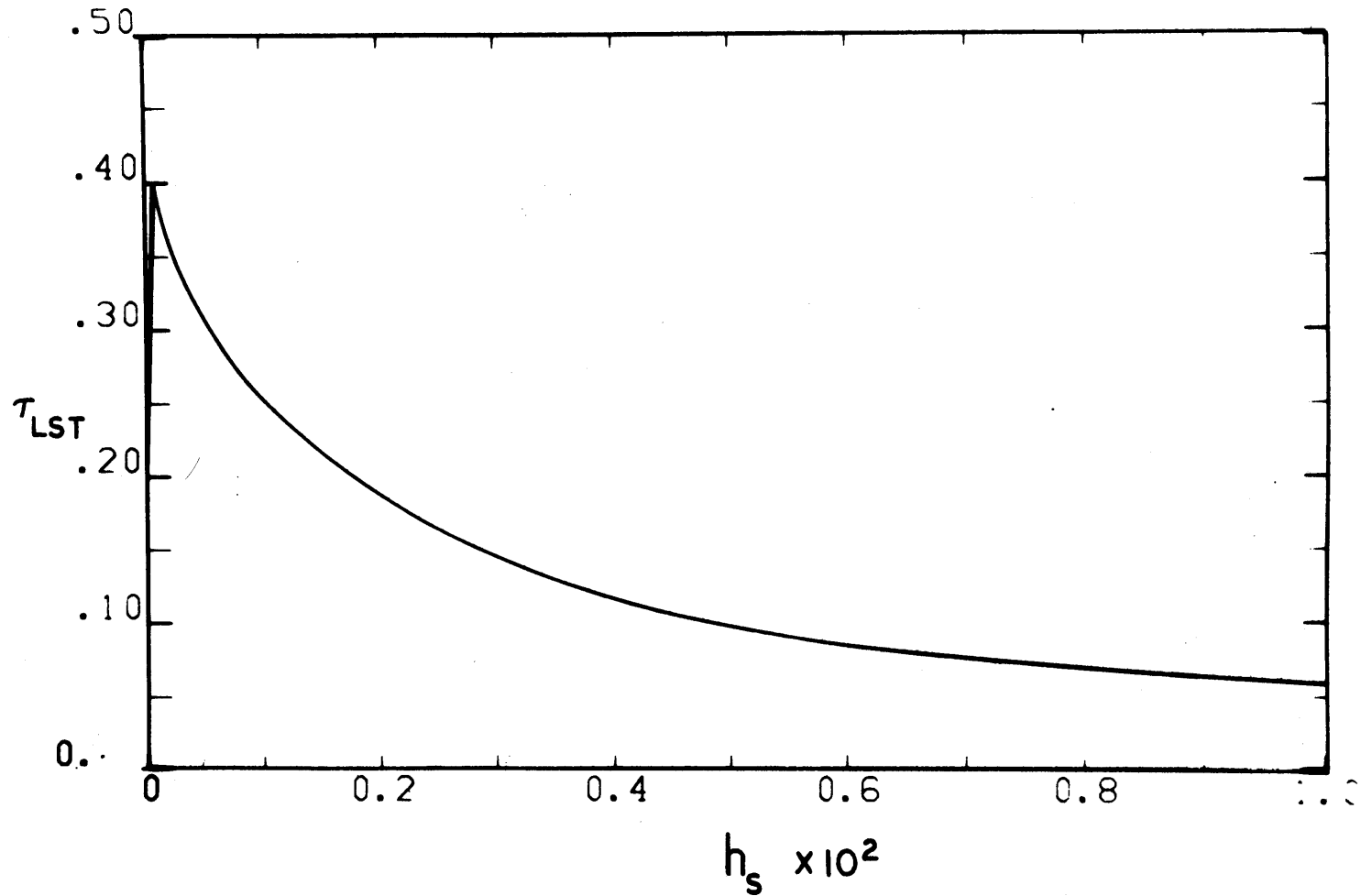


Figure 24. Local solidification time at  $\lambda = 0.75$  versus  $h_s$ , for conditions of Figure (22),  $w = 1$  cm.,  $L = 15$ .

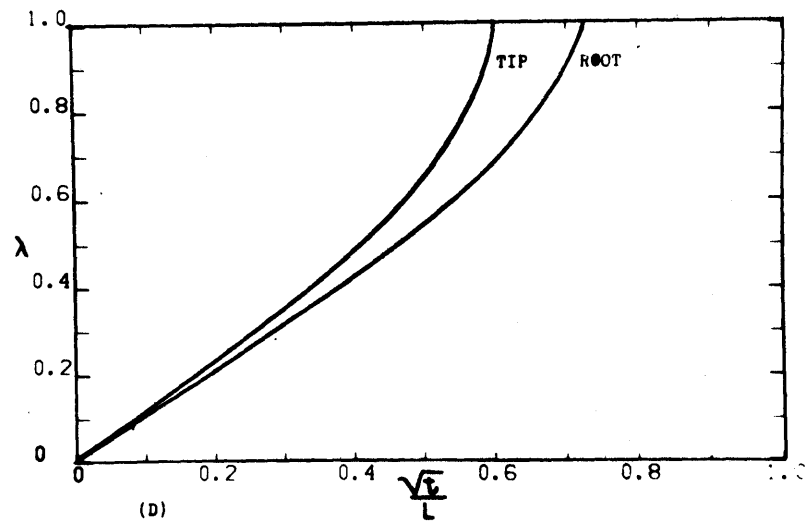
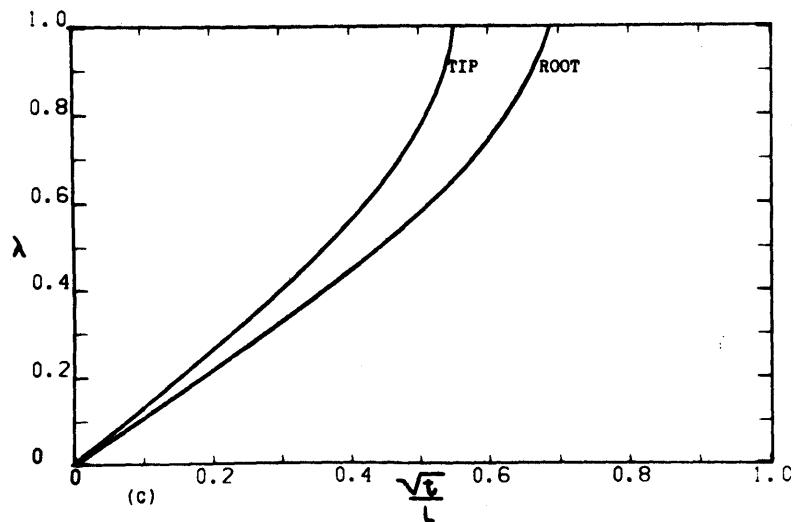
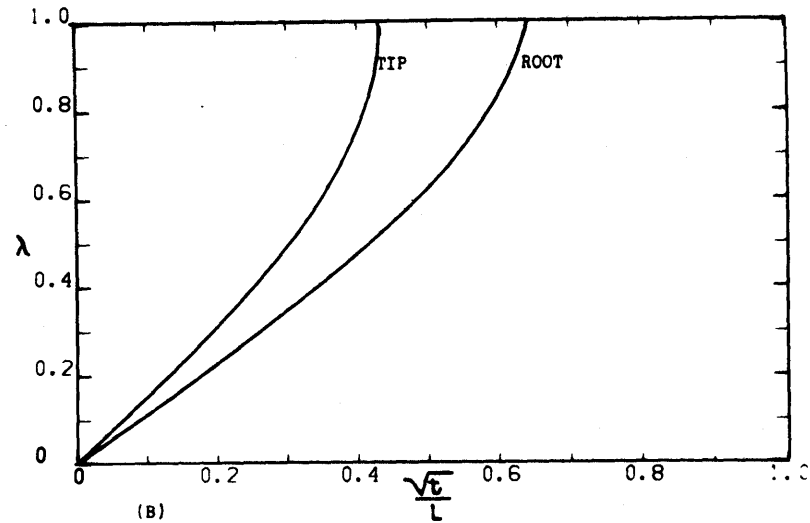
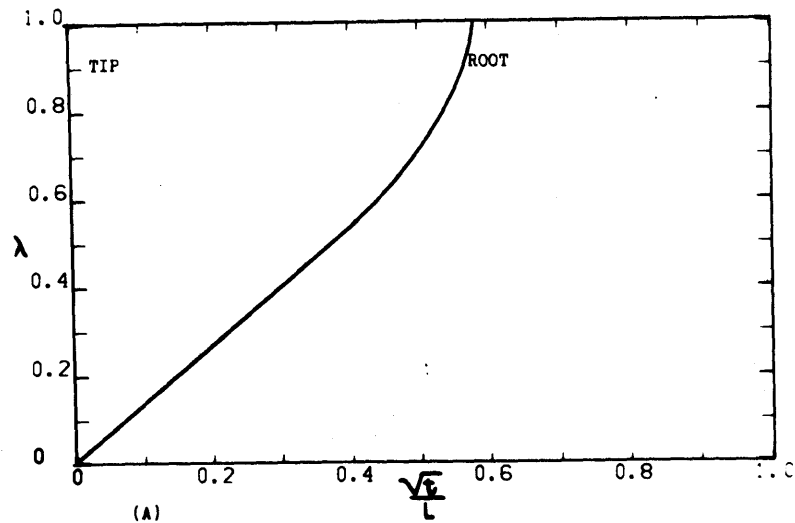


Figure 25. Position of the tip and root versus  $\sqrt{t}/L$ , Al-4.5% Cu alloy, side heat flow,  $h_S L^2/W = 0.232$ ,  $h_B L/\bar{K} = \infty$ , for (A)  $\Delta T_S = 0^\circ\text{C}$ , (B)  $\Delta T_S = 50^\circ\text{C}$ , (C)  $\Delta T_S = 150^\circ\text{C}$ , (D)  $\Delta T_S = 250^\circ\text{C}$ .

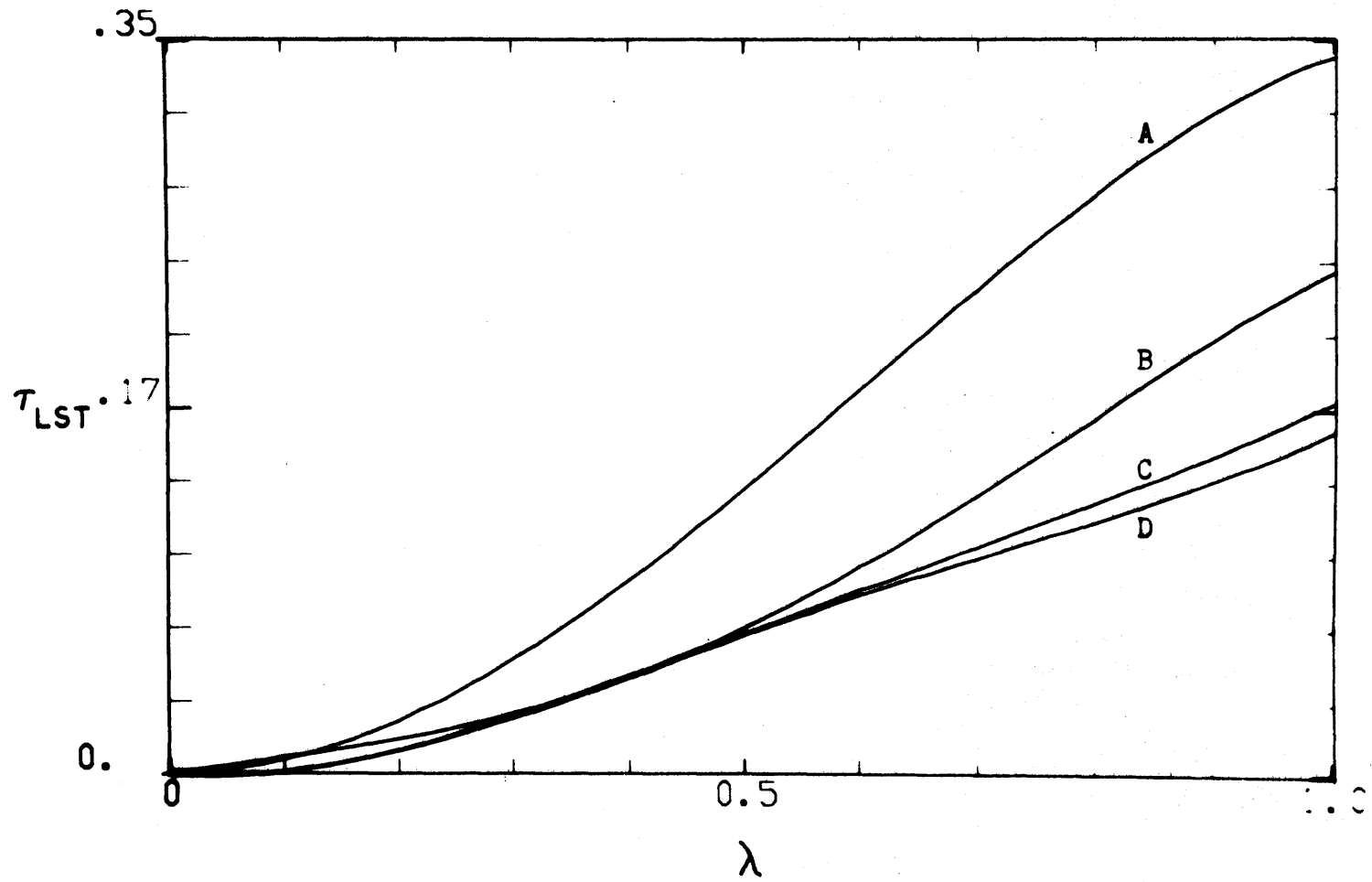


Figure 26. Local solidification time versus position, for conditions of Figure (25).

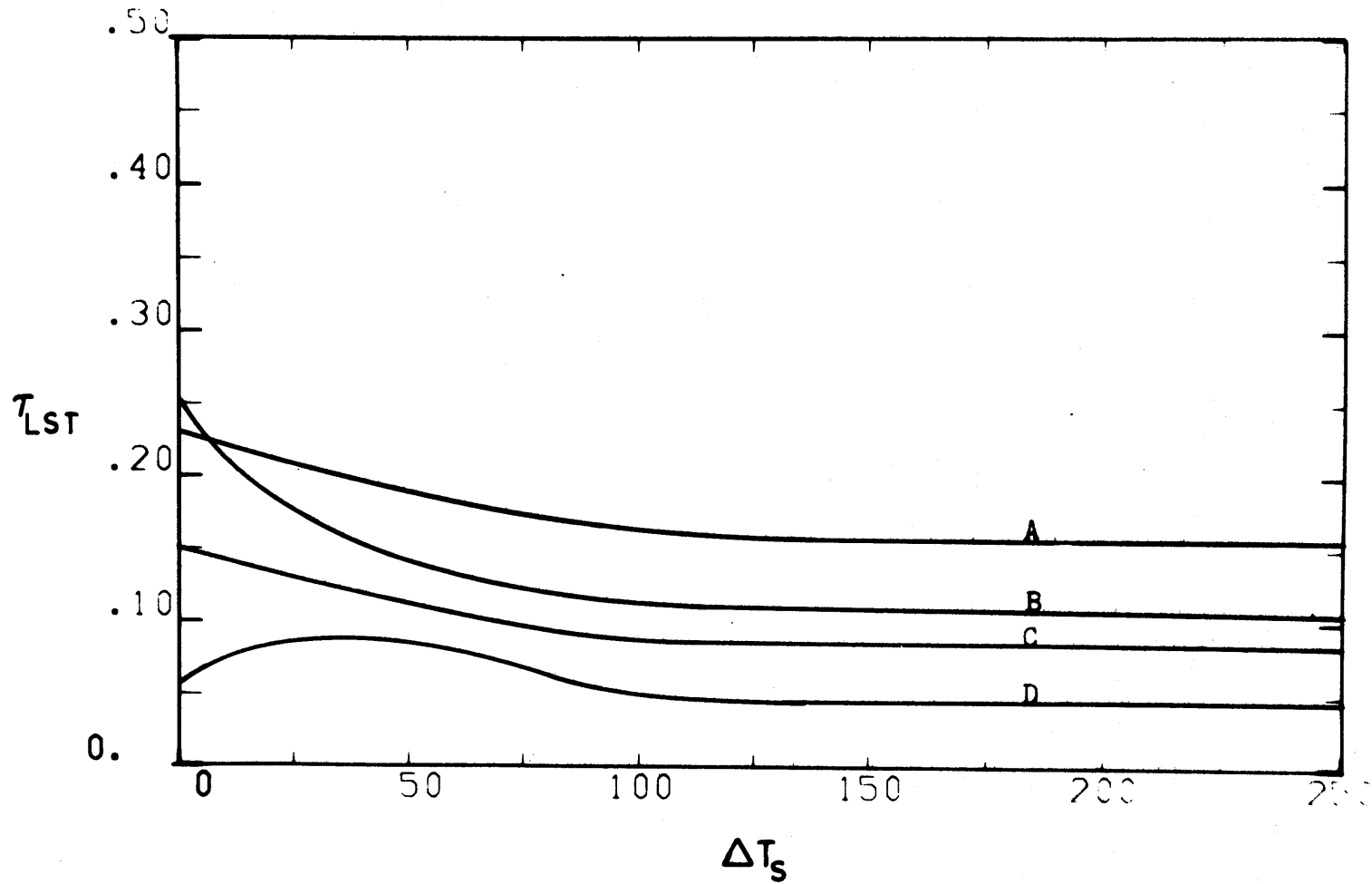


Figure 27. Local solidification time versus superheat, Al-4.5% Cu alloy, side heat flow,  $h_B L / \bar{K} = \infty$ , for (A) no side heat loss, (B)  $h_S L^2 / W = 0.232$ , (C)  $h_S L^2 / W = 0.696$ , (D)  $h_S L^2 / W = 2.32$ .

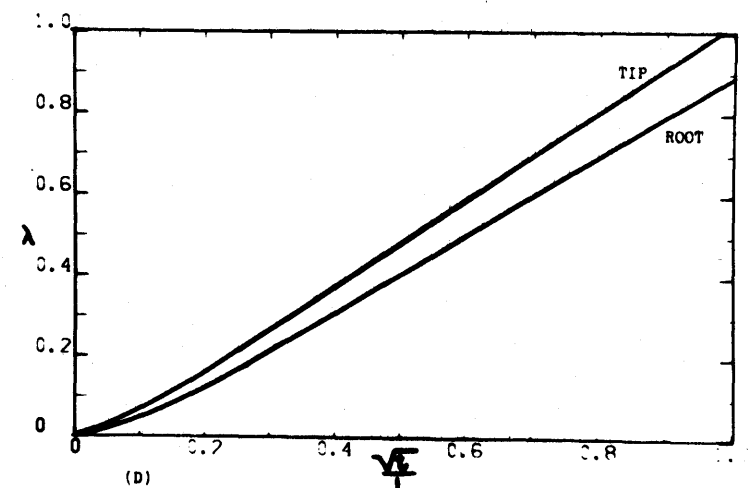
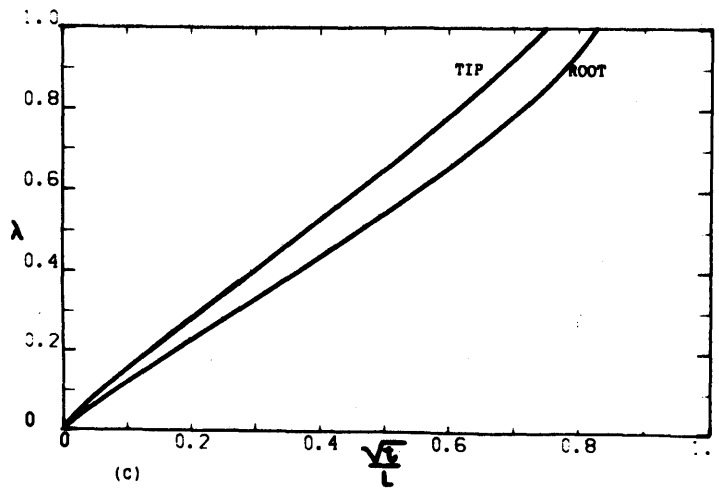
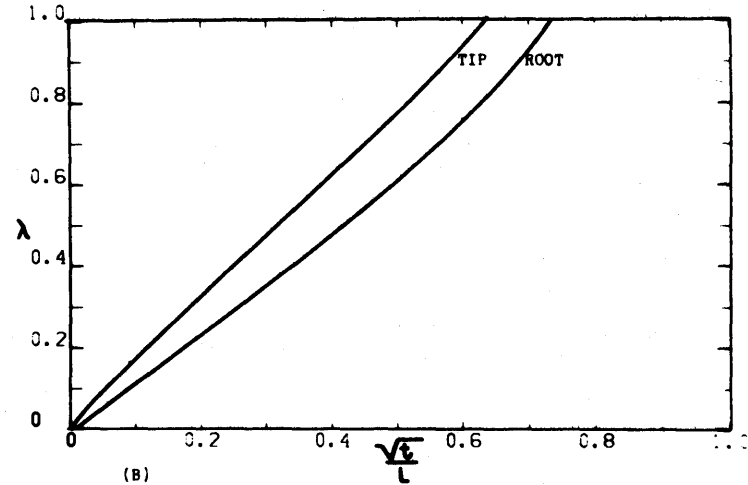
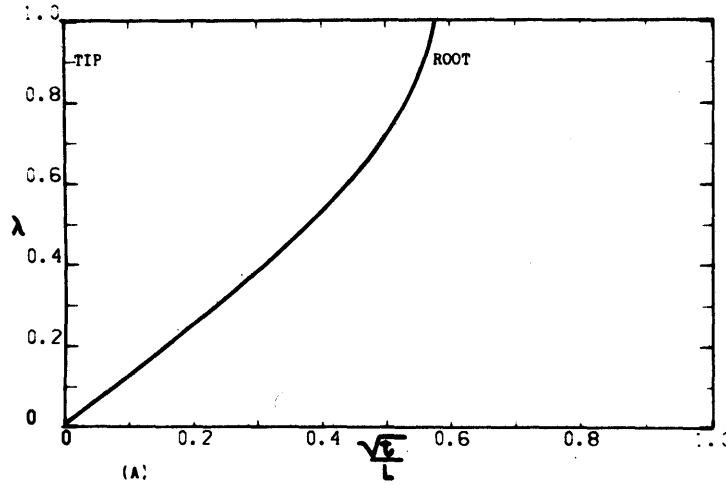


Figure 28. Position of the tip and root versus  $\sqrt{t}/L$ , Al-4.5% Cu alloy, side heat loss, high convection with heat input,  $h_b L / \bar{K} = \infty$ ,  $h_s L^2 / W = 0.232$ , for (A) no heat input, (B)  $q' = 1.27 \times 10^{-2}$ , (C)  $q' = 2.54 \times 10^{-2}$ , (D)  $q' = 5.08 \times 10^{-2}$ .

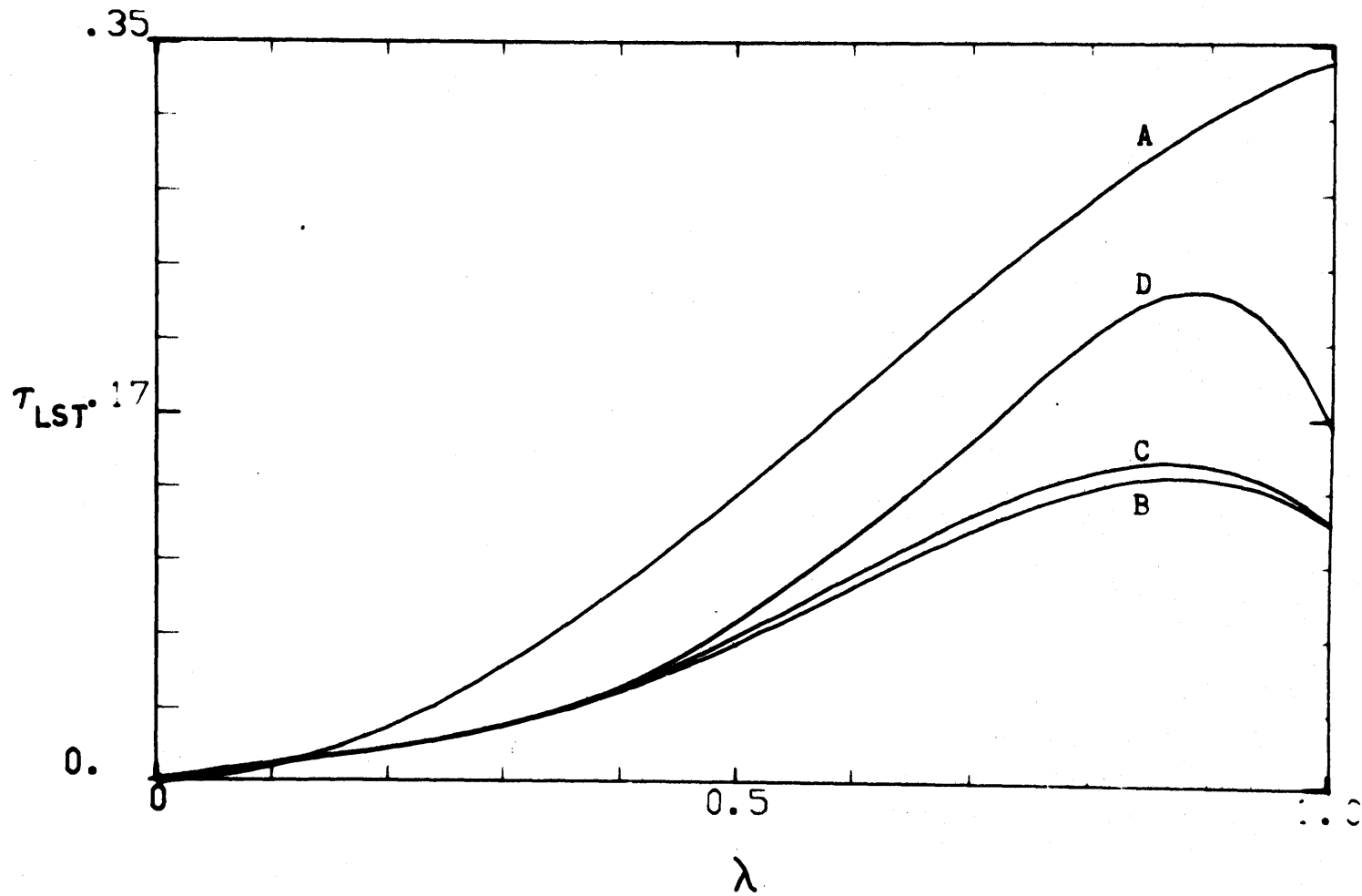


Figure 29. Local solidification time versus position, for condition of Figure (28).

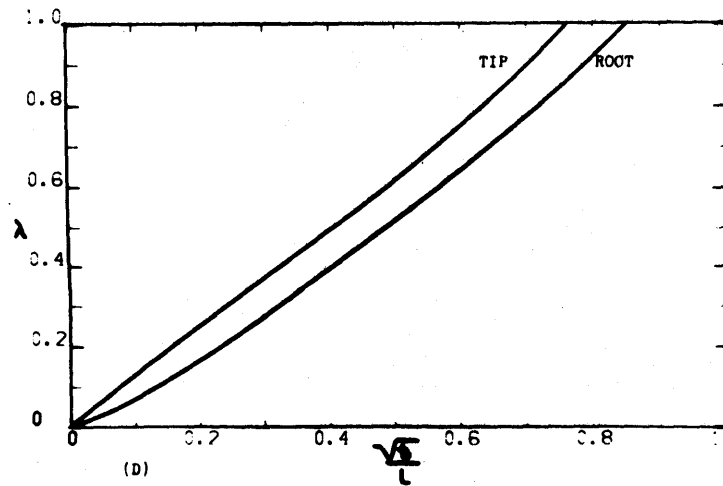
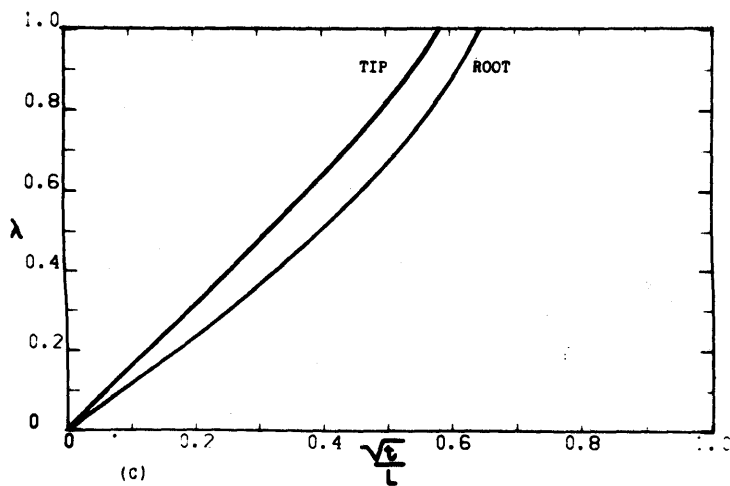
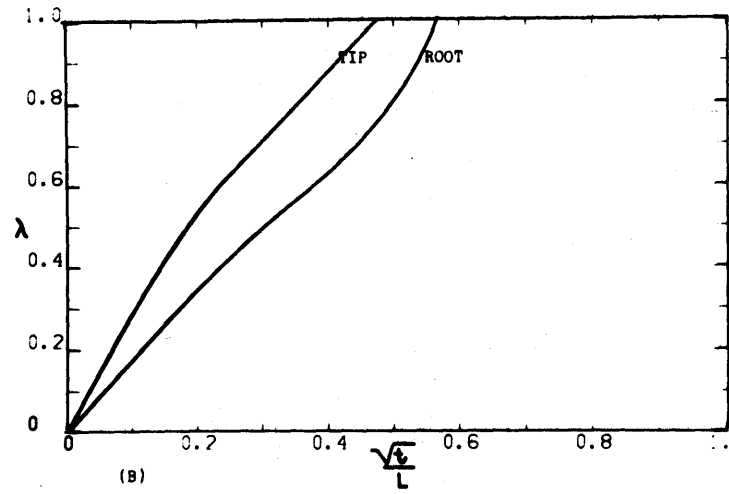
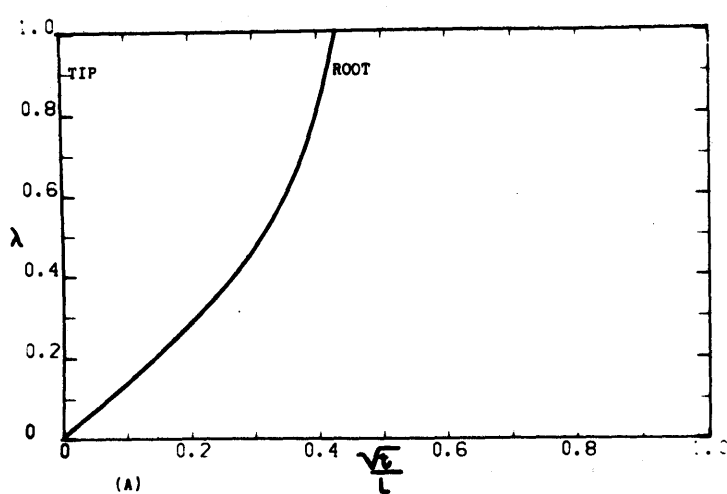


Figure 30. Position of the tip and root versus  $\sqrt{t}/L$ , Al-4,5% Cu alloy, side heat flow, high convection, heat input,  $h_B L / \bar{K} = \infty$ ,  $h_B L^2 / W = 0.696$ , for (A) no heat input, (B)  $q' = 1.27 \times 10^{-2}$ , (C)  $q' = 2.54 \times 10^{-2}$ , (D)  $q' = 5.08 \times 10^{-2}$ .



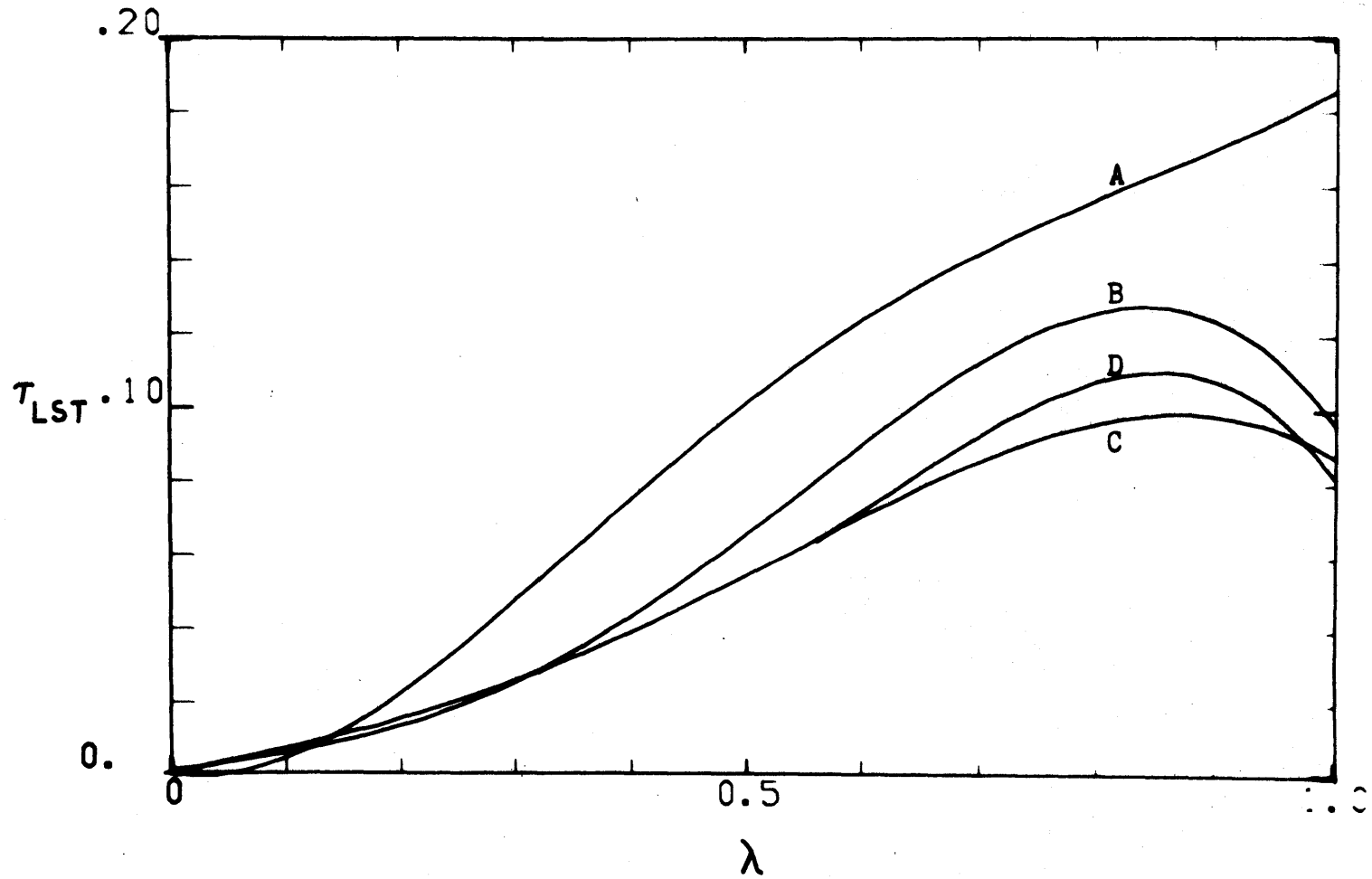


Figure 31. Local solidification time versus position, for conditions of Figure (30).

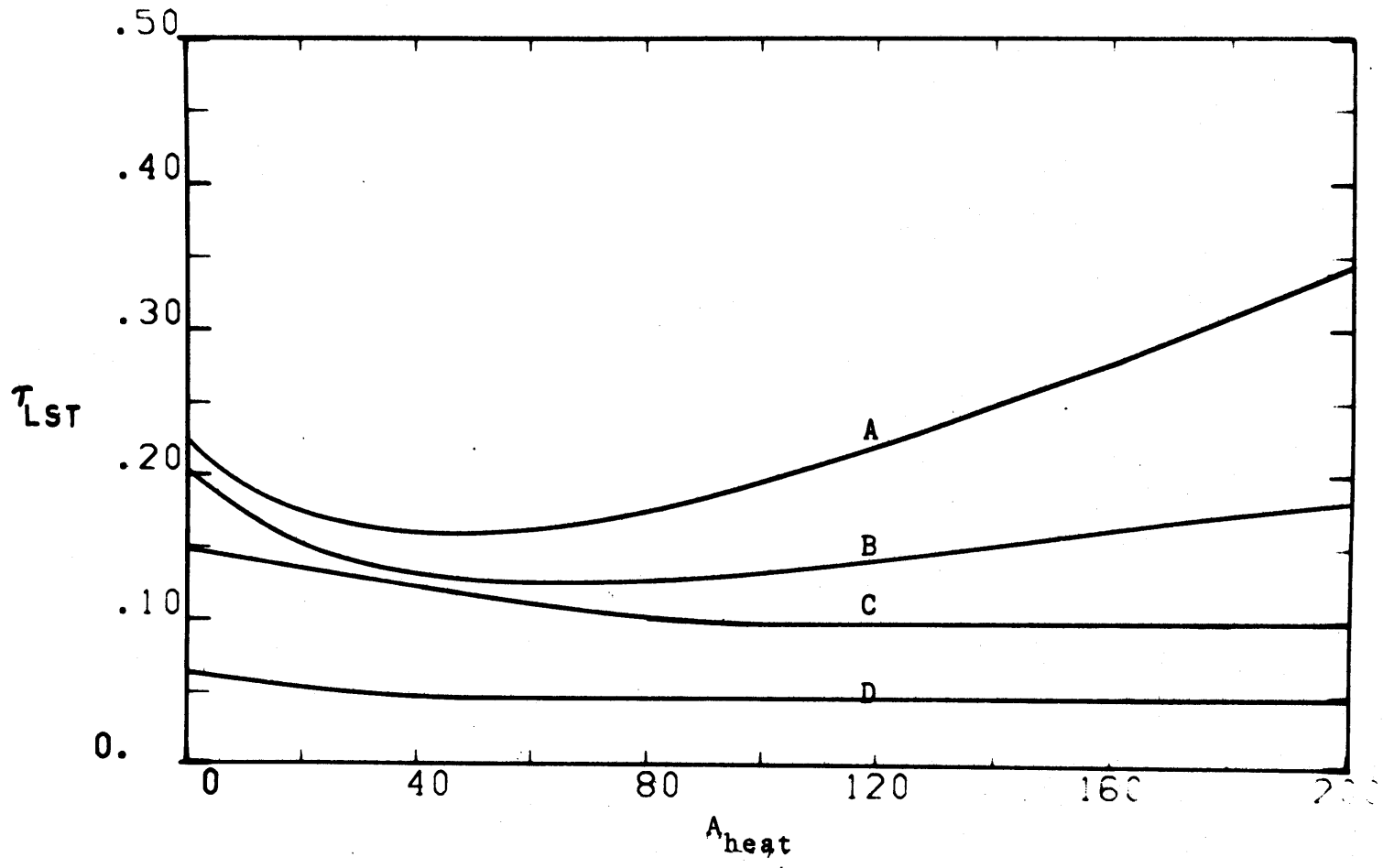


Figure 32. Local solidification time at  $\lambda = 0.75$  versus heat input, side heat flow, high convection, no superheat,  $h_B L / \bar{K} = \infty$ , for (A)  $h_S L^2 / W = 0$ , (B)  $h_S L^2 / W = 0.232$ , (C)  $h_S L^2 / W = 0.696$ , (D)  $h_S L^2 / W = 2.32$ .

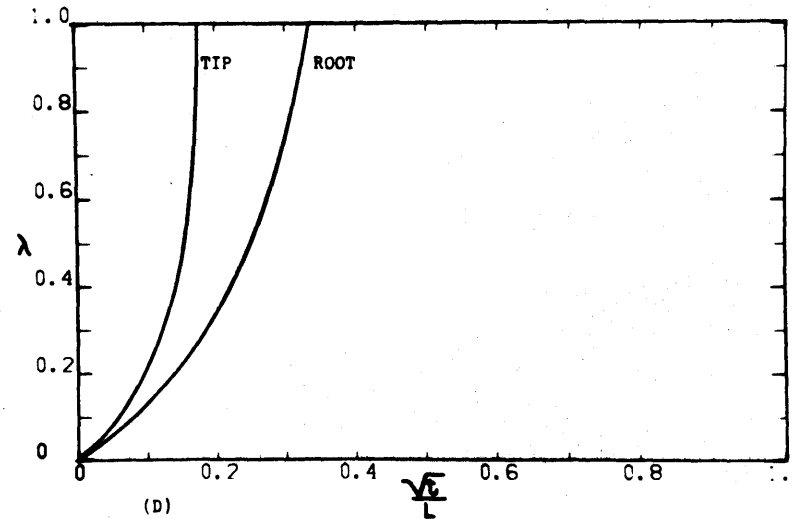
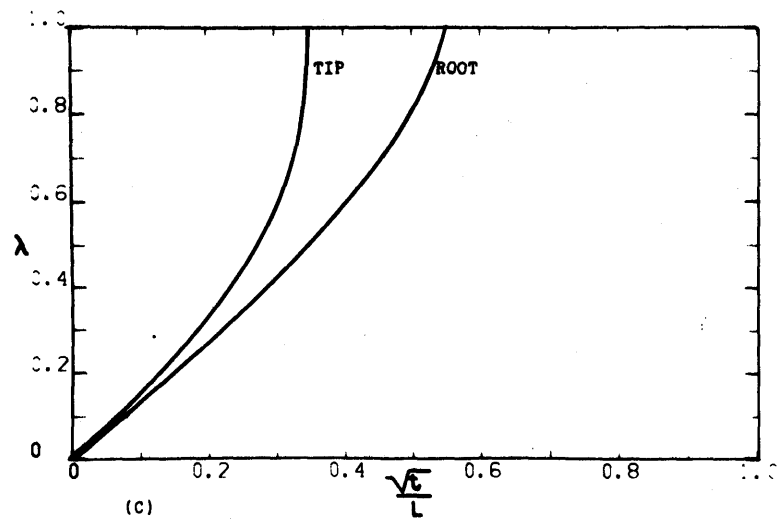
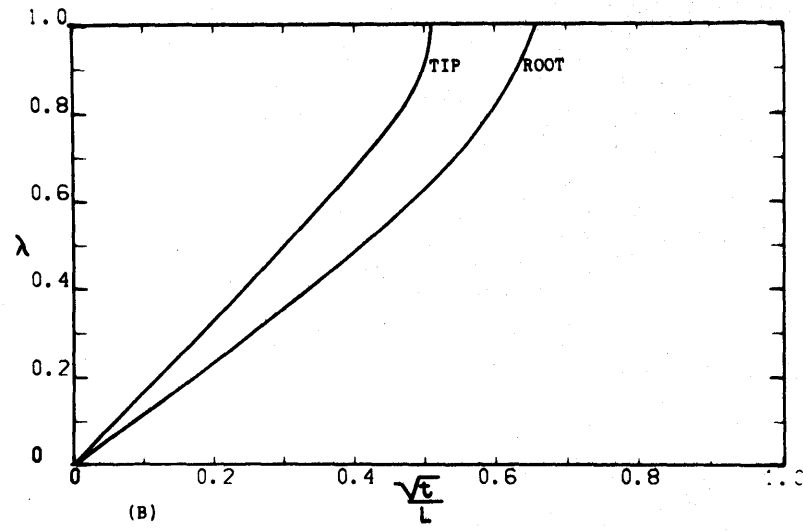
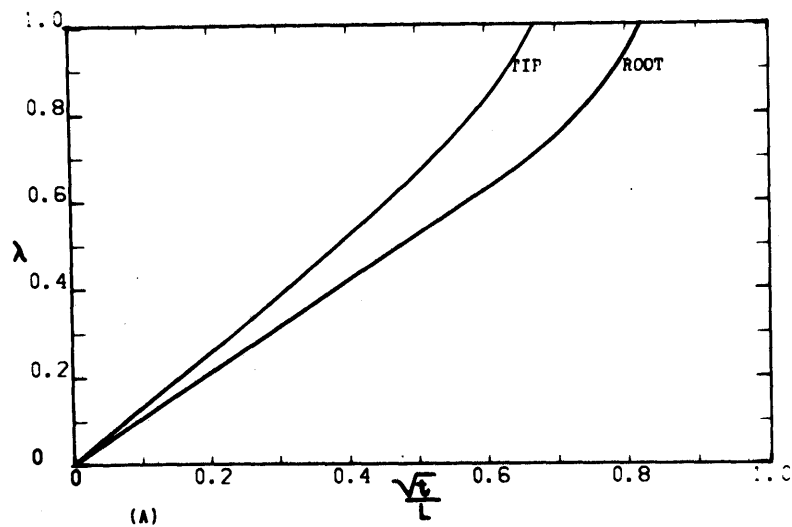


Figure 33. Position of the tip and root versus  $\sqrt{t}/L$ , Al-4.5% Cu alloy, parabolic side heat flow,  $h_B L / \bar{k} = \infty$ ,  $T_S = 150^\circ\text{C}$ , for (A)  $aL/W = 0$ , (B)  $aL/W = 68$ , (C)  $aL/W = 136$ , (D)  $aL/W = 272$ .

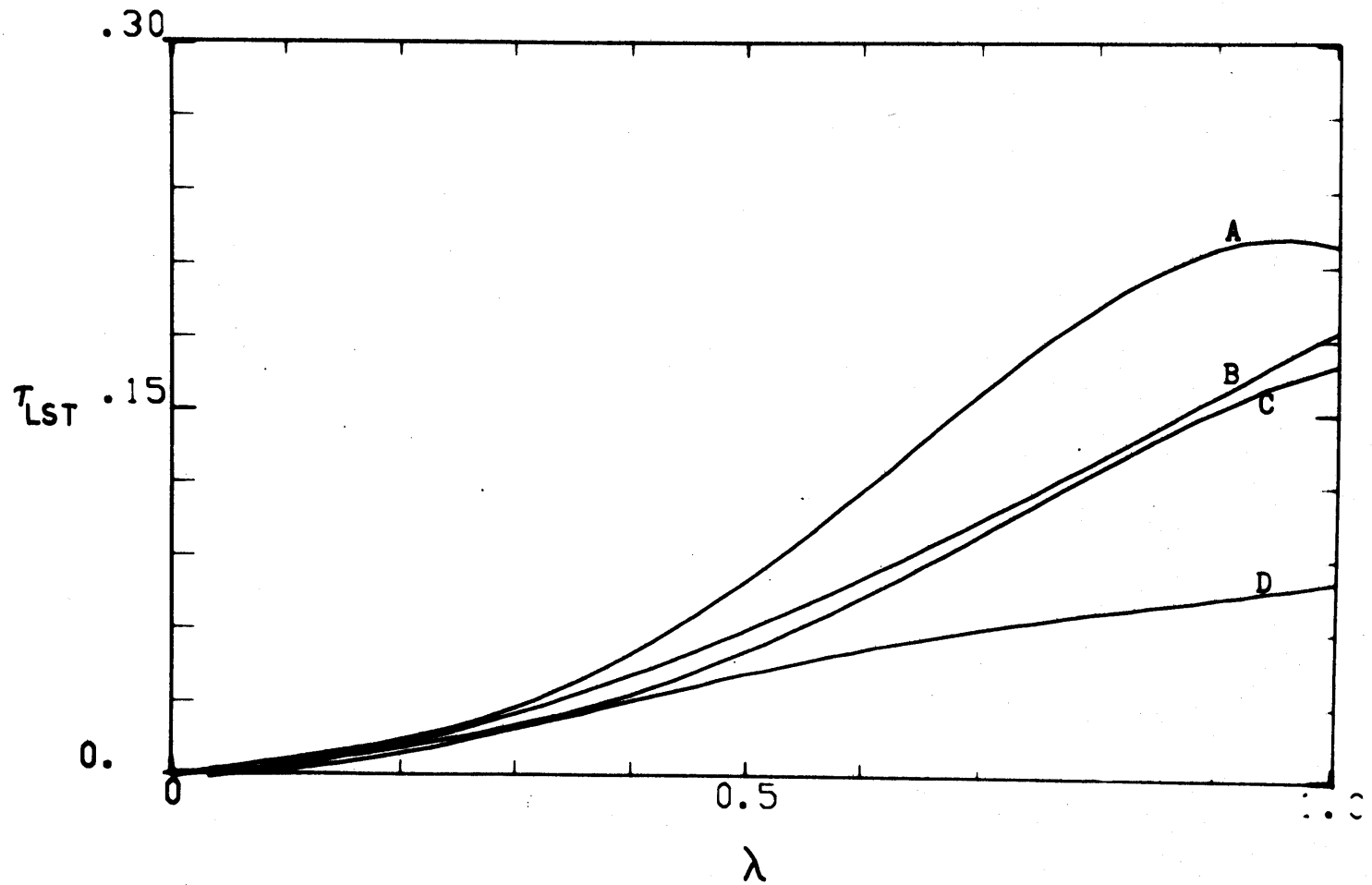


Figure 34. Local solidification time versus position, for conditions of Figure (33).

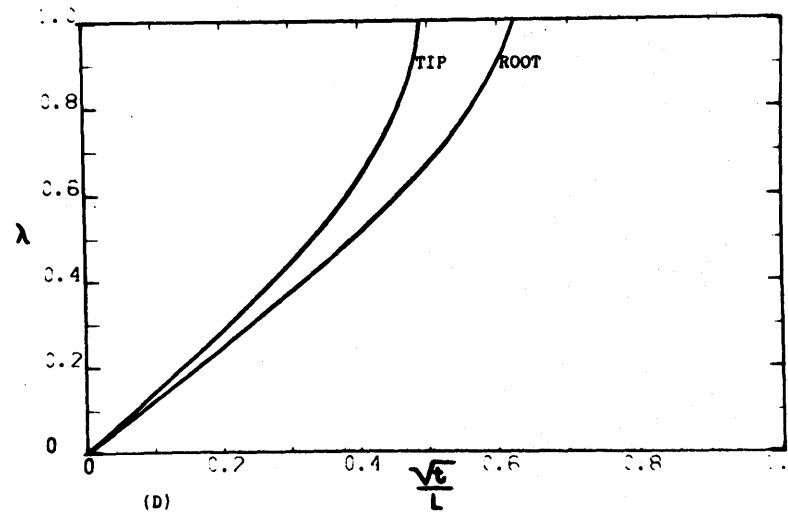
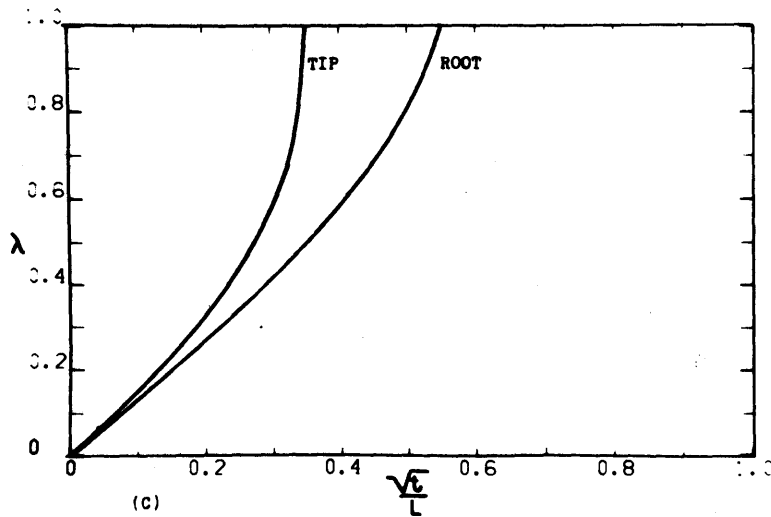
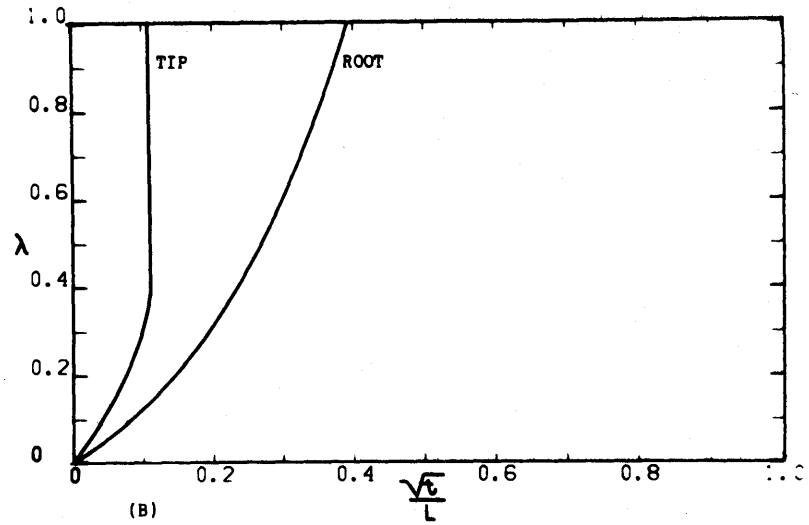
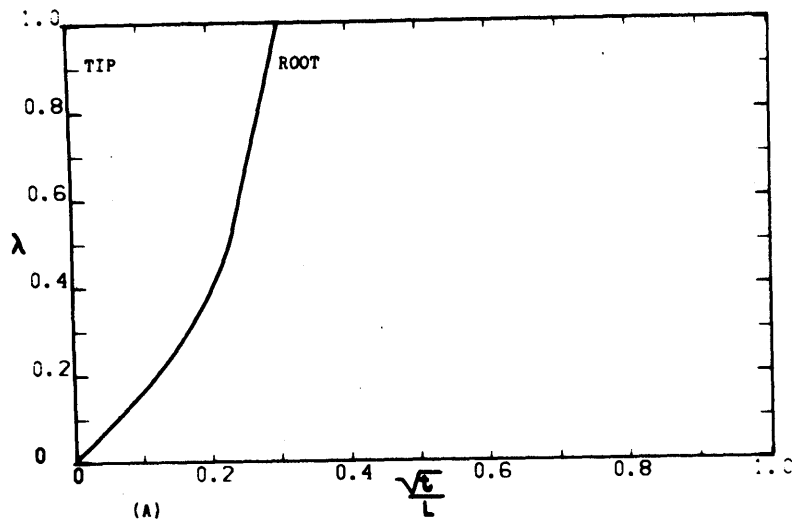


Figure 35. Position of the tip and root versus  $\sqrt{t}/L$ , Al-4.5% Cu alloy, parabolic side heat flow,  $h_B L / \bar{K} = \infty$ ,  $aL/W = 136$ , for (A)  $\Delta T_S = 0$ , (B)  $\Delta T_S = 50^\circ\text{C}$ , (C)  $\Delta T_S = 150^\circ\text{C}$ , (D)  $\Delta T_S = 250^\circ\text{C}$ .

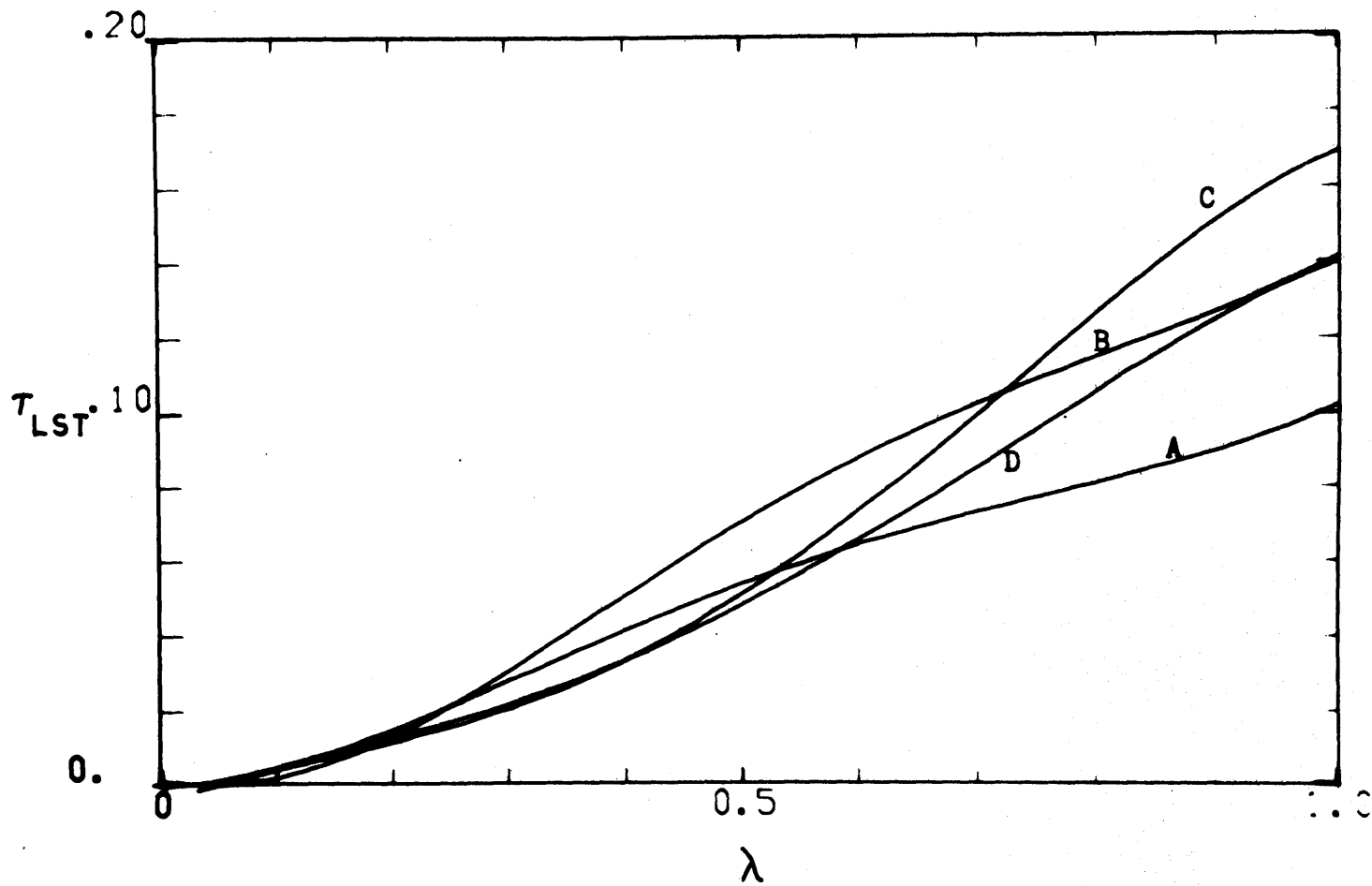


Figure 36. Local solidification time versus position, for conditions of Figure (35).

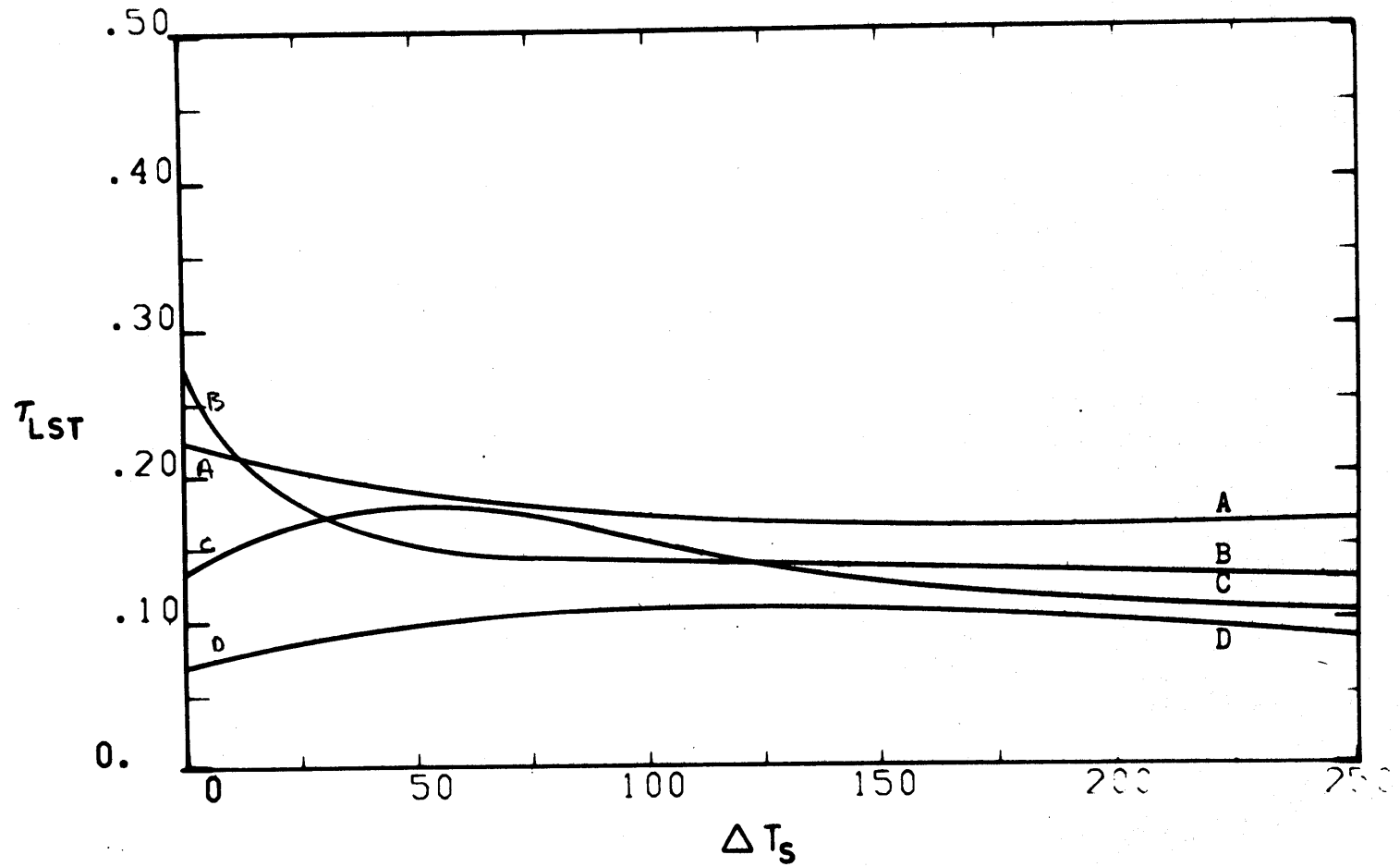


Figure 37. Local solidification time at  $\lambda = 0.75$  versus superheat, Al-4.5% Cu alloy,  $h_B L / \bar{K} = \infty$ , no convection, for (A)  $aL/W = 0$ , (B)  $aL/W = 24$ , (C)  $aL/W = 75$ , (D)  $aL/W = 136$ .

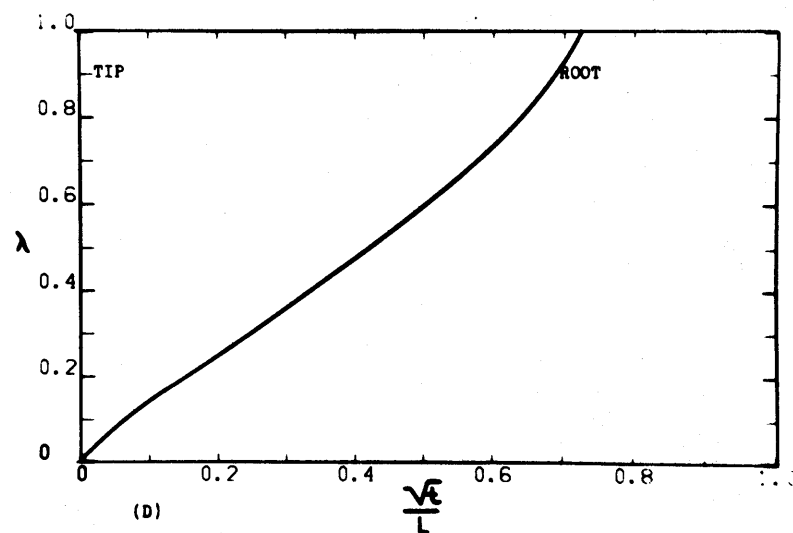
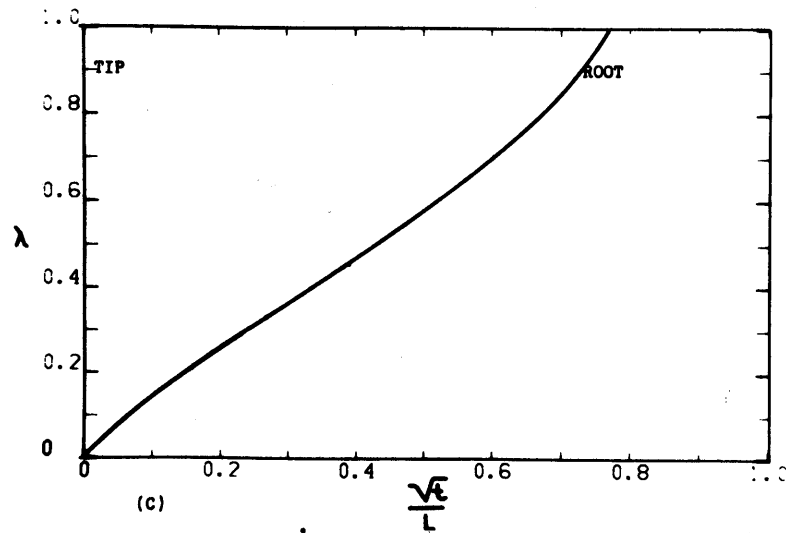
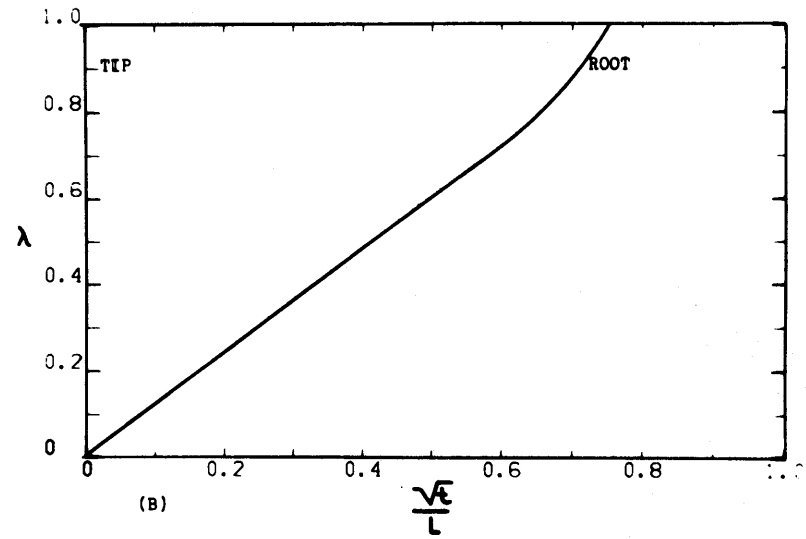
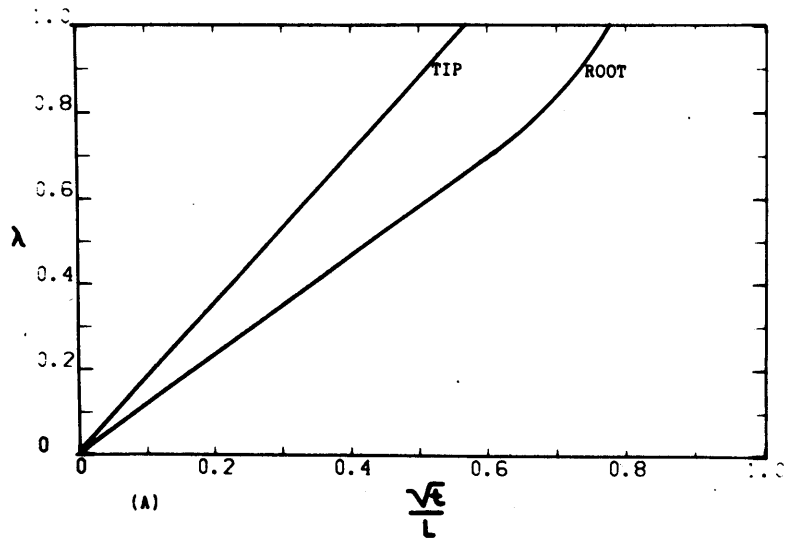


Figure 38. Position of the tip and root versus  $\sqrt{t}/L$ , Al-4.5% Cu alloy, equiaxed growth, high convection,  $h_B L / \bar{K} = \infty$ , no superheat, for (A) no convection, (B) critical fraction solid ( $f_{SC}$ ) = 0.15, (C)  $f_{SC}$  = 0.30, (D)  $f_{SC}$  = 0.45.



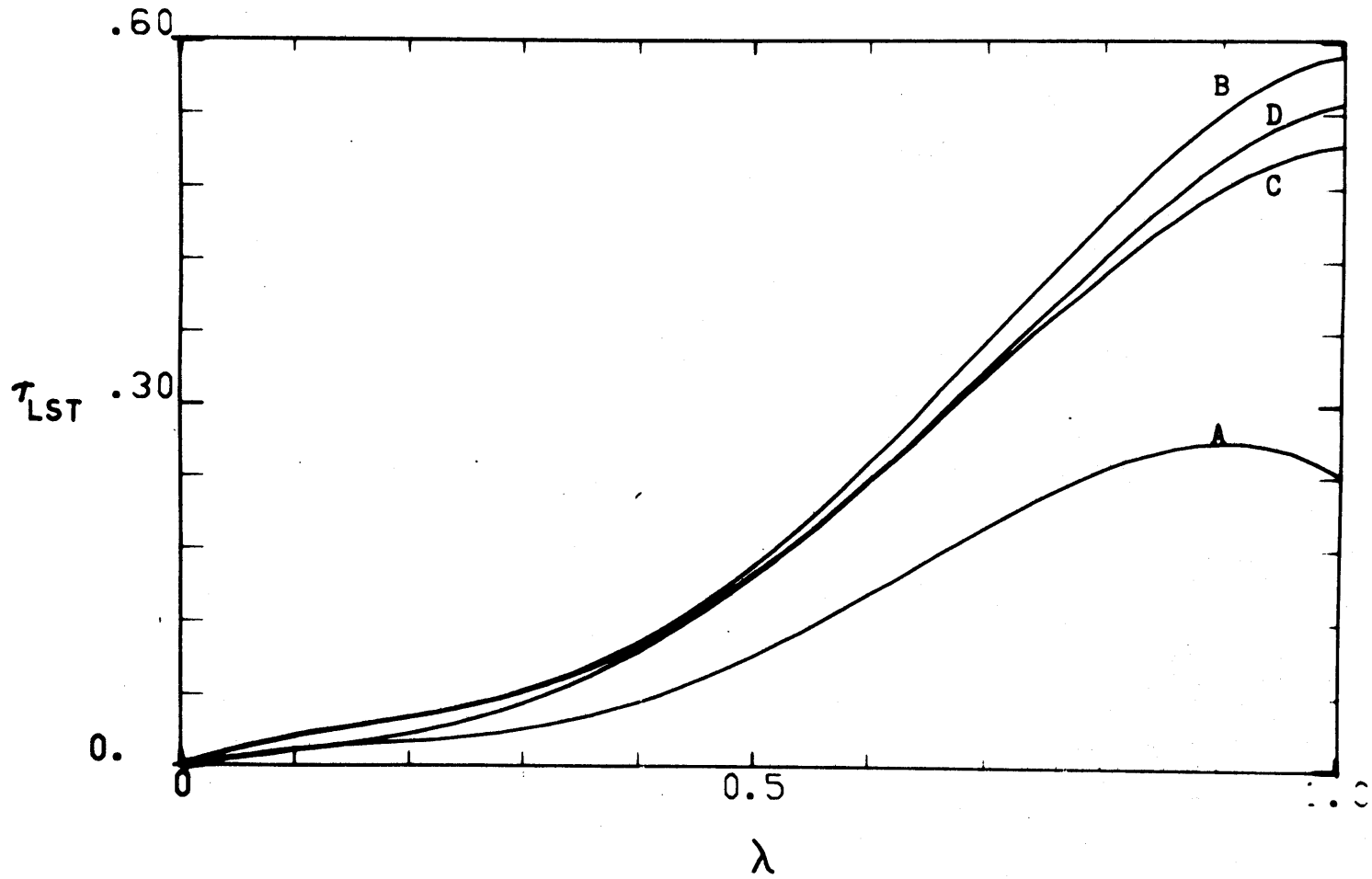


Figure 39. Local solidification time versus position, for conditions of Figure (38).

## Chapter III

## DISCUSSION

A. General; Effects on Local Solidification Time of h, Superheat, Convection and Geometry

The results presented in the previous section represent a survey of the characteristics of alloy solidification for several important variables; geometry, convection, superheat, heat transfer rate at the surface, and heat loss in two dimensions. To the engineer, the effect that each of these variables can have on the "local solidification time,"\* and therefore on the dendrite arm spacing of the final cast structure is important. From these results, several methods for reducing or controlling the local solidification time are evident. These will be reviewed here.

For the unidirectional solidification of plates, with no convection, superheat lowers local solidification time. Figure 13 shows that  $\tau_{1st}$  at  $\lambda = .85$  is reduced from 0.27 at  $0^{\circ}\text{C}$  superheat to 0.24 at  $50^{\circ}\text{C}$  to 0.22 at  $250^{\circ}\text{C}$ . In general, the presence of a positive gradient of temperature in front of the dendrite tips\*\* causes the velocity of the tip to be retarded to a greater extent than the root velocity (the mushy

---

\* "Local solidification time" is defined as the time at a given location in a casting or ingot elapsing between passage of the "start of freeze" isotherm and the "end of freeze" isotherm.

\*\* The term dendrite "tips" is used herein as a short hand designation for "start of freeze" isotherm. The term dendrite "roots" is designation for "end of freeze" isotherm. See note on page 9. The actual structure in the mushy zone may be columnar, in which case the terms, dendrite "tips" and "roots" have direct and intuitive physical significance. More often, the structure is equiaxed as in Figure 5, in which case the terms "start of freeze" and "end of freeze" isotherms more accurately convey the physical reality.

region width at a given time is shortened), and the overall effect of this is to reduce the local solidification time.

The effect of the heat transfer coefficient on  $\tau_{1st}$  depends on the value of  $hL/\bar{K}$ . For values of  $hL/\bar{K} > 1$ , the solidification is controlled by thermal diffusion through the metal, and  $\tau_{1st}$  is not affected significantly. For values of  $hL/\bar{K} < .1$ , the heat flow and therefore solidification is controlled by the heat flow across the chill interface, according to the equation (R3). For intermediate values,  $5 > hL/\bar{K} > .1$ , Figure 15 shows that  $\tau_{1st}$  is strongly affected by  $h$ , with an order of magnitude drop in  $h$  from .1 to .01 producing an order of magnitude rise in  $\tau_{1st}$  at  $\lambda = .75$  from .38 to 3.4.

For radial solidification, the effects of superheat and the heat transfer coefficient on local solidification time are qualitatively the same as for unidirectional solidification. However, a comparison of radial versus unidirectional heat flow shows that for a given superheat, and heat transfer coefficient,  $\tau_{1st}$  at a given distance from the chill is always lower for radial geometry. For example, at  $0^{\circ}\text{C}$  superheat,  $h = \infty$ ,  $\tau_{1st}$  at  $\lambda = .85$  is 0.1 for the radial case, and  $\tau_{1st}$  at  $\lambda = .85$  is 0.27 for the unidirectional case. This is due to the higher cooling rate which is caused by heat flowing in more than one direction.

For a case in which heat flows in two directions linearly, i.e., the side heat loss examples in the Results section, the effect on  $\tau_{1st}$  is quite marked. For example,

at  $0^{\circ}\text{C}$  superheat,  $h = \infty$  at the chill,  $\tau_{1st}$  at  $\lambda = .85$  is 0.27 for no side heat loss, and with side heat loss,  $h_s L^2/W = 2.32$ ,  $\tau_{1st}$  at  $\lambda = .85$  is 0.08. Sidewise heat loss has two separate effects; (1) the width of the mushy region is increased, and thus can lead to problems of macrosegregation, hot tearing and feeding defects, and (2) the local solidification time at a given position is increased if the loss of heat causes the tip to be affected much more than the root (low values of side heat loss, Figure 24), but for high values of side heat loss the local solidification time is greatly decreased. In general the results of the radial and side heat loss studies show that one method for the reduction of local solidification times in the casting or large ingots is to design a mold with as small a characteristic distance (half-width of a plate, length, or radius of a cylinder) as possible, and to attain as much multi-dimensionality to the heat flow as possible.

Another implication of the results of the previous section for the practice of casting large ingots, especially sand castings, is clear. If a high degree of convection is present during the pouring and early stages of solidification in these castings, most or all of the superheat will be removed before solidification starts, with the result that the local solidification times obtained will be much higher than they would be if either (1) the

convection could be retained, so that the superheat would be present during solidification, or (2) this convection could be used to carry an artificial superheat, in the form of heat input, into the convecting melt to the dendrite tips. Results in the previous section support the conclusion that either of these methods would work to reduce the local solidification time.

#### B. Fraction Liquid and Cooling Curves

Another way of looking at the way in which the dendrite arm spacing at a given point in a casting is affected by geometry, convection, and two-dimensionality of heat flow is to consider the rate of solid formation at a given point as a function of time. Figures 40, 41 and 42 present the fraction liquid (or 1.-fraction solid) and the dimensionless temperature versus reduced solidification time (the time from the start of solidification to the finish, normalized to 1) for a position  $\lambda = 0.5$ , for four typical cases: (1) no convection, columnar, unidirectional growth; (2) no convection, columnar, radial growth; (3) high convection, equi-axed unidirectional growth, and (4) no convection, equi-axed, two-dimensional growth (side heat loss). In all cases, the heat transfer rate at the chill was infinite, and there was no superheat at the start of solidification.

The information which these curves reveal is more than that obtained from the simple consideration of local

solidification time. Specifically, the local solidification time at a given point in an ingot has been shown to be a good measure of what the final dendrite arm spacing will be, (3,5) and for most of the interpretation of the results presented here, the local solidification time alone has and will be used as the indicator of what the dendrite arm spacing will be. It should always be true that if the local solidification time at a given position can be reduced, the dendrite arm spacing will also be reduced. What these fraction liquid curves indicates is a different kind of information, which is important as several other areas of solidification behavior are considered, namely, the effect on microsegregation, hot tearing, and macrosegregation. Research in these areas has indicated that the length of time which a point in an ingot spends at a particular fraction liquid, or between a certain range of fractions liquid is very important to the final morphology of the dendrites and to the final distribution of solute in the interdendritic region and across the length of the casting. A detailed analysis of the implications of the results presented in Figures 40, 41 and 42 is beyond the scope of the present work, rather, a general description is more germane.

The characteristics of these curves are: (1) the slope at time  $t = 0$  is zero, and changes rapidly as solidification progresses, and (2) as a result of this, proportionally more time was spent by this position in the range of low fraction solid. It must be noted here that the

nature of the fraction liquid curves is very much determined by the assumption made concerning the fraction solid versus distance distribution, Figure 3. As a direct result of that assumption, the fraction liquid curves presented in Figures 40, 41 and 42 are exactly convertible to the temperature curves. That is, the fraction liquid curves are linearly calculated from the cooling curves. In a later portion of this section this assumption of linearity of the fraction solid distribution will be examined as to the change in the fraction liquid and temperature curves which would result from the use of a Scheil distribution, Equation (9) in the Introduction.

Figure 40 compares the curves for two types of geometry; (a) unidirectional, and (b) radial heat flow, both for no convection, columnar growth, and no superheat, and infinite surface cooling rate. There is not a large effect here, but it is interesting to note that while the radial geometry produces a much lower local solidification time at a given position, the change in cooling rate over the solidification time is a little slower.

Figure 41 compares the curves for the effect of convection and growth morphology; (a) columnar, no convection and (b) equi-axed, high convection, both for no superheat and infinite surface cooling rate. Here there is a very marked effect, showing in the high convection case that after an initial drop to .45 fraction solid, the mushy

liquid at this position remains at this value of fraction liquid (.55) for 60% of the solidification time before resuming its drop to the eutectic fraction liquid (.09). In general, this sort of behavior indicates that in large castings, with convection high enough that dendrites physically transported in the direction opposite heat flow, the mushy zone is rapidly extended and solidification starts at very early times across the entire length. Thus, a large portion of the ingot, at any given time, is essentially mushy in nature, relatively early in solidification. The effect that this has on the final cast structure and solute distribution is great, and, in general, not beneficial. Results of engineering importance, to be expected from the convection are (1) increased dendrite arm spacing as a result of increased local solidification time (Figures 38 and 39), and (2) increase macrosegregation, hot tearing, and shrinkage defects as a result of the wide mushy zone produced by dendrites being swept out in front of the non-convecting portion of the mushy region.

It is worthwhile to point out the difference between the results of Figures 11 and Figures 38 and 39. The effect thought to be observed in practice of equi-axed growth producing longer local solidification time cannot be explained by the difference in thermal conductivities between equi-axed and columnar mushy regions, as seen by the small difference in the curves in Figure 11. If convection can carry equi-axed grains out into the melt, which effectively causes the mushy region to extend over the length of the casting, this would explain



the observed behavior much better. A method of reducing the local solidification time at any given position is suggested by the analogous results for side heat loss (Figures 37 and 32), which is to remove the convection and preserve the superheat or to replace the superheat loss by means of inputting heat to the convecting melt.

Figure 42 compares the cooling curves, or analogously the fraction liquid curves, for the effect of two-dimensional heat flow, (a) columnar, no heat loss from the side, and (b) equi-axed, with heat loss at the side,  $h_s = .001$ , both for no convection, no superheat, and infinite surface cooling rate at the chill. Here the effect is large, with the curve for side heat loss showing that for this position in the ingot, the local solidification time is much larger in the case of side heat loss, compared to the unidirectional case. This result indicates another reason why foundry engineers might appropriately concern themselves with finding ways of minimizing convection during solidification of sand castings. By reducing it, they could preserve some superheat, which would reduce the deleterious affect of the side heat loss discussed above, as shown earlier in the Results sections, H, I, and J.

#### C. Scheil Versus Linear Fraction Solid Distribution

The effect of the linear distribution of fraction solid versus temperature assumption employed for the previous results must be examined. For the four cases

presented above, (Figures 40, 41 and 42), the model was modified to utilize the Scheil equation for the  $f_L$  versus  $T$  distribution (Equation 9). The results were that the temperatures and positions of the tip and root were affected by less than 0.1%. Therefore, the temperature curves of Figures 40b, 41b, and 42b apply to both the linear and Scheil distribution results. The major change, therefore, is found in the  $f_L$  versus reduced time curves, which are presented in Figures 43, 44, and 45. These curves indicate that the major difference in behavior is that if the Scheil distribution applies to the mushy region, a large portion of solidification takes place in the very early periods of the freezing time. The significant difference between the Scheil results and the linear results occurs for the case of equi-axed convection. Figure 44 shows that solidification takes place in the later time period, with the fraction liquid equal to .55 for 60% of the time period, whereas for columnar, no convection growth the fraction liquid has dropped to .2 in this time period. The implications of this comparison on macrosegregation and hot tearing depend on the analysis of these results, but it is clear that a significant difference in structure and properties of an ingot would result from the difference in casting conditions for curves (a) and (b) of Figure 44.

#### D. Continuous Casting

One of the most important areas for engineering application of solidification studies is the field of continuous casting. Some studies of the solidification of alloys during the continuous casting process have been done (15,18,27), in particular, with various models for heat flow. The model employed in this work can be used to represent the continuous casting process under the following conditions: (1) heat flow along the length of the continuously cast ingot can be neglected compared to the radial component of heat flow; (2) variations of heat transfer coefficient along the length of the ingot are neglected, that is, if this heat transfer coefficient is considered to be constant, for the purposes of discussion here.

It is apparent from the work of the authors cited above that the foregoing assumptions are reasonable only for certain cases of continuous cast ingots. As example, the work of Mizikar (15), and Adenis (18), shows that the continuous casting of steel ingots is well approximated by the above, whereas the solidification of large aluminum ingots is not. Kroeger (27), who considers the continuous castings of commercial copper, indicates that he includes the axial conduction in his analysis, but some of his results, showing pool depths, indicate that the assumption

of no axial (or lengthwise) heat flow would not affect the results by more than 10 - 20%.

Where the assumptions apply, therefore, the results of the preceding sections should apply to the local solidification time distribution in continuously cast ingots. The time axis in the plots shown in the previous section is directly convertible to length along the z axis. Since most of the plots in the results section are presented for the square root of time, these would have to be replotted for linear time in order to make a direct comparison to the pool shapes which the model presented here would predict.

The local solidification time curves versus radius (Figures 17 and 19) are indicative of the behavior to be expected in continuous cast ingots, especially the curve at  $h = .01$ , which might approximate the chilling conditions for the type of molds used in the casting of steel. The curves of Figure 19 indicate that an order of magnitude increase in the heat transfer coefficient from  $h = .01$  to  $h = .1$  would result in a shortening of the local solidification time, but only by a factor of about 1.2 to 1.5. It may be concluded that for values of  $hL/K$  in the vicinity of .5 to 1 or larger, the process of solidification is very much controlled by thermal diffusion through the metal rather than by heat removal at the surface, so that increasing the heat transfer coefficient at these levels of

$hL/K$  does not result in an appreciable benefit in the local solidification time distribution.

As mentioned above, the results of the previous section cannot be applied to the continuous casting of aluminum, especially in the 'direct chill' process, where the ingot radius is large and the casting rate (linear velocity in the  $Z$  direction) is small, so that heat flow in the  $Z$  direction is important. Research into the area of heat flow during the continuous casting of aluminum alloys could be conducted by using the model for solidification and the method of numerical solution presented here, with the addition of a consideration of axial heat flow. A method for considering this axial heat flow is presented by Kroeger(27), which is especially useful for his definition of the boundary conditions at  $Z = m$ , the axial length over which heat flow is considered. There are other approaches for numerical procedures for two-dimensional initial value problems which might also be applied.

#### E. Experimental Examples

The discussion and results have been presented in terms of dimensionless numbers up to this point. It will be useful and illustrative to present some examples of the most pertinent results in terms of laboratory experiments which might be carried out.

Consider the following casting; a plate 12" long, 1.57" thick, and at least 6" wide, chilled at one end with a very high heat removal rate (a water pipe or very smooth water-cooled copper chill). This plate can be cast in a sand, plaster, or foamed plaster mold or with an insulating material around the sides. For an Al-4.5% Cu grain refined alloy, the local solidification times at a distance of 9" from the chill, for various casting conditions, are reported in Table II.

Figures 46, 47, 48 and 49 present the local solidification time in seconds versus the distance from the chill in inches; Figures 50 through 53 present the width of the mushy region (inches) versus position of the end of freeze isotherm, or "root" (inches), for the conditions of Table II. The width reported is the distance between the root and the isotherm at  $f_L = 0.75$ , which is  $646.1^{\circ}\text{C}$ , assuming a Scheil distribution of  $f_L$  versus  $T$  in the mushy region. The reason this isotherm is chosen rather than the liquidus isotherm is simply due to the experimental difficulty in detecting the exact position of the liquidus with thermocouples in the laboratory. The detection of the range 650 - 646.1 is simpler and adds no great inaccuracy to the thermocouple results.

The characteristics of the local solidification time versus distance curves have been discussed earlier, in the Results section. At high rates of heat removal

from the side (Figure 47, for sand), superheat and heat input with convection raise the local solidification time, whereas for low rates of side heat removal (Figure 49), the local solidification time at a given distance from the chill is lowered by the presence of heat at the tip. Table II clearly shows the directions and relative magnitudes of the local solidification times to be expected for this laboratory casting, which are typical of the results presented dimensionlessly earlier.

The widths of the mushy region versus position of the root curves are presented to give an indication of the macrosegregation effects and feeding problems which might be encountered during these laboratory experiments.

Table II. End Chilled Laboratory Casting, 12" x 6" x 1.57"

|   | unidirectional<br>heat flow |     |     |                       | sand mold† |     |                       | plaster mold |     |                       | foamed<br>plaster mold |     |                       |
|---|-----------------------------|-----|-----|-----------------------|------------|-----|-----------------------|--------------|-----|-----------------------|------------------------|-----|-----------------------|
|   |                             |     |     |                       |            |     |                       |              |     |                       |                        |     |                       |
| superheat   | 0                           | 0   | 150 | 0                     | 0          | 150 | 0                     | 0            | 150 | 0                     | 0                      | 150 | 0                     |
| heat,<br>cal/cm <sup>2</sup> /sec <sup>1/2</sup>            | 0                           | 0   | 0   | $\frac{50}{\sqrt{t}}$ | 0          | 0   | $\frac{50}{\sqrt{t}}$ | 0            | 0   | $\frac{50}{\sqrt{t}}$ | 0                      | 0   | $\frac{50}{\sqrt{t}}$ |
| local solidifi-<br>cation time,<br>sec. at 9"<br>from chill | 200                         | 330 | 155 | 160                   | 70         | 110 | 105                   | 135          | 115 | 120                   | 255                    | 130 | 140                   |
| convection  | 0                           | ∞*  | 0   | ∞                     | 0          | 0   | ∞                     | 0            | 0   | ∞                     | 0                      | 0   | ∞                     |

\* Assuming liquid with up to 15% solid convects as pure liquid. At higher fraction solid, liquid - solid mixtures do not convect.

† The parabolic heat loss constants (a) used were: 8.9 for sand, 4.95 for plaster, and 1.57 for foamed plaster.



## Chapter IV

## CONCLUSIONS

1. A numerical procedure is presented for calculation of heat flow in solidification of alloys. Results are given, using Al-4.5% Cu as example, for unidirectional heat flow and for radial heat flow in a mold at constant temperature (e.g., water cooled mold).
2. In unidirectional solidification of an ingot of finite length, with infinite mold-metal heat transfer coefficient and no superheat, the "start of freeze" isotherm moves such that its position is proportional to the square root of time. The "end of freeze" isotherm moves such that its position is proportional to the square root of time until the "start of freeze" isotherm reaches the ingot extremity; thereafter it moves at greater velocity.
3. With superheat and no convection, the "start of freeze" and "end of freeze" isotherms also move such that their positions are proportional to the square root of time (until the upper extremity is approached). The velocity of these isotherms decreases with increasing superheat, and both isotherms move at greater rate near the upper extremity of the ingot than that given by the square root relationship.
4. If convection is high and mold-metal interface heat transfer coefficient infinite, any superheat present is lost immediately on pouring and heat flow is as if

the ingot were poured with zero superheat. If convection is high and mold-metal interface coefficient is finite, solidification is delayed until all superheat is exhausted. Thereafter, solidification is as if the ingot were poured with zero superheat.

5. A second effect of convection is postulated and studied quantitatively. The effect is that of convection sweeping away equi-axed dendrites from the outer edge of the mushy zone, thus extending mushy zone thickness. A corollary of the postulated model is that the convection greatly increases the width of the mushy zone during much of solidification. Calculations show that local solidification time is then also greatly increased in much of the ingot.
6. An "imperfect" unidirectional solidification (i.e., some lateral heat loss) start of freeze and end of freeze isotherms always move faster than for "perfect" unidirectional solidification, other conditions being equal. At zero superheat, the start of freeze isotherm moves at infinite velocity in "imperfect" unidirectional heat flow.
7. "Local solidification time" is strongly affected by the above variables. It increases linearly with distance from chill in unidirectionally solidified ingots with no interface resistance (except near the final extremity where it may decrease slightly).

Small amounts of side heat loss increase local solidification time. Larger amounts decrease it. Convection, where strong enough to sweep solid dendrites in the direction of advancing isotherms, increases local solidification time. Small amounts of heat added to the melt in "perfect" or "imperfect" unidirectional solidification decrease local solidification time. Larger amounts increase it.

8. Results of radial heat flow calculations are qualitatively similar to those presented above for unidirectional heat flow. Major quantitative differences are that (1) velocities of start of freeze and end of freeze isotherms at a given distance from the mold are substantially higher for radial heat flow, (2) local solidification times are reduced, and (3) the transient effects at the ingot extremity (ingot center in the case of radial heat flow) are enhanced.
9. For an end chilled, plate casting, 12" long from chill to riser, 6" wide and 1.57" thick, cast into an insulated mold, with no superheat and no convection present, detailed results are presented as numerical examples of the results obtained. The local solidification time at a distance 9" from the chill is ~200 second. With 150°C superheat and no convection, it will be ~155 sec. With a

grain refiner and high convection, the local solidification time at 9" from the chill will be ~330 seconds.

10. For the above end chilled plate, cast into a sand mold, the local solidification time at 9" from the chill will be ~70 seconds with no superheat and ~110 seconds with 150<sup>o</sup>C superheat and no convection.
11. For the above and chilled plate cast into a foamed plaster mold, the local solidification time at 9" from the chill will be ~250 seconds with no superheat and ~130 seconds with 150<sup>o</sup>C superheat and no convection.

## Chapter V

## SUGGESTIONS FOR FUTURE WORK

1. The solidification of alloys other than Al-4.5% Cu should be studied, such as those which are of commercial interest. This could be accomplished easily with the present computer model.
2. The analysis should be extended to treat heat flow in two dimensions fully. This is important for the study of continuous casting and ingot solidification, where the results of the unidirectional analysis presented here will not apply. This extension to more than one dimension can be accomplished within the framework of the present method, which treats the tip and root boundary conditions explicitly in the solution. A method for two dimensional heat flow analysis with finite differences is available in the literature, known as the 'alternating direction' method.
3. A mathematical description of the effect of heat input into a highly convecting melt is needed. The results presented in the Results Section for only one form of heat input,  $q = q'/(t)^{1/2}$ , showed that there is a strong possibility for reducing local solidification times in castings in which convection is present, but that the effect of this heat input on the positions and velocities of the tip and root

is complex. Since the forms of heat input (the function  $q = F(t)$ ) are limitless, the most efficient method of searching for an optimal function (the definition of optimal is itself a problem) would be to use a mathematical optimizing procedure. Such a procedure, available in the literature of numerical analysis, is the unsteady state optimization algorithm referred to as "Hill climbing in function space". The procedure is well defined, but calls for repeated integration of the differential (or difference) equations, which will result in a large amount of computer time spent in reaching the optimal function. Just the definition of the problem and setting up of the optimizing procedure may reveal much more about the process of heat input and its effects on the local solidification time.

4. A survey of the Results Section will reveal that over the wide range of values of the parameters (see Appendix C for the list of all parameters), only a small portion of the possible values was considered in this work. Therefore it is possible that many interesting and useful results were not uncovered here (such as, what the effect of finite heat transfer coefficient at the chill is on the results for the side heat loss studies presented, which were for  $h = \infty$ ). The dimensional analysis in Appendix C shows that there are many dimensionless groups which

were held at a constant value for this study, and these groups, such as  $h_s/h_b$  indicate areas for future study.

5. Experimental studies, such as proposed in the Discussion, should be carried out to determine:
  - (a) whether the magnitude of the changes in the dendrite arm spacing presented there is found in the laboratory, and
  - (b) whether actual laboratory or foundry conditions of heat transfer at the chill, amount of convection, etc., can be measured accurately enough to be used as data for the computer model for the prediction of final dendrite arm spacings more accurately.

## Chapter VI

## BIBLIOGRAPHY

1. E. M. Passmore, M. C. Flemings, H. F. Taylor, "Fundamental Studies on Effects of Solution Treatment, Iron Content, and Chilling of Sand Case Aluminum-Copper Alloy," *Trans. AFS*, v. 66, 1968, pp. 96-104.
2. S. N. Singh, M. C. Flemings, "Influence of Ingot Structure and Processing on Mechanical Properties and Fracture of a High Strength Wrought Aluminum Alloy," (to be published), *Trans. Met. Soc. AIME*.
3. T. F. Bower, H. D. Brody, and M. C. Flemings, *Trans. Met. Soc. AIME*, v. 236, 1966, p. 624.
4. T. Z. Kattamis, J. M. Coughlin, M. C. Flemings, "Influence of Coarsening on Dendrite Arm Spacing of Aluminum-Copper Alloys," *Trans. Met. Soc. AIME*, v. 239, 1967, pp. 1504-1511.
5. M. C. Flemings, "Application of Solidification Theory to Large Castings and Ingots," The Solidification of Metals, J.I.S.I., Publication 110, 1968, pp. 13-24.
6. F. Neumann, Cf P. Frank, and Baron Mises, "Die Differential und Integral Gleichungen der Mechanik und Physick," v. 2, Vieweg, Branunschweig, 1927.
7. H. S. Carslaw and J. C. Jaeger, "Conduction of Heat in Solids," Oxford University Press, London and New York, 1959.
8. P. V. Danckwets, *Trans. Faraday Society*, v. 46, 1950, p. 701.
9. B. A. Boley, *Quart. Appl. Math.*, v. 1, 1963, p. 300.
10. C. M. Adams, Liquid Metals and Solidification, ASM, Cleveland, 1958, pp. 174-186.
11. V. Koump, R. H. Tien, and W. J. Kim, *Trans. Met. Soc. AIME*, v. 239, 1967, p. 1305.
12. A. W. D. Hills, *Trans. Met. Soc. AIME*, v. 245, 1969, p. 1471.
13. J. C. Muehlbauer and J. E. Sunderland, *Appl. Mech. Rev.*, v. 18, No. 12, 1965, p. 951.
14. S. G. Bankoff, *Advance in Chem. Eng.*, v. 5, 1965, p. 75.



15. E. A. Mizikar, *Trans. Met. Soc. AIME*, v. 239, 1967, p. 1747.
16. R. D. Phelke and M. J. Sinnott, "Unidirectional Analysis of Heat Transfer During Continuous Casting," Computer Applications in Metallurgical Engineering, ASM, 1964, pp. 75-81.
17. W. B. Eisen and A. J. Campagna, "A Computer Simulation of Vacuum Remelted Ingots," *TMS-AIME*, v. 1, no. 4, p. 849.
18. Adenis et al., *J. Inst. of Metals*, v. 91, 1963, pp. 395-403.
19. H. D. Brody and M. C. Flemings, *Trans. Met. Soc. AIME*, v. 236, 1966, p. 301.
20. M. C. Flemings and G. E. Nereo, *Trans. Met. Soc. AIME*, v. 239, 1967, p. 1449.
21. D. Kingery, Introduction to Ceramics, p. 501.
22. A. W. D. Hills and M. R. Moore, *Trans. Met. Soc. AIME*, v. 245, 1969, p. 1481.
23. W. D. Murray and F. Landis, *Journal of Heat Transfer*, May, 1959, pp. 106-112.
24. L. W. Ehrlich, *Journal of Assoc. Comp. Machinery*, v. 5, 1968, p. 161.
25. A. Kohn, "Auto Radiograph Study of the Process of Solidification in Killed Steel Ingots," The Solidification of Metals, J.I.S.I., Publication 10, 1968, pp. 356-362.
26. H. D. Brody, Sc.D. Thesis, Department of Metallurgy, Massachusetts Institute of Technology, 1965.
27. P. G. Kroeger, "A Heat Transfer Analysis of Solidification of Pure Materials in Continuous Casting Processes," to be published at the Fourth International Heat Transfer Conference, Paris, 1970.
28. H. Silberberg and J. J. McKetta, "Learning How to Use Dimensional Analysis," *Petroleum Refiner*, v. 32, no. 7, p. 129.
29. R. W. Ruddle, "The Solidification of Castings", Institute of Metals, 1950.
30. H. H. Rosenbrook and C. Storey, "Computational Techniques for Chemical Engineers," Pergamon Press, 1966.
31. B. P. Bardes, M. C. Flemings, "Dendrite Arm Spacing and Solidification Time in Cast Aluminum-Copper Alloy," *Trans. AFS*, v. 74, 1966, pp. 406-412.

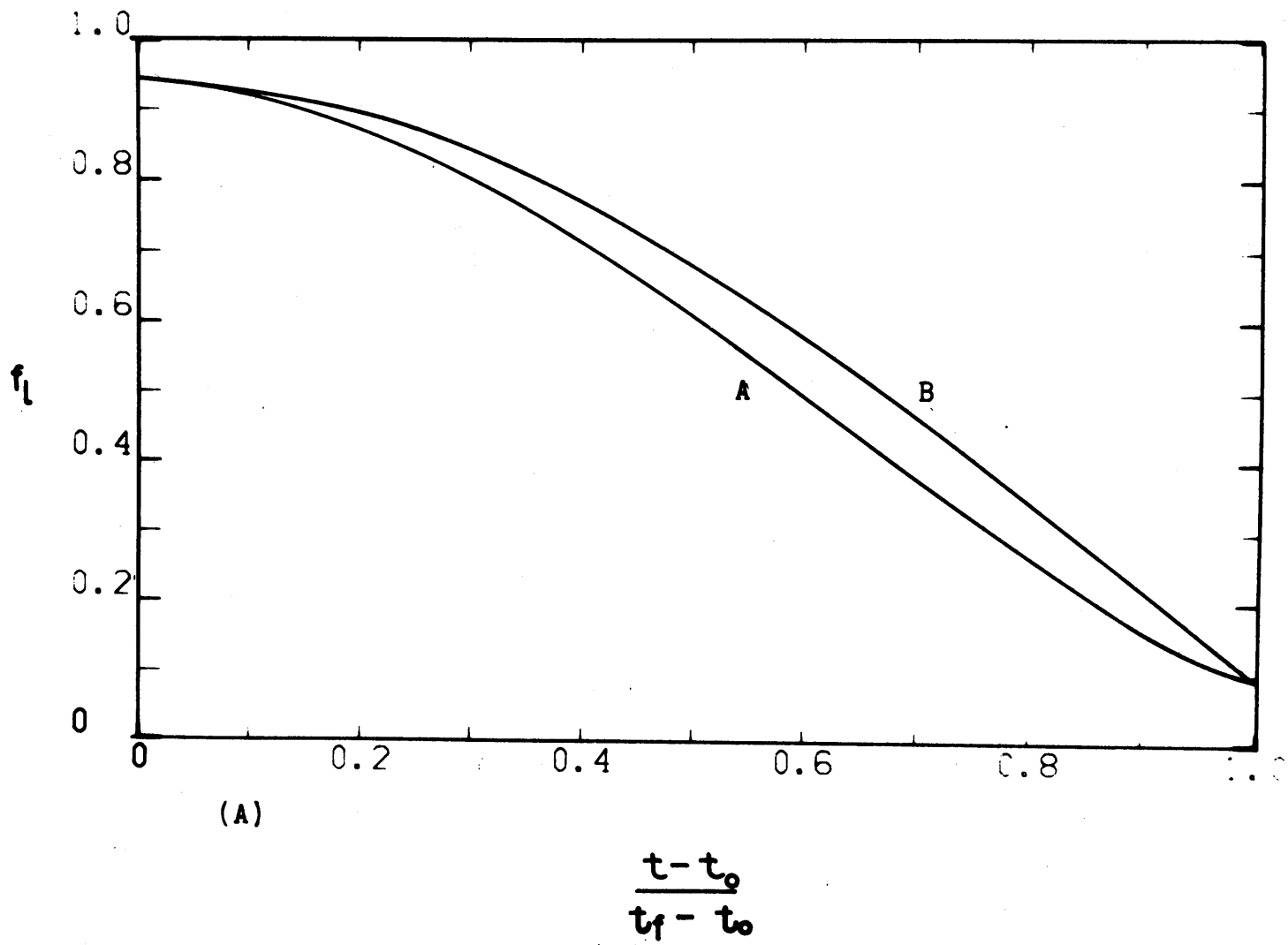


Figure 40A. Fraction liquid at  $\lambda = 0.5$  versus reduced time,  $h_B L / \bar{K} = \infty$ , no superheat, no convection, for (A) unidirectional heat flow (Figure 12A), (B) radial heat flow (Figure 16A).

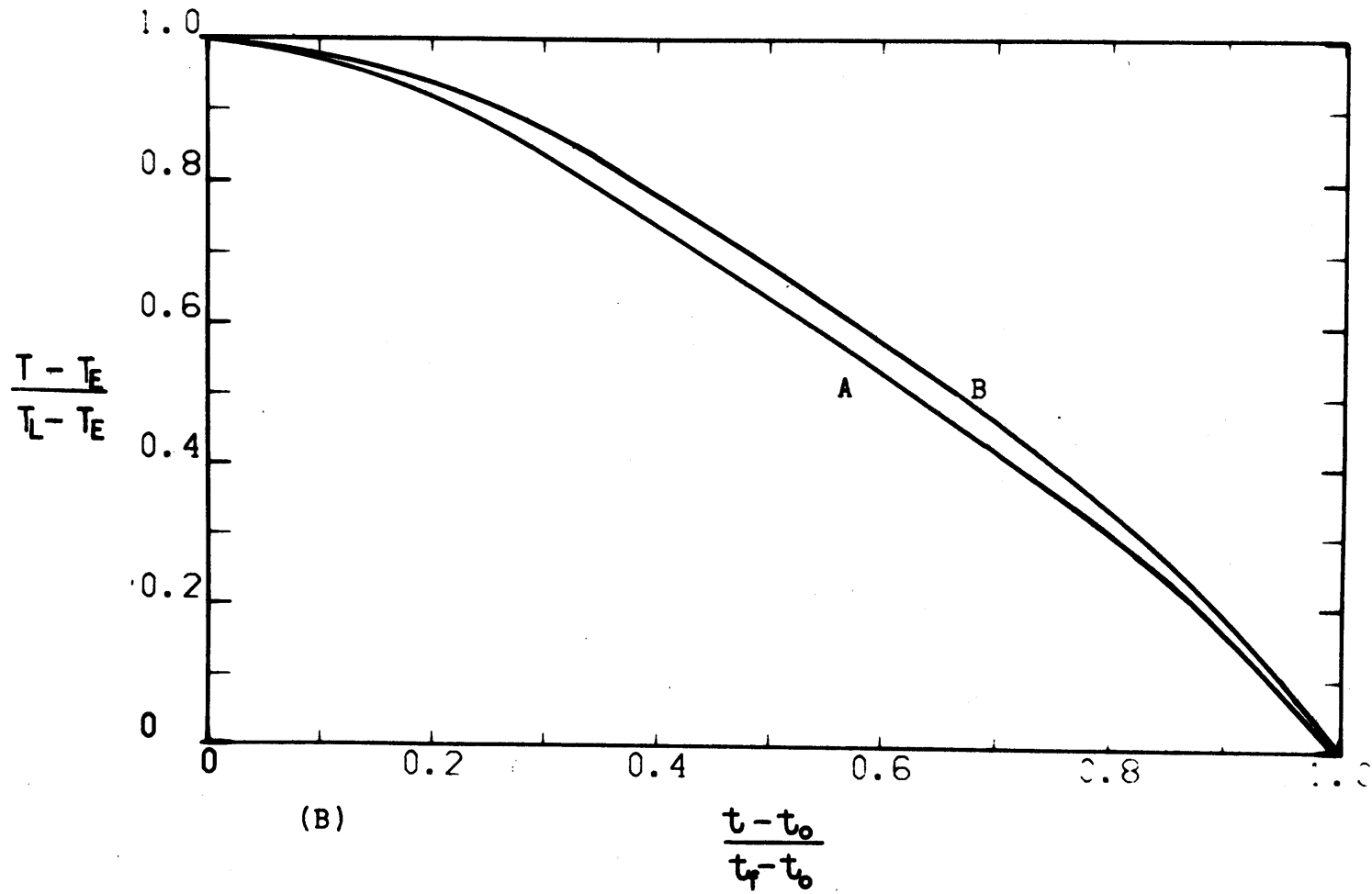


Figure 40B. Dimensionless temperature at  $\lambda = 0,5$  versus reduced time, for conditions of Figure 40A.

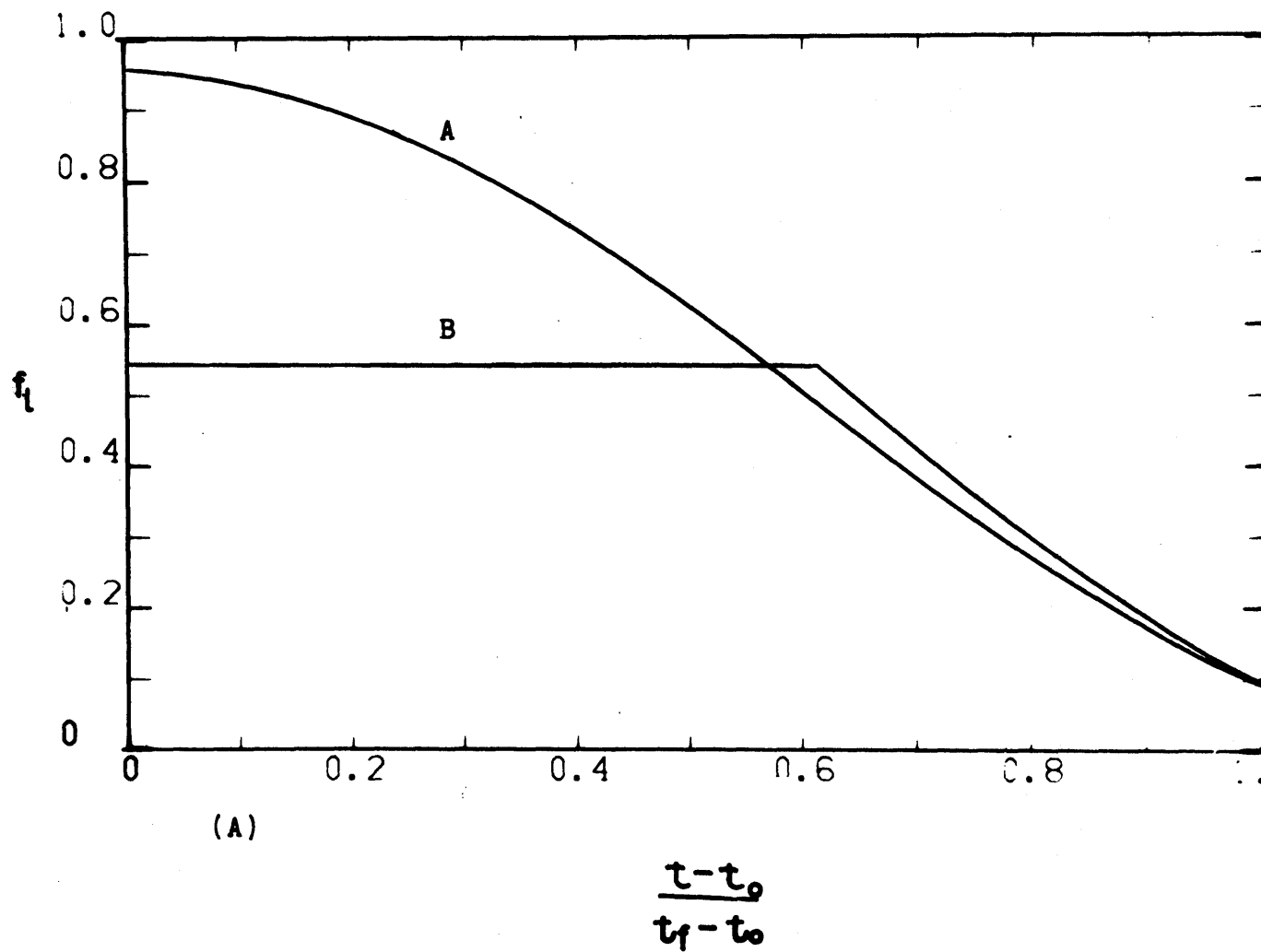


Figure 41A. Fraction liquid at  $\lambda = 0.5$  versus reduced time,  $h_b L / \bar{K} = \infty$ , no superheat, for (A) no convection, columnar growth (Figure 12A), (B) high convection, equiaxed growth,  $f_{SC} = 0.45$  (Figure 38D).

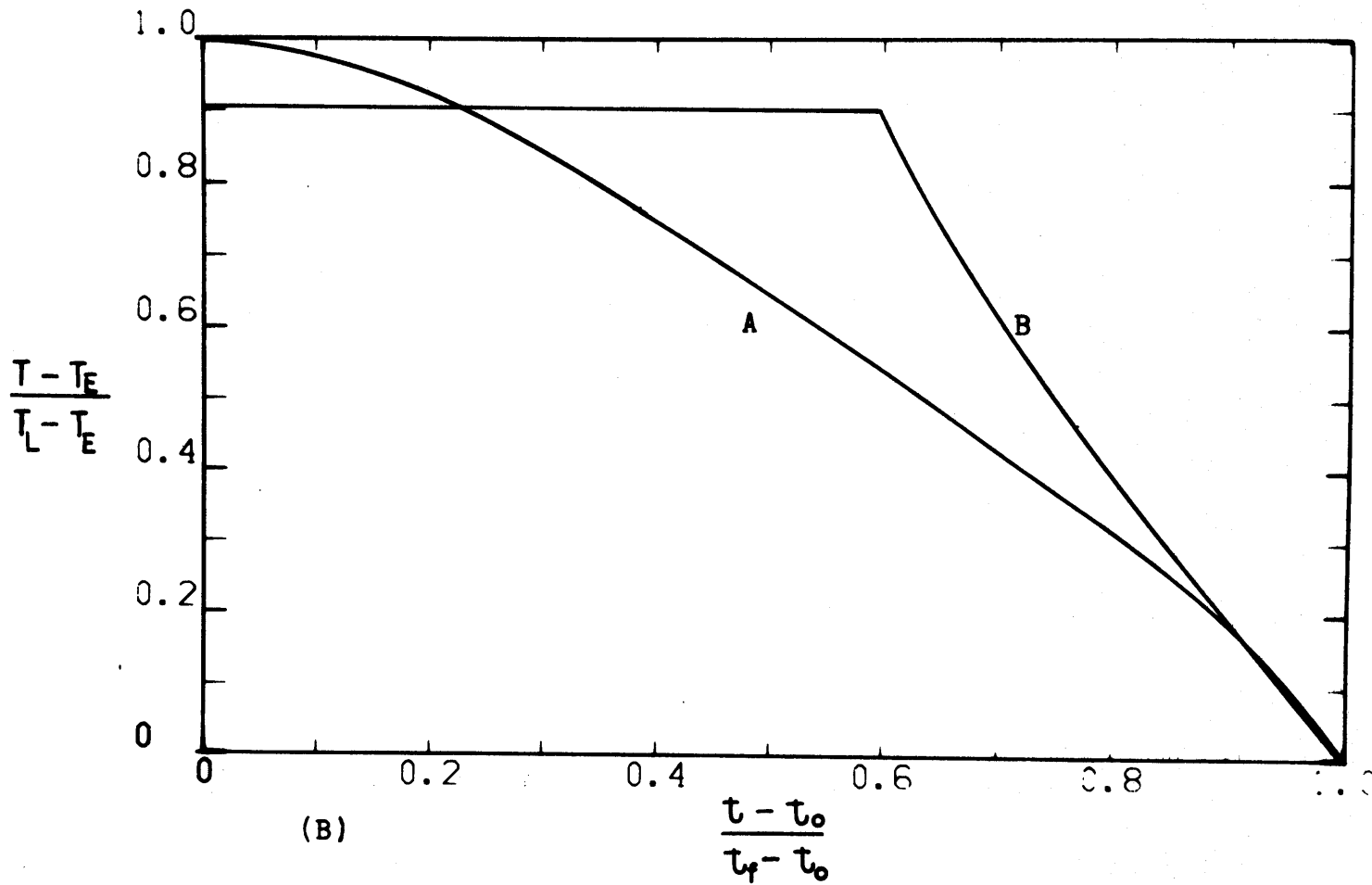


Figure 41B. Dimensionless temperature at  $\lambda = 0.5$  versus reduced time, for conditions of Figure 41A.

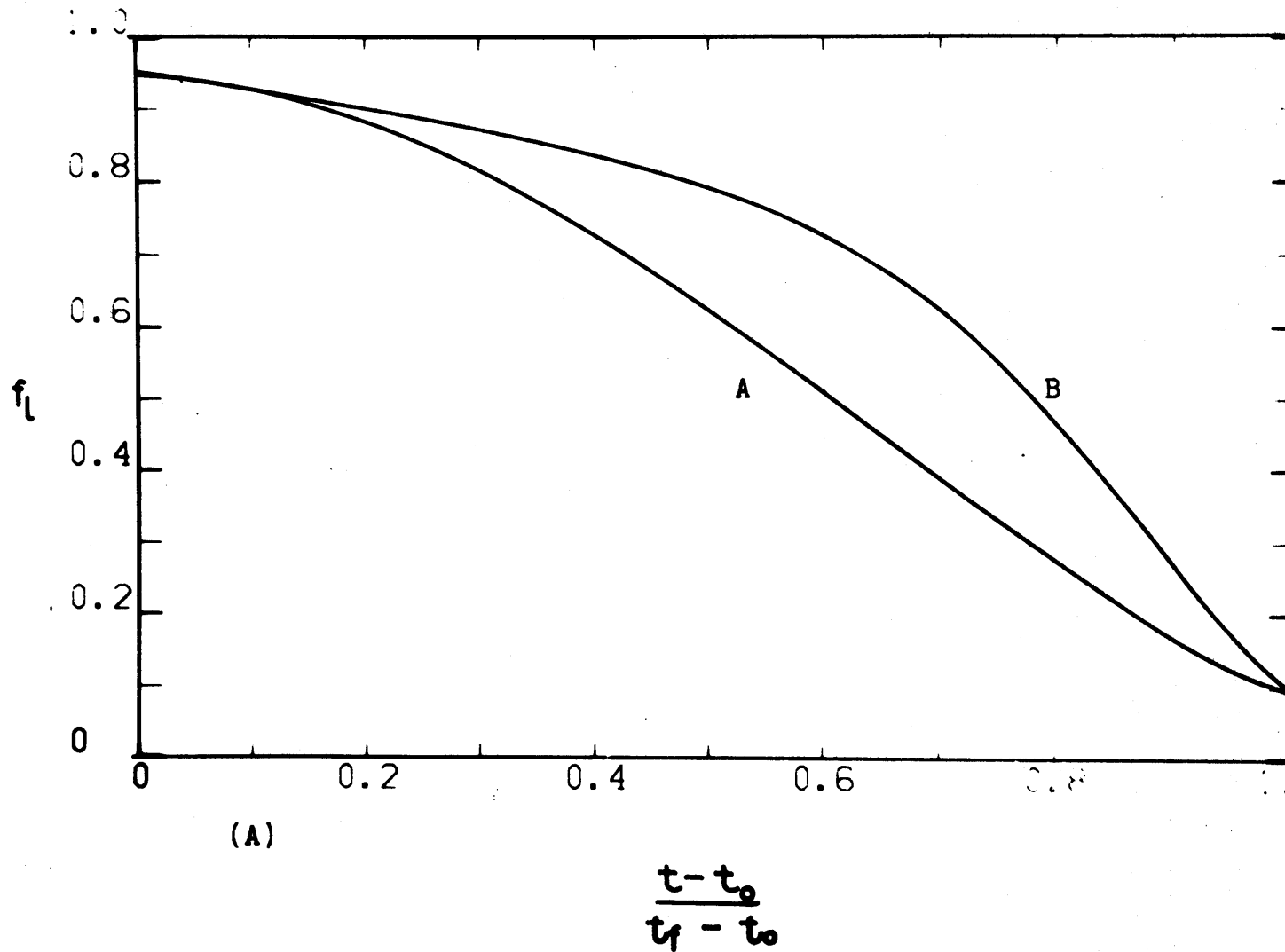


Figure 42A. Fraction liquid at  $\lambda = 0,5$  versus reduced time,  $h_B L / \bar{K} = \infty$ , no superheat, no convection, for (A) unidirectional heat flow (Figure 12A), (B) side heat flow,  $h_S L^2 / W = 0,232$  (Figure 22B).

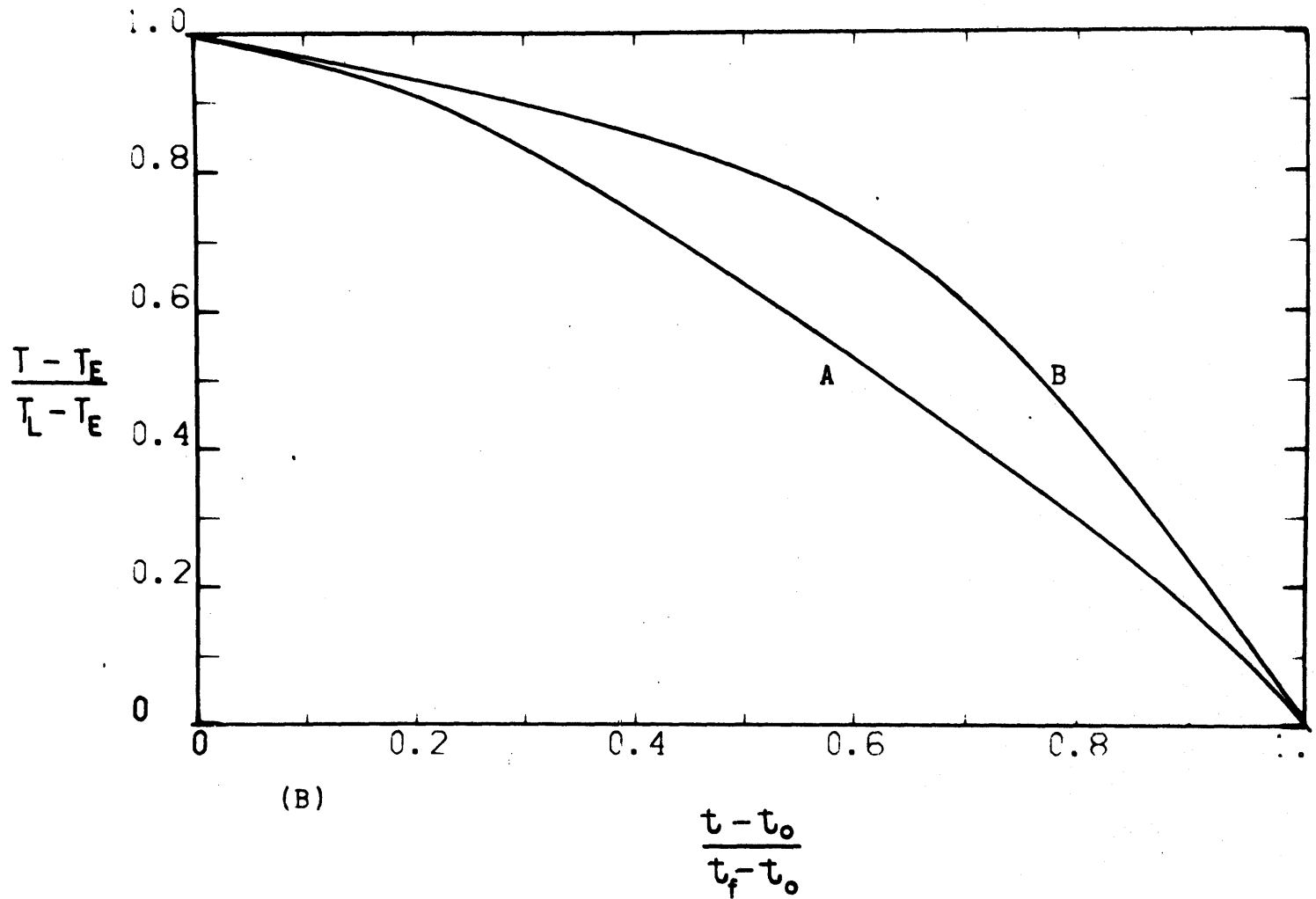


Figure 42B. Dimensionless temperature at  $\lambda = 0,5$  versus reduced time, for conditions of Figure 42A.

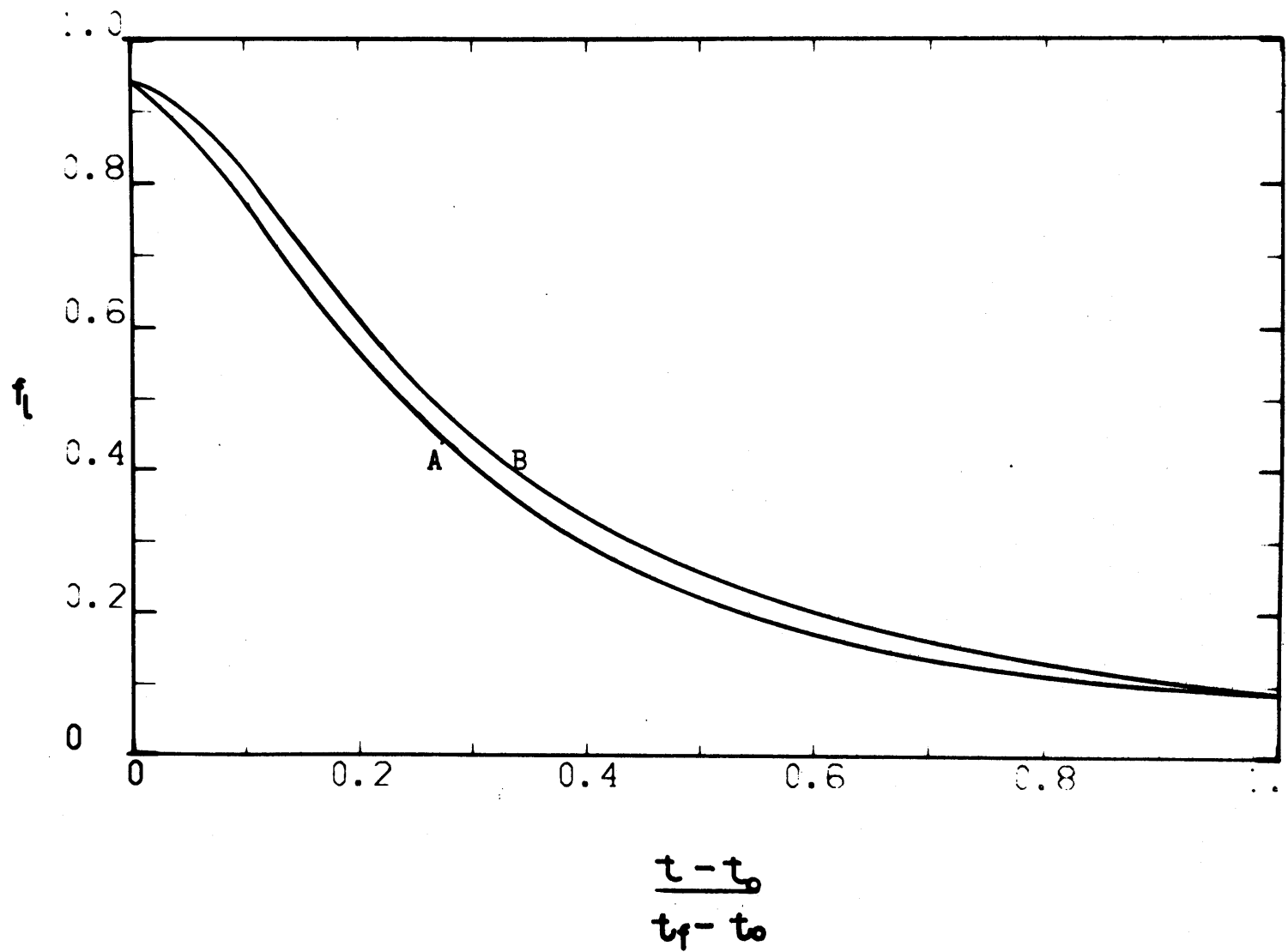


Figure 43. Fraction liquid at  $\lambda = 0.5$  versus reduced time, for conditions of Figure 41A, with Scheil distribution of fraction liquid versus temperature used in the mushy region.



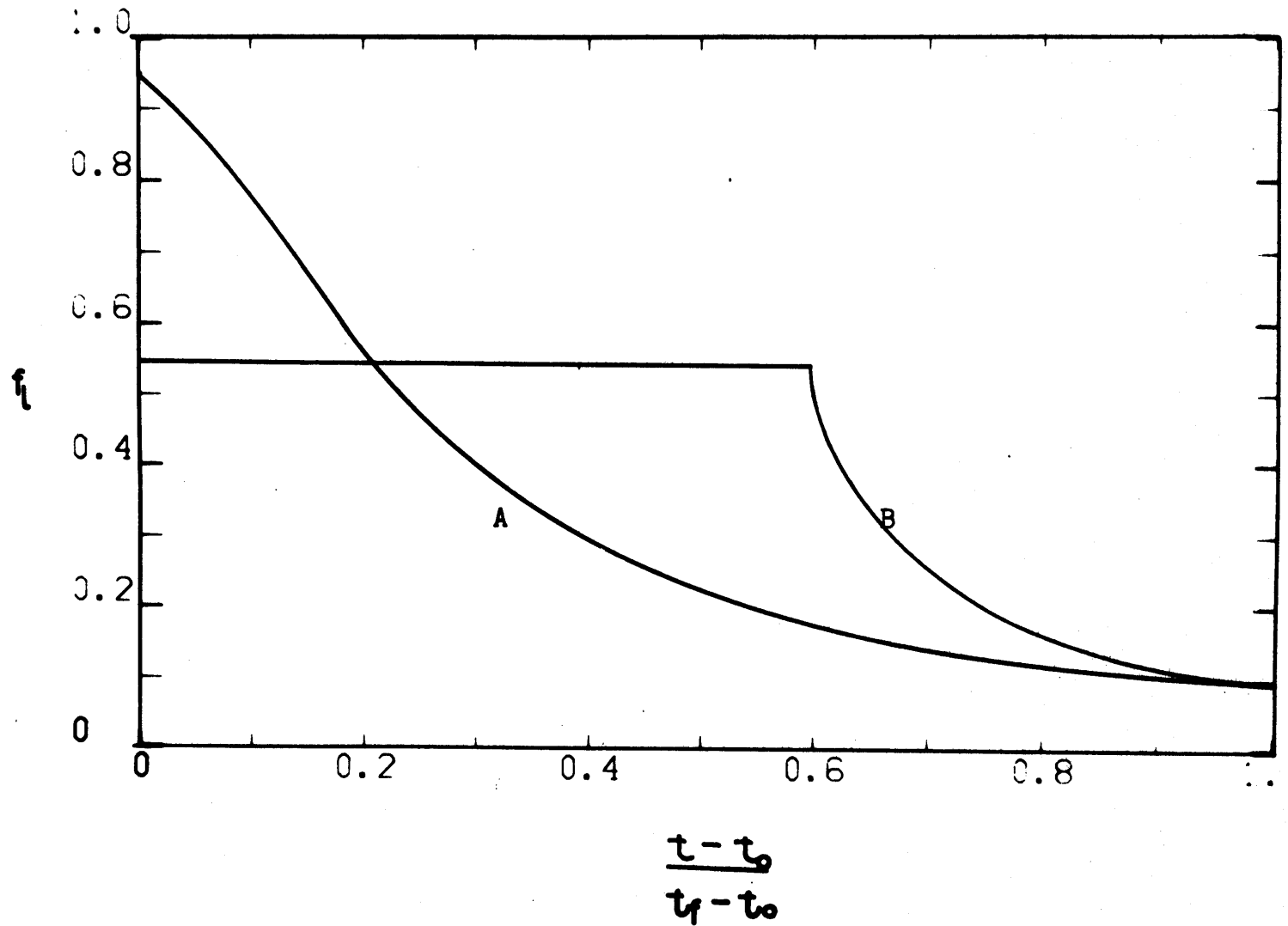


Figure 44. Fraction liquid at  $\lambda = 0.5$  versus reduced time, for conditions of Figure 42A, with Scheil distribution of fraction liquid versus temperature used in the mushy region.

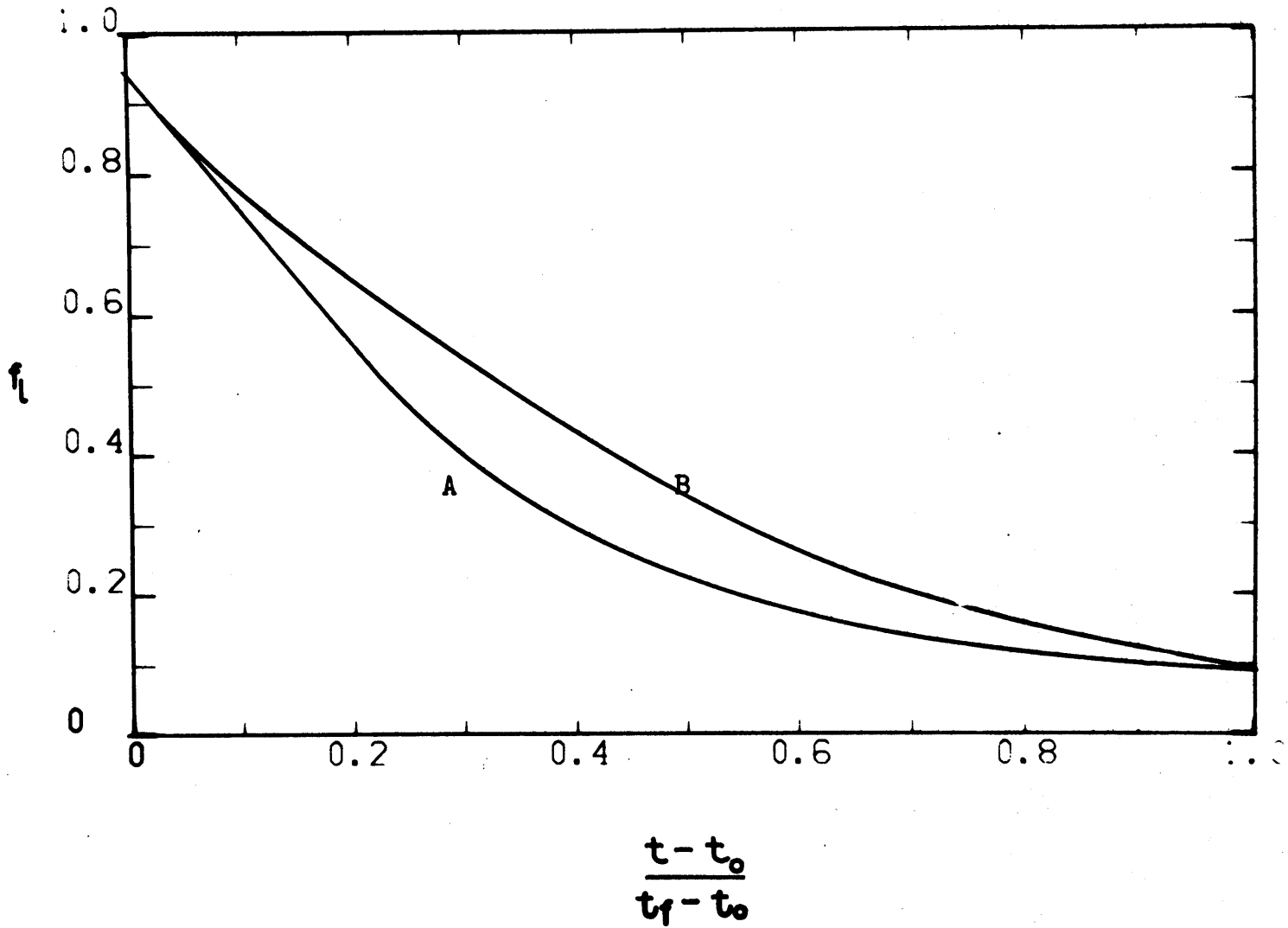


Figure 45. Fraction liquid at  $\lambda = 0.5$  versus reduced time, for conditions of Figure 42A, with Scheil distribution of fraction liquid versus temperature used in the mushy region.

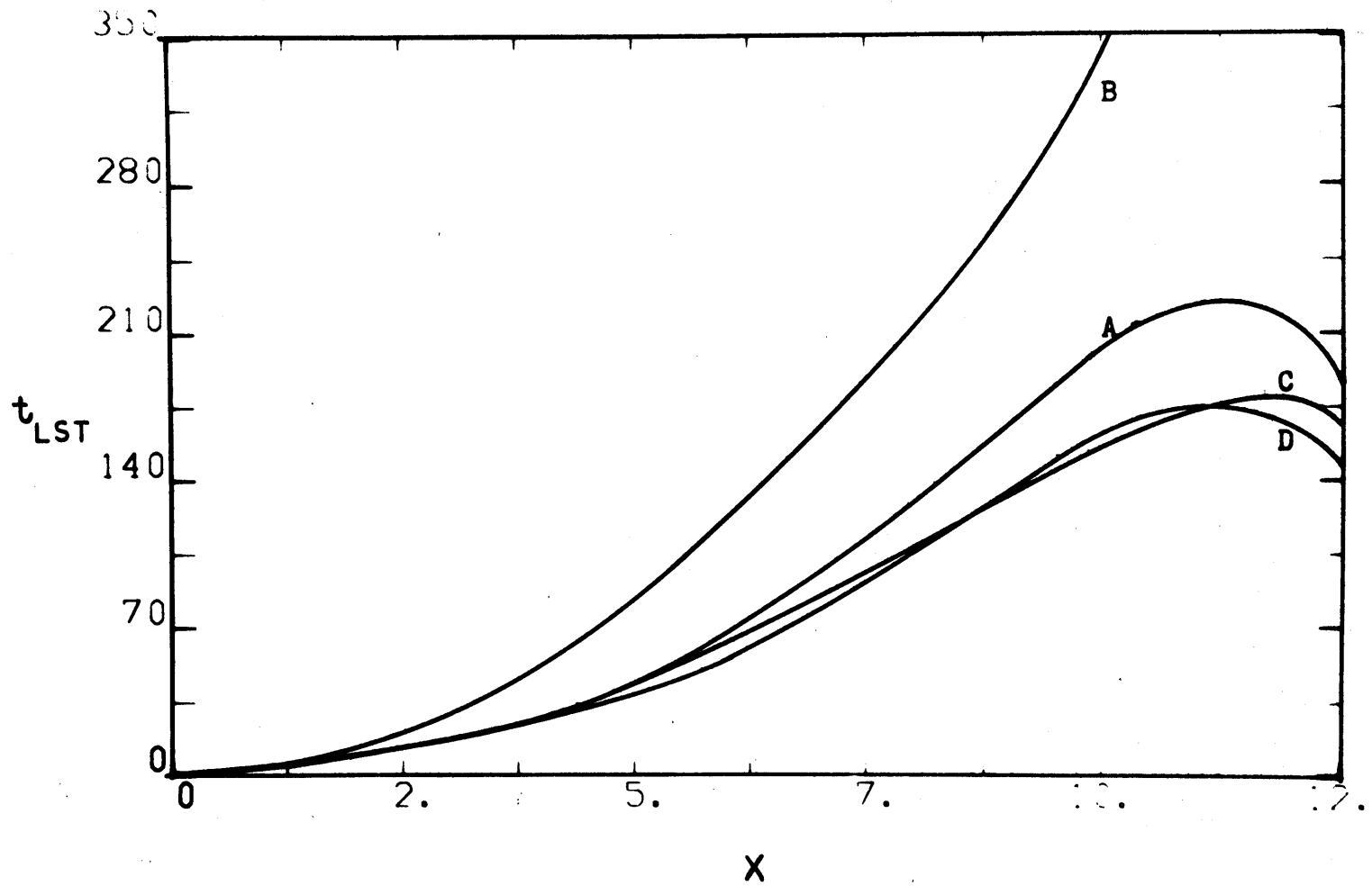


Figure 46. Local solidification time versus distance from the chill, 12" end-chilled plate casting, 6" wide, 1.57" thick, insulated mold, for (A)  $\Delta T_S = 0$ , no convection, (B)  $\Delta T_S = 0$ , equiaxed growth, high convection (C)  $\Delta T_S = 150^\circ\text{C}$ , no convection, (D) high convection, heat at centerline =  $50/\sqrt{t}$  cal/sec/cm<sup>2</sup>.

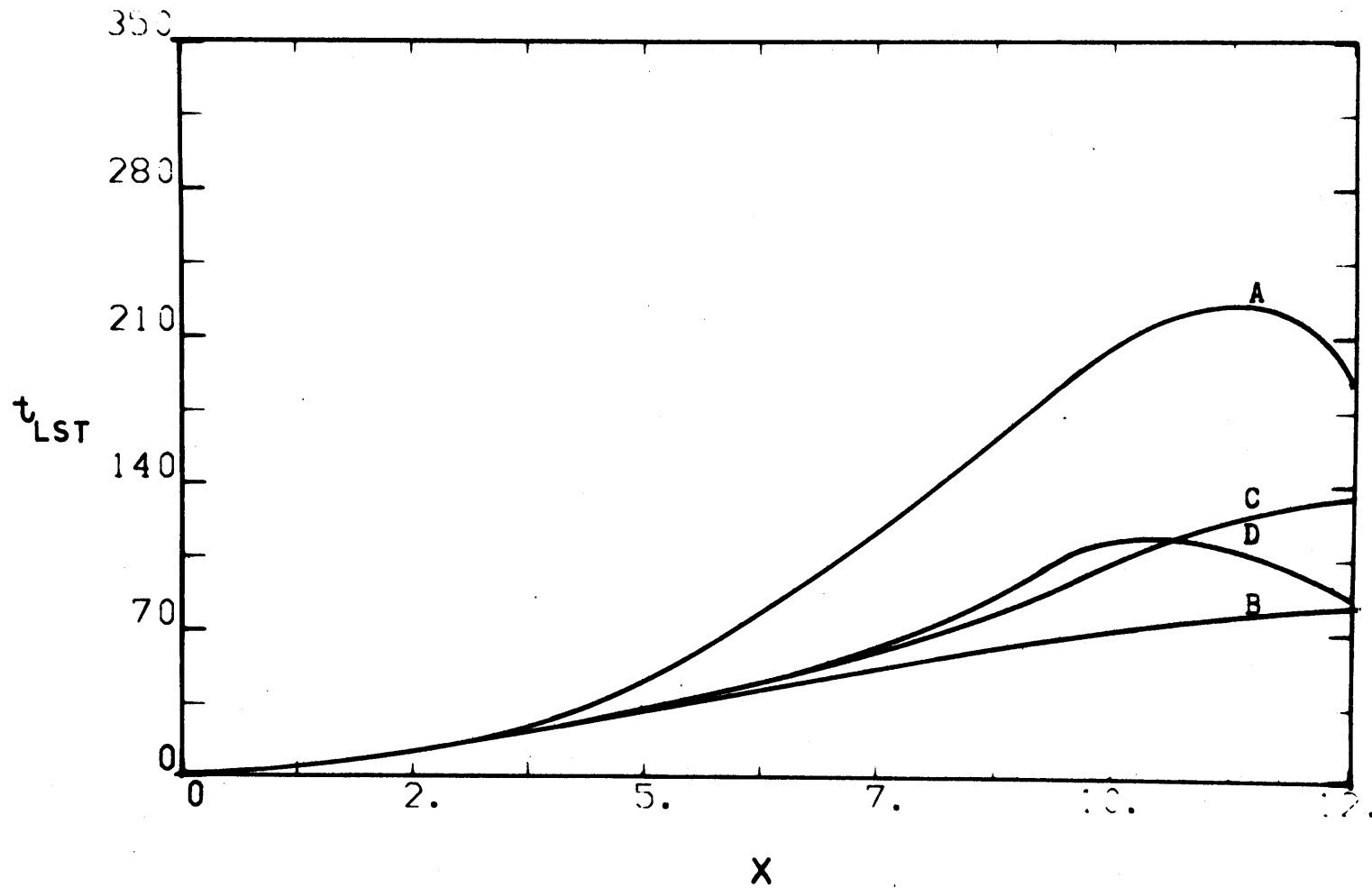


Figure 47. Local solidification time versus distance from the chill, for the casting of Figure 46, for (A) insulated mold,  $\Delta T_s = 0$ , no convection, (B) sand mold,  $\Delta T_s = 0^\circ\text{C}$ , no convection, (C) sand mold,  $\Delta T_s = 150^\circ\text{C}$ , no convection, (D) sand mold, high convection, heat in =  $50/\sqrt{t}$  cal/sec/cm<sup>2</sup>, where  $a = 8.9$  for sand,

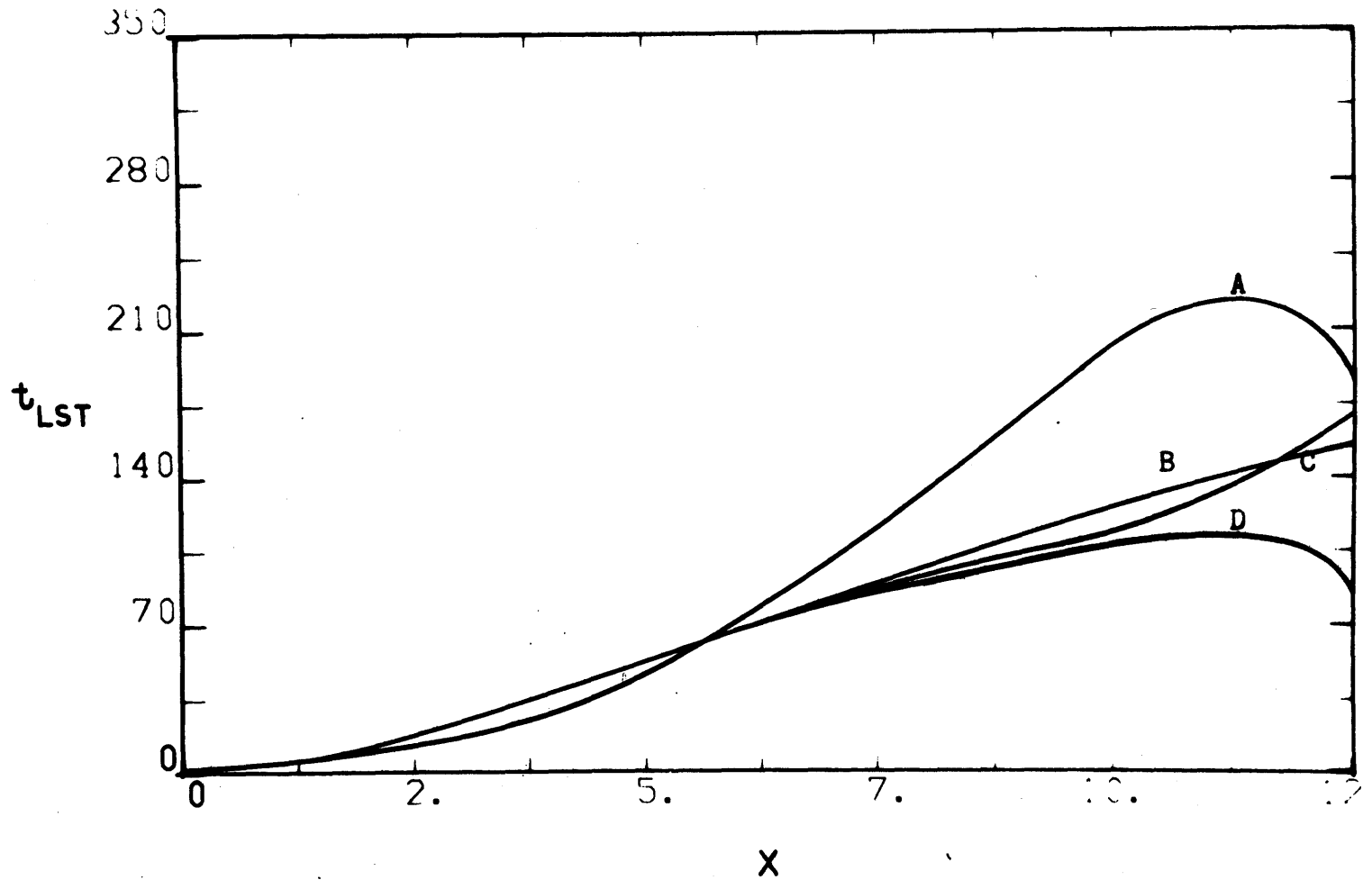


Figure 48. Local solidification time versus distance from the chill, for the casting of Figure 46, for (A) insulated mold,  $\Delta T_S = 0$ , no convection, (B) plaster mold,  $\Delta T_S = 0^\circ C$ , no convection, (C) plaster mold,  $\Delta T_S = 150^\circ C$ , no convection, (D) plaster mold, high convection, heat  $ip = 50/\sqrt{t}$  cal/sec/cm<sup>2</sup>, where  $a = 4.95$  for plaster.

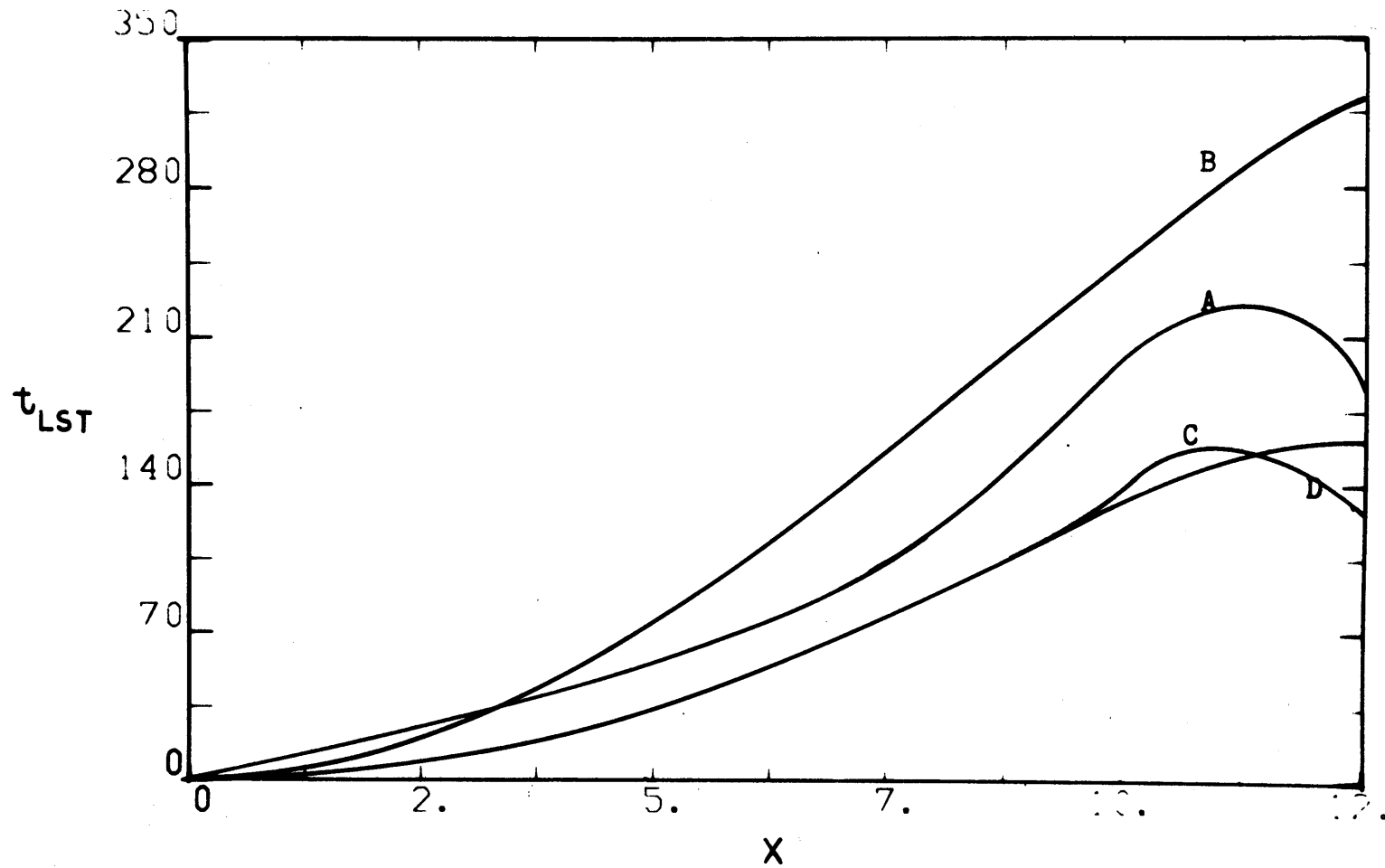


Figure 49. Local solidification time versus distance from the chill for the casting of Figure 46, for (A) insulated mold,  $\Delta T_s = 0$ , no convection, (B) foamed plaster mold,  $\Delta T_s = 0^\circ\text{C}$ , no convection, (C) foamed plaster mold,  $\Delta T_s = 150^\circ\text{C}$ , no superheat, (D) foamed plaster mold, high convection, heat in =  $50/\sqrt{t}$  cal/sec/cm<sup>2</sup>, where  $a = 1.57$  for foamed plaster.

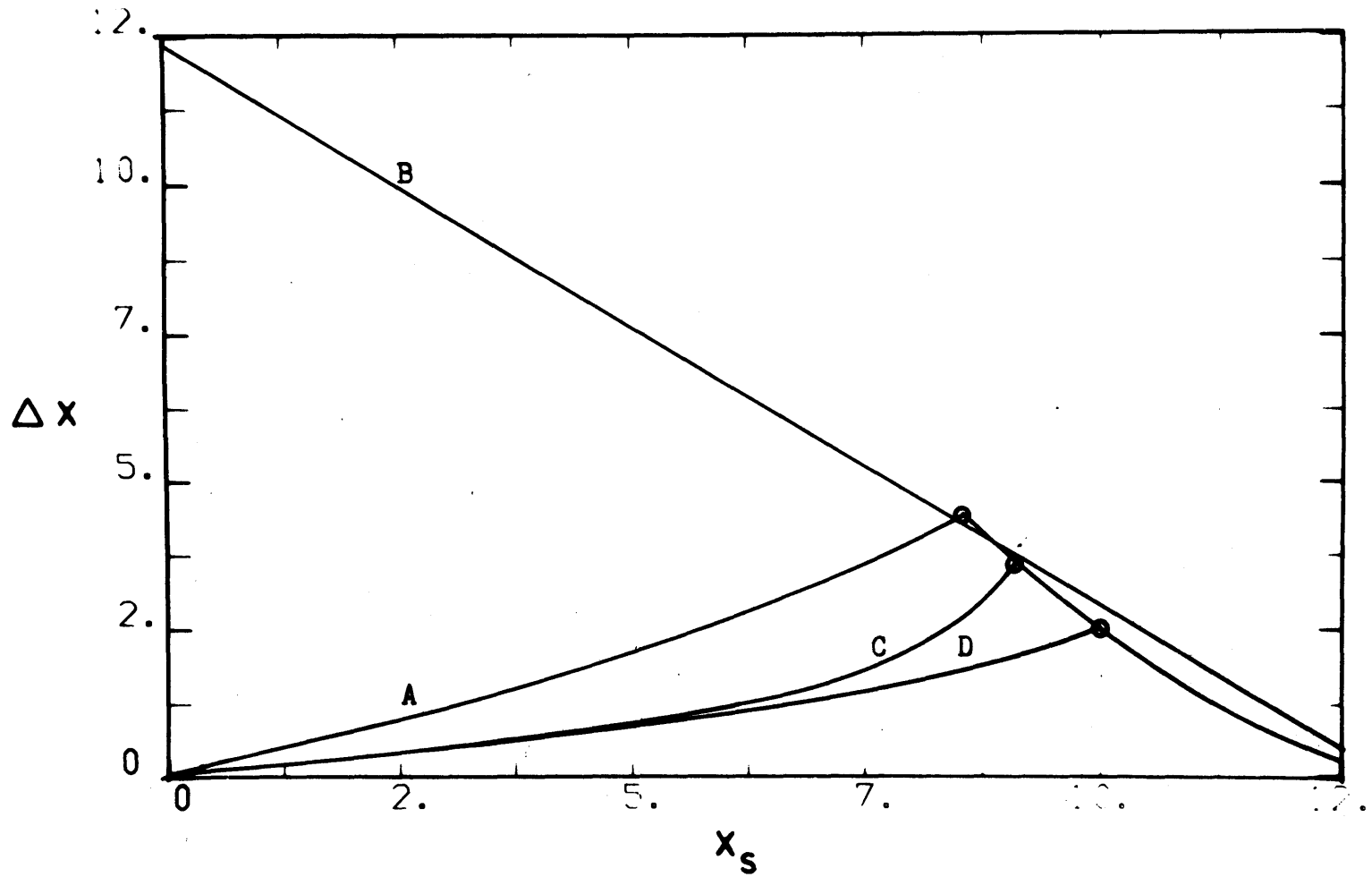


Figure 50. Width of the mushy region versus position of the root for cases of Figure 46.

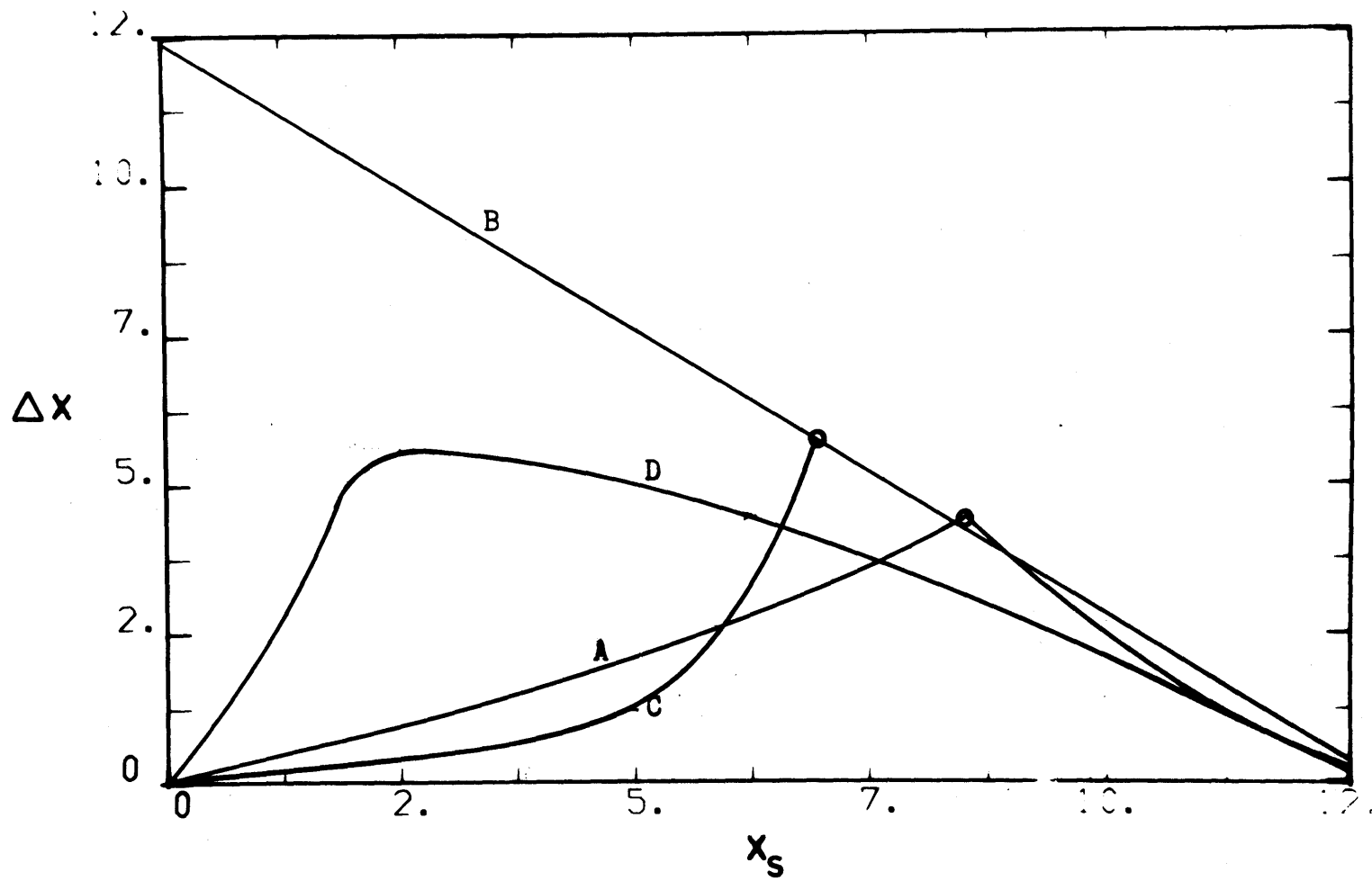


Figure 51. Width of the mushy region versus position of the root for cases of Figure 47.



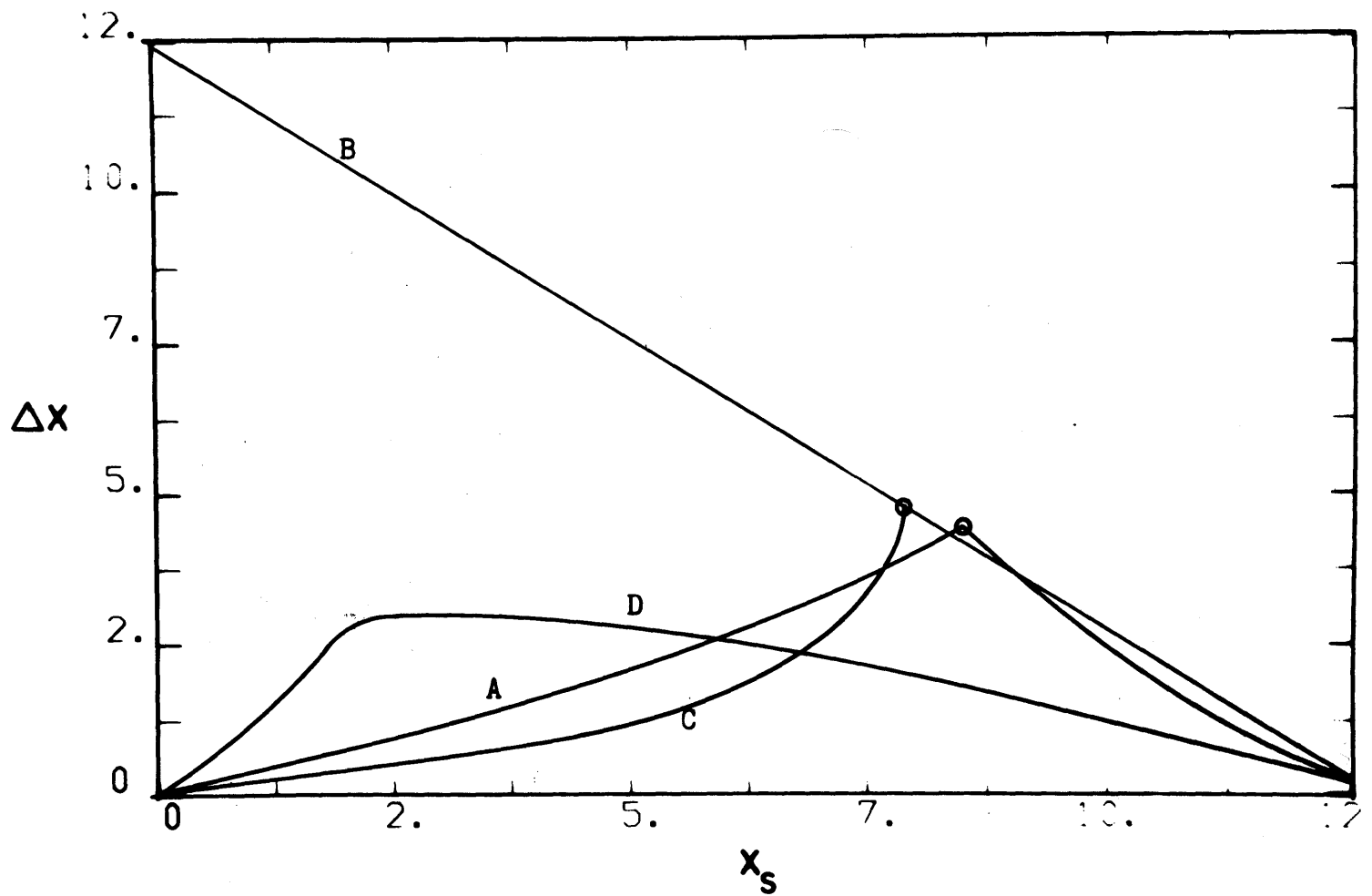


Figure 52. Width of the mushy region versus position of the root for cases of Figure 48.

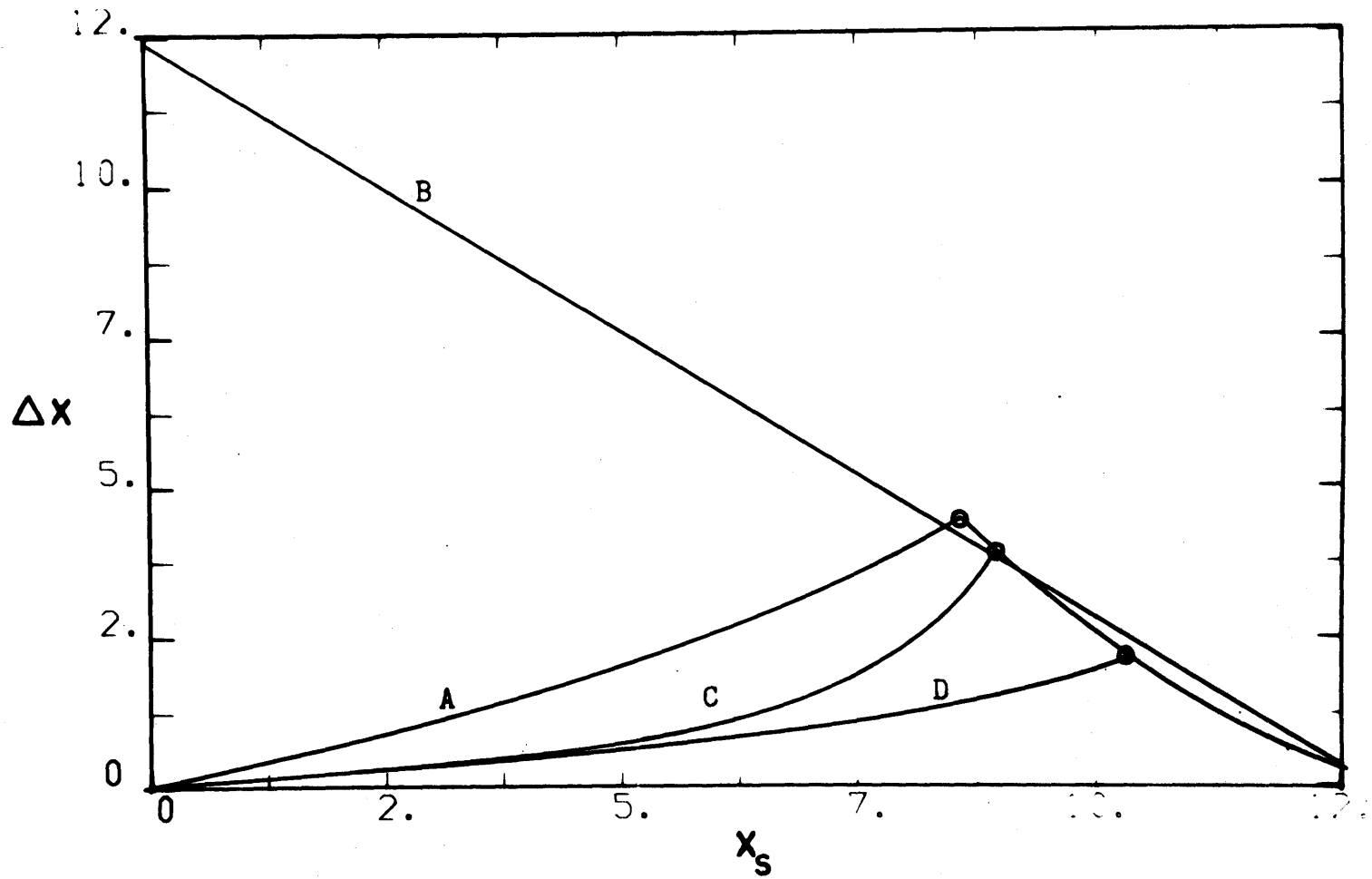


Figure 53. Width of the mushy region versus position of the root for cases of Figure 49.

## Chapter VII

## APPENDIX A

Numerical Procedure Used in Calculation  
of Heat Flow in Unidirectional  
Solidification of Alloys

A. Standard Solution of the Heat Flow Equation (Explicit)

The standard method of solving Equation (1) numerically is to set up a grid of  $N$  points across the length of interest, and write a separate heat balance for each of these  $N$  points or nodes such as:

$$\rho C_p \frac{dT}{dt} = \frac{(K \frac{\Delta T}{\Delta x} \Big|_x^+ - K \frac{\Delta T}{\Delta x} \Big|_x^-)}{x} + \rho_s H \frac{\Delta f_s}{\Delta t} \quad (A1)$$

where the symbols are as defined earlier and the  $+$  and  $-$  refer to the right and left sides of the point, respectively.

With the solid distribution assumed in Figure 1b, the term  $\rho_s H \Delta f_s / \Delta T$  can be reduced to a constant additive term  $H / (T_t - T_E)$  where  $T_t$  is the liquidus temperature,  $T_L$ , minus a small amount of dendrite tip undercooling. The term is zero for all slabs whose temperature is greater than  $T_L$  or less than  $T_E$ , because  $df_s / dt$  is zero in these regions.

If an explicit technique is used to solve the  $N$  equations of the form (A1):

$$\begin{aligned} dT(1)/dt &= f_1(T, t) \\ &\vdots \\ dT(N)/dt &= f_N(T, t) \end{aligned} \quad (A2)$$

then the left hand side is replaced by some form of the time derivative such as:

$$dT(J)/dt = \frac{T_{t+\Delta t}(J) - T_t(J)}{\Delta t} \quad (A3)$$

Although higher order terms of the expansion of the time derivative around time = t may be used, the method is called explicit as long as the temperature at time, t+Δt may be expressed as a function of temperature at time, t. In a following section of this appendix, an implicit technique will be presented which will be shown to be more advantageous than the explicit technique.

For the explicit technique, a set of N equations is formed as follows:

$$T'(J) = \frac{T(J+1) - (2-M)T(J) + T(J-1)}{M} \quad (A4)$$

For J = 1 to N

where

$$\begin{aligned} M &= \Delta x^2 / \alpha \Delta t \\ \alpha &= \bar{k} / (\bar{\rho} \cdot (\bar{C}_p + H / (T_t - T_E))) \\ T' &= T_{t+\Delta t} \end{aligned}$$

This set can be solved for T' (1) to T' (N) at each time step, then replacing T by T' and repeated for the next time step (Δt). The technique is known as Euler's method, and the size of the time step is constrained to be small.

B. Murray and Landis' Treatment of Solidification Discontinuities

Due to the presence of a heat generation event which occurs during solidification of an alloy at the dendrite tip and root (represented by Equations (6b) and (7) in the text), the temperature discontinuities resulting from these moving internal boundaries must be properly included into the heat flow solution.

Murray and Landis (ref. 19) present a method for including these calculations in a numerical solution to the heat flow equation for melting or freezing of a pure material. This method was used and applied to both the tip and root isotherms. The slight modification of the method required comes about when the tip and root are within two or less grid points of each other. The method will be presented here for a single discontinuity, since both tip and root are treated exactly alike.

Let the solidification isotherm be contained in slab I, which is  $\Delta x$  wide with the grid point I at the mid-point. The heat which is given off at this isotherm,  $H(I)dx/dt$ , is assumed to be felt only in this slab. All other slabs are treated as in equation (A4). Slab I is not included in the heat flow calculations, but rather its temperature is calculated by forming a three point interpolation on both sides of the isotherm, which gives rise to two temperatures for the mid-point temperature of slab I,  $T_{SE}^+$  and  $T_{SE}^-$  (refer to Figure 6). The formulae used were:

$$T_{SE}^+ = T_x \cdot \frac{2}{(2 - \delta x/\Delta x)(1 - \delta x/\Delta x)} \quad (A5)$$

$$- T(I + 1) \cdot \frac{2 \cdot \delta x/\Delta x}{(1 - \delta x/\Delta x)}$$

$$+ T(I + 2) \cdot \frac{\delta x/\Delta x}{(2 - \delta x/\Delta x)}$$

$$T_{SE}^- = T_x \cdot \frac{2}{(2 + \delta x/\Delta x)(1 + \delta x/\Delta x)} \quad (A6)$$

$$+ T(I - 1) \cdot \frac{2 \cdot \delta x/\Delta x}{(1 + \delta x/\Delta x)}$$

$$- T(I - 2) \cdot \frac{\delta x/\Delta x}{(2 + \delta x/\Delta x)}$$

where:  $T_x = T_E$  or  $T_t$ , depending on whether the tip or root was in slab I

$\delta x =$  distance between grid point I and the isotherm (refer to Figure 6, where I is referred

$$\therefore -\frac{\Delta x}{2} < \delta x < \frac{\Delta x}{2} \quad \text{to as K)}$$

Although  $\delta x$  may be positive or negative, and Equations (A5) and (A6) are defined over the full range of  $\delta x$ , the temperature of slab I is set to  $T_{SE}^-$  when  $0 < \delta x$  and to  $T_{SE}^+$  when  $0 > \delta x$ .

$T_{SE}^+$  and  $T_{SE}^-$  are also used in the equations set (A4) for the calculation of the temperatures in slabs I + 1 and I - 1.

After the new temperature of the slabs have been calculated from Equations (A4) and set with Equations (A5)

or (A6) in slab I, the new position of the boundary can be calculated from Equations (6b) for the tip and (7) for the root:

$$\Delta \delta x_m = (\Delta t / (f_m \cdot \rho_m - H)) \left\{ \frac{(\bar{K}_m (T_{SE}^- - T(I-1))}{\Delta x} - \frac{\bar{K}_M (T(I+1) - T_{SE}^+)}{\Delta x} \right\} \quad (A7)$$

where: the subscript m refers to the properties at either the tip or root, depending on which new position is to be calculated.

Then  $\delta x_{t+\Delta t} = \delta x_t + \Delta \delta x_x$ , for both the tip and root, and the calculation may proceed for the next time step.

The cycle for each calculation is:

- (1) Calculate new positions of the boundaries;
- (2) Interpolate temperatures of the boundary-containing slabs and set them;
- (3) Perform heat flow calculations in the solid, mushy, and liquid regions, excluding the boundary-containing slabs;
- (4) Replace T by T' and start at (1) again.

The two problems in keeping track of the two internal boundaries by the above method are:

- (1) The start up and final stages of the process must be treated separately. That is, when either discontinuity is within one grid point of the surface or center of the simulated casting, special two point formulae

must replace Equations (A5) and (A6).

(2) When and if the tip and root are within 2 or less grid points of each other, special formulae must again be used to replace Equations (A5) and (A6). These formulae are of the same form as (A5) or (A6) with appropriate substitutions made for  $T(I + 1)$ ,  $T(I + 2)$ ,  $T(I - 1)$ , or  $T(I - 2)$  where necessary.

The above problems present no mathematical difficulty, but rather the inclusion of the tests for each possible condition increases the run-time of the program considerably.

### C. Temperature Dependent Properties

In addition to the discontinuities, there are temperature (and, therefore, space) dependent properties to be included, which arise from conditions in the mushy zone. The most important of these is the thermal conductivity variation, as can be seen in Equation (A1), where the right hand side must be treated as  $\underline{d}/dx (\bar{K} dT/dx)$  rather than  $\bar{K} d^2T/dx^2$ .

Therefore, the following method is used during the solution at each time step: the thermal properties of the slab J, in the mushy zone, are determined from Equations (13), (14) and (15) or (16). The thermal conductivities to be used for heat into slab J ( $\bar{K} \Delta T / \Delta x^+$  in Equation A1) and heat out ( $\bar{K} \Delta T / \Delta x^-$ ) are taken as an average, since the



heat flows through a distance  $\Delta x/2$  with one  $\bar{K}_m$  and then  $\Delta x/2$  with the other  $\bar{K}_m$ . (Refer to Figure 2a). That is for slab J ( $T_E < T(J) < T_L$ ),

$$\begin{aligned}(\bar{K}_m)^+ &= (\bar{K}_m(J+1) + \bar{K}_m(J))/2 \\ (\bar{K}_m)^- &= (\bar{K}_m(J-1) + \bar{K}_m(J))/2\end{aligned}\tag{A8}$$

where:  $\bar{K}_m(J)$ ,  $\bar{K}_m(J+1)$ ,  $\bar{K}_m(J-1)$  are thermal conductivities of slabs J, J+1, J-1 respectively; these are calculated using Equations (15) or (16).

It should be noted that the above method is also used in heat flow in the solid and liquid regions; but since  $\bar{K}_m(J+1) = \bar{K}_m(J)$  in these regions, the effect is as if the right hand side of Equation (1) where  $\bar{K} d^2T/dx^2$ .

For the case of high convection in the liquid, the above method is employed. But since the slabs containing the tip and root are treated separately, the thermal conductivity in front of the tip,  $\bar{K}_x$  in Equation (A7), becomes important. Physically, there is a fluid mechanical boundary layer in front of the tip, so that a good approximation for  $\bar{K}_x$  is that it has the same value as  $\bar{K}_L$  for still liquid. Thus the liquid directly in front of the tip is considered to be still, but that the liquid at the next slab ahead of the tip is considered to be highly convecting.

D. Implicit Versus Explicit Finite Difference Techniques

As noted previously there are two general methods of solution for a set of differential equations of the type (A2). The explicit technique, which was presented above, is derived by using the first term of the Taylor series expansion of the function  $T$  around time,  $t$ . (Equation A3).

If the higher order terms are neglected, this is called Euler's Method, and the error in using Equation (A8) is on the order of  $(\Delta t)^2$ . However, when Equation (A3) is substituted into the set (A2) to obtain (A4), the stability parameter  $M$  must be numerically greater than or equal to 2.

This puts a severe restriction on the size of the time step  $(\Delta t)$  for a given  $\Delta x$ . For instance, for  $\alpha = .65$  (solid Al-4.5% Cu alloy),  $N = 25$ , length = 50 cm, this restricts  $\Delta t$  to  $\leq 3.07$  sec. Note that since we assign a high thermal conductivity to the liquid to approximate the effect of convection in the melt, (as much as 10 times as high as the solid thermal conductivity) this will force the time step to be  $\leq 0.3$  sec. This requirement provides unnecessary accuracy, since for  $\Delta t = 0.3$  sec, the error in the resultant  $dT/dt$  is  $\sim (\Delta t)^2$  or 0.09 sec. The advantage of the implicit technique is that the solution is stable (conditionally), so that the error requirement rather than the stability requirement may be used to determine the appropriate time step.

To derive the implicit method, we substitute (A3) into (A2) and rearrange:

$$T_{t+\Delta t}(J) = T_t(J) + \Delta t \cdot f_{J,t} \quad (A9)$$

To increase the stability of this equation, a substitution is made for  $f_J(T,t)$ :

$$T_{t+\Delta t}(J) = T_t(J) + \Delta t \left( \frac{1}{2} f_J(T,t) + \frac{1}{2} f_J(T,t+\Delta t) \right) \quad (A10)$$

where: the temperature at the time,  $t+\Delta t$  appears on both sides of the equation. The unknown temperature at time,  $t+\Delta t$  is implicit on the right hand side of the equation, thus, the name of the method. That the method is more stable than the explicit can be seen qualitatively from the consideration that the averaging of the slopes ( $f_J$ ) at time,  $t$ , and  $t+\Delta t$ , tends to smooth out highly transient behavior in  $dT/dt$ , therefore, the "overshooting" problem of the explicit method is partially avoided.

The system of Equations (A10) could be solved iteratively at each time step to obtain  $T_{t+\Delta t}$ . However, due to the nature of the finite difference forms of the heat flow equation, Crank and Nicholson (Ref. 7, p. 474) have presented a method of solution which involves solving a new system of equations:

$$L_r = \Delta t \left\{ f_r(T, t) + \frac{1}{2} \sum_{J=1}^N L_J \frac{2}{2T_J} (f_r(T, t)) \right\}$$

$$\text{for } r = 1 \text{ to } N \quad (A11)$$

which rearranges to a matrix equation:

$$\bar{L} = [\bar{A}]^{-1} \bar{B} \quad (A12)$$

Then:

$$T_{t+\Delta t}(J) = T_t(J) + L_J \quad (A13)$$

The method we use to solve the matrix equation (A12) simultaneously with a Gaussian elimination type of solution, taking advantage of the fact that the matrix A in the matrix Equation (A12) is tri-diagonal. This saves computer time and storage, and makes the implicit method all the more useful.

This implicit method is used to solve the heat flow equations in the solid, liquid and mushy regions. Each region is treated separately, with the surface BC (Equation 2) and the root (Equation 4a) boundaries for the solid, the root and the tip (Equation 4b) for the mushy region, and the tip and the center (Equation 3) for the liquid boundaries. The coupling of the regions is included by Equations (6b) and (7), which are solved via Equation (A7). Equation (A7) is solved for both the tip and root position with Euler's method, and since the stability requirement of these equations forces a smaller  $\Delta t$  to be used than for the heat flow calculations, a separate loop is included in

the computer program to cycle through P time steps of the solution of (A7) for each single time step of the heat flow solution, where

$$P = \frac{\text{time step of heat flow calculation}}{\text{time step of position (A7) calculation}}.$$

An estimate of the error involved in the method is presented in Appendix E.

## Appendix B

Modifications of the Uni-Directional Numerical  
Procedure, for the Solution of Radial and  
Side Heat Loss Heat Flow

A. Radial Heat Flow

Consider a shell balance for heat made on a cylindrical element:

Heat accumulated = Heat in - Heat out + Heat generated

$$\begin{aligned}
 V\rho C_p \frac{dT}{dt} &= A_1 \bar{K}_1 \left. \frac{dT}{dr} \right|_1 \\
 &\quad - A_2 \bar{K}_2 \left. \frac{dT}{dr} \right|_2 + V\rho_s H \frac{df_s}{dt}
 \end{aligned}
 \tag{B1}$$

where A is the area across which heat flows into the element, V is the volume of the element, and the subscripts 1 and 2 refer to the two surfaces across which heat flows,  $r_1 > r_2$ .

In finite different form, this becomes:

$$\begin{aligned}
 \rho C_p \frac{\Delta T_J}{\Delta t} &= \frac{1}{\Delta r} \left( \frac{2r_1}{r_1 + r_2} \right) \bar{K} \frac{(T_J - T_{J+1})}{\Delta r} \\
 &\quad - \left( \frac{2r_2}{r_1 + r_2} \right) \bar{K} \frac{(T_{J-1} - T_J)}{\Delta r} \\
 &\quad + \rho_s H \Delta f_s / \Delta t
 \end{aligned}
 \tag{B2}$$

where the volume of the element has been approximated by

$$2\pi \Delta r (r_1 + r_2) / 2$$

A comparison of Equations (B2) with Equation (A1) shows that the finite difference forms of the heat flow equations differ only in the coefficients in the  $\Delta T/\Delta x$  terms. This means that the solution for the radial case is found in exactly the same manner as for the uni-directional case except for the coefficients  $(2r_J/r_J+r_{J+1})$  and  $(2r_{J+1}/(r_J+r_{J+1}))$  which are calculated for each element J and included in the matrix solution, Equations (A11) - (A13).

B. Side Heat Loss

The effect of heat loss from the side has been presented mathematically in the Introduction. The computer model implements this heat loss by simply reducing the temperature of each slab by

$$\Delta T_{J \text{ side}} = \frac{\Delta t}{\rho C_p} q_x$$

where  $q_x$  is either  $h(T_J - T_{A, \text{side}})$  or  $a/\sqrt{t}$ , as presented in the introduction. This is accomplished by a simple calculation made at each time step after the x-direction heat flow equations have been solved.

The slabs which contain the tip or root are not treated in the same manner. Rather than reducing the temperature of these slabs, the heat loss to the side,  $q_x$ , is included in the position equation (6b) at each time step.

## APPENDIX C

Results of Dimensional Analysis of the Problem  
of Heat Flow During Solidification

A consideration of the differential equations and the solidification model (presented in the Introduction) pertinent to this problem shows that the variables which must be included in the analysis are: (refer to Table I for definitions)

| <u>property</u> | <u>units<br/>(absolute)</u> | <u>property</u>     | <u>units<br/>(absolute)</u> |
|-----------------|-----------------------------|---------------------|-----------------------------|
| 1. $h_b$        | $M/\theta^3 T$              | 13. $\alpha_s$      | $L^2/\theta$                |
| 2. $K_s$        | $ML/\theta^3 T$             | 14. $C_{pl}$        | $L^2/\theta^2 T$            |
| 3. $\alpha_L$   | $L^2/\theta$                | 15. $H_l$           | $L^2/\theta^2$              |
| 4. $T_m - T_s$  | T                           | 16. $H_s$           | $L^2/\theta^2$              |
| 5. $T_p - T_s$  | T                           | 17. $C_{pm}$        | $L^2/\theta^2 T$            |
| 6. $T_o - T_m$  | T                           | 18. $\alpha_m$      | $L^2/\theta$                |
| 7. $K_l$        | $ML/\theta^3 T$             | 19. $\bar{K}_m$     | $ML/\theta^3 T$             |
| 8. L            | L                           | 20. $q'$            | $M/\theta^3$                |
| 9. $x_s$        | L                           | 21. $T_m - T_{a,s}$ | T                           |
| 10. H           | $L^2/\theta^2$              | 22. W               | L                           |
| 11. t           | $\theta$                    | 23. $h_s$           | $M/\theta^3 T$              |
| 12. $C_{ps}$    | $L^2/\theta^2 T$            | 24. $T_{le}$        | T                           |
|                 |                             | 25. $C_{ple}$       | $L^2/\theta^2 T$            |
|                 |                             | 26. a               | $M/\theta^{2.5}$            |



The Buckingham Pi method was applied to the problem (see Reference 28 for details). The first four variables,  $h_b$ ,  $K_s$ ,  $\alpha_L$ , and  $T_m - T_s$  were chosen as the base of the analysis. The resultant groups of dimensionless numbers produced are listed below. It should be noted that the Buckingham Pi method assures that the dimensionless groups produced will completely describe the problem (as much as the variables used will), but the exact form of the groups produced depends on the choice of the variables used as the base of the analysis. According to the rules of dimensional analysis, however, any dimensionless group may be replaced by a combination of other groups with no loss in information. Therefore, the groups listed below do not represent the actual groups produced by this analysis, rather they are the groups which are commonly associated with heat flow. The forms of many of these groups come from the form of the differential equations and boundary problems, but as noted above, they also can be obtained by combinations of the groups formed by the Buckingham Pi method.

For Unidirectional Solidification of Pure Metals with Superheat, Infinite or Finite Heat Transfer Coefficient, and Any Degree of Convection:

- |                            |                             |
|----------------------------|-----------------------------|
| 1. $T_p - T_s / T_m - T_s$ | 6. $(T_p - T_m) C_{ps} / H$ |
| 2. $T - T_s / T_m - T_s$   | 7. $\alpha_s t / L^2$       |
| 3. $K_l / K_s$             | 8. $(T_m - T_s) C_{ps} / H$ |
| 4. $h_b L / K_s$           | 9. $\alpha_l / \alpha_s$    |
| 5. $x_s / L$               | 10. $C_{ps} / C_{pl}$       |

For radial solidification, replace L by R and  $X_s$  by  $R-r_s$ .

For the solidification of alloys, add:

- |     |                 |     |                     |
|-----|-----------------|-----|---------------------|
| 11. | $x_s/x_1$       | 14. | $\alpha_m/\alpha_s$ |
| 12. | $H_s/H_1$       | 15. | $K_m/K_s$           |
| 13. | $C_{pm}/C_{ps}$ |     |                     |

For the parabolic heat input, add:

16.  $q/K_s(T_m - T_s)$  or  $q\sqrt{\alpha}/K_s L(T_m - T_s)$  cal/sec/cm<sup>2</sup>

For side heat loss, with constant heat transfer coefficient on the side, add:

- |     |                         |     |                             |
|-----|-------------------------|-----|-----------------------------|
| 17. | $h_s L^2 / W \bar{K}_s$ | 19. | $T_{a,s} - T_s / T_m - T_s$ |
| 18. | $h_s / h_b$             |     |                             |

For equi-axed, high convection growth add:

- |     |                            |     |                    |
|-----|----------------------------|-----|--------------------|
| 20. | $T_{le} - T_s / T_m - T_s$ | 21. | $C_{ple} / C_{ps}$ |
|-----|----------------------------|-----|--------------------|

For parabolic heat loss from the side, add:

22.  $a L(\alpha_s)^{1/2} / K_s W$

## APPENDIX D

## A Listing of the Program

The following program was written in Fortram IV, and was compiled with the I.B.M. Level H compiler, with an optimization level of 2. Various statistics for compilation and execution are:

(These apply to the I.B.M. 360/65/40 system at M.I.T.)

Number of Fortran statements = 850

Compile time (H Compiler) = 90 seconds

Core storage necessary for program and Fortran routines = 30K bytes

Number of implementation dependent routines = none

Number of iterations (time steps) per second of computer time = 20 to 27.

The number of iterations per computer second varies as the variable 'CYLL' varies.

The run time required to simulate the solidification of a casting of given length depends on the accuracy and external conditions read into the program. A typical time is 50 seconds of computer time to simulate the solidification of a 6" casting, of an alloy with 0 degrees superheat, no convection, infinite h, and accuracy level between 0.1% to 0.03%.

The listing of the program follows.

C MAIN PROG FOR CASTING PROBLEM

C

PROGRAM LAST MODIFIED MAY,1970

C

C

C

C

THIS ROUTINE IS A SOLUTION OF A ONE DIMENSIONAL HEAT FLOW PROBLEM

C

IT USES A METHOD OF FINITE

C

DIFFERENCES,AND DOES A LINE RELAXATION(SINGLE STEP)

C

FEATURES OF THE PROGRAM..

C

1) HEAT AT CENTER IS SPECIFIED FUNCTION OF TIME

C

2) SURFACE TEMPERATURE IS SPECIFIED IN ONE OF TWO WAYS;

C

A) AS A SPECIFIC FUNCTION OF TIME, OR B) AS A CONSTANT HEAT TRANSFER  
COEFFICIENT(FROM WHICH EACH TEMPERATURE IS CALCULATED. )

C

THE SURFACE SLAB IS NEVER INCLUDED IN THE SIMULATION DIRECTLY,  
ONLY INDIRECTLY AS A CONSTANT TEMPERATURE.

C

3) THE POSITIONS OF THE LIQUIDUS AND SOLIDUS ARE CALCULATED

C

AT EACH TIME STEP FROM SEPERATE EQUATIONS(Q IN = Q OUT+HEAT)

C

THIS METHOD IS SIMILIAR TO(AN EXTENSION OF) THE METHOD

C

OF MURRY AND LANDIS. IT IS NECESSARY IN ORDER TO TAKE

C

ACCOUNT OF THE HEAT EVENTS AT THE TIP AND ROOT PROPERLY.

C

4) INTEPPOLATION NECESSARY IS DONE BY USING A THREE POINT FIT

C

WHENEVER POSSIBLE,AND TWO POINT FITS IF NOT.

C

5) THE TEMPERATURES OF THE SLABS WHICH CONTAIN THE ROOT OR THE TIP ARE

C

TREATED SPECIALLY,IE,THEIR TEMPERATURES ARE SET FROM INTERPOLATION,

C

NOT CALCULATED FROM THE FINITE DIF. EQNS. THESE SLABS ARE INCLUDED

C

IN THE HEAT FLOW SOLUTION,HOWEVER,AS THE RESULTANT TEMPERATURES ARE

C

USED TO SET THE POSITIONS AT THE TIME STEP.

C

A CRANK-NICHOLSON METHOD IS USED TO SOLVE THE EQUATIONS

C

C

C

C

C

THE CONSTANTS APPEARING IN VARIOUS PLACES IN THIS PROGRAM

C

ARE THOSE WHICH APPLY TO A AL-4.5%CU ALLOY

C

THE THERMAL DATA MAY BE READ IN,SO THAT THE PROGRAM ITSELF

C

C WOULD BE APPLICABLE TO ANY ALLOY(THE COOLING OF SOLIDS  
 C OR THE FREEZING OF PURE MATERIALS IS A SUBSET OF THIS)  
 C THE ONLY CONSTANTS WHICH APPLY ONLY TO AL-4.5%CU ARE  
 C THOSE USED IN THE SCHEIL DISTRIBUTION EQUATIONS...  
 C IF A LINEAR DISTRIBUTION IS USED, HOWEVER(CHOSEN BY  
 C SPECIFYING A VALUE OF '0' FOR THE FLAG ISHEIL,BELOW) THEN  
 C THIS MODIFICATION OF THE EQUATIONS IS NOT NECESSARY  
 C RESULTS INDICATE THAT THE SCHEIL DISTRIBUTION HAS PRACTICALLY  
 C NO EFFECT ON THE TEMPERATURE DISTRIBUTION OR POSITIONS OF  
 C THE TIP AND ROOT, THEREFORE IF A SCHEIL DISTRIBUTION IS DESIRED,  
 C THE SIMULATION COULD BE RUN WITH A LINEAR DISTRIBUTION, AND THE  
 C RESULTANT TEMPERATURES CONVERTED TO FRACTION SOLID WITH  
 C THE SCHEIL EQUATION WITH THE SAME RESULTS  
 C

C -----  
 C IF THE SURFACE TEMPERATURE AT TIME ONE(SURTEM(1)) IS LESS  
 C THAN ZERO, THEN THE CONSTANT HEAT TRANS. COEF READ IN WILL BE USED  
 C OTHERWISE, THE GIVEN SURFACE TEMP. WITH TIME WILL BE USED.  
 C -----

C RADIAL HEAT FLOW SIMULATION CAPABILITY ADDED... MARCH 13, 1970  
 C THIS IS ACCOMPLISHED BY RE-DERIVING THE HEAT FLOW EQUATIONS FOR  
 C RADIAL(CYLINDRICAL) SHELLS... THE RESULTANT HEAT FLOW EQUATIONS  
 C DIFFER FROM THE UNI-DIRECTIONAL ONES ONLY IN THE COEFFICIENT  
 C WHICH REPRESENTS THE AREA... SEE BLOCK 'MATX' FOR DETAILS  
 C -----

|  |      |
|--|------|
| DIMENSION TSAV(50), TSAVL(50), TSAVT(50), TSAVC(50)                    | INIT |
| DIMENSION S(100), TKS AV(50), EX(50), AK(2), TKINT(50), TT(20), TR(20) | INIT |
| DIMENSION EM1(3), EM(3), LIST(50), DIST(10), IN(10)                    | INIT |
| DIMENSION F(100), Q(100), A(100,3)                                     | INIT |
| COMMON SURTEM(20), GLOBAR(40), R(50), EPSILO(20), T(50)                | INIT |
| COMMON PT, DELT, DCYL, CYLL, HIGHC, FLOWC, TSEC, TL, TE, TKS, TKL      | INIT |
| COMMON CPS, CPL, RHS, RHL, HOF, FRE, FRT, FSC, TKFACT, ALEN, DELX      | INIT |
| COMMON TIN, POSL, POSX, SEC, H, DELTS, TA, HS, XS, TAS, ANU, DELTQ     | INIT |
| COMMON NAME(10), N, NCYCLE, NSCYL, ICONT, KTFLG, KGR, NEPS, LCONT      | INIT |
| COMMON ISHEIL, IRADFL, ISTFLG, KHIN                                    | INIT |
| REAL*8 A, Q, F, EM   | INIT |



|   |   |      |
|---|---|------|
|   | READ(5,819) DIST  | INIT |
|   | IF(DELT.LT.0.) STOP   | INIT |
| C |   | INIT |
| C | THE FOLLOWING VALUES OF THE THERMAL PROPERTIES ARE CONSIDERED | INIT |
| C | STANDARD....FOR SPECIAL RUNS,THEY MAY BE READ IN BY           | INIT |
| C | USING THE FLAG 'ITHPRO'                                       | INIT |
| C |   | INIT |
|   | TKS=0.43  | INIT |
|   | TKL=0.243   | INIT |
|   | CPS=.220  | INIT |
|   | CPL=0.24  | INIT |
|   | RHS=2.75  | INIT |
|   | RHL=2.645   | INIT |
|   | HOF=75.   | INIT |
|   | TE=548.   | INIT |
|   | IF(ITHPRO.EQ.1)READ(5,818)TKS,TKL,CPS,CPL,RHS,RHL,HOF,TE      | INIT |
|   | HIGHC=1.  | INIT |
|   | FLOWC=0.  | INIT |
| C |   | INIT |
| C | THE FOLLOWING READ TAKES PLACE IF THE USER HAS SPECIFIED      | INIT |
| C | THAT CONTROL OF THE LOOP WITH RESPECT TO DEL TIME IS TO TAKE  | INIT |
| C | PLACE.IF NO CONTROL(LCONT=0) THE STANDARD VALUES OF THE       | INIT |
| C | CONTROL VARIABLES ARE SUCH THAT NO TESTING SHOULD TAKE        | INIT |
| C | PLACE,AND THEREFORE,THE PROGRAM WILL OPERATE AT THE           | INIT |
| C | SAME SPEED AS BEFORE  | INIT |
| C | THE VARIABLES TO CONTROL THE LOOP ARE;                        | INIT |
| C | 1) ICONT...THE NUMBER OF ITERATIONS AT WHICH THE CONTROL IS   | INIT |
| C | TO BE APPLIED   | INIT |
| C | 2) FLOWC...THE LIMIT AT WHICH THE TIME STEP MAY BE DOUBLED    | INIT |
| C | 3) HIGHC... THE LIMIT AT WHICH THE TIME STEP WILL BE REPEATED | INIT |
| C | AT HALF THE CURRENT TIME STEP                                 | INIT |
| C |   | INIT |
|   | ICONT=10000   | INIT |
|   | IF(LCONT.EQ.1)READ(5,871) ICONT,FLOWC,HIGHC                   | INIT |
|   | TCONT=ICONT*DELT  | INIT |
| C |   | INIT |

```

C          CONDITIONAL READ IF POINTS SPECIFIED          INIT
C                                                     INIT
C          IF(NEPS.NE.0) READ(5,819) EPSTLO             INIT
C.....                                                     INIT
C                                                     BEGIN  INITIALIZATION  INIT
C                                                     INIT
C          THE PURPOSE OF BLOCK 'INIT' IS              INIT
C          1) INITIALIZE THE TEMPERATURE PROFILE AT TIME T=0.  INIT
C          2) INITIALIZE THE CONSTANTS WHICH WILL BE USED IN THE TIME  INIT
C              LOOP WHICH DO NOT CHANGE                INIT
C          3) SET UP THE VALUES OF THE THERMAL PROPERTIES AND  INIT
C              THE FLAGS FOR THE FIRST ITERATION,WHICH WILL BE  INIT
C              CONTROLLED BY THE TIME STEP LOOP THEREAFTER  INIT
C                                                     INIT
C          DELTCY USED BELOW IS THE NUMBER OF TIMES THAT THE POSITIONS ARE  INIT
C          CALCULATED PER TIME STEP OF HEAT FLOW        INIT
C                                                     INIT
C          KROLD=1                                       INIT
C          KTOLD=1                                       INIT
C          IHCFLG=1                                       INIT
C          DELTCY=DELT/NCYCLF                               INIT
C          HPRINT=PT                                       INIT
C          DELX=ALEN/N                                     INIT
C          DCYL=DELX/CYLL                                   INIT
C          IF(NSCYL.EQ.0) NSCYL=1                           INIT
C          CONST=DELX*DELX/DELT                             INIT
C          EX(1)=CONST*RHL*CPL                             INIT
C                                                     INIT
C                                                     INIT
C          DELT IS THE TIME STEP(INITIAL)                INIT
C                                                     INIT
C          KCNTL=1                                         INIT
C          DO 7777 J=1,N                                    INIT
C          R(J)=0.                                         INIT
C          S(J)=0.                                         INIT
7777  CONTINUE                                           INIT

```



|     |   |      |
|-----|---|------|
| C   |   | INIT |
| C   | ARRAYS 'IN','S','R','DIST' ARE USED TO CALC. THE TEMPERATURES | INIT |
| C   | AT SPECIFIED POINTS ALONG THE LENGTH OF THE CASTING,          | INIT |
| C   | ...FOR THE PURPOSE OF COMPARISON TO T.C. READINGS             | INIT |
| C   |   | INIT |
|     | IF(NDIST.EQ.0) GO TO 858                                      | INIT |
| C   |   | INIT |
| C   | R WILL BE WRITTEN OUT AND LATER RE-USED                       | INIT |
| C   |   | INIT |
|     | DO 859 J=1,NDIST  | INIT |
| 859 | R(J)=DIST(J)  | INIT |
|     | DO 961 J=1,20   | INIT |
|     | TR(J)=0.  | INIT |
| 961 | TT(J)=0.  | INIT |
|     | DO 855 J=1,40   | INIT |
|     | GLOBAR(J)=GLOBAR(J)*FACT                                      | INIT |
| 855 | CONTINUE  | INIT |
|     | DO 856 J=1,10   | INIT |
|     | DIST(J)=DIST(J)+DELX/2.                                       | INIT |
|     | IN(J)=(DIST(J)/DELX)+1  | INIT |
|     | S(J)=DIST(J)-((IN(J)-1)*DELX+DELX/2.)                         | INIT |
| 856 | CONTINUE  | INIT |
| 858 | CONTINUE  | INIT |
|     | IT=0  | INIT |
|     | IP=0  | INIT |
|     | I=0   | INIT |
|     | DO 13 J=1,N   | INIT |
| 13  | T(J)=TIN  | INIT |
| C   |   | INIT |
| C   | INITIALIZATION FOR H COEFFICIENT SIMULATION                   | INIT |
| C   |   | INIT |
|     | KHIN=2  | INIT |
|     | IF(SURTEM(1).LE.0.) KHIN=1                                    | INIT |
|     | H=0.  | INIT |
|     | IF(KHIN.EQ.1)H=SURTEM(2)                                      | INIT |
| C   | FIRST ITERATION ALWAYS USES LIQUID PROPERTIES...              | INIT |



|      |   |      |
|------|---|------|
| C    | 1) ANALYTIC STARTING CONDITIONS...T (1) IS 0 AT TIME=0      | INIT |
| C    | 2) RESTART STARTING CONDITIONS...READ IN OLD STATUS OF LOOP | INIT |
| C    | AND CONTINUE SIMULATION                                     | INIT |
| C    |   | INIT |
| 2303 | READ(5,816)IQ,IR  | INIT |
|      | READ(5,817) TQP,TQM,TRP,TRM                                 | INIT |
|      | READ(5,817) POSL,POSX,SEC,HPRINT                            | INIT |
|      | READ(5,819) (T(NTP),NTP=1,N)                                | INIT |
|      | SL=POSL-((IQ-1)*DELX+DELX/2.)                               | INIT |
|      | SX=POSX-((IR-1)*DELX+DELX/2.)                               | INIT |
|      | TSD=T(1)  | INIT |
|      | ILFL=1  | INIT |
|      | IRFL=1  | INIT |
|      | ISKP=0  | INIT |
|      | MST=SEC/DELT  | INIT |
|      | GO TO 2301  | INIT |
| 2302 | CONTINUE  | INIT |
|      | MST=1   | INIT |
|      | IQ=1  | INIT |
|      | IR=1  | INIT |
|      | ILFL=1  | INIT |
|      | IRFL=1  | INIT |
|      | SX=(DELX/2.)*(TE/TIN)**2                                    | INIT |
|      | SL=(DELX/2.)*(TL/TIN)**2                                    | INIT |
|      | POSL=(DELX/2.)+SL   | INIT |
|      | POSX=(DELX/2.)+SX   | INIT |
|      | PJSLS=POSL  | INIT |
|      | PJSXS=POSX  | INIT |
|      | T(1)=SURTEM(1)  | INIT |
|      | TSD=SURTEM(1)   | INIT |
| C    |   | INIT |
| C    | ISKP IS USED AS A FLAG TO SKIP THE FIRST EXECUTION OF TH    | INIT |
| C    | POSITIONS ARE SPECIFIED IN THE INPUT(ANALYTIC STARTING)     | INIT |
| C    | POSITION CALCULATION BLOCKS,IN THE CASE WHERE THE INITIAL   | INIT |
| C    |   | INIT |
|      | ISKP=1  | INIT |



```

C KGR=0...SERIES HEAT FLOW,NO CONVECTION INIT
C KGR=1...PARALLEL HEAT FLOW,NO CONVECTION INIT
C KGR=2...SERIES HEAT FLOW,INFINITE CONVECTION(IN THE LIQUID) INIT
C KGR=3...PARALLEL HEAT FLOW,INFINITE CONVECTION INIT
C INIT
C TKEM=TKS INIT
C TKEP=TKS INIT
C TKLM=TKL INIT
C INIT
C THIS VERSION OF THE THERMAL CONDUCTIVITY IN FRONT OF INIT
C OF THE INTERFACE IS EQUIVALENT TO A FINITE BOUNDARY INIT
C LAYER TYPE OF CONVECTION...PREVIOUSLY,THE CONVECTION WAS INIT
C BROUGHT UP TO THE INTERFACE,WITH UNSTABLE RESULTS INIT
C INIT
C TKLP=TKL INIT
C INIT
C TKA,THE AVG SOLID&LIQUID CONDUCTIVITY,IS USED IN THE MOTION INIT
C EQUATIONS WHENEVER THE TIP AND ROOT ARE CLOSER THAN 2 SLABS INIT
C APART,IE,WHEN IQ<=IR+1 INIT
C TKA=(TKL+TKS)/2. INIT
C TLM=TL-.5 INIT
C TS=T(1) INIT
C NN=N+1 INIT
C DO 2305 J=1,NN INIT
2305 TSAB(J)=T(J) INIT
ANU=HS*XS/TKS INIT
C END INITIALIZATION INIT
C..... INIT
C SUBROUTINE 'WRITES' SIMPLY OUTPUTS THE SIMULATION PARAMETERS INIT
C TO THIS POINT ,THROUGH THE COMMON BLOCK ABOVE INIT
C INIT
C CALL WRITES INIT
C..... TVAR
C TVAR
C MAIN CALCULATION LOOP...J IS DISTANCE TVAR

```









|   |   |          |
|---|---|----------|
| C |   | TVAR     |
| C |   | TVAR     |
| 1 | CONTINUE  | TVAR     |
|   | SEC=SEC+DELT  | TVAR     |
|   | I=I+1   | TVAR     |
| C |   | TVAR     |
| C | CALCULATE SURFACE TEMPERATURE AND HEAT INPUT                          | TVAR     |
| C | DELTS IS THE INCREMENT OF TIME AT WHICH THE SURFACE TEMP IS TABULATED | TVAR     |
| C | DELTO IS THE TIME INTERVAL AT WHICH GLOBAR IS TABULATED               | TVAR     |
| C | DELTS IS IN SECONDS   | TVAR     |
| C | SURTEM IS THE ARRAY WHICH CONTAINS THE TEMPERATURES                   | TVAR     |
| C | TS IS THE SURFACE TEMP AT TIME 'SEC'                                  | TVAR     |
| C |   | TVAR     |
| C | .....   | CONTROLT |
| C | BLOCK CONTROL IS ASSOCIATED WITH BLOCK CONTROLX...                    | CONTROLT |
| C | IT SAVES THE STATUS OF THE TEMPERATURE AND POSITIONS SO THAT          | CONTROLT |
| C | IF THE CURRENT TIME STEP DOES NOT MEET THE ACCURACY TEST, IT          | CONTROLT |
| C | MAY BE REPEATED   | CONTROLT |
|   | ICNTL=0   | CONTROLT |
|   | IF(SEC.LT.TCONT) GO TO 1001   | CONTROLT |
|   | KCNTL=-1  | CONTROLT |
|   | ICNTL=1   | CONTROLT |
|   | SLST=SL   | CONTROLT |
|   | SXST=SX   | CONTROLT |
|   | SECST=SEC   | CONTROLT |
|   | POSLST=POSL   | CONTROLT |
|   | POSXST=POSX   | CONTROLT |
|   | IQST=IQ   | CONTROLT |
|   | IRST=IR   | CONTROLT |
|   | ILFLST=ILFL   | CONTROLT |
|   | IRFLST=IRFL   | CONTROLT |
|   | ISKPST=ISKP   | CONTROLT |
|   | TSOST=TSO   | CONTROLT |
|   | TK1ST=TKSAV(1)  | CONTROLT |
|   | LLCT=0  | CONTROLT |
|   | DO 1000 J=1,N   | CONTROLT |

|      |  |          |
|------|--|----------|
| 1000 | TSAVT(J)=T(J)  | CONTROLT |
| 1001 | CONTINUE   | CONTROLT |
| C    | .....  | CONTROLT |
|      | IF(KHIN.EQ.1) GO TO 1111                                       | TVAR     |
|      | SDS=SEC/DELTS  | TVAR     |
|      | IKL=SDS  | TVAR     |
|      | TS=(SURTEM(IKL+2)-SURTEM(IKL+1))*(SDS-IKL)+SURTEM(IKL+1)       | TVAR     |
|      | TSDEL=TS-TSO   | TVAR     |
|      | IF(TA.EQ.TS) GO TO 1112  | TVAR     |
|      | HBC=TKSAV(1)*(T(2)-T(1))/((TS-TA)*DELX)                        | TVAR     |
|      | GO TO 1112   | TVAR     |
| 1111 | CONTINUE   | TVAR     |
| C    |  | TVAR     |
| C    | SURFACE TEMPERATURE LOOP ADDED DUE TO STABILITY PROBLEM        | TVAR     |
| C    |  | TVAR     |
|      | EXSE=EX(1)*NSCYL   | TVAR     |
|      | DO 1002 NSC=1,NSCYL  | TVAR     |
|      | TS=TS+((TA-TS)*H*DELX/EXSE )+((T(2)-TS)*TKSAV(1)/EXSE )        | TVAR     |
| 1002 | CONTINUE   | TVAR     |
|      | IHCFLG=0   | TVAR     |
| C    |  | TVAR     |
| C    | NOTE THAT THE H COEF IS USED TO MATCH THE TWO POINT SLOPE      | TVAR     |
| C    | AT THE SURFACE   | TVAR     |
| C    |  | TVAR     |
| 1112 | CONTINUE   | TVAR     |
|      | TSO=TS   | TVAR     |
|      | LCT=0  | TVAR     |
| C    |  | TVAR     |
| C    | FORMS OF GLOBAR TO SPECIFY HEAT INPUT;                         | TVAR     |
| C    | 1) LIST DV VALUES, ALL >0. ... THIS FUNCTION USED DIRECTLY     | TVAR     |
| C    | 2) GLOBAR(1)<0.,GLOBAR(2)>0.,...GLOBAR(3) USED AS CONSTANT     | TVAR     |
| C    | FOR TIME UP TO SEC=GLOBAR(4), THEN SHUT OFF                    | TVAR     |
| C    | 3) GLOBAR(1)<0.,GLOBAR(2)<0.,... GLOBAR(3) IS USED AS CONSTANT | TVAR     |
| C    | OF PARABOLIC HEAT INPUT, IE,GLOBAR(3)/SQRT(SEC) IS HEAT IN     | TVAR     |
| C    |  | TVAR     |
| C    |  | TVAR     |
|      | IF(GLOBAR(1))2222,2229,2229                                    | TVAR     |

|      |  |          |
|------|--|----------|
| 2222 | IF (GLOBAL(2))2223,2224,2224                                     | TVAR     |
| 2223 | GLUG=(GLOBAL(3)/SQRT(SEC+.0001))*(DELT/DELX)                     | TVAR     |
|      | GO TO 2228   | TVAR     |
| 2224 | GLUG=GLOBAL(3)*(DELT/DELX)                                       | TVAR     |
|      | IF(SEC.GT.GLOBAL (4)) GLUG=0.                                    | TVAR     |
|      | GO TO 2228   | TVAR     |
| 2229 | CONTINUE   | TVAR     |
|      | SDQ=SEC/DELTQ  | TVAR     |
|      | IKQ=SDQ  | TVAR     |
|      | GLUG=(GLOBAL(IKQ+2)-GLOBAL(IKQ+1))*(SDQ-IKQ)+GLOBAL(IKQ+1)       | TVAR     |
|      | GLUG=GLUG*DELT/DELX  | TVAR     |
| 2228 | CONTINUE   | TVAR     |
|      | LCT=LCT+1  | TVAR     |
| C    | .....  | TVAR     |
| C    | .....  | CONTROLS |
| C    |  | CONTROLS |
| C    |  | CONTROLS |
| C    | THIS CONTROL BLOCK SAVES THE VARIOUS PARAMETERS FOR USE BY THE   | CONTROLS |
| C    | CONTROL BLOCK FOLLOWING THE POSITION AND TEMPERATURE SETTING     | CONTROLS |
| C    | LOOP   | CONTROLS |
| C    |  | CONTROLS |
|      | DO 5051 J=1,NN   | CONTROLS |
| 5051 | TS AVL(J)=T(J)   | CONTROLS |
|      | POSLS=POS L  | CONTROLS |
|      | POSXS=POS X  | CONTROLS |
|      | SLS=SL   | CONTROLS |
|      | SXS=SX   | CONTROLS |
|      | IQS=IQ   | CONTROLS |
|      | IRS=IR   | CONTROLS |
|      | ILFLS=ILFL   | CONTROLS |
|      | IRFLS=IRFL   | CONTROLS |
|      | ISKPS=ISKP   | CONTROLS |
| C    | .....  | CONTROLS |
| C    | .....  | PSET     |
| C    |  | PSET     |
| C    | PSFT: CALCULATES AND SETS THE NEW LIQUIDUS AND SOLIDUS POSITIONS | PSET     |

|      |  |      |
|------|--|------|
| C    |  | PSET |
|      | DD 4060 J=1,NCYCLE   | PSET |
| C    |  | PSET |
| C    | LIQUIDUS BOUNDARY  | PSET |
| C    |  | PSET |
|      | IP=IP+1  | PSET |
|      | IF(T(1).GE.TL.OR.IQ.GT.N.OR.ISKP.EQ.1) GO TO 4141                | PSET |
|      | IF(ILFL.EQ.0) GO TO 4110   | PSET |
|      | IF(IQ-2)4121,4115,4116   | PSET |
| 4115 | IF(SL)4122,4122,4123   | PSET |
| 4122 | HEATOT=TKLM*(TL-T(1))/(POSL-DELX/2.)                             | PSET |
|      | GO TO 4120   | PSET |
| 4123 | HEATOT=TKLM*(TL-T(2))/SL   | PSET |
|      | GO TO 4120   | PSET |
| 4121 | HEATOT=TKLM*(TL-T(1))/SL   | PSET |
|      | GO TO 4120   | PSET |
| 4116 | HEATOT=TKLM*(((TQM-T(IQ-2))/(2*DELX))+((DELX+SL)*((T(IQ-2)       | PSET |
|      | 1 -2.*T(IQ-1)+TQM)/(DELX*DELX)))                                 | PSET |
| 4120 | CONTINUE   | PSET |
|      | IF(IQ-(N-1))4117,4118,4118                                       | PSET |
| 4118 | HEATIN=TKLP*(T(N)-TL)/((N*DELX-DELX/2.)-POSL)                    | PSET |
|      | GO TO 4119   | PSET |
| 4117 | HEATIN=TKLP*(((T(IQ+2)-TQP)/(2*DELX))-((DELX-SL)*((TQP-2*T(IQ+1) | PSET |
|      | 1 +T(IQ+2))/(DELX*DELX)))  | PSET |
| 4119 | CONTINUE   | PSET |
| C    |  | PSET |
| C    | THE FOLLOWING STMT SHOULD BE A BETTER APPROXIMATION IF THE       | PSET |
| C    | TWO BOUNDARIES ARE IN THE SAME SLAB                              | PSET |
| C    |  | PSET |
|      | IF(IQ.EQ.IR) HEATOT=TKA *((TL-TE)/(POSL-POSX))                   | PSET |
| C    |  | PSET |
| C    | THE IQ=IR+1 TEST IS DUE TO THE LOSS OF HEAT IN THIS CASE         | PSET |
| C    | WHICH MUST BE TAKEN INTO ACCOUNT...ESPECIALLY IN CASES           | PSET |
| C    | WHERE THE TIP AND ROOT SPEND A LOT OF TIME NEAR EACHOTHER        | PSET |
| C    |  | PSET |
|      | IF(IQ.EQ.IR+1) HEATOT=TKA *((TL-TE)/(POSL-POSX))                 | PSET |

|      |  |      |
|------|--|------|
| C    |  | PSET |
| C    | SIDE HEAT ADDITION MADE AS HEAT OUT TERM..ADDITIVE           | PSET |
| C    |  | PSET |
|      | HTSIDE=HS*(T(IQ)-TAS)*DELX/XS                                | PSET |
|      | IF(HS.LT.0.) HTSIDE=TAS*DELX/(SQRT(SEC+10**(-4))*XS)         | PSET |
|      | DPOSL=(DELTCY/THEAT)*(HTSIDE+HEATOT-HEATIN)                  | PSET |
|      | GO TO 4140   | PSET |
| 4110 | ILFL=1   | PSET |
|      | DO 4111 L=1,N  | PSET |
|      | IF(T(L).GT.TL) GO TO 4112                                    | PSET |
| 4111 | CONTINUE   | PSET |
|      | IQ=N+1   | PSET |
|      | GO TO 4141   | PSET |
| 4112 | IQ=L-1   | PSET |
|      | AAB=TKLM*(TL-T(IQ))*DELX/(TKLP*(T(IQ+1)-TL)+TKLM*(TL-T(IQ))) | PSET |
|      | IF(AAB.GT.DELX/2.) GO TO 4113                                | PSET |
|      | SL=AAB   | PSET |
|      | GO TO 4114   | PSET |
| 4113 | SL=AAB-DELX  | PSET |
|      | IQ=IQ+1  | PSET |
| 4114 | POSL=(IQ-1)*DELX+DELX/2.+SL                                  | PSET |
|      | GO TO 4141   | PSET |
| 4140 | POSL=POSL+DPOSL  | PSET |
|      | IQ=(POSL/DELX)+1   | PSET |
|      | SL=POSL-((IQ-1)*DELX+DELX/2.)                                | PSET |
|      | IF(IQ.LE.0) ILFL=0   | PSET |
|      | IF(IQ.EQ.N.AND.SL.GT.0.) IQ=NN                               | PSET |
|      | IF(IQ.GT.N) GO TO 4141                                       | PSET |
| 4160 | CONTINUE   | PSET |
| 4141 | CONTINUE   | PSET |
| C    |  | PSET |
| C    | SOLIDUS BOUNDARY   | PSET |
| C    |  | PSET |
|      | IF(T(1).GE.TE.OR.IR.GT.N.OR.ISKP.EQ.1) GO TO 4041            | PSET |
|      | IF(IRFL.EQ.0) GO TO 4010                                     | PSET |
|      | IF(IR-2)4021,4015,4016                                       | PSET |

|      |   |      |
|------|---|------|
| C    |   | PSET |
| C    | TWO POINT FORMULA USED FOR POINTS IN PROXIMITY OF ENDS          | PSET |
| C    |   | PSET |
| 4015 | IF(SX)4022,4022,4023  | PSET |
| 4022 | HEATOT=TKEM*(TE-T(1))/(POSX-DELX/2.)                            | PSET |
|      | GO TO 4020  | PSET |
| 4023 | HEATOT=TKEM*(TE-T(2))/SX  | PSET |
|      | GO TO 4020  | PSET |
| 4021 | HEATOT=TKEM*(TE-T(1))/SX  | PSET |
|      | GO TO 4020  | PSET |
| C    |   | PSET |
| C    | THREE POINT FORM OF THE FINITE DIFFERENCE FORM OF THE           | PSET |
| C    | TAYLOR'S EXPANSION IS USED TO OBTAIN THE SLOPE OF TEMPERATURE   | PSET |
| C    | REQUIRED BY THE MOTION EQUATIONS OF THE TIP AND ROOT            | PSET |
| C    |   | PSET |
| 4016 | HEATOT=TKEM*(((TRM-T(IR-2))/(2*DELX))+(DELX+SX)*((T(IR-2)       | PSET |
| 1    | -2.*T(IR-1)+TRM)/(DELX*DELX)))                                  | PSET |
| 4020 | CONTINUE  | PSET |
|      | IF(IR-(N-1))4017,4018,4018                                      | PSET |
| 4018 | HEATIN=TKEP*(T(N)-TE)/((N*DELX-DELX/2.)-POSX)                   | PSET |
|      | GO TO 4019  | PSET |
| 4017 | HEATIN=TKEP*(((T(IR+2)-TRP)/(2*DELX))-(DELX-SX)*((TRP-2*T(IR+1) | PSET |
| 1    | +T(IR+2))/(DELX*DELX)))   | PSET |
| 4019 | CONTINUE  | PSET |
|      | IF(IQ.EQ. IR) HEATIN=TKA *((TL-TE)/(POSL-POSX))                 | PSET |
|      | IF(IQ.EQ. IR+1) HEATIN=TKA *((TL-TE)/(POSL-POSX))               | PSET |
|      | HTSIDE=HS*(T(IR)-TAS)*DELX/XS                                   | PSET |
|      | IF(HS.LT.0.) HTSIDE=TAS*DELX/(SQRT(SEC+10**(-4))*XS)            | PSET |
|      | DPOSX=(DELTCY/RHEAT)*(HTSIDE+HEATOT-HEATIN)                     | PSET |
|      | GO TO 4040  | PSET |
| 4010 | IRFL=1  | PSET |
|      | DO 4011 L=1,N   | PSET |
|      | IF(T(L).GT.TE) GO TO 4012                                       | PSET |
| 4011 | CONTINUE  | PSET |
| 4012 | IR=L-1  | PSET |
|      | AAB=DELX*((TE-T(IR))/(T(IR+1)-T(IR)))                           | PSET |

|      |  |      |
|------|--|------|
|      | IF(AAB.GT.DELX/2.) GO TO 4013                                | PSET |
|      | SX=AAB   | PSET |
|      | GO TO 4014   | PSET |
| 4013 | SX=AAB-DELX  | PSET |
|      | IR=IR+1  | PSET |
| 401  | POSX=(IR-1)*DELX+DELX/2.+SX                                  | PSET |
|      | GO TO 4041   | PSET |
| 4040 | POSX=POSX+DPOSX  | PSET |
|      | IR=(POSX/DELX)+1   | PSET |
|      | SX=POSX-((IR-1)*DELX+DELX/2.)                                | PSET |
|      | IF(IR.LE.0) IRFL=0   | PSET |
|      | IF(IR.EQ.N.AND.SX.GT.0.) IR=NN                               | PSET |
|      | IF(IR.GT.N) GO TO 4042                                       | PSET |
| 4041 | CONTINUE   | PSET |
| 4042 | CONTINUE   | PSET |
|      | ISKP=0   | PSET |
| C    |  | PSET |
| C    | POSITIONS HAVE NOW BEEN SET                                  | PSET |
| C    |  | PSET |
| C    | .....  | PSET |
| C    | .....  | TSET |
| C    |  | TSET |
| C    | C:TSET: SET TQ,TR,TQP,TQM,TRP,TRM                            | TSET |
| C    |  | TSET |
| C    | C: FIND MODULUS AND TEST                                     | TSET |
| C    |  | TSET |
|      | NDQ=(IQ+N-1)/N   | TSET |
|      | NDR=(IR+N-1)/N   | TSET |
|      | IF(NDQ.NE.1) GO TO 5000                                      | TSET |
|      | ASD=SL/DELX  | TSET |
|      | BSD=1.-ASD   | TSET |
|      | CSD=BSD+1.   | TSET |
|      | DSD=1.+ASD   | TSET |
|      | ESD=1.+DSD   | TSET |
|      | IF(IQ-2) 5010,5011,5012                                      | TSET |
| 5010 | TQP=TL*(2./(CSD*BSD))-T(IQ+1)*(2.*ASD/BSD)+T(IQ+2)*(ASD/CSD) | TSET |

|      |   |  |
|------|---|--|
| 5011 | GO TO 5000<br>TQP=TL*(2./(CSD*BSD))-T(IQ+1)*(2.*ASD/BSD)+T(IQ+2)*(ASD/CSD)<br>TQM=T(IQ-1)+(DELX/(DELX+SL))*(TL-T(IQ-1))                     | TSET<br>TSET<br>TSET                                 |
| 5012 | GO TO 5000<br>IF(IQ-(N-1)) 5013,5014,5015   | TSET<br>TSET   |
| 5015 | TQM=-T(IQ-2)*(ASD/ESD)+T(IQ-1)*(2.*ASD/DSD)+TL*(2./(DSD*ESD))   | TSET   |
| 5014 | GO TO 5000<br>TQM=-T(IQ-2)*(ASD/ESD)+T(IQ-1)*(2.*ASD/DSD)+TL*(2./(DSD*ESD))<br>TQP=T(IQ+1)-(DELX/(DELX-SL))*(T(IQ+1)-TL)                    | TSET<br>TSET<br>TSET                                 |
| 5013 | GO TO 5000<br>TQP=TL*(2./(CSD*BSD))-T(IQ+1)*(2.*ASD/BSD)+T(IQ+2)*(ASD/CSD)<br>TQM=-T(IQ-2)*(ASD/ESD)+T(IQ-1)*(2.*ASD/DSD)+TL*(2./(DSD*ESD)) | TSET<br>TSET<br>TSET                                 |
| 5000 | CONTINUE<br>IF(NDR.NE.1) GO TO 5001<br>ASD=SX/DELX<br>BSD=1.-ASD<br>CSD=BSD+1.<br>DSD=1.+ASD<br>ESD=DSD+1.<br>IF(IR-2) 5020,5021,5022       | TSET<br>TSET<br>TSET<br>TSET<br>TSET<br>TSET<br>TSET |
| 5020 | TRP=TE*(2./(CSD*BSD))-T(IR+1)*(2.*ASD/BSD)+T(IR+2)*(ASD/CSD)<br>GO TO 5001  | TSET<br>TSET   |
| 5021 | TRP=TE*(2./(CSD*BSD))-T(IR+1)*(2.*ASD/BSD)+T(IR+2)*(ASD/CSD)<br>TRM=T(IR-1)+(DELX/(DELX+SX))*(TE-T(IR-1))                                   | TSET<br>TSET   |
| 5022 | GO TO 5001<br>IF(IR-(N-1)) 5023,5024,5025   | TSET<br>TSET   |
| 5025 | TRM=-T(IR-2)*(ASD/ESD)+T(IR-1)*(2.*ASD/DSD)+TE*(2./(DSD*ESD))<br>GO TO 5001   | TSET<br>TSET   |
| 5024 | TRM=-T(IR-2)*(ASD/ESD)+T(IR-1)*(2.*ASD/DSD)+TE*(2./(DSD*ESD))<br>TRP=T(IR+1)-((DELX/(DELX-SX))*(T(IR+1)-TE))                                | TSET<br>TSET   |
| 5023 | GO TO 5001<br>TRM=-T(IR-2)*(ASD/ESD)+T(IR-1)*(2.*ASD/DSD)+TE*(2./(DSD*ESD))<br>TRP=TE*(2./(CSD*BSD))-T(IR+1)*(2.*ASD/BSD)+T(IR+2)*(ASD/CSD) | TSET<br>TSET<br>TSET                                 |
| 5001 | CONTINUE  | TSET   |
| 5002 | CONTINUE<br>IF(IQ.NE.IR.OR.IR.LT.2) GO TO 5006  | TSET<br>TSET   |



|      |   |          |
|------|---|----------|
|      | TRP=TQP   | TSFT     |
|      | TQM=TRM   | TSET     |
| 5006 | CONTINUE  | TSET     |
|      | IF(NDR.NE.1) GO TO 5003                                       | TSET     |
|      | IF(IR.EQ.1) GO TO 5003  | TSET     |
|      | T(IR)=TRM   | TSFT     |
|      | IF(SX.LT.0) T(IR)=TRP   | TSET     |
| C    | TR=T(IR)  | TSET     |
| 5003 | CONTINUE  | TSET     |
|      | IF(NDQ.NE.1) GO TO 5004                                       | TSET     |
|      | IF(IQ.EQ.1) GO TO 5004  | TSET     |
|      | T(IQ)=TQM   | TSET     |
|      | IF(SL.LT.0.) T(IQ)=TQP  | TSET     |
| C    | TQ=T(IQ)  | TSET     |
| 5004 | CONTINUE  | TSET     |
| 4060 | CONTINUE  | TSET     |
| C    |   | TSET     |
| C    | .....   | TSET     |
| C    | .....   | CONTROLC |
| C    | CONTROL BLOCK...MONITOR THE POSITION AND TEMPERATURE LOOP     | CONTROLC |
| C    |   | CONTROLC |
| C    | THE AVERAGE CHANGE IN POSITIONS IS COMPARED TO A CONTROL      | CONTROLC |
| C    | VALUE READ IN,AND IF THE TOLERANCE LIMIT IS EXCEEDED,         | CONTROLC |
| C    | NEW LOOP PARAMETERS(DELTQY,NCYCLE) ARE SET ACCORDING TO       | CONTROLC |
| C    | THE DEVIATION FROM THE LIMIT,AND THE OLD POSITIONS,TEMPS,     | CONTROLC |
| C    | AND SUCH ARE RESET,AND THE LOOP IS EXECUTED AGAIN.            | CONTROLC |
| C    | ALSO,IF THE TOLERANCE LIMIT IS MET,THE LOOP PARAMETERS ARE    | CONTROLC |
| C    | INCREASED TO MATCH THE AMOUNT OVER THE LIMIT,SO THE           | CONTROLC |
| C    | TOTAL EFFECT OF THE CONTROL BLOCK IS TO KEEP THE LOOP RUNNING | CONTROLC |
| C    | AT THE MAXIMUN SPEED  | CONTROLC |
| C    |   | CONTROLC |
|      | ADPOSL=(POSL-POSLS)/NCYCLE                                    | CONTROLC |
|      | ADPOSX=(POSX-POSXS)/NCYCLE                                    | CONTROLC |
|      | RFACT=ADPOSL  | CONTROLC |
|      | IF(ADPOSL.LT.ADPOSX) RFACT=ADPOSX                             | CONTROLC |
|      | IF(ADPOSX.GT.DCYL.OR.ADPOSL.GT.DCYL) GO TO 5050               | CONTROLC |

|      |   |         |
|------|---|---------|
|      | NCYCLE=NCYCLE*(RFACT/DCYL)                          | CONTROL |
|      | IF(NCYCLE.LE.1) NCYCLE=1                            | CONTROL |
|      | DELTCY=DELT/NCYCLE                                  | CONTROL |
|      | GO TO 5060  | CONTROL |
| 5050 | NCYCLE=NCYCLE*((RFACT/DCYL)+0.5) +1                 | CONTROL |
|      | IF(LCT.GT.5) GO TO 5055                             | CONTROL |
|      | IF(NCYCLE.LT.500) GO TO 5052                        | CONTROL |
|      | WRITE(6,959)  | CONTROL |
|      | WRITE(6,5053) NCYCLE                                | CONTROL |
| 5053 | FORMAT(' PROGRAM HALTED DUE TO NCYCLE SIZE'110)     | CONTROL |
|      | GO TO 880   | CONTROL |
| 5055 | CONTINUE  | CONTROL |
|      | WRITE(6,959)  | CONTROL |
|      | WRITE(6,5056)                                       | CONTROL |
| 5056 | FORMAT(' PROGRAM HALTED DUE TO MORE THAN 5 CYCLES') | CONTROL |
|      | GO TO 880   | CONTROL |
| 5052 | DELTCY=DELT/NCYCLE                                  | CONTROL |
| C    |   | CONTROL |
| C    | . RESET OLD PARAMETERS                              | CONTROL |
| C    |   | CONTROL |
|      | DO 5054 J=1,NN                                      | CONTROL |
| 5054 | T(J)=TSAVL(J)                                       | CONTROL |
|      | SL=SLS  | CONTROL |
|      | SX=SXS  | CONTROL |
|      | POSL=POSLS  | CONTROL |
|      | POSX=POSXS  | CONTROL |
|      | IR=IRS  | CONTROL |
|      | IQ=IQS  | CONTROL |
|      | ILFL=ILFLS  | CONTROL |
|      | IRFL=IRFLS  | CONTROL |
|      | ISKP=ISKPS  | CONTROL |
|      | GO TO 2228  | CONTROL |
| 5060 | CONTINUE  | CONTROL |
| C    | .....   | CONTROL |
| C    | .....   | MUSHY   |
| C    |   | MUSHY   |

|    |  |       |
|----|--|-------|
| C  | BLOCK MUSHY CALCULATES THE CONSTANTS FOR EACH SLAB, AS A | MUSHY |
| C  | FUNCTION OF TEMPERATURE                                  | MUSHY |
| C  |  | MUSHY |
|    | EM(1)=CONST*RHS*CPS                                      | MUSHY |
|    | EM(2)=CONST*RHL*CPL                                      | MUSHY |
|    | DO 3333 J=1,N  | MUSHY |
| C  |  | MUSHY |
| C  | DECIDE WHICH REGION THIS ELEMENT IS IN                   | MUSHY |
| C  |  | MUSHY |
|    | IF(T(J).GE.TL) GO TO 4                                   | MUSHY |
|    | IF(T(J).LE.TE) GO TO 2                                   | MUSHY |
|    | GO TO 5  | MUSHY |
| 2  | K1=1   | MUSHY |
|    | GO TO 3  | MUSHY |
| 4  | K1=2   | MUSHY |
|    | GO TO 3  | MUSHY |
| C  |  | MUSHY |
| C  | CALCULATE CONSTANTS FOR MUSHY REGION                     | MUSHY |
| C  |  | MUSHY |
| 5  | CONTINUE   | MUSHY |
|    | GS=FRL*((TL-T(J))/(TL-TE))+FRT+FSC                       | MUSHY |
| C  |  | MUSHY |
| C  | THE OPTION OF CHOOSING EITHER A SHEIL DISTRIBUTION       | MUSHY |
| C  | OF FRACTION SOLID IN THE MUSHY REGION OR A LINEAR ONE    | MUSHY |
| C  | IS DECIEDED BY THE FLAG(READ IN) ISHEIL                  | MUSHY |
| C  |  | MUSHY |
|    | IF(ISHEIL.EQ.1) GS=1.-(1.+SCHC*(TL-T(J)))**SCHE          | MUSHY |
|    | GL=1.-GS   | MUSHY |
|    | IF(KGR.EQ.0.OR.KGR.FQ.2) GO TO 31                        | MUSHY |
|    | TKM=GS*TKS+GL*TKL  | MUSHY |
|    | GO TO 32   | MUSHY |
| 31 | TKM=TKS*TKL/(GS*TKL+GL*TKS)                              | MUSHY |
| 32 | CONTINUE   | MUSHY |
|    | RHM=GS*RHS+GL*RHL  | MUSHY |
|    | CPM=GS*CPS+GL*CPL  | MUSHY |
|    | CPMH=HOF*FRL/(TE-TL)                                     | MUSHY |

```

IF (ISHEIL.EQ.1) CPMH=HOF*FRL*SCHC*SCHE*(1+SCHC*(TL-T(J)))**(SCHE-1) MUSHY
EM(3)=CONST*RHM*(CPM-CPMH) MUSHY
K1=3 MUSHY
3 CONTINUE MUSHY
FX(J)=EM(K1) MUSHY
IF(K1-2) 3334,3335,3336 MUSHY
3334 TKS AV(J)=TKS MUSHY
GO TO 3333 MUSHY
3335 TKS AV(J)=TKLL MUSHY
GO TO 3333 MUSHY
3336 TKS AV(J)=TKM MUSHY
3333 CONTINUE MUSHY
C..... MUSHY
C..... TKFILL
C TKFILL
C BLOCK TKFILL STORES THE VALUES OF THE AVERAGE THERMAL TKFILL
C CONDUCTIVITIES,TO BE USED IN 'MATRIX' TKFILL
C TKFILL
C TKFILL
C K BETWEEN J AND J+1 IS IN TKINT(J) TKFILL
C TKFILL
KKK=N-1 TKFILL
DO 5500 J=1,KKK TKFILL
IF(IR-J) 5501,5502,5501 TKFILL
5502 IF(IQ-J) 5503,5504,5503 TKFILL
5504 TKINT(J)=TKLP TKFILL
GO TO 5500 TKFILL
5503 IF(IQ-(J+1))5505,5506,5505 TKFILL
5505 TKINT(J)=TKEP TKFILL
GO TO 5500 TKFILL
5506 TKINT(J)=(TKEP+TKLM)/2. TKFILL
GO TO 5500 TKFILL
5501 IF(IR-(J+1))5507,5508,5507 TKFILL
5508 TKINT(J)=TKEM TKFILL
GO TO 5500 TKFILL
5507 IF(IQ-J) 5509,5510,5509 TKFILL

```

|      |  |        |
|------|--|--------|
| 5510 | TKINT(J)=TKLP  | TKFILL |
|      | GO TO 5500   | TKFILL |
| 5509 | IF(IQ-(J+1))5511,5512,5511                                     | TKFILL |
| 5512 | TKINT(J)=TKLM  | TKFILL |
|      | GO TO 5500   | TKFILL |
| 5511 | TKINT(J)=(TKSAV(J)+TKSAV(J+1))/2.                              | TKFILL |
| 5500 | CONTINUE   | TKFILL |
| C    |  | TKFILL |
| C    | .....  | TKFILL |
| C    | .....  | MATRIX |
| C    |  | MATRIX |
| C    | BLOCK MATRIX STORES THE CONSTANTS (COEFFICIENTS) FOR THE SOLVE | MATRIX |
| C    | BLOCK  | MATRIX |
| C    |  | MATRIX |
| C    | P MEANS LOOKING FROM THE POSITIVE SIDE, M FROM THE MINUS (J-1) | MATRIX |
| C    |  | MATRIX |
|      | DO 6600 J=2,N  | MATRIX |
|      | IF(J.EQ.N) GO TO 6602  | MATRIX |
| C    |  | MATRIX |
| C    | INTERIOR   | MATRIX |
| C    |  | MATRIX |
|      | AK(1)=TKINT(J)   | MATRIX |
|      | AK(2)=TKINT(J-1)   | MATRIX |
|      | IF(IRADFL.NE.1) GO TO 6613                                     | MATRIX |
|      | Z=J  | MATRIX |
|      | ZZ=(N-Z)+0.5   | MATRIX |
| C    |  | MATRIX |
| C    | NOTE THAT THE PROGRAM COUNTS FROM THE OUTSIDE (CHILL SURFACE)  | MATRIX |
| C    | IN TO THE CENTER...FOR THE RADIAL CASE,THIS REQUIRES A         | MATRIX |
| C    | SLIGHT MODIFICATION TO THE EQUATIONS                           | MATRIX |
| C    |  | MATRIX |
|      | AK(2)=AK(2)*(ZZ+0.50)/ZZ                                       | MATRIX |
|      | AK(1)=AK(1)*(ZZ-0.50)/ZZ                                       | MATRIX |
| 6613 | CONTINUE   | MATRIX |
|      | IF(IR-(J+1)) 6603,6604,6603                                    | MATRIX |
| 6604 | F(J)=-AK(1)*TRM-AK(2)*T(J-1)+(AK(1)+AK(2))*T(J)                | MATRIX |

|   |        |
|---|--------|
| GO TO 6660  | MATRIX |
| 6603 IF((IQ-J)+1)6605,6606,6605                         | MATRIX |
| 6606 F(J)=-AK(1)*T(J+1)-AK(2)*TOP+(AK(1)+AK(2))*T(J)    | MATRIX |
| GO TO 6660  | MATRIX |
| 6605 IF(IQ-(J+1)) 6607,6608,6607                        | MATRIX |
| 6608 IF(IR-(J-1)) 6609,6610,6609                        | MATRIX |
| 6609 F(J)=-AK(1)*TQM-AK(2)*T(J-1)+(AK(1)+AK(2))*T(J)    | MATRIX |
| GO TO 6660  | MATRIX |
| 6610 F(J)=-AK(1)*TQM-AK(2)*TRP+(AK(1)+AK(2))*T(J)       | MATRIX |
| GO TO 6660  | MATRIX |
| 6607 IF((IR-J)+1)6611,6612,6611                         | MATRIX |
| 6611 F(J)=-AK(1)*T(J+1)-AK(2)*T(J-1)+(AK(1)+AK(2))*T(J) | MATRIX |
| GO TO 6660  | MATRIX |
| 6612 F(J)=-AK(1)*T(J+1)-AK(2)*TRP+(AK(1)+AK(2))*T(J)    | MATRIX |
| 6660 A(J,1)=AK(2)/2.                                    | MATRIX |
| A(J,2)=-((AK(1)+AK(2))/2.+EX(J))                        | MATRIX |
| A(J,3)=AK(1)/2.   | MATRIX |
| GO TO 6600  | MATRIX |
| 6602 AK(2)=TKINT(N-1)                                   | MATRIX |
| IF(IQ-(N-1))6630,6631,6630                              | MATRIX |
| 6631 F(N)=T(N)-TOP                                      | MATRIX |
| GO TO 6680  | MATRIX |
| 6630 IF(IR-(N-1))6633,6632,6633                         | MATRIX |
| 6632 F(N)=T(N)-TRP                                      | MATRIX |
| GO TO 6680  | MATRIX |
| 6633 F(N)=T(N)-T(N-1)                                   | MATRIX |
| 6680 A(N,1)=.5  | MATRIX |
| A(N,2)=- (EX(J)/AK(2)+.5)                               | MATRIX |
| A(N,3)=0.0  | MATRIX |
| 6600 CONTINUE   | MATRIX |
| C.....  | MATRIX |
| C.....  | SOLVE  |
| C   | SOLVE  |
| C   | SOLVE  |
| C   | SOLVE  |
| C   | SOLVE  |

SOLVE SIMULTANEOUS EQNS

|      |  |       |
|------|--|-------|
| C    | EACH GROUP OF EQUATIONS(REPRESENTING ONE REGION OF THE CASTING)        | SOLVE |
| C    | IS SOLVED AS A SEPERATE MATRIX   | SOLVE |
| C    | THIS TECHNIQUE IS USED TO HANDLE THE SURFACE BC'S AS WELL AS THE       | SOLVE |
| C    | LIQUIDUS AND SOLIDUS INTERNAL BOUNDARIES                               | SOLVE |
| C    | THE VARIALBE ARRAY 'LIST' IS USED TO KEEP TRACK OF THE CURRENT         | SOLVE |
| C    | POSITIONS OF THE TIP AND ROOT, FOR USE BY THE SOLVE BLOCK, IN ORDER TO | SOLVE |
| C    | SET UP THE CORRECT SUB-MATRICES TO BE SOLVED                           | SOLVE |
| C    |  | SOLVE |
|      | DO 7002 J=2,N  | SOLVE |
| 7002 | LIST(J)=0  | SOLVE |
|      | IF(IQ) 7003,7003,7004  | SOLVE |
| 7004 | LIST(IQ)=1   | SOLVE |
| 7003 | CONTINUE   | SOLVE |
|      | IF(IR) 7005,7005,7006  | SOLVE |
| 7006 | LIST(IR)=1   | SOLVE |
| 7005 | CONTINUE   | SOLVE |
| 7014 | CONTINUE   | SOLVE |
|      | DO 7007 J=2,N  | SOLVE |
|      | IF(LIST(J).EQ.0) GO TO 7008  | SOLVE |
| 7007 | CONTINUE   | SOLVE |
|      | GO TO 7009   | SOLVE |
| 7008 | KSTART=J   | SOLVE |
|      | DO 7010 J=KSTART,NN  | SOLVE |
|      | IF(LIST(J).EQ.1) GO TO 7011  | SOLVE |
| 7010 | CONTINUE   | SOLVE |
| 7011 | KEND=J-1   | SOLVE |
|      | DO 7012 J=KSTART,KEND  | SOLVE |
| 7012 | LIST(J)=1  | SOLVE |
| C    |  | SOLVE |
| C    | THE FOLLOWING TWO STMTS ARE NECESSARY IN ORDER TO CORRECTLY            | SOLVE |
| C    | SET THE SLAB TEMPERATURES FOR SLABS NEXT TO BOJNDARIES                 | SOLVE |
| C    | IF THESE CORRECTIONS ARE IGNORED, ERRORS ARE INCURRED WHICH            | SOLVE |
| C    | CAUSE OSCILLATION OF THE POSITONS XE, XL EVEN THOUGH THE               | SOLVE |
| C    | TEMPERATURES ARE STABLE  | SOLVE |
| C    |  | SOLVE |
|      | TDELL=T(KSTART-1)-TSAV(KSTART-1)                                       | SOLVE |

|      |   |       |
|------|---|-------|
|      | TDELH=T(KEND+1)-TSAV(KEND+1)                                    | SOLVE |
|      | IF(KSTART.LT.KEND) GO TO 7013                                   | SOLVE |
| C    |   | SOLVE |
| C    | SOLUTION FOR ONE SLAB MATRICES                                  | SOLVE |
| C    |   | SOLVE |
|      | F(KSTART)=F(KSTART)-(A(KSTART,1)*TDELL)-(A(KSTART,3)*TDELH)     | SOLVE |
|      | T(KSTART)=(F(KSTART)/A(KSTART,2) )+T(KSTART)                    | SOLVE |
|      | GO TO 7014  | SOLVE |
| 7013 | CONTINUE  | SOLVE |
|      | F(KSTART)=F(KSTART)-(A(KSTART,1)*TDELL)                         | SOLVE |
|      | F(KEND)=F(KEND)-(A(KEND,3)*TDELH)                               | SOLVE |
| C    |   | SOLVE |
| C    | THE CORRECTIONS REPRESENTED BY THE USE OF TDELL AND TDELH       | SOLVE |
| C    | IN THE ABOVE BLOCK ARE NECFSITATED BY THE WAY IN WHICH THE      | SOLVE |
| C    | SURFACE TEMPERATURE,THE CENTER TEMPERATURE,AND THE TWO INTERNAL | SOLVE |
| C    | TEMPERATURES ARE HANDLED  | SOLVE |
| C    | THAT IS,BECAUSE THESE VARIOUS TEMPERATURES ARE SET BY           | SOLVE |
| C    | VARIOUS EQUATIONS RATHER THAN INCLUDED IN THE HEAT FLOW         | SOLVE |
| C    | EQUATIONS,THEY MUST BE TAKEN INTO ACCOUNT IN THE MATRIX         | SOLVE |
| C    | SOLUTION TO THE H/F EQUATIONS,NAMELY,BY INCLUDING THE RESULTANT | SOLVE |
| C    | TEMPERATURE CHANGES IN THE 'SET' SLABS INTO THE MATRIX          | SOLVE |
| C    |   | SOLVE |
| C    | TDELL AND TDELH THEREFORE REPRESENT THE RESULTS OF              | SOLVE |
| C    | TEMPERATURES BEING SET BY EQUATIONS EXTRANEIOUS TO THE          | SOLVE |
| C    | HEAT FLOW EQUATION SET.   | SOLVE |
| C    |   | SOLVE |
|      | KKHIN=KSTART+1  | SOLVE |
|      | DO 7015 K=KKHIN,KEND  | SOLVE |
| C    |   | SOLVE |
| C    |   | SOLVE |
| C    | THESE STMTS SET UP TO PREVENT BUILD-UP OF LARGE NUMBER DURING   | SOLVE |
| C    | SOLUTION OF THE MATRIX  | SOLVE |
| C    |   | SOLVE |
|      | RRR=A(K,1)  | SOLVE |
|      | RRH=A(K-1,2)  | SOLVE |
|      | A(K,2)=(A(K,2)/RRR)-(A(K-1,3)/RRH)                              | SOLVE |



|      |   |       |
|------|---|-------|
|      | A(K,3)=A(K,3)/RRR   | SOLVE |
|      | F(K)=(F(K)/RRR)-(F(K-1)/RRH)                                    | SOLVE |
| 7015 | CONTINUE  | SOLVE |
|      | Q(KEND)=F(KEND)/A(KEND,2)                                       | SOLVE |
|      | K2=KEND-1   | SOLVE |
|      | DO 7016 J=KSTART,K2   | SOLVE |
|      | K3=K2-(J-KSTART)  | SOLVE |
|      | Q(K3)=(F(K3)-Q(K3+1)*A(K3,3))/A(K3,2)                           | SOLVE |
| 7016 | CONTINUE  | SOLVE |
|      | HTS=-TAS*DELT/(SQRT(SFC+10**(-4))*RHS*CPS*XS)                   | SOLVE |
|      | DO 7017 J=KSTART,KEND   | SOLVE |
| C    |   | SOLVE |
| C    | SIDE HEAT ADDITION...H CONTROLLED HEAT ASSUMED FOR THE SIDE     | SOLVE |
| C    | NOTE THAT LIQUID DENSITY AND HEAT CAPACITY ARE USED TO SIMPLIFY | SOLVE |
| C    |   | SOLVE |
|      | IF(HS.LT.0.) GO TO 7101   | SOLVE |
|      | HTS=(TAS-T(J))*(HS*DELT)/(RHL*CPL*XS)                           | SOLVE |
| 7101 | CONTINUE  | SOLVE |
|      | T(J)=T(J)+Q(J)+HTS  | SOLVE |
| 7017 | CONTINUE  | SOLVE |
|      | GO TO 7014  | SOLVE |
| 7009 | CONTINUE  | SOLVE |
| C    |   | SOLVE |
| C    | SAVED TEMPERATURES USED TO CORRECT SOLUTION FOR NEXT STEP       | SOLVE |
| C    |   | SOLVE |
|      | DO 7020 J=1,NN  | SOLVE |
| 7020 | TSAV(J)=T(J)  | SOLVE |
|      | T(N)=T(N)+(GLUG/EX(N))*CONST                                    | SOLVE |
|      | T(1)=TS   | SOLVE |
| C    |   | SOLVE |
| C    | ASYNCHRONOUS TIP MOVEMENT...                                    | SOLVE |
| C    |   | SOLVE |
| C    | THE PRESENCE OF SIDE-WISE HEAT LOSS MAY CAUSE                   | SOLVE |
| C    | NUCLEATION OF DENDRITIES IN THE MELT AHEAD OF THE               | SOLVE |
| C    | UNIDIRECTIONAL TIP POSITION...THIS NECESSITATES THE SEARCH      | SOLVE |
| C    | FOR A NEW TIP POSITION IN THESE CASES.AT THIS POINT,            | SOLVE |

|      |   |          |
|------|---|----------|
| C    | ONLY A FLAG(ILFL) IS SET...THE SEARCH IS DONE AS PART OF THE  | SOLVE    |
| C    | TIP MOVEMENT BLOCK PSET.                                      | SOLVE    |
| C    |   | SOLVE    |
|      | ISTIP=IQ+1  | SOLVE    |
|      | IF(ISTIP.GE.N) GO TO 7022                                     | SOLVE    |
|      | DO 7021 J=ISTIP,N   | SOLVE    |
|      | IF(T(J).LT.TLM) ILFL=0  | SOLVE    |
| 7021 | CONTINUE  | SOLVE    |
| 7022 | CONTINUE  | SOLVE    |
| C    | .....   | SOLVE    |
| C    | .....   | CONTROLX |
| C    |   | CONTROLX |
| C    | BLOCK CONTROLX CONTROLS THE ACCURACY OF THE SIMULATION        | CONTROLX |
| C    |   | CONTROLX |
| C    | THIS IS DONE BY   | CONTROLX |
| C    | 1) THE DIFFERENCE BETWEEN THE TEMPERATURE AT THE              | CONTROLX |
| C    | CURRENT TIME STEP WITH THE CURRENT TIME STEP SIZE             | CONTROLX |
| C    | AND THAT OBTAINED BY USING A TIME STEP OF 1/2 THE CURRENT     | CONTROLX |
| C    | SIZE IS COMPARED TO A VALUE FOR ACCURACY LEVEL,READ IN        | CONTROLX |
| C    | 2) IF THIS VALUE OF ACCURACY IS NOT MET,THE PROGRAM           | CONTROLX |
| C    | LEAVES THE TIME STEP AT THE HALVED VALUE,AND CONTINUES        | CONTROLX |
| C    | THE ACCURACY WILL BE CHECKED AT THE NEXT ITERATION AGAIN      | CONTROLX |
| C    | SO THAT THE TIME STEP WILL CONSTANTLY BE HALVED UNTIL THE     | CONTROLX |
| C    | ACCURACY IS MET OR THE LOWEST LIMIT ALLOWED IS REACHED        | CONTROLX |
| C    | 3) IF THE ACCURACY IS MET,THE PROGRAM COMPARES THE            | CONTROLX |
| C    | DIFFERENCE TO A NUMBER READ IN FOR DOUBLING THE TIME STEP     | CONTROLX |
| C    | 4) THIS ACCURACY IS CHECKED EVERY N CYCLES,WHERE N IS READ IN | CONTROLX |
| C    | ALSO  | CONTROLX |
| C    | 5) IN THIS MANNER,THE EFFECT OF THE CONTROL BLOCK IS TO       | CONTROLX |
| C    | MAINTAIN THE ACCURACY OF THE SIMULATION BETWEEN THE           | CONTROLX |
| C    | TWO LIMITS READ IN,AND THIS MAY RESULT IN EITHER VERY         | CONTROLX |
| C    | SHORT INNACCURATE OR LONG INEFFICIENT RUNS IF THE LIMITS      | CONTROLX |
| C    | ARE NOT CHOSEN CAREFULLY                                      | CONTROLX |
| C    |   | CONTROLX |
|      | IT=IT+1   | CONTROLX |
|      | IF(ICNTL.EQ.0) GO TO 9000                                     | CONTROLX |



|      |   |          |
|------|---|----------|
| 9002 | CONTINUE  | CONTROLX |
|      | DELT=DELT*2.  | CONTROLX |
|      | IF(IDBFL.EQ.1) DELT=DELT*2.                                     | CONTROLX |
|      | TCONT=SEC +ICONT*DELT   | CONTROLX |
|      | ICNTL=0   | CONTROLX |
|      | CONSTS=DELX*DELX/DELT   | CONTROLX |
|      | EX(1)=EX(1)*CONSTS/CONST  | CONTROLX |
|      | CONST=CONSTS  | CONTROLX |
|      | DELTCY=DELT/NCYCLE  | CONTROLX |
|      | GO TO 9000  | CONTROLX |
| 9012 | CONTINUE  | CONTROLX |
|      | WRITE(6,959)  | CONTROLX |
|      | WRITE(6,9013) DELT  | CONTROLX |
| 9013 | FORMAT(' PROGRAM HALTED DUE TO DELT SIZE, = ',F10.6)            | CONTROLX |
|      | GO TO 880   | CONTROLX |
| 9000 | CONTINUE  | CONTROLX |
| C    |   | CONTROLX |
| C    | TIMES OF TIP AND ROOT ARE STORED AT THIS POINT FOR LATER OUTPUT | CONTROLX |
| C    |   | CONTROLX |
| C    | .....   | CONTROLX |
| C    | .....   | OUTPUTC  |
|      | POSXN=(POSX-DELX/2.)/(ALEN-DELX)                                | OUTPUTC  |
|      | POSLN=(POSL-DELX/2.)/(ALEN-DELX)                                | OUTPUTC  |
|      | IF(NEPS.EQ.0) GO TO 8014  | OUTPUTC  |
|      | IF(KTOLD.GT.NEPS) GO TO 8013                                    | OUTPUTC  |
|      | IF(POSLN.LT.EPSILO(KTOLD))GO TO 8013                            | OUTPUTC  |
|      | TT(KTOLD)=SEC   | OUTPUTC  |
|      | EPSILO(KTOLD)=POSLN   | OUTPUTC  |
|      | KTOLD=KTOLD+1   | OUTPUTC  |
| 8013 | CONTINUE  | OUTPUTC  |
|      | IF(KROLD.GT.NEPS) GO TO 8014                                    | OUTPUTC  |
|      | IF(POSXN.LT.EPSILO(KROLD))GO TO 8014                            | OUTPUTC  |
|      | TR(KROLD)=SEC   | OUTPUTC  |
|      | KROLD=KROLD+1   | OUTPUTC  |
| 8014 | CONTINUE  | OUTPUTC  |
|      | IF(SEC.GE.HPRINT) GO TO 11                                      | OUTPUTC  |

|      |  |         |
|------|--|---------|
|      | GO TO 20   | OUTPUTC |
| 11   | CONTINUE   | OUTPUTC |
|      | HPRINT=HPRINT+PT   | OUTPUTC |
|      | WRITE (6,40) SEC,HBC,IHCFLG                                  | OUTPUTC |
|      | IF(KTFLG.GT.1) GO TO 8012                                    | OUTPUTC |
|      | WRITE(6,41) (T(J),J=1,N)                                     | OUTPUTC |
| C    |  | OUTPUTC |
| C    | LOOP TO WRITE OUT THE INTERPOLATED TEMPERATURES AT SPECIFIED | OUTPUTC |
| C    | LOCATIONS ALONG THE LENGTH                                   | OUTPUTC |
| C    |  | OUTPUTC |
| 8012 | CONTINUE   | OUTPUTC |
|      | IF (NDIST.LT.1) GO TO 8010                                   | OUTPUTC |
|      | IF(KTFLG.GT.2) GO TO 8010                                    | OUTPUTC |
|      | DO 8001 J=1,NDIST  | OUTPUTC |
|      | IF(S(J))8002,8003,8004                                       | OUTPUTC |
| 8002 | IF (IN(J).EQ.1) GO TO 8001                                   | OUTPUTC |
|      | TX=(T(IN(J))-T(IN(J)-1))*((DELX+S(J))/DELX)                  | OUTPUTC |
|      | R(J)=T(IN(J)-1)+TX   | OUTPUTC |
|      | GO TO 8001   | OUTPUTC |
| 8003 | R(J)=T(IN(J))  | OUTPUTC |
|      | GO TO 8001   | OUTPUTC |
| 8004 | IF(IN(J).EQ.N) GO TO 8001                                    | OUTPUTC |
|      | TX=(T(IN(J)+1)-T(IN(J)))*(S(J)/DELX)                         | OUTPUTC |
|      | R(J)=T(IN(J))+TX   | OUTPUTC |
| 8001 | CONTINUE   | OUTPUTC |
|      | WRITE(6,857) (R(J),J=1,NDIST)                                | OUTPUTC |
| 857  | FORMAT(' T.C.T',10F10.3)                                     | OUTPUTC |
| C    | DIST IS AVAILAIBLE FOR STORAGE AFTER INIT LOOP               | OUTPUTC |
|      | DO 860 J=1,NDIST   | OUTPUTC |
|      | DIST(J)=FRL*((TL-R(J))/(TL-TE))+FRT+FSC                      | OUTPUTC |
|      | IF(R(J).GE.TL) GO TO 862                                     | OUTPUTC |
|      | IF(ISHEIL.EQ.1) DIST(J)=1.-(1.+SCHC*(TL-R(J)))*SCHE          | OUTPUTC |
| 862  | CONTINUE   | OUTPUTC |
|      | IF(R(J).LT.TE)DIST(J)=1.                                     | OUTPUTC |
|      | IF(TIN.EQ.TL) GO TO 860                                      | OUTPUTC |
|      | IF(R(J).GT.TL ) DIST(J)=((TIN-R(J))/(TIN-TL))*FSC            | OUTPUTC |

|      |   |         |
|------|---|---------|
| 860  | CONTINUE                                      | OUTPUTC |
|      | WRITE(6,861) (DIST(J),J=1,NDIST)              | OUTPUTC |
| 861  | FORMAT(' FR.S.',10F10.4)                      | OUTPUTC |
| 8010 | CONTINUE                                      | OUTPUTC |
|      | IF(KTFLG.GT.0) GO TO 8011                     | OUTPUTC |
|      | WRITE(6,831) NCYCLE                           | OUTPUTC |
|      | WRITE(6,26) TQP,TQM,TRP,TRM                   | OUTPUTC |
|      | WRITE(6,25) IQ,IR                             | OUTPUTC |
| 8011 | CONTINUE                                      | OUTPUTC |
|      | WRITE(6,825) POSL,POSX,POSLN,POSXN            | OUTPUTC |
|      | IF(IR.LT.N) GO TO 8015                        | OUTPUTC |
|      | WRITE(6,826)                                  | OUTPUTC |
|      | GO TO 880                                     | OUTPUTC |
| 8015 | CONTINUE                                      | OUTPUTC |
| 8888 | IF(SEC.LE.TSEC) GO TO 8016                    | OUTPUTC |
|      | WRITE(6,827)                                  | OUTPUTC |
|      | GO TO 880                                     | OUTPUTC |
| 8016 | CONTINUE                                      | OUTPUTC |
|      | IF(I.LT.10000) GO TO 8017                     | OUTPUTC |
|      | WRITE(6,828)                                  | OUTPUTC |
|      | GO TO 880                                     | OUTPUTC |
| 8017 | CONTINUE                                      | OUTPUTC |
| 20   | CONTINUE                                      | OUTPUTC |
|      | GO TO 1                                       | OUTPUTC |
| 601  | CONTINUE                                      | OUTPUTC |
| 880  | CONTINUE                                      | OUTPUTC |
|      | WRITE(6,883)                                  | OUTPUTC |
|      | WRITE(6,881) DELT,I                           | OUTPUTC |
|      | WRITE(6,882) SEC                              | OUTPUTC |
|      | WRITE(6,884) IP,IT                            | OUTPUTC |
|      | IF(NEPS.EQ.0) GO TO 8018                      | OUTPUTC |
|      | WRITE(6,829)                                  | OUTPUTC |
|      | WRITE(6,830) (EPSILO(J),TT(J),TR(J),J=1,NEPS) | OUTPUTC |
| 8018 | CONTINUE                                      | OUTPUTC |
|      | WRITE(6,883)                                  | OUTPUTC |
|      | WRITE(6,250) NAME                             | OUTPUTC |



```
871  FORMAT(I5,2F10.5)
959  FORMAT(///' $$$$$ EXECUTION ERROR')
833  FORMAT(' AVERAGE STEP SIZE LIMIT ',F10.5,' = ',F10.5,
1     ' DIVISIONS OF DELX')
      END
```

```
INIT
INIT
INIT
INIT
END
```



## Appendix E

### Error Estimates

The following conclusions concerning the errors in and stability criterion of the Crank-Nicholson method are based on the presentation given in Reference (31), Chapter 7, pages 120-188.

#### 1. Reasons for Choosing an Implicit Technique

The Crank-Nicholson method of implicit solution of the finite difference equations is useful because it is more stable than the explicit techniques. The Euler or Rungu-Kutta techniques, which are explicit, constrain the time step of integration to be very small in order to obtain a stable solution. This yields a unnecessary degree of precision in the results, with a resultant high cost of computation. The implicit Crank-Nicholson technique requires more computation at each time step, but a larger time step may be chosen so that the overall effect is a reduction in computer time to integrate over a given number of seconds.

#### 2. Error in the Crank-Nicholson Method

Error estimates can be obtained only for linear problems, and it is expected that the error estimated for the linear problem will serve only as a lower limit on the

error to be expected in a non-linear problem, such as the one considered in this work.

The truncation error (the difference between the exact solution at time  $t+\Delta t$  and the finite difference solution at time  $t+\Delta t$ , over one time step) at each time step is found to be on the order of  $(\Delta t)^3$  for one linear problem, using the Crank-Nicholson technique. The round-off error is very small, and for most conditions the round-off error is swamped by other errors (truncation, non-linearity). At extremely low values of the heat transfer coefficients, the round-off error becomes important, but can be overcome if a sufficiently large time step is used.

Since the technique is stable for linear problems, the choice of an appropriate time step can be made easily. However, instability can be re-introduced in non-linear problems, where this estimate of  $\Delta t^3$  may not apply. Therefore, the most practical way to test the accuracy of the solution of a non-linear problem is to do two things; (1) compare the finite difference solution to a known analytic solution where one is available, and (2) make a series of numerical experiments, varying the time step and space mesh size, to test accuracy and convergence. Step (1) above has been presented in Figure (7) of the Results, and the results obtained there were that the finite difference solution was always within 0.5 sec. of the analytic solution, with the error growing slightly at higher times. Step (2), the convergence tests, is presented below.

### 3. Sensitivity of the Method to Time Step and Mesh Size Changes

Table III presents the results of the computer program for the following boundary and initial conditions; infinite surface cooling (constant temperature boundary conditions =  $0^{\circ}\text{C}$ ), initial temperature =  $700^{\circ}\text{C}$  ( $50^{\circ}\text{C}$  superheat), no convection, columnar growth morphology. The results are presented for 7 cases, for varying time steps and mesh sizes.

For comparison, the results at 60 seconds are useful, since both the tip and root positions are within the bounds of the casting at this time. The temperature at or near the centerline, the position of the tip and root at 60 seconds are presented; with these the local solidification time at  $\lambda = 0.75$  is presented for each case, in Table IV.

#### A. Space Mesh Size

Parts 1, 2 and 3 show the effect of doubling the number of nodes used. Table IV indicates that as the mesh size is reduced (number of nodes increased), the effect is that the cooling takes place at a slightly lower rate. An equation of the form  $az^3 + bz^2 + c = F$  may be fitted to the points in order to extrapolate the results at a mesh size = 0, where  $z$  is the mesh size and  $F$  is temperature,  $x_L$ ,  $x_E$  or  $t_{1st}$  ( $\lambda = 0.75$ ). The results of interpolating back to  $z = 0$  are presented in Part 8 of Table IV.

### B. Time Step Size

Parts 2, 4 and 5 of Table IV show the effect of halving the time step with a constant number of nodes ( $N = 38$ ). Once again, the higher accuracy results ( $\Delta t = 0.05$  sec) show a slower cooling rate than the lower accuracy ones. The fitting equation  $az^3 + bz^2 + c = F$  was used to extrapolate the temperature,  $x_L$ ,  $x_E$  and  $t_{1st}$  ( $\lambda = 0.75$ ) back to zero time step, and the results are presented in Part 9 of Table IV.

Parts 6 and 7 of Table IV show that for two typical values of the accuracy limits, with  $N = 38$ , the temperatures at the centerline are within  $1^\circ\text{C}$  of the interpolated zero time step value after 60 seconds, the positions of the liquidus and solidus isotherms are within 0.2 cm of the interpolated value, and the local solidification times are 5.4% to 9.4% shorter than the interpolated values.

### 4. Validity of the Curves in the Results Section

Table IV gives an estimate of the degree of numerical accuracy and the degree of convergence which was obtained in the curves plotted in the Results section. In general, the parameters used to generate the Results (time step = 0.1 sec and mesh size = 38 nodes) generate values close to the more accurate results in Table IV. Specifically, the positions of the liquidus and solidus with  $N = 38$  and  $\Delta t = 0.1$  sec are within 0.13 cm of the positions extrapolated to an infinite number of nodes, and are within 0.2 cm of the positions extrapolated to a zero time step. The local solidification

times at  $\lambda = 0.75$  are within 1.0 to 2.5 seconds of the interpolated values. More importantly, it can be seen that the error in the results is systematic, i.e., that the errors occur in the same direction for changes in time step or mesh size (as the time step is decreased the temperatures at a given time increase, for instance). Also, a comparison of the results in Table IV with those in Table VI, which is for different heat flow conditions, shows that the errors occur in the same direction for other conditions, as should be expected. Therefore the changes in the curves in the Results section which occur as external conditions are changed (such as superheat or heat transfer coefficient) are quite meaningful, since the numerical error in each of the curves is systematically reproduced in each of a given set of curves. All sets of curves in the Results section, showing the effect of a change in an external condition, were generated with exactly the same mesh sizes and time steps in order to insure that this systematic error would be reproduced.

Parts 6 and 7 of Table IV were generated by allowing the program to control the size of the time step by holding the accuracy of the temperature calculations between an upper and lower limit, which are given in the table. The exact method is described in Appendix A, and can be followed directly in the computer program (Appendix D) in the blocks labelled 'CONTROLX'. These results, Part 6 and 7, are presented here because most of the curves in the Results

section were generated using this controlled time step technique.

#### 5. Side Heat Loss

Since the computer model for side heat loss adds some additional computational inaccuracy to temperature profiles and tip and root position results, a computational analysis of the errors in one typical side heat flow case is presented here. Tables V and VI are completely analogous to Tables III and IV, for the same external conditions; initial temperature =  $700^{\circ}\text{C}$ , no convection,  $h_B = \text{infinite}$  (constant temperature boundary condition =  $0^{\circ}\text{C}$ ), columnar growth. In addition, heat loss out the side was assumed, with  $h_s = 0.001$ ,  $W = 1$  cm (plate half thickness),  $T_{a,s} = 0^{\circ}\text{C}$ . The parts of Tables V and VI correspond to those in Tables III and IV, and the discussion of the preceding section of this appendix apply to the results presented in these tables. Hence, the general conclusion is again that the curves presented in the Results section are valid and meaningful, and that the numerical values presented there are close to the fully convergent values (presented in Parts 8 and 9 of Table VI for one specific case).

TABLE III, PART 1

NUMBER OF NODES 74  
 TIME STEP= 0.100 SECONDS  
 DISTANCE BETWEEN NODES= 0.2005 CENTIMETERS

DISTANCES FROM THE SURFACE AT EACH NODE (CENTIMETERS)

|       |       |       |       |       |       |       |       |       |       |       |       |       |       |       |       |
|-------|-------|-------|-------|-------|-------|-------|-------|-------|-------|-------|-------|-------|-------|-------|-------|
| 0.10  | 0.30  | 0.50  | 0.70  | 0.90  | 1.10  | 1.30  | 1.50  | 1.70  | 1.90  | 2.11  | 2.31  | 2.51  | 2.71  | 2.91  | 3.11  |
| 3.11  | 3.51  | 3.71  | 3.91  | 4.11  | 4.31  | 4.51  | 4.71  | 4.91  | 5.11  | 5.31  | 5.51  | 5.71  | 5.92  | 6.12  | 6.32  |
| 6.52  | 6.72  | 6.92  | 7.12  | 7.32  | 7.52  | 7.72  | 7.92  | 8.12  | 8.32  | 8.52  | 8.72  | 8.92  | 9.12  | 9.32  | 9.52  |
| 9.73  | 9.93  | 10.13 | 10.33 | 10.53 | 10.73 | 10.93 | 11.13 | 11.33 | 11.53 | 11.73 | 11.93 | 12.13 | 12.33 | 12.53 | 12.73 |
| 12.93 | 13.13 | 13.33 | 13.54 | 13.74 | 13.94 | 14.14 | 14.34 | 14.54 | 14.74 | 14.94 | 15.14 |       |       |       |       |

TIME (SECONDS) NODAL TEMPERATURES (DEGREES C)

|        |  |       |       |       |       |       |       |       |       |       |       |       |       |       |       |
|--------|--|-------|-------|-------|-------|-------|-------|-------|-------|-------|-------|-------|-------|-------|-------|
| 0.0    | POSITIONS: TIP 0.0 (SLAB 0), ROOT 0.0 (SLAB 0)       |       |       |       |       |       |       |       |       |       |       |       |       |       |       |
| 700.0  | 700.0  | 700.0 | 700.0 | 700.0 | 700.0 | 700.0 | 700.0 | 700.0 | 700.0 | 700.0 | 700.0 | 700.0 | 700.0 | 700.0 | 700.0 |
| 700.0  | 700.0  | 700.0 | 700.0 | 700.0 | 700.0 | 700.0 | 700.0 | 700.0 | 700.0 | 700.0 | 700.0 | 700.0 | 700.0 | 700.0 | 700.0 |
| 700.0  | 700.0  | 700.0 | 700.0 | 700.0 | 700.0 | 700.0 | 700.0 | 700.0 | 700.0 | 700.0 | 700.0 | 700.0 | 700.0 | 700.0 | 700.0 |
| 700.0  | 700.0  | 700.0 | 700.0 | 700.0 | 700.0 | 700.0 | 700.0 | 700.0 | 700.0 | 700.0 | 700.0 | 700.0 | 700.0 | 700.0 | 700.0 |
| 10.10  | POSITIONS: TIP 4.80 (SLAB 25), ROOT 3.20 (SLAB 17)   |       |       |       |       |       |       |       |       |       |       |       |       |       |       |
| 0.0    | 39.1   | 78.1  | 116.9 | 155.1 | 192.8 | 229.9 | 266.2 | 301.7 | 336.3 | 370.1 | 402.9 | 434.9 | 466.9 | 502.1 | 547.4 |
| 566.5  | 554.7  | 542.2 | 529.0 | 512.4 | 492.4 | 473.4 | 455.8 | 439.1 | 423.2 | 407.9 | 392.4 | 376.7 | 360.9 | 345.1 | 329.2 |
| 682.7  | 685.7  | 687.2 | 687.2 | 685.8 | 682.4 | 677.2 | 670.7 | 662.8 | 653.8 | 643.8 | 632.9 | 621.2 | 608.8 | 595.8 | 582.4 |
| 654.8  | 649.7  | 643.7 | 636.8 | 629.0 | 620.4 | 611.2 | 601.5 | 591.3 | 580.6 | 569.4 | 557.7 | 545.5 | 532.9 | 520.0 | 506.8 |
| 700.0  | 700.0  | 700.0 | 700.0 | 700.0 | 700.0 | 700.0 | 700.0 | 700.0 | 700.0 | 700.0 | 700.0 | 700.0 | 700.0 | 700.0 | 700.0 |
| 20.10  | POSITIONS: TIP 6.60 (SLAB 34), ROOT 4.99 (SLAB 25)   |       |       |       |       |       |       |       |       |       |       |       |       |       |       |
| 0.0    | 24.1   | 42.1  | 61.1  | 103.9 | 129.5 | 154.9 | 180.1 | 205.0 | 229.5 | 253.7 | 277.5 | 300.9 | 323.7 | 346.2 | 368.1 |
| 389.4  | 417.1  | 435.4 | 453.3 | 469.4 | 484.9 | 500.0 | 523.5 | 541.3 | 557.9 | 576.0 | 592.6 | 607.4 | 620.1 | 630.8 | 639.4 |
| 666.5  | 665.9  | 665.7 | 664.9 | 663.5 | 661.6 | 659.3 | 656.6 | 653.5 | 649.9 | 645.9 | 641.6 | 637.1 | 632.4 | 627.5 | 622.4 |
| 691.1  | 692.7  | 693.1 | 693.9 | 694.7 | 695.3 | 695.9 | 696.4 | 696.9 | 697.3 | 697.6 | 697.9 | 698.2 | 698.4 | 698.6 | 698.8 |
| 699.0  | 699.1  | 699.2 | 699.3 | 699.4 | 699.5 | 699.6 | 699.6 | 699.6 | 699.7 | 699.7 | 699.7 | 699.7 | 699.7 | 699.7 | 699.7 |
| 30.10  | POSITIONS: TIP 8.14 (SLAB 41), ROOT 6.15 (SLAB 31)   |       |       |       |       |       |       |       |       |       |       |       |       |       |       |
| 0.0    | 20.9   | 41.4  | 62.4  | 83.1  | 103.7 | 124.2 | 144.6 | 164.9 | 185.0 | 204.9 | 224.6 | 244.1 | 263.4 | 282.4 | 301.2 |
| 319.7  | 337.9  | 355.9 | 373.5 | 390.7 | 407.7 | 424.3 | 443.5 | 456.4 | 471.9 | 487.1 | 501.9 | 516.3 | 530.4 | 544.7 | 558.4 |
| 573.1  | 586.9  | 599.5 | 611.0 | 621.1 | 629.8 | 637.3 | 643.4 | 649.0 | 653.7 | 657.0 | 660.7 | 664.1 | 667.2 | 670.1 | 672.8 |
| 675.3  | 677.6  | 679.7 | 681.6 | 683.3 | 684.9 | 686.4 | 687.7 | 688.9 | 690.0 | 691.0 | 691.9 | 692.7 | 693.5 | 694.1 | 694.7 |
| 695.2  | 695.7  | 696.1 | 696.4 | 696.7 | 697.0 | 697.2 | 697.4 | 697.5 | 697.7 | 697.7 | 697.7 | 697.7 | 697.7 | 697.7 | 697.7 |
| 40.10  | POSITIONS: TIP 9.41 (SLAB 48), ROOT 7.10 (SLAB 36)   |       |       |       |       |       |       |       |       |       |       |       |       |       |       |
| 0.0    | 18.0   | 35.9  | 53.8  | 71.7  | 89.5  | 107.3 | 124.9 | 142.5 | 160.0 | 177.4 | 194.7 | 211.8 | 228.9 | 245.6 | 262.2 |
| 279.7  | 295.0  | 311.1 | 327.0 | 342.7 | 358.1 | 373.4 | 389.4 | 403.1 | 417.6 | 431.9 | 445.9 | 459.6 | 473.0 | 486.2 | 499.1 |
| 511.7  | 524.0  | 536.0 | 548.3 | 560.3 | 573.1 | 585.1 | 596.2 | 606.4 | 615.6 | 623.8 | 631.1 | 637.4 | 642.9 | 647.5 | 651.6 |
| 655.0  | 658.3  | 661.4 | 664.3 | 667.0 | 669.6 | 671.9 | 674.1 | 676.1 | 678.0 | 679.7 | 681.3 | 682.8 | 684.1 | 685.3 | 686.4 |
| 687.5  | 688.4  | 689.2 | 689.9 | 690.5 | 691.0 | 691.5 | 691.9 | 692.2 | 692.4 | 692.5 | 692.6 | 692.6 | 692.6 | 692.6 | 692.6 |
| 50.10  | POSITIONS: TIP 10.52 (SLAB 53), ROOT 7.91 (SLAB 40)  |       |       |       |       |       |       |       |       |       |       |       |       |       |       |
| 0.0    | 16.1   | 32.1  | 48.1  | 64.1  | 80.0  | 96.0  | 111.9 | 127.6 | 143.3 | 159.0 | 174.5 | 190.0 | 205.3 | 220.6 | 235.7 |
| 250.7  | 265.6  | 280.3 | 294.9 | 309.3 | 323.6 | 337.7 | 351.6 | 365.4 | 378.7 | 392.3 | 405.5 | 418.5 | 431.3 | 443.8 | 456.2 |
| 468.4  | 480.3  | 492.0 | 503.5 | 514.7 | 525.8 | 536.5 | 547.4 | 558.3 | 569.7 | 580.6 | 590.8 | 600.2 | 609.0 | 617.0 | 624.2 |
| 630.7  | 635.4  | 641.4 | 645.7 | 649.7 | 652.6 | 655.6 | 659.3 | 660.9 | 663.4 | 665.6 | 667.8 | 669.7 | 671.6 | 673.2 | 674.8 |
| 675.2  | 677.5  | 678.4 | 679.7 | 680.6 | 681.4 | 682.0 | 682.6 | 683.1 | 683.4 | 683.6 | 683.7 | 683.7 | 683.7 | 683.7 | 683.7 |
| 60.10  | POSITIONS: TIP 11.57 (SLAB 58), ROOT 8.63 (SLAB 44)  |       |       |       |       |       |       |       |       |       |       |       |       |       |       |
| 0.0    | 14.7   | 29.3  | 43.9  | 58.6  | 73.1  | 87.7  | 102.2 | 116.7 | 131.1 | 145.4 | 159.7 | 173.9 | 188.1 | 202.1 | 216.1 |
| 230.0  | 243.7  | 257.4 | 270.9 | 284.3 | 297.6 | 310.8 | 323.8 | 336.7 | 349.5 | 362.1 | 374.5 | 386.9 | 399.0 | 411.0 | 422.8 |
| 434.5  | 445.0  | 457.3 | 468.4 | 479.4 | 490.2 | 500.9 | 511.3 | 521.5 | 531.5 | 541.9 | 551.5 | 561.3 | 571.6 | 581.3 | 590.5 |
| 599.0  | 607.0  | 614.4 | 621.1 | 627.2 | 632.7 | 637.6 | 641.8 | 645.5 | 648.9 | 651.4 | 653.7 | 655.9 | 657.7 | 659.8 | 661.5 |
| 663.1  | 664.6  | 666.0 | 667.2 | 668.2 | 669.1 | 669.9 | 670.6 | 671.1 | 671.5 | 671.8 | 671.9 | 671.9 | 671.9 | 671.9 | 671.9 |
| 70.09  | POSITIONS: TIP 12.66 (SLAB 64), ROOT 9.31 (SLAB 47)  |       |       |       |       |       |       |       |       |       |       |       |       |       |       |
| 0.0    | 13.6   | 27.2  | 40.7  | 54.3  | 67.8  | 81.3  | 94.8  | 108.2 | 121.4 | 134.9 | 148.1 | 161.5 | 174.6 | 187.7 | 200.8 |
| 213.7  | 224.6  | 235.4 | 245.1 | 254.7 | 264.7 | 274.7 | 284.5 | 301.8 | 316.0 | 326.1 | 336.0 | 345.9 | 354.6 | 363.1 | 371.7 |
| 407.0  | 418.1  | 428.9 | 439.7 | 450.3 | 460.7 | 471.0 | 481.1 | 491.0 | 500.7 | 510.5 | 520.0 | 529.3 | 538.5 | 547.7 | 556.8 |
| 566.4  | 575.4  | 584.3 | 592.5 | 600.2 | 607.4 | 614.1 | 620.2 | 625.8 | 630.8 | 635.2 | 639.2 | 642.6 | 645.4 | 648.1 | 650.3 |
| 651.5  | 652.8  | 654.0 | 655.0 | 656.0 | 656.9 | 657.5 | 658.1 | 658.6 | 659.0 | 659.2 | 659.4 | 659.4 | 659.4 | 659.4 | 659.4 |
| 80.09  | POSITIONS: TIP 13.91 (SLAB 70), ROOT 9.93 (SLAB 50)  |       |       |       |       |       |       |       |       |       |       |       |       |       |       |
| 0.0    | 12.7   | 25.4  | 38.1  | 50.8  | 63.5  | 76.2  | 88.9  | 101.4 | 113.9 | 126.5 | 138.9 | 151.4 | 163.7 | 176.1 | 188.3 |
| 200.5  | 212.7  | 224.7 | 236.7 | 248.6 | 260.4 | 272.2 | 283.3 | 295.4 | 306.9 | 318.2 | 329.5 | 340.6 | 351.6 | 362.6 | 373.4 |
| 384.1  | 394.7  | 405.2 | 415.5 | 425.7 | 435.8 | 445.8 | 455.6 | 465.3 | 474.7 | 484.3 | 493.6 | 502.7 | 511.7 | 520.6 | 529.3 |
| 537.9  | 546.6  | 555.0 | 563.8 | 572.4 | 580.5 | 588.3 | 595.6 | 602.5 | 609.9 | 614.8 | 620.3 | 625.2 | 629.6 | 633.6 | 637.1 |
| 640.2  | 642.8  | 645.1 | 647.0 | 648.6 | 649.9 | 650.2 | 650.3 | 650.5 | 650.6 | 650.7 | 650.7 | 650.7 | 650.7 | 650.7 | 650.7 |
| 90.09  | POSITIONS: TIP 15.07 (SLAB 76), ROOT 10.53 (SLAB 53) |       |       |       |       |       |       |       |       |       |       |       |       |       |       |
| 0.0    | 12.0   | 24.0  | 36.0  | 48.0  | 59.0  | 71.0  | 83.0  | 95.0  | 107.0 | 119.4 | 131.2 | 142.9 | 154.6 | 166.3 | 177.9 |
| 199.5  | 201.0  | 212.4 | 223.8 | 235.1 | 246.4 | 257.5 | 268.6 | 279.6 | 290.5 | 301.4 | 312.2 | 322.9 | 333.4 | 343.9 | 354.3 |
| 364.6  | 374.8  | 384.9 | 394.8 | 404.7 | 414.5 | 424.1 | 433.5 | 443.0 | 452.3 | 461.5 | 470.6 | 479.5 | 488.3 | 497.0 | 505.5 |
| 514.0  | 522.3  | 530.5 | 538.5 | 546.7 | 554.5 | 562.8 | 570.8 | 578.4 | 585.7 | 592.6 | 599.1 | 605.2 | 610.9 | 616.1 | 620.9 |
| 625.2  | 629.2  | 632.7 | 635.8 | 638.6 | 641.0 | 643.1 | 644.9 | 646.5 | 647.9 | 649.0 | 649.0 | 649.0 | 649.0 | 649.0 | 649.0 |
| 100.09 | POSITIONS: TIP 15.24 (SLAB 77), ROOT 11.11 (SLAB 56) |       |       |       |       |       |       |       |       |       |       |       |       |       |       |
| 0.0    | 11.4   | 22.8  | 34.2  | 45.5  | 56.9  | 68.2  | 79.5  | 90.8  | 102.1 | 113.3 | 124.6 | 135.7 | 146.9 | 158.0 | 169.0 |
| 180.0  | 191.0  | 201.9 | 212.8 | 223.6 | 234.3 | 245.0 | 255.6 | 266.1 | 276.6 | 287.0 | 297.3 | 307.5 | 317.7 | 327.7 | 337.7 |
| 347.6  | 357.5  | 367.2 | 376.8 | 386.3 | 395.8 | 405.1 | 414.4 | 423.5 | 432.5 | 441.5 | 450.3 | 459.0 | 467.6 | 476.1 | 484.5 |
| 492.8  | 500.9  | 509.0 | 516.9 | 524.7 | 532.4 | 540.0 | 547.4 | 555.0 | 562.8 | 570.3 | 577.5 | 584.3 | 590.8 | 596.9 | 602.6 |
| 607.9  | 612.8  | 617.3 | 621.3 | 624.9 | 628.0 | 630.8 | 633.0 | 634.8 | 636.2 | 637.1 | 637.5 | 637.5 | 637.5 | 637.5 | 637.5 |
| 110.09 | POSITIONS: TIP 15.24 (SLAB 77), ROOT 11.69 (SLAB 59) |       |       |       |       |       |       |       |       |       |       |       |       |       |       |
| 0.0    | 10.9   | 21.7  | 32.6  | 43.4  | 54.2  | 65.0  | 75.8  | 86.6  | 97.4  | 108.1 | 118.8 | 129.5 | 140.1 | 150.7 | 161.3 |
| 171.8  | 182.3  | 192.8 | 203.1 | 213.5 | 223.8 | 234.0 | 244.2 | 254.3 | 264.3 | 274.3 | 284.2 | 294.1 | 303.9 | 313.6 | 323.2 |
| 332.7  | 342.2  | 351.6 | 360.9 | 370.1 | 379.1 | 388.3 | 397.3 | 406.2 | 414.9 | 423.6 | 432.2 | 440.7 | 449.1 | 457.4 | 465.6 |
| 473.7  | 481.7  | 489.6 | 497.3 | 505.0 | 512.5 | 520.0 | 527.3 | 534.5 | 541.6 | 548.8 | 555.7 | 563.0 | 569.9 | 576.5 | 582.7 |
| 598.5  | 601.0  | 603.4 | 605.8 | 607.5 | 611.1 | 614.3 | 616.9 | 619.0 | 620.5 | 621.7 | 622.2 | 622.2 | 622.2 | 622.2 | 622.2 |
| 120.09 | POSITIONS: TIP 15.24 (SLAB 77), ROOT 12.29 (SLAB 62) |       |       |       |       |       |       |       |       |       |       |       |       |       |       |
| 0.0    | 10.4   | 20.8  | 31.2  | 41.5  | 51.9  | 62.3  | 72.6  | 82.9  | 93.2  | 103.5 | 113.8 | 124.0 | 134.2 | 144.3 | 154.5 |
| 164.6  | 174.6  | 184.6 | 194.6 | 204.6 | 214.4 | 224.2 | 234.0 | 243.8 | 253.4 | 263.0 | 272.6 | 282.1 | 291.5 | 300.8 | 310.1 |
| 319.3  | 328.5  | 337.6 | 346.5 | 355.5 | 364.3 | 373.1 | 381.7 | 390.3 | 398.8 | 407.2 | 415.5 | 423.8 | 431.9 | 440.0 | 447.9 |
| 455.8  | 463.4  | 471.2 | 478.8 | 486.2 | 493.6 | 500.9 | 507.9 | 515.0 | 521.9 | 528.6 | 535.3 | 541.9 | 548.5 | 554.8 | 561.3 |
| 567.4  | 573.1  | 578.4 | 583.2 | 587   |       |       |       |       |       |       |       |       |       |       |       |















Table IV

## Results for 60 Seconds

Sensitivity of the Results to Time Step and Space Mesh Size  
Unidirectional Heat Flow

$T_0 = 700^\circ\text{C}$ ,  $L = 15.24$  cm., no convection, surface temperature =  $0^\circ\text{C}$  ( $t > 0$ ),  
columnar growth.

| part | N          | $\Delta t$ , sec        | $x_L$ , cm | $x_E$ , cm | $T_{\text{center}}$ , $^\circ\text{C}$ | $t_{1st}$<br>$\lambda = 0.75$ |
|------|------------|-------------------------|------------|------------|--|-------------------------------|
| 1    | 76         | .1                      | 11.47      | 8.53       | 671.5                                  | 46.9                          |
| 2    | 38         | .1                      | 11.57      | 8.56       | 668.6                                  | 46.5                          |
| 3    | 19         | .1                      | 12.03      | 8.81       | 661.6                                  | 45.1                          |
| 4    | 38         | .2                      | 11.84      | 8.80       | 666.2                                  | 44.4                          |
| 5    | 38         | .05                     | 11.41      | 8.43       | 670.1                                  | 48.0                          |
| 6    | 38         | *.0002 max<br>.0001 min | 11.45      | 8.48       | 669.8                                  | 46.0                          |
| 7    | 38         | *.0006 max<br>.0003 min | 11.53      | 8.56       | 669.4                                  | 44.0                          |
| 8    | $\infty$ † | .1                      | 11.44      | 8.52       | 672.7                                  | 47.0                          |
| 9    | 38         | 0**                     | 11.34      | 8.37       | 670.8                                  | 48.7                          |

† Extrapolated back to zero slab width.

\* Time steps controlled by program. These are accuracy limits.

\*\* Extrapolated back to zero time steps.







TABLE V, PART 3  
SIDE HEAT LOSS

NUMBER OF NODES 76  
TIME STEP= 0.100 SECONDS  
DISTANCE BETWEEN NODES= 0.2125 CENTIMETERS

DISTANCES FROM THE SURFACE AT EACH NODE(CENTIMETERS)

|       |       |       |       |       |       |       |       |       |       |       |       |       |       |       |       |
|-------|-------|-------|-------|-------|-------|-------|-------|-------|-------|-------|-------|-------|-------|-------|-------|
| 0.10  | 0.30  | 0.50  | 0.70  | 0.90  | 1.10  | 1.30  | 1.50  | 1.70  | 1.90  | 2.11  | 2.31  | 2.51  | 2.71  | 2.91  | 3.11  |
| 3.21  | 3.41  | 3.61  | 3.81  | 4.01  | 4.21  | 4.41  | 4.61  | 4.81  | 5.01  | 5.21  | 5.41  | 5.61  | 5.81  | 6.01  | 6.21  |
| 6.42  | 6.62  | 6.82  | 7.02  | 7.22  | 7.42  | 7.62  | 7.82  | 8.02  | 8.22  | 8.42  | 8.62  | 8.82  | 9.02  | 9.22  | 9.42  |
| 9.63  | 9.83  | 10.03 | 10.23 | 10.43 | 10.63 | 10.83 | 11.03 | 11.23 | 11.43 | 11.63 | 11.83 | 12.03 | 12.23 | 12.43 | 12.63 |
| 12.83 | 13.03 | 13.23 | 13.43 | 13.63 | 13.83 | 14.03 | 14.23 | 14.43 | 14.63 | 14.83 | 15.03 | 15.23 | 15.43 | 15.63 | 15.83 |

TIME(SECONDS) NODE TEMPERATURE(DEGREES C)

| C.O   | POSITIONS: TIP 0.0 (SLAB 0) , ROOT 0.0 (SLAB 0)       |       |       |       |       |       |       |       |       |       |       |       |       |       |       |       |
|-------|---|-------|-------|-------|-------|-------|-------|-------|-------|-------|-------|-------|-------|-------|-------|-------|
|       | T00.0   | T00.0 | T00.0 | T00.0 | T00.0 | T00.0 | T00.0 | T00.0 | T00.0 | T00.0 | T00.0 | T00.0 | T00.0 | T00.0 | T00.0 | T00.0 |
| 0.0   | 700.0   | 700.0 | 700.0 | 700.0 | 700.0 | 700.0 | 700.0 | 700.0 | 700.0 | 700.0 | 700.0 | 700.0 | 700.0 | 700.0 | 700.0 | 700.0 |
| 10.10 | POSITIONS: TIP 4.96 (SLAB 25) , ROOT 3.53 (SLAB 14)   |       |       |       |       |       |       |       |       |       |       |       |       |       |       |       |
| 0.0   | 38.6  | 77.2  | 115.8 | 154.4 | 193.0 | 231.6 | 270.2 | 308.8 | 347.4 | 386.0 | 424.6 | 463.2 | 501.8 | 540.4 | 579.0 | 617.6 |
| 52.7  | 544.4   | 565.5 | 587.8 | 607.1 | 622.2 | 633.5 | 641.7 | 648.7 | 652.7 | 656.9 | 660.6 | 664.0 | 667.0 | 669.7 | 672.1 | 674.2 |
| 174.2 | 676.1   | 677.8 | 679.3 | 680.6 | 681.8 | 682.8 | 683.7 | 684.4 | 685.1 | 685.7 | 686.2 | 686.6 | 687.0 | 687.3 | 687.6 | 687.9 |
| 267.8 | 688.3   | 688.2 | 688.3 | 688.4 | 688.5 | 688.6 | 688.7 | 688.7 | 688.8 | 688.8 | 688.8 | 688.8 | 688.9 | 688.9 | 688.9 | 688.9 |
| 362.9 | 688.9   | 688.9 | 688.9 | 688.9 | 688.9 | 688.9 | 688.9 | 688.9 | 688.9 | 688.9 | 688.9 | 688.9 | 688.9 | 688.9 | 688.9 | 688.9 |
| 20.10 | POSITIONS: TIP 7.27 (SLAB 37) , ROOT 5.37 (SLAB 27)   |       |       |       |       |       |       |       |       |       |       |       |       |       |       |       |
| 0.0   | 24.5  | 49.1  | 73.5  | 97.8  | 121.9 | 145.9 | 169.7 | 193.2 | 216.4 | 239.4 | 262.2 | 284.7 | 306.9 | 328.8 | 350.4 | 371.8 |
| 368.9 | 389.3   | 408.5 | 427.5 | 446.0 | 463.9 | 481.3 | 498.2 | 514.5 | 530.2 | 546.5 | 562.3 | 577.7 | 592.7 | 607.4 | 621.8 | 636.0 |
| 628.3 | 635.6   | 641.7 | 646.5 | 651.4 | 655.7 | 659.2 | 662.4 | 665.4 | 668.1 | 670.7 | 673.1 | 675.4 | 677.5 | 679.4 | 681.1 | 682.7 |
| 675.3 | 677.5   | 679.3 | 680.9 | 682.3 | 683.6 | 684.7 | 685.7 | 686.5 | 687.2 | 687.8 | 688.3 | 688.7 | 689.0 | 689.3 | 689.5 | 689.7 |
| 677.3 | 677.4   | 677.5 | 677.6 | 677.7 | 677.7 | 677.7 | 677.8 | 677.8 | 677.8 | 677.9 | 677.9 | 677.9 | 677.9 | 677.9 | 677.9 | 677.9 |
| 30.10 | POSITIONS: TIP 9.33 (SLAB 47) , ROOT 6.60 (SLAB 36)   |       |       |       |       |       |       |       |       |       |       |       |       |       |       |       |
| 0.0   | 19.6  | 39.2  | 58.7  | 78.2  | 97.6  | 116.9 | 136.2 | 155.3 | 174.2 | 193.0 | 211.6 | 230.0 | 248.2 | 266.2 | 284.0 | 301.6 |
| 301.2 | 318.8   | 335.9 | 352.5 | 368.9 | 385.0 | 400.8 | 416.3 | 431.4 | 446.3 | 460.8 | 475.0 | 488.9 | 502.7 | 516.5 | 529.8 | 543.0 |
| 543.3 | 554.6   | 566.9 | 579.6 | 591.1 | 601.5 | 610.7 | 618.8 | 625.8 | 631.7 | 636.9 | 641.8 | 646.4 | 650.7 | 654.7 | 658.4 | 661.9 |
| 652.0 | 653.1   | 654.2 | 655.2 | 656.2 | 657.1 | 657.8 | 658.4 | 658.8 | 659.2 | 659.5 | 659.8 | 660.1 | 660.3 | 660.5 | 660.7 | 660.8 |
| 663.8 | 664.2   | 664.5 | 664.7 | 664.9 | 665.0 | 665.1 | 665.2 | 665.3 | 665.4 | 665.4 | 665.5 | 665.5 | 665.6 | 665.7 | 665.7 | 665.7 |
| 40.10 | POSITIONS: TIP 11.46 (SLAB 57) , ROOT 7.74 (SLAB 37)  |       |       |       |       |       |       |       |       |       |       |       |       |       |       |       |
| 0.0   | 16.7  | 33.4  | 50.2  | 66.8  | 83.5  | 100.0 | 116.5 | 132.9 | 149.3 | 165.5 | 181.6 | 197.6 | 213.4 | 229.2 | 244.7 | 260.2 |
| 260.2 | 275.4   | 290.5 | 305.4 | 320.2 | 334.5 | 348.8 | 362.9 | 376.9 | 390.4 | 403.8 | 417.0 | 429.9 | 442.6 | 455.0 | 467.2 | 479.2 |
| 479.1 | 490.8   | 502.2 | 513.4 | 524.3 | 534.9 | 545.9 | 556.3 | 567.0 | 577.0 | 587.6 | 597.4 | 606.4 | 615.5 | 624.7 | 633.3 | 641.8 |
| 628.1 | 632.2   | 635.8 | 638.8 | 641.5 | 643.7 | 645.7 | 647.3 | 648.8 | 649.9 | 650.6 | 651.0 | 651.4 | 651.7 | 651.9 | 652.1 | 652.3 |
| 650.7 | 650.9   | 651.1 | 651.3 | 651.5 | 651.7 | 651.9 | 652.0 | 652.1 | 652.2 | 652.3 | 652.3 | 652.3 | 652.3 | 652.3 | 652.3 | 652.3 |
| 50.10 | POSITIONS: TIP 15.24 (SLAB 77) , ROOT 9.78 (SLAB 44)  |       |       |       |       |       |       |       |       |       |       |       |       |       |       |       |
| 0.0   | 14.8  | 29.6  | 44.3  | 59.1  | 73.8  | 88.4  | 102.9 | 117.6 | 132.1 | 146.5 | 160.9 | 175.1 | 189.3 | 203.4 | 217.3 | 231.2 |
| 231.2 | 244.9   | 258.5 | 272.0 | 285.3 | 298.5 | 311.5 | 324.6 | 337.1 | 349.7 | 362.1 | 374.4 | 386.4 | 398.2 | 409.9 | 421.4 | 432.7 |
| 432.7 | 443.8   | 454.7 | 465.4 | 475.9 | 486.2 | 496.5 | 506.2 | 516.0 | 525.5 | 534.8 | 544.0 | 553.3 | 562.9 | 571.9 | 580.4 | 588.4 |
| 588.2 | 595.3   | 601.8 | 607.6 | 612.7 | 617.3 | 621.7 | 625.6 | 629.6 | 633.1 | 636.2 | 639.9 | 643.4 | 646.6 | 649.6 | 652.4 | 655.0 |
| 655.1 | 655.6   | 655.1 | 654.6 | 654.0 | 653.9 | 653.9 | 653.8 | 653.7 | 653.6 | 653.5 | 653.4 | 653.3 | 653.2 | 653.1 | 653.0 | 652.9 |
| 60.10 | POSITIONS: TIP 19.24 (SLAB 77) , ROOT 9.80 (SLAB 50)  |       |       |       |       |       |       |       |       |       |       |       |       |       |       |       |
| 0.0   | 13.3  | 26.7  | 40.0  | 53.2  | 66.5  | 79.7  | 92.9  | 106.1 | 119.2 | 132.3 | 145.3 | 158.2 | 171.0 | 183.8 | 196.5 | 209.2 |
| 209.1 | 221.7   | 234.1 | 246.4 | 258.7 | 270.8 | 282.8 | 294.6 | 306.4 | 318.0 | 329.5 | 340.9 | 352.1 | 363.2 | 374.1 | 384.9 | 395.5 |
| 395.5 | 406.0   | 416.3 | 426.5 | 436.5 | 446.3 | 456.0 | 465.5 | 474.9 | 484.0 | 493.0 | 501.9 | 510.5 | 519.0 | 527.4 | 535.5 | 543.5 |
| 543.2 | 552.1   | 559.8 | 567.7 | 575.7 | 583.6 | 591.2 | 598.7 | 606.1 | 613.3 | 620.4 | 627.3 | 634.1 | 640.7 | 647.2 | 653.6 | 659.8 |
| 659.8 | 665.4   | 670.7 | 675.7 | 680.5 | 685.2 | 689.7 | 694.0 | 698.1 | 702.0 | 705.7 | 709.2 | 712.5 | 715.7 | 718.8 | 721.8 | 724.7 |
| 70.09 | POSITIONS: TIP 15.24 (SLAB 77) , ROOT 10.94 (SLAB 55) |       |       |       |       |       |       |       |       |       |       |       |       |       |       |       |
| 0.0   | 12.2  | 24.3  | 36.5  | 48.6  | 60.6  | 72.6  | 84.6  | 96.5  | 108.3 | 120.0 | 131.6 | 143.1 | 154.5 | 165.8 | 177.0 | 188.1 |
| 188.1 | 203.7   | 214.5 | 225.9 | 237.2 | 248.4 | 259.5 | 270.5 | 281.4 | 292.2 | 302.9 | 313.5 | 324.0 | 334.3 | 344.6 | 354.8 | 364.9 |
| 364.9 | 374.6   | 384.4 | 394.0 | 403.5 | 412.8 | 422.0 | 431.1 | 440.1 | 448.8 | 457.4 | 465.8 | 474.1 | 482.3 | 490.4 | 498.5 | 506.5 |
| 506.5 | 513.9   | 521.3 | 528.6 | 535.8 | 542.9 | 549.8 | 556.7 | 563.4 | 570.0 | 576.4 | 582.7 | 588.9 | 595.0 | 601.0 | 606.9 | 612.7 |
| 612.7 | 618.4   | 624.0 | 629.4 | 634.7 | 639.8 | 644.8 | 649.6 | 654.3 | 658.8 | 663.2 | 667.4 | 671.5 | 675.5 | 679.4 | 683.2 | 686.9 |
| 686.9 | 690.5   | 694.0 | 697.4 | 700.7 | 703.9 | 707.0 | 710.0 | 712.9 | 715.6 | 718.2 | 720.7 | 723.1 | 725.4 | 727.6 | 729.7 | 731.8 |
| 80.09 | POSITIONS: TIP 15.24 (SLAB 77) , ROOT 11.92 (SLAB 63) |       |       |       |       |       |       |       |       |       |       |       |       |       |       |       |
| 0.0   | 11.2  | 22.4  | 33.6  | 44.8  | 56.0  | 67.2  | 78.4  | 89.6  | 100.8 | 111.9 | 122.9 | 133.8 | 144.7 | 155.5 | 166.2 | 176.9 |
| 176.9 | 187.5   | 198.2 | 208.7 | 219.2 | 229.6 | 240.0 | 250.3 | 260.6 | 270.8 | 280.9 | 290.9 | 300.8 | 310.6 | 320.3 | 329.9 | 339.4 |
| 339.4 | 348.8   | 357.1 | 365.2 | 373.2 | 381.0 | 388.7 | 396.3 | 403.8 | 411.1 | 418.3 | 425.4 | 432.4 | 439.3 | 446.0 | 452.6 | 459.1 |
| 459.1 | 465.5   | 471.8 | 477.9 | 483.8 | 489.5 | 495.0 | 500.4 | 505.7 | 510.8 | 515.8 | 520.6 | 525.3 | 529.9 | 534.4 | 538.8 | 543.1 |
| 543.1 | 547.3   | 551.4 | 555.4 | 559.3 | 563.1 | 566.8 | 570.4 | 573.9 | 577.3 | 580.6 | 583.8 | 586.9 | 589.9 | 592.8 | 595.6 | 598.3 |
| 60.09 | POSITIONS: TIP 15.24 (SLAB 77) , ROOT 13.16 (SLAB 64) |       |       |       |       |       |       |       |       |       |       |       |       |       |       |       |
| 0.0   | 10.4  | 20.8  | 31.2  | 41.6  | 52.0  | 62.4  | 72.7  | 83.0  | 93.3  | 103.5 | 113.8 | 124.0 | 134.1 | 144.2 | 154.3 | 164.4 |
| 164.4 | 174.5   | 184.7 | 194.8 | 204.9 | 214.9 | 224.9 | 234.9 | 244.8 | 254.7 | 264.5 | 274.3 | 284.0 | 293.7 | 303.4 | 313.0 | 322.6 |
| 322.6 | 332.1   | 341.6 | 351.0 | 360.4 | 369.7 | 378.9 | 388.0 | 397.0 | 405.9 | 414.7 | 423.4 | 432.0 | 440.5 | 448.9 | 457.2 | 465.4 |
| 465.4 | 473.5   | 481.5 | 489.4 | 497.2 | 504.9 | 512.5 | 520.0 | 527.4 | 534.7 | 541.9 | 549.0 | 556.0 | 562.9 | 569.6 | 576.2 | 582.7 |
| 582.7 | 589.1   | 595.4 | 601.6 | 607.7 | 613.7 | 619.6 | 625.4 | 631.1 | 636.7 | 642.2 | 647.6 | 652.9 | 658.1 | 663.2 | 668.2 | 673.1 |

TABLE V, PART 4  
SIDE HEAT LOSS

-----  
NUMBER OF NODES 39  
TIME STEP= 0.200 SECONDS  
DISTANCE BETWEEN NODES= 0.4011 CENTIMETERS  
-----

DISTANCES FROM THE SURFACE AT EACH NODE(CENTIMETERS)

|       |       |       |       |       |       |      |      |      |       |       |       |       |       |       |       |
|-------|-------|-------|-------|-------|-------|------|------|------|-------|-------|-------|-------|-------|-------|-------|
| C-20  | 0.60  | 1.00  | 1.40  | 1.80  | 2.21  | 2.61 | 3.01 | 3.41 | 3.81  | 4.21  | 4.61  | 5.01  | 5.41  | 5.82  | 6.22  |
| 6.62  | 7.02  | 7.42  | 7.82  | 8.22  | 8.62  | 9.02 | 9.42 | 9.83 | 10.23 | 10.63 | 11.03 | 11.43 | 11.83 | 12.23 | 12.63 |
| 13.03 | 13.44 | 13.84 | 14.24 | 14.64 | 15.04 |      |      |      |       |       |       |       |       |       |       |

TIME(SECONDS)      NODE TEMPERATURES(DEGREES C)

| TIME  | POSITIONS: TIP    0.0 (SLAB 0) , ROOT    0.0 (SLAB 0)       |       |       |       |       |       |       |       |       |       |       |       |       |       |       |       |
|-------|---|-------|-------|-------|-------|-------|-------|-------|-------|-------|-------|-------|-------|-------|-------|-------|
| 0.0   | 700.0   | 700.0 | 700.0 | 700.0 | 700.0 | 700.0 | 700.0 | 700.0 | 700.0 | 700.0 | 700.0 | 700.0 | 700.0 | 700.0 | 700.0 | 700.0 |
| 10.20 | POSITIONS: TIP    5.61 (SLAB 15) , ROOT    4.25 (SLAB 11)   |       |       |       |       |       |       |       |       |       |       |       |       |       |       |       |
| 0.0   | 667.6   | 673.3 | 677.5 | 680.7 | 683.1 | 684.9 | 686.2 | 687.1 | 687.7 | 688.1 | 688.4 | 688.5 | 688.7 | 688.8 | 688.8 | 688.8 |
| 20.20 | POSITIONS: TIP    7.86 (SLAB 20) , ROOT    5.80 (SLAB 15)   |       |       |       |       |       |       |       |       |       |       |       |       |       |       |       |
| 0.0   | 603.6   | 624.4 | 638.7 | 649.0 | 657.7 | 658.2 | 662.1 | 665.3 | 668.0 | 670.1 | 671.9 | 673.3 | 674.5 | 675.3 | 676.0 | 676.5 |
| 30.20 | POSITIONS: TIP    9.84 (SLAB 25) , ROOT    7.74 (SLAB 18)   |       |       |       |       |       |       |       |       |       |       |       |       |       |       |       |
| 0.0   | 521.0   | 545.9 | 568.9 | 592.1 | 611.0 | 625.5 | 636.2 | 643.7 | 649.6 | 651.7 | 653.0 | 655.8 | 657.6 | 659.2 | 660.6 | 661.7 |
| 40.20 | POSITIONS: TIP    12.03 (SLAB 33) , ROOT    8.13 (SLAB 21)  |       |       |       |       |       |       |       |       |       |       |       |       |       |       |       |
| 0.0   | 464.7   | 487.5 | 509.4 | 530.5 | 551.7 | 570.6 | 589.0 | 605.9 | 618.7 | 628.5 | 635.9 | 641.4 | 645.5 | 648.4 | 649.4 | 649.4 |
| 50.20 | POSITIONS: TIP    15.24 (SLAB 39) , ROOT    9.17 (SLAB 23)  |       |       |       |       |       |       |       |       |       |       |       |       |       |       |       |
| 0.0   | 421.2   | 442.8 | 463.7 | 483.9 | 503.3 | 521.9 | 540.8 | 557.8 | 575.3 | 590.6 | 603.4 | 613.7 | 621.7 | 627.6 | 631.9 | 634.9 |
| 60.20 | POSITIONS: TIP    15.24 (SLAB 39) , ROOT    10.19 (SLAB 26) |       |       |       |       |       |       |       |       |       |       |       |       |       |       |       |
| 0.0   | 386.1   | 406.6 | 426.5 | 445.8 | 464.4 | 482.4 | 499.7 | 516.3 | 532.3 | 548.4 | 563.0 | 577.6 | 589.9 | 600.0 | 608.1 | 614.3 |
| 70.20 | POSITIONS: TIP    15.24 (SLAB 39) , ROOT    11.22 (SLAB 29) |       |       |       |       |       |       |       |       |       |       |       |       |       |       |       |
| 0.0   | 356.5   | 376.2 | 395.1 | 413.4 | 431.1 | 448.4 | 465.0 | 481.1 | 496.7 | 511.7 | 526.2 | 539.7 | 552.5 | 564.6 | 576.0 | 587.6 |
| 80.20 | POSITIONS: TIP    15.24 (SLAB 39) , ROOT    12.32 (SLAB 31) |       |       |       |       |       |       |       |       |       |       |       |       |       |       |       |
| 0.0   | 331.9   | 350.1 | 368.0 | 385.3 | 402.2 | 418.7 | 434.7 | 450.1 | 465.1 | 479.6 | 493.5 | 506.9 | 519.7 | 532.1 | 544.0 | 555.3 |
| 90.20 | POSITIONS: TIP    15.24 (SLAB 39) , ROOT    13.68 (SLAB 35) |       |       |       |       |       |       |       |       |       |       |       |       |       |       |       |
| 0.0   | 310.0   | 327.2 | 344.0 | 360.4 | 376.4 | 392.0 | 407.2 | 421.9 | 436.1 | 449.9 | 463.2 | 475.9 | 488.2 | 499.8 | 511.0 | 521.6 |





TABLE V, PART 7  
SIDE HEAT LOSS

NUMBER OF NODES 38  
TIME STEP (CONTROLLED) HIGH LIMIT= 0.00003 LOW LIMIT= 0.00003  
DISTANCE BETWEEN NODES= 0.4311 CENTIMETERS

DISTANCES FROM THE SURFACE AT EACH NODE (CENTIMETERS)

|       |       |       |       |       |       |      |      |      |       |       |       |       |       |       |       |
|-------|-------|-------|-------|-------|-------|------|------|------|-------|-------|-------|-------|-------|-------|-------|
| 0.20  | 0.60  | 1.03  | 1.47  | 1.80  | 2.21  | 2.61 | 3.01 | 3.41 | 3.81  | 4.21  | 4.61  | 5.01  | 5.41  | 5.82  | 6.22  |
| 6.62  | 7.07  | 7.42  | 7.92  | 8.22  | 8.62  | 9.02 | 9.42 | 9.83 | 10.23 | 10.63 | 11.03 | 11.43 | 11.83 | 12.23 | 12.63 |
| 13.03 | 13.44 | 13.84 | 14.24 | 14.64 | 15.04 |      |      |      |       |       |       |       |       |       |       |

TIME (SECONDS) NODE TEMPERATURES (DEGREES C)

| Time (s) | POSITIONS: TIP C.C. (SLAB 0) , ROOT C.C. (SLAB 37)    |       |       |       |       |       |       |       |       |       |       |       |       |       |       |       |
|----------|---|-------|-------|-------|-------|-------|-------|-------|-------|-------|-------|-------|-------|-------|-------|-------|
|          | 700.0   | 700.0 | 700.0 | 700.0 | 700.0 | 700.0 | 700.0 | 700.0 | 700.0 | 700.0 | 700.0 | 700.0 | 700.0 | 700.0 | 700.0 | 700.0 |
| 0.00     | 700.0   | 700.0 | 700.0 | 700.0 | 700.0 | 700.0 | 700.0 | 700.0 | 700.0 | 700.0 | 700.0 | 700.0 | 700.0 | 700.0 | 700.0 | 700.0 |
| 10.02    | POSITIONS: TIP 5.33 (SLAB 14) , ROOT 3.96 (SLAB 17)   |       |       |       |       |       |       |       |       |       |       |       |       |       |       |       |
|          | 674.0   | 678.3 | 681.5 | 683.9 | 685.6 | 686.7 | 687.5 | 688.0 | 688.4 | 688.6 | 688.8 | 688.9 | 688.9 | 688.9 | 688.9 | 688.9 |
| 20.02    | POSITIONS: TIP 7.47 (SLAB 19) , ROOT 5.46 (SLAB 14)   |       |       |       |       |       |       |       |       |       |       |       |       |       |       |       |
|          | 622.2   | 637.7 | 648.0 | 653.9 | 658.4 | 662.3 | 665.5 | 668.2 | 670.4 | 672.2 | 673.6 | 674.7 | 675.6 | 676.2 | 676.9 | 677.1 |
| 30.02    | POSITIONS: TIP 9.40 (SLAB 24) , ROOT 6.66 (SLAB 17)   |       |       |       |       |       |       |       |       |       |       |       |       |       |       |       |
|          | 544.3   | 568.1 | 591.1 | 610.2 | 625.1 | 636.1 | 644.1 | 650.0 | 652.1 | 654.2 | 656.2 | 657.9 | 659.5 | 660.9 | 662.0 | 663.0 |
| 40.02    | POSITIONS: TIP 11.50 (SLAB 29) , ROOT 7.86 (SLAB 20)  |       |       |       |       |       |       |       |       |       |       |       |       |       |       |       |
|          | 481.0   | 504.1 | 526.2 | 548.1 | 568.3 | 588.3 | 604.9 | 618.2 | 628.4 | 636.0 | 641.7 | 645.9 | 649.4 | 649.6 | 649.9 | 650.2 |
| 50.02    | POSITIONS: TIP 15.24 (SLAB 39) , ROOT 8.81 (SLAB 23)  |       |       |       |       |       |       |       |       |       |       |       |       |       |       |       |
|          | 434.3   | 456.4 | 477.8 | 498.4 | 518.2 | 537.8 | 556.7 | 573.2 | 588.2 | 602.5 | 613.2 | 621.5 | 627.3 | 632.3 | 634.5 | 637.3 |
| 60.02    | POSITIONS: TIP 15.24 (SLAB 39) , ROOT 9.85 (SLAB 25)  |       |       |       |       |       |       |       |       |       |       |       |       |       |       |       |
|          | 397.1   | 418.0 | 438.2 | 457.8 | 476.7 | 494.9 | 512.4 | 528.2 | 546.0 | 561.1 | 576.1 | 588.9 | 599.5 | 608.0 | 614.7 | 619.8 |
| 70.01    | POSITIONS: TIP 15.24 (SLAB 39) , ROOT 10.87 (SLAB 28) |       |       |       |       |       |       |       |       |       |       |       |       |       |       |       |
|          | 366.2   | 385.9 | 405.1 | 423.7 | 441.8 | 459.3 | 476.2 | 492.8 | 509.3 | 523.5 | 537.9 | 552.6 | 565.1 | 577.3 | 587.4 | 595.7 |
| 80.09    | POSITIONS: TIP 15.24 (SLAB 39) , ROOT 11.94 (SLAB 30) |       |       |       |       |       |       |       |       |       |       |       |       |       |       |       |
|          | 339.7   | 358.3 | 376.5 | 394.2 | 411.4 | 428.1 | 444.3 | 460.0 | 475.2 | 489.8 | 504.0 | 517.6 | 530.7 | 543.4 | 554.1 | 563.9 |
| 90.09    | POSITIONS: TIP 15.24 (SLAB 39) , ROOT 12.17 (SLAB 33) |       |       |       |       |       |       |       |       |       |       |       |       |       |       |       |
|          | 310.9   | 328.5 | 345.6 | 362.4 | 378.7 | 394.6 | 410.1 | 425.1 | 439.6 | 453.6 | 467.2 | 480.4 | 493.2 | 505.7 | 517.4 | 528.0 |

Table VI

## Results at 60 Seconds

Sensitivity of the Results to Time Step and Space Mesh Size  
Side Heat Loss

$T_o = 700^\circ\text{C}$ ,  $L = 15.24$  cm, no convection, surface temperature =  $0^\circ\text{C}$ , ( $t < 0$ ),  
columnar growth,  $h_s = 0.001$ ,  $w = 1$  cm,  $T_{a,s} = 0^\circ\text{C}$

| <u>part</u> | <u>N</u>         | <u><math>\Delta t</math></u> | <u><math>x_L</math></u> | <u><math>x_E</math></u> | <u><math>T_{\text{center}}</math></u> | <u><math>t_{1st}</math></u><br><u><math>\lambda = 0.75</math></u> |
|-------------|------------------|------------------------------|-------------------------|-------------------------|---------------------------------------|---|
| 1           | 19               | .1                           | 15.24                   | 10.21                   | 626.5                                 | 34.5  |
| 2           | 38               | .1                           | 15.24                   | 9.84                    | 629.2                                 | 35.4  |
| 3           | 76               | .1                           | 15.24                   | 9.80                    | 630.1                                 | 35.5  |
| 4           | 38               | .2                           | 15.24                   | 10.19                   | 628.0                                 | 33.8  |
| 5           | 38               | .05                          | 15.24                   | 9.65                    | 631.2                                 | 37.0  |
| 6           | 38               | *.0002 max<br>.0001 min      | 15.24                   | 9.66                    | 635.6                                 | 36.9  |
| 7           | 38               | *.0006 max<br>.0003 min      | 15.24                   | 9.85                    | 630.7                                 | 35.1  |
| 8           | $\infty^\dagger$ | .1                           | 15.24                   | 9.80                    | 630.4                                 | 35.5  |
| 9           | 38               | 0**                          | 15.24                   | 9.57                    | 632.2                                 | 37.8  |

† Extrapolated back to zero slab width.

\* Fine steps controlled by program. These are accuracy limits.

\*\* Extrapolated back to zero time step.

## Appendix F

## Thin Plate Castings

This appendix describes the physical model and analytical approximations made in describing heat flow in end chilled plates with h controlled side heat flow.

1. Physical Basis

Many experiments made on thin plate castings(31) have shown that for h controlled heat flow ( $h_s w/\bar{K} \ll 1$ ),\* and for mushy alloys that freeze over a wide range of temperature, the structure during the process of solidification is as pictured in Figure 54a. For example, the work of Bardes and Flemings(31) with thin plates ( $w = 0.114$  cm to  $w = 0.447$  cm) cast in a copper mold ( $h_s = 0.04$  cal/cm<sup>2</sup>°C sec) of Al-4.5% Cu alloy showed that the temperature gradients across the specimen were very small, that the dendrite arm spacing was nearly constant across the specimen, and that both the start of freeze isotherm and eutectic or end of freeze isotherm occurred throughout the specimen at nearly the same time, respectively.

Thus, solidification does not proceed inwards from the mold walls as is often intuitively thought to be the case, but proceeds at a nearly uniform rate throughout the casting by nucleation and/or growth of dendrite arms. The simple Scheil equation shown to approximately apply for this

\* Note: w will be used for the half width (y direction) of the casting in this appendix.

and many other alloys (3,19) quantitatively relates local fraction solid,  $f_s$ , to liquid composition,  $C_L$ , at any location:

$$f_s = 1 - \left(\frac{C_L}{C_0}\right)^{1/k-1} \quad (F1)$$

where  $C_0$  = starting alloy composition

$k$  = equilibrium partition ratio,  $C_s/C_L$

and liquid composition is a function only of temperature  $T$ :

$$C_L = C_0 + \frac{T - T_L}{m} \quad (F2)$$

where  $T_L$  = liquidus temperature

$m$  = slope of the liquidus.

Thus, fraction solid at a given location is a function only of temperature. Since temperature varies only slightly from center to surface of a casting when  $h_s w / \bar{K} \ll 1$ , fraction solid must also vary only slightly, as sketched in Figure 54. As a specific example, consider a variation in center to surface temperature of  $1^\circ\text{C}$ , for Al-4.5% Cu alloy. Calculations using equations (F1) and (F2) shows that at no temperature above the eutectic can there be more than a 7% difference in fraction solid between center and surface.

Consider now the same plate casting, where  $h_s w / \bar{K} \ll 1$ , but with a water chill at one end of the casting, such that  $h_p L / \bar{K} \gg 1$ , where  $h_p$  is the heat transfer coefficient at the metal-water cooled chill interface, and  $L$  is the length of the casting in the  $x$  direction. Now the



distribution of fraction solid during solidification must be as sketched in Figure 54b, with a marked variation in  $f_s$  along the plate length, but negligible variation across the plate thickness. Fraction solid at any time during solidification remains a single valued fraction of temperature as given by equations (F1) and (F2).

## 2. Mathematical Statement of the Assumptions

This section justifies the mathematical technique used herein of treating two dimensional heat flow in end chilled plate castings (where  $h_g w / \bar{K} \ll 1$ ) by adding a simple term to a one dimensional heat flow analysis. The heat flow equation in two dimensions, in the absence of a change of phase, is:

$$\frac{1}{\alpha} \frac{\partial T}{\partial t} = \frac{\partial^2 T}{\partial x^2} + \frac{\partial^2 T}{\partial y^2} \quad (\text{F3})$$

where  $\alpha$  is thermal diffusivity,  $\bar{K}/\rho C_p$ .

Integrating equation (F3) from 0 to  $y$ , holding  $x$  and  $t$  constant yields:

$$\frac{1}{\alpha} \int_0^y \frac{\partial T}{\partial t} dy = \int_0^y \frac{\partial^2 T}{\partial x^2} dy + \left. \frac{\partial T}{\partial y} \right|_0^y \quad (\text{F4})$$

Since  $T = f(x, y, t)$  where  $f$  is continuous and differentiable with respect to  $t$  and  $x$ , then

$$\int_0^y \frac{\partial T}{\partial t} dy = \frac{\partial}{\partial t} \int_0^y T dy \quad (\text{F5})$$

and

$$\int_0^y \frac{\partial^2 T}{\partial x^2} dy = \frac{\partial^2}{\partial x^2} \int_0^y T dy \quad (F6)$$

The term  $\frac{\partial T}{\partial y} \Big|_0^y$  may be evaluated directly at  $y = 0$  and  $y = w$ ,

$$\frac{\partial T}{\partial y} \Big|_{y=0} = 0 \quad (F7)$$

(centerline)

$$\frac{\partial T}{\partial y} \Big|_{y=w} = \frac{h_s}{\bar{K}} (T_w - T_{a,s}) \quad (F8)$$

(surface)

where  $T_w$  is the temperature at the surface, °C

$T_{a,s}$  is the ambient temperature at the interface, °C

$h_s$  is the heat transfer coefficient at the interface in the  $y$  direction,  $\text{cal/cm}^2 \text{ } ^\circ\text{C sec}$

Therefore

$$\frac{\partial T}{\partial y} \Big|_0^w = \frac{h_s}{\bar{K}} (T_w - T_{a,s}) - 0 \quad (F9)$$

Substituting (F5), (F6), and (F9) into equation (F4) yields

$$\frac{1}{\alpha} \frac{\partial}{\partial t} \int_0^w T dy = \frac{\partial^2}{\partial x^2} \int_0^w T dy + \frac{h_s}{\bar{K}} (T_w - T_{a,s}) \quad (F10)$$

Define the average temperature in the  $y$  direction,  $\bar{T}$ , as

$$\bar{T} \equiv \frac{1}{w} \int_0^w T dy \quad (F11)$$

Substituting (F11) into (F10) and dividing by  $w$  gives

$$\frac{1}{\alpha} \frac{\partial \bar{T}}{\partial t} = \frac{\partial^2}{\partial x^2} \bar{T} + \frac{h_s}{\bar{K}w} (T_w - T_{a,s}) \quad (\text{F12})$$

The only assumption to be made is the following; if  $T_w \approx \bar{T}$ , which is approximately correct for  $h_s w / \bar{K} \ll 1$ , then a substitution of  $\bar{T}$  for  $T_w$  in equation (F12) yields a differential equation

$$\frac{1}{\alpha} \frac{\partial \bar{T}}{\partial t} = \frac{\partial^2 \bar{T}}{\partial x^2} + \frac{h_s}{\bar{K}w} (\bar{T} - T_{a,s}) \quad (\text{F13})$$

which may be integrated in  $x$  to be solved.

Equation (F13) is the result desired. That is, it shows that for the case considered, heat flow can be treated as in a one dimensional problem with an added term (the term at the right of equation F13). The only assumption made in obtaining equation (F13) is that  $h_s w / \bar{K}$  is much less than unity.

In the foregoing discussion, no mention has been made of change in state (i.e., solidification). However, if fraction solid is a function only of temperature, as discussed above and as depicted in Figure 54b, then this formation of solid will affect only the apparent macroscopic heat capacity ( $C_p$ ) of the solid liquid mixture. Therefore, the constant  $\alpha$  ( $\bar{K} / \rho C_p$ ) in equation (F13) will be changed, but the equation will apply without modification.

In the computer model herein discussed below, a discontinuity in fraction solid occurs at the eutectic temperature as predicted by the Scheil equation (9% for Al-4.5% Cu). In addition, for mathematical convenience, a discontinuity is assumed at the dendrite tips (5% for most of this work). These discontinuities are relatively small and mean simply that even with extremely small temperature differences across the plate thickness, differences in fraction solid across the plate thickness is 5% at the beginning of solidification and 9% at the end.

### 3. Computer Model

The computer model for the side heat loss is as follows. The removal of heat through the y direction is calculated separately, applied to each slab after the x direction heat flow equations have been applied at the particular time step. The finite difference equation

$$\Delta T = \Delta t h_s (T_{a,s} - T(J)) / w C_p \rho \quad (F14)$$

where  $T(J)$  is the temperature of the J-th slab is applied to all slabs except those containing the tip or root.\*

---

\* Here, the terms "tip" or "root" are used for "start of freeze" or "end of freeze" isotherms.

The two slabs which contain the tip or root use the condition;

$$q_y = h_s (T_{a,s} - T(J))/w \quad (F15)$$

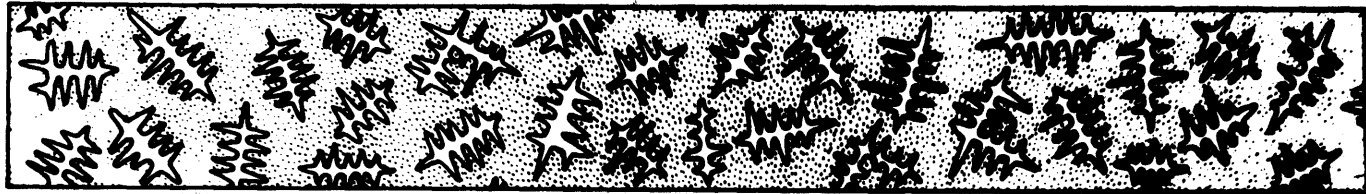
where  $q_y$  is the heat out in the y direction, cal/cm<sup>2</sup>/sec and this heat is included in the motion equations (for example, at the tip)

$$\Delta x_L / \Delta t = \frac{\text{heat in, x direction} - \text{heat out, x direction} - q_y}{f_t \rho H} \quad (F16)$$

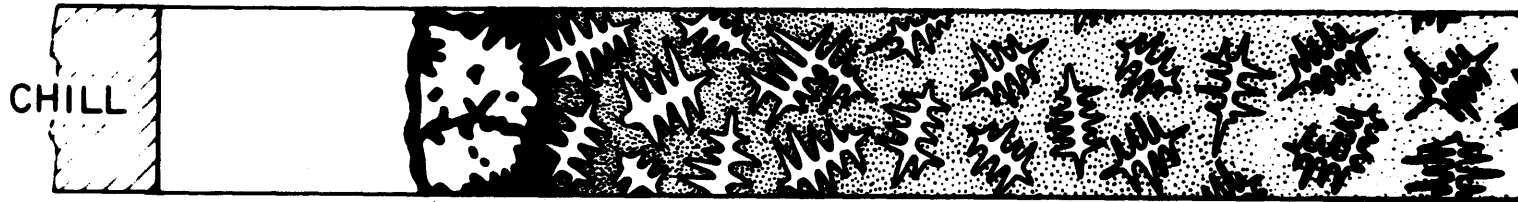
where  $f_t$  is the fraction solid at the tip

H is the heat of fusion.

Finally, if sidewise cooling of liquid ahead of the position of the tip has caused the temperature of the liquid to drop below the start of freeze temperature, a new position of the tip is set by interpolating the intersection of the temperature profile with the liquidus temperature. The program treats the position of the tip as if it represents the boundary between the region  $T > T_L$  and the region  $T < T_L$ . This treatment of the tip position can result in an apparently infinite velocity of the tip, as seen in Figures 22, 25. This effect is realistic only when "tip" and "root" are defined as in the footnote on the previous page, i.e., solid nucleates along the length of the ingot in slightly under-cooled liquid.



a) h controlled cast plate



b) h controlled end-chilled cast plate

RISER END →

Figure 54. Schematic representation of an h controlled cast plate.

## BIOGRAPHICAL NOTE

The author was born on April 23, 1945 in New York, New York. The first 12 years were spent travelling with his family courtesy of the U.S. Air Force. He was graduated from Boston Latin School in 1962, and has been at M.I.T. since then. He received the degree of S.B. in Metallurgy in 1966, and entered graduate school thereafter.

His professional interests include computer applications in process metallurgy, specifically to heat flow, and solidification, as well as other computer related fields. He intends to pursue a career related to the use of computers in the engineering disciplines.

He was married on June 4, 1966, and now has two children, whose education and growth form the basis for his interest in the psychology of education, personal motivation, and artificial intelligence. Along with music and literature, these are the avocations which fill any spare time.